University of Bath

PHD

Synthetic and spectroscopic studies of platinum and gold sigma-acetylide complexes with conjugated arene ligands

Jura, Marek

Award date:
2006

Awarding institution:
University of Bath

Link to publication

Alternative formats
If you require this document in an alternative format, please contact:
openaccess@bath.ac.uk

Copyright of this thesis rests with the author. Access is subject to the above licence, if given. If no licence is specified above, original content in this thesis is licensed under the terms of the Creative Commons Attribution-NonCommercial 4.0 International (CC BY-NC-ND 4.0) Licence (https://creativecommons.org/licenses/by-nc-nd/4.0/). Any third-party copyright material present remains the property of its respective owner(s) and is licensed under its existing terms.

Take down policy
If you consider content within Bath's Research Portal to be in breach of UK law, please contact: openaccess@bath.ac.uk with the details. Your claim will be investigated and, where appropriate, the item will be removed from public view as soon as possible.

Download date: 05. May. 2023

Synthetic and Spectroscopic Studies of Platinum and Gold σ-Acetylide Complexes with Conjugated Arene Ligands

Marek Jura

Department of Chemistry

University of Bath, September 2006

TITLE : SYNTHETIC AND SPECTROSCOPIC STUDIES OF PLATINUM AND GOLD σ-ACETYLIDE COMPLEXES WITH CONJUGATED ARENE LIGANDS

Attention is drawn to the fact that the copyright of this thesis rests with its author. This copy of the thesis has been supplied on condition that anyone who consults it is understood to recognise that the copyright rests with its author and that no quotation from the thesis and no information derived from it may be published without the prior written consent of the author.

This thesis may be made available for consultation within the University Library and may be photocopied or lent to other libraries for the purpose of consultation.

Signed : 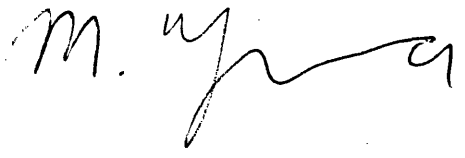

UMI Number: U490447

All rights reserved

INFORMATION TO ALL USERS
The quality of this reproduction is dependent upon the quality of the copy submitted.

In the unlikely event that the author did not send a complete manuscript
and there are missing pages, these will be noted. Also, if material had to be removed,
a note will indicate the deletion.

UMI U490447
Published by ProQuest LLC 2013. Copyright in the Dissertation held by the Author.
Microform Edition © ProQuest LLC.
All rights reserved. This work is protected against
unauthorized copying under Title 17, United States Code.

ProQuest LLC
789 East Eisenhower Parkway
P.O. Box 1346
Ann Arbor, MI 48106-1346

UNIVERSITY OF BATH
LIBRARY
30 10 JUL 2007
.....Ph.D.....

Dla Moich Rodziców

For My Parents

"This paper will no doubt be found interesting by those who take an interest in it."

John Dalton 1766-1844

Table of Contents

Declaration viii
Acknowledgements ix
Abstract x
Abbreviations used in the Text xi
1. Introduction 1
1.1 Luminescence and Light Emitting Diodes (LEDs) 2
1.2 Transition Metal σ-Acetylide Complexes 11
1.2.1 Platinum and Palladium 13
1.3.1 Gold and Silver 17
1.3.2 Ruthenium and Osmium 20
1.3 Properties of Transition Metal σ-Acetylide Complexes 22
1.3.1 Nonlinear Optics 22
1.3.2 Liquid Crystal Phases 25
1.5 Summary and Thesis Aims 28
1.6 References 29
Compound Naming and Numbering Scheme 33
2. Oligophenylene Systems 45
2.1 Introduction 45
2.1.1 Background 45
2.1.2 Objectives 47
2.2 Results and Discussion 48
2.2.1 Synthetic Strategy 48
2.2.2 Ligand Synthesis 49
2.2.3 Complex Synthesis 51
2.3 Molecular Structures 55
2.4 UV-visible Spectroscopic Studies 60
2.5 Density functional theory (DFT) calculational studies 69
2.6 Conclusions 72
2.7 References 73
3. Chalcogenophene Systems 75
3.1 Introduction 75
3.1.1 Background 75
3.1.2 Objectives 78
3.2 Results and Discussion 79
3.2.1 Synthesis of Chalcogenophene- Containing Ligands 79
3.2.2 Synthesis of di-platinum complexes (22), (26) and (32) 87
3.2.3 UV-visible spectroscopic studies of complexes (22), (26) and (32) 88
3.3.4 DFT calculational studies of compounds (21), (25) and (31) 91
3.2.5 Synthetic details for the platinum complexes (36), (40) and (43) 93
3.2.6 UV-visible spectroscopic studies of complexes (36), (40) and (43) 96
3.2.7 DFT calculational studies of compounds (35), (39) and (42) 98
3.2.8 Synthetic details for the diazole containing compounds 100
3.2.9 UV-visible spectroscopic studies of complexes (48) and (52) 103
3.2.10 DFT calculational studies of compounds (47) and (51) 105
3.2.11 Synthetic details for the dicarbonyl compounds (53) – (55) and UV-visible studies of (55) 106
3.2.12 Synthetic details for the gold(I) systems (56) and (57) and UV-visible spectroscopic studies 108

3.4 NMR Studies of Chalcogenophene- Containing Platinum(II) and Gold(I) Complexes 111
3.4.1 ^{1}H NMR Spectroscopy 111
3.4.2 ^{13}C NMR Spectroscopy 112
3.4.3 ^{31}P NMR Spectroscopy 113
3.4.4 Group 16 NMR Spectroscopy 114
3.5 Molecular structures determined by X-ray crystallography 117
3.6 Summary of Results and Conclusions 128
3.7 References 130
4. Luminescent Pyrrole- Containing Systems 133
4.1 Introduction 133
4.1.1 Background 133
4.1.2 Objectives 135
4.2 Synthesis of the pyrrole containing ligands 135
4.3 Synthesis of the pyrrole containing platinum (II) complexes 140
4.4 UV-visible spectroscopic studies of pyrrole containing platinum (II) complexes 142
4.4 Solid state X-ray structure of (61) 146
4.5 Summary and Conclusions 149
4.6 References 150
5. Tuneable 'Twisted' Systems 152
5.1 Introduction 152
5.1.1 Background 152
5.1.2 Objectives 153
5.2 Synthesis of 4,4"-bis-(trans-(phenyl,bis-triethylphosphine) platinum) ethynyl-2',3',5',6'-tetrafluoro-terphenyl (86) 154
5.3 Synthesis of 1,4-di-((trans-(phenyl,bis-triethylphosphine) platinum)ethynyl)-2,3,5,6-tetrafluoro-benzene (89) 157
5.4 UV-visible studies of the tetra-fluoride containing complexes (86) and (89) 159
5.5 Synthesis of 4,4"-di-(trans-(phenyl,bis-triethylphosphine) platinum) ethynyl-2',3',5',6'-tetramethyl-terphenyl (95) 162
5.6 UV-visible studies complex (95) 164
5.7 Synthesis and UV-visible studies of complex (90) 165
5.8 Synthesis of Aza-cyclic ligands (99) and (101) 169
5.9 UV-visible studies of Aza-cyclic ligands (99) and (101) 172
5.10 Synthesis and characterisation of complex (106) 173
5.11 UV-visible studies of complex (106) 177
5.12 Conclusions 178
5.13 References 179
6. Experimental Details 180
6.1 General methods and instrumentation 180
6.2 Experimental details for Chapter Two 182
6.2.1 Synthesis of 1,4-*di*-(*trans*-(phenyl,*bis*-triethylphosphine)platinum) ethynyl-benzene (3) 182
6.2.2 Synthesis of 4,4'-*di*-(*trans*-(phenyl,*bis*-triethylphosphine)platinum) ethynyl-biphenyl (6) 183
6.2.3 Synthesis of 4,4"-*di*-(*trans*-(phenyl,*bis*-(diethyl) (phenyl) phosphine) platinum) ethynyl-biphenyl (7) 184
6.2.4 Synthesis of 4,4"-*bis*-(trimethylsilyl)-terphenyl (8) 185
6.2.5 Synthesis of 4,4"-diiodo-*p*-terphenyl (9) 186

6.2.6 Synthesis of 4,4"-*bis*trimethylsilylethynyl-*p*-terphenyl (10) 186
6.2.7 Synthesis of 4,4"-*di*-ethynyl-terphenyl (11) 187
6.2.8 Synthesis of 4,4"-*bis*-(*trans*-(phenyl,*bis*-triethylphosphine)platinum) ethynyl-terphenyl (12) 188
6.2.9 Synthesis of 4,4'''-*bis*-(trimethylsilyl)-quaterphenyl (13) 189
6.2.10 Synthesis 4,4'''-diiodo-*p*-quaterphenyl (14) 190
6.2.11 Synthesis of 4,4'''-*bis*-(trimethylsilylethynyl)-quaterphenyl (15) 190
6.2.12 Attempted synthesis of 4,4'''-*di*-(ethynyl)-quaterphenyl (16) 191
6.2.13 Synthesis of 4,4'''-*di*-(*trans*-(phenyl,*bis*-triethylphosphine) platinum)ethynyl-tetraphenyl (17) 192
6.3 Experimental details for Chapter Three 193
6.3.1 Synthesis of 1,4-*di*-(4-bromo-phenyl)-butane-1,4-dione (18) 193
6.3.2 Synthesis of 2,5-*di*-(4-bromo-phenyl)-furan (19) 194
6.3.3 Synthesis of 2,5-*bis*-(4-trimethylsilylethynyl-phenyl)-furan (20) 194
6.3.4 Synthesis of 2,5-*di*-(4-ethynyl-phenyl)-furan (21) 195
6.3.5 Synthesis of 2,5-*di*-(4-(*trans*-(phenyl,*bis*-triethylphosphine)platinum ethynyl))phenyl)-furan (22) 196
6.3.6 Synthesis of 2,5-*di*-(4-bromo-phenyl)-thiophene (23) 197
6.3.7 Synthesis of 2,5-*bis*-(4-trimethylsilylethynyl-phenyl)-thiophene (24) 197
6.3.8 Synthesis of 2,5-*di*-(4-ethynyl-phenyl)-thiophene (25) 198
6.3.9 Synthesis of 2,5-*di*-(4-(*trans*-(phenyl,*bis*-triethylphosphine)platinum ethynyl))phenyl)-thiophene (26) 199
6.3.10 Synthesis of 2,5-dibromoselenophene (27) 200
6.3.11 Synthesis of 2,5-*bis*-(4-trimethylsilyl-phenyl)-selenophene (28) 201
6.3.12 Synthesis of 2,5-*di*-(4-iodo-phenyl)selenophene (29) 202
6.3.13 Synthesis of 2,5-*bis*-(4-trimethylsilylethynyl-phenyl)selenophene (30) 202
6.3.14 Synthesis of 2,5-*di*-(4-ethynyl-phenyl)selenophene (31) 203
6.3.15 Synthesis of 2,5-*di*-(4-(*trans*-(phenyl,*bis*-triethylphosphine)platinum ethynyl))phenyl)- selenophene (32) 204
6.3.16 Synthesis of 2,5-dibromofuran (33) 205
6.3.17 Synthesis of 2,5-*bis*(trimethylsilyethynyl)furan (34) 206
6.3.18 Synthesis of 2,5-diethynyl furan (35) 206
6.3.19 Synthesis of 2,5-di(*trans-bis*(triethylphosphine)(phenyl)platinum)ethynyl furan (36) 207
6.3.20 Synthesis of 2,5-di(*trans-bis*(triethylphosphine)(phenyl)platinum)ethynyl thiophene (40) 208
6.3.21 Synthesis of 2,5-*bis*(trimethylsilyethynyl)selenophene (41) 209
6.3.22 Synthesis of 2,5-diethynyl selenophene (42) 210
6.3.22 Synthesis of 2,5-di(*trans-bis*(triethylphosphine)(phenyl)platinum)ethynyl selenophene (43) 211
6.3.23 Synthesis of 1,2-di(4-bromobenzoyl)hydrazine (44) 212
6.3.24 Synthesis of 2,5-di(4-bromophenyl)-1,3,4-oxadiazole (45) 212
6.3.25 Synthesis of 2,5-*bis*(4-trimethylsilylethynylphenyl)-1,3,4-oxadiazole (46) 213
6.3.26 Synthesis of 2,5-di(4-ethynylphenyl)-1,3,4-oxadiazole (47) 214
6.3.27 Synthesis of 2,5-*di*-(4-(*trans*-(phenyl,*bis*-triethylphosphine)platinum ethynyl))phenyl)-1,3,4-oxadiazole (48) 215
6.3.28 Synthesis of 2,5-di(4-bromophenyl)-1,3,4-thiadiazole (49) 216
6.3.29 Synthesis of 2,5-*bis*(4-trimethylsilylethynylphenyl)-1,3,4-thiadiazole (50) 217

6.3.30 Synthesis of 2,5-di(4-ethynylphenyl)-1,3,4-thiadiazole (51) 218
6.3.31 Synthesis of 2,5-*di*-(4-(*trans*-(phenyl,*bis*-triethylphosphine)platinum ethynyl))phenyl)-1,3,4-thiadiazole (52) 219
6.3.32 Synthesis of 1,4-*bis*-(4-(trimethylsilylethynyl)phenyl)-butane-1,4-dione (53) 220
6.3.33 Synthesis of 1,4-*bis*-(4-(ethynyl)phenyl)-butane-1,4-dione (54) 221
6.3.34 Synthesis of 2,5-*di*-(4-(*trans*-(phenyl,*bis*-triethylphosphine)platinum ethynyl))phenyl)- butane-1,4-dione (55) 221
6.3.35 Synthesis of 2,5-*bis*-(4-triphenylphosphine gold(I)ethynyl-phenyl)-1,3,4-oxadiazole (56) 223
6.3.36 Synthesis of 2,5-*bis*-(4-triphenylphosphine gold(I)ethynyl-phenyl)selenophene (57) 224
6.4 Experimental details for Chapter Four 225
6.4.1 Synthesis of 2,5-*di*-(4-bromo-phenyl)-pyrrole (58) 225
6.4.2 Synthesis of 2,5-*bis*-(4-trimethylsilylethynyl-phenyl)-pyrrole (59) 225
6.3.3 Synthesis of 2,5-*di*-(4-ethynyl-phenyl)-1*H*-pyrrole (60) 226
6.4.4 Synthesis of 2,5-*bis*-(4-(*trans*-(phenyl,*bis*-triethylphosphine)platinum ethynyl))phenyl)-1*H*-pyrrole (61) 227
6.4.5 Synthesis of 2,5-*di*-(4-bromo-phenyl)-1-methyl-pyrrole (62) 228
6.4.6 Synthesis of 2,5-*bis*-(4-trimethylsilylethynyl-phenyl)-1-methyl-pyrrole (63) 229
6.4.7 Synthesis of 2,5-*di*-(4-ethynyl-phenyl)-1-methyl-pyrrole (64) 230
6.4.8 Synthesis of 2,5-*di*-(4-bromo-phenyl)-1-n-butyl-pyrrole (66) 231
6.4.9 Synthesis of 2,5-*bis*-(4-trimethylsilylethynyl-phenyl)-1-n-butyl-pyrrole (67) 233
6.4.10 Synthesis of 2,5-*bis*-(4-trimethylsilylethynyl-phenyl)-1-n-butyl-pyrrole (68) 234
6.4.11 Synthesis of 2,5-*bis*-(4-(*trans*-(phenyl,*bis*-triethylphosphine)platinum ethynyl))phenyl)-1-butyl-1H-pyrrole (69) 235
6.4.12 Synthesis of 2,5-*di*-(4-bromo-phenyl)-1-phenyl-pyrrole (70) 236
6.4.14 Synthesis of 2,5-*di*-(4-ethynyl-phenyl)-1-phenyl-pyrrole (72) 238
6.4.15 Synthesis of 2,5-*di*-(4-(*trans*-(phenyl,*bis*-triethylphosphine)platinum ethynyl))phenyl)-1-phenyl-1H-pyrrole (73) 238
6.4.16 Synthesis of 2,5-*di*-(4-bromo-phenyl)-1-methoxyphenyl-pyrrole (74) .240
6.4.17 Synthesis of 2,5-*bis*-(4-trimethylsilylethynyl-phenyl)-1-methoxyphenyl-pyrrole (75) 241
6.4.18 Synthesis of 2,5-*di*-(4-(*trans*-(phenyl,*bis*-triethylphosphine)platinum ethynyl))phenyl-1-(4-methoxy-phenyl)-1H-pyrrole (77) 242
6.4.19 Synthesis of 2,5-*di*-(4-bromo-phenyl)-1-phenol-pyrrole (78) 243
6.4.20 Synthesis of 2,5-*di*-(4-bromo-phenyl)-1-pyren-1-yl-1H-pyrrole (79) ..244
6.4.21 Synthesis of 4-[2,5-*di*-(4-bromo-phenyl)-pyrrol-1-yl]-benzonitrile (80) 244
6.4.22 Synthesis of 4-[2,5-*di*-(4-bromo-phenyl)-pyrrol-1-yl]-phenylamine (81) 245
6.5 Experimental details for Chapter Five 246
6.5.1 Synthesis of 1,2,4,5-tetrafluoro-3,6-(*bis*-*p*-trimethylsilylphenyl)benzene (82) 246
6.5.2 Synthesis of 1,2,4,5-tetrafluoro-3,6-(*di*-*p*-iodophenyl)benzene (83) 247
6.5.3 Synthesis of 1,2,4,5-tetrafluoro-3,6-(*bis*-*p*-trimethylsilylethynylphenyl) benzene (84) 247
6.5.4 Synthesis 1,2,4,5-tetrafluoro-3,6-(*di*-*p*-ethynylphenyl)benzene (85) 248

6.5.5 Synthesis of 4,4"-*bis*-(*trans*-(phenyl,*bis*-triethylphosphine)platinum) ethynyl-2',3',5',6'-tetrafluoro-terphenyl (86) 249
6.5.6 Synthesis of 1,2,4,5-tetrafluoro-3,6-*bis*-trimethylsilylethynyl-benzene (87) 250
6.5.7 Synthesis of 1,2,4,5-tetrafluoro-3,6-*di*-ethynyl-benzene (88)....251
6.5.8 Synthesis of 1,4-*bis*-((*trans*-(phenyl,*bis*-triethylphosphine)platinum) ethynyl) 2,3,5,6-tetrafluoro-benzene (89) 252
6.5.9 Synthesis of *trans*- *bis*(triethylphosphine)(phenyl)platinum(II) ethynyl benzene (90) 253
6.5.10 Synthesis of 1,2,4,5-tetramethyl-3,6-(*bis*-*p*-trimethylsilylphenyl)benzene (92) 254
6.5.11 Synthesis of 1,2,4,5-tetramethyl-3,6-(*di*-*p*-iodophenyl)benzene (93)...255
6.5.12 Synthesis of 1,2,4,5-tetramethyl-3,6-(*bis*-*p*-trimethylsilylethynyl)benzene (94) 255
6.5.13 Synthesis of 4,4"-*bis*-(trans-(phenyl,*bis*-triethylphosphine)platinum) ethynyl-2',3',5',6'-tetramethyl-terphenyl (95) 256
6.5.14 Synthesis of 2,5-*bis*-(4-trimethylsilyl-phenyl)-pyrimidine (98) 257
6.5.15 Synthesis of 2,5-*di*-(4-iodo-phenyl)-pyrimidine (99) 258
6.5.16 Synthesis of 2,5-*bis*-(4-trimethylsilylethynyl-phenyl)-pyrimidine (100) 259
6.5.17 Synthesis of 3,6-*di*-(4-bromo-phenyl)-[1,2,4,5]-tetrazine (101)....260
6.5.18 Synthesis of 3,6-*bis*-(4-trimethylsilylethynyl-phenyl)-[1,2,4,5]-tetrazine (102) 260
6.5.19 Synthesis of 1,3,5-*tris*-[(4-trimethylsilylethynyl)phenyl]benzene (106) 261
6.6 References 263

Declaration

The work described in this Thesis was conducted by the author at the University of Bath between October 2002 and December 2005. It represents the author's original and independent work, except where specific reference is made to the contrary. Neither the whole nor any part of this Thesis has been submitted previously in support of a degree at this or any other university. It does not exceed the prescribed limit, including tables, references and appendices.

Marek Jura

University of Bath, August 2006

Acknowledgements

I would like to thank my supervisors, Professor Paul Raithby and Dr. Paul Wilson for their constant support and guidance throughout my PhD. I would like to particularly thank Professor Paul Raithby for his patience and faith, and for a being a great source of ideas. I wish to particularly thank Dr. Paul Wilson for all his time spent in the lab, training me up to be a synthetic chemist, as well as for the enjoyable times spent in UBSA after a long day in the lab.

Thanks to Dr. Mary Mahon and Dr. Gabriele Kociok-Köhn for X-ray solid state structures.

I also wish to thank all the members of the Raithby and Wilson groups, past and present, for making my time at Bath so enjoyable. A special thank you to Emma Sharp and David Bandy for making my time in the lab so much fun and to Hazel Sparkes for her assistance with all things crystallographic, as well as making lunchtimes and breaks so enjoyable.

Thanks also to Gillian Eade for three enjoyable years living at Laura Place, to the rest of the Department of Chemistry at Bath, and to Ali Cullen for reminding me there is more to life than Chemistry (I am still working on that "electron bike" design).

As always, thanks to my family, Mum, Dad and Karolina for everything.

The financial support from the University of Bath is gratefully acknowledged.

Abstract

The research presented in this Thesis is concerned with the synthesis and physical properties of a range of organometallic compounds, with a particular emphasis on the opto-electronic properties of these systems.

Chapter one introduces the principles of luminescence and Light Emitting Diodes (LEDs), and describes how transition metal σ-acetylide complexes have been studied with respect to their luminescent properties. The chemistry of this class of compounds is also reviewed with specific references to Pt, Pd, Au, Ag, Os and Ru complexes.

Chapter two reports the synthesis and characterisation of a series of dinuclear *trans*-platinum complexes ($PhPt(PR'_3)_2C{\equiv}C\text{-}R\text{-}C{\equiv}CPt(PR'_3)_2Ph$) with oligophenyl spacer di-yne ligands (R = $-(C_6H_4)-$, $-(C_6H_4)_2-$, $-(C_6H_4)_3-$, $-(C_6H_4)_4-$, R' = Et, Et_2Ph). The photophysical properties of these complexes as well as the bridging ligands are discussed. Density Functional Theory (DFT) calculations are also reported in support of experimental observations.

Chapter three reports the synthesis and characterisation of a series of platinum and gold complexes with di-yne ligands containing heterocyclic groups of the form $PhPt(PEt_3)_2C{\equiv}C\text{-}R\text{-}C{\equiv}CPt(PEt_3)_2Ph$ where R = $-(C_6H_4)C_4H_2O(C_6H_4)-$, $-(C_6H_4)C_4H_2S(C_6H_4)-$, $-(C_6H_4)C_4H_2Se(C_6H_4)-$, $-C_4H_2O-$, $-C_4H_2S-$, $-C_4H_2Se-$, $-(C_6H_4)C_2N_2O(C_6H_4)-$, and $-(C_6H_4)C_2N_2S(C_6H_4)-$ and the form $Ph_3PAuC{\equiv}C\text{-}R\text{-}C{\equiv}CAuPPh_3$ where R = $-(C_6H_4)C_2N_2O(C_6H_4)-$, and $-(C_6H_4)C_4H_2Se(C_6H_4)-$. The steric and electronic effects of the heteroatoms in the di-yne ligands are investigated by solution state UV-visible spectroscopy correlated with solid state structures and DFT calculations. Comparisons of analogous platinum and gold complexes are also made.

Chapter four reports the synthesis and characterisation of a series of platinum complexes with pyrrole containing di-yne ligands of the form $PhPt(PEt_3)_2C{\equiv}C\text{-}(C_6H_4)C_4H_2(NR)(C_6H_4)\text{-}C{\equiv}CPt(PEt_3)_2Ph$ where R = H, CH_3, $CH_2CH_2CH_2CH_3$, C_6H_5, $C_6H_4OCH_3$. The effects of the various R groups on the physical properties of the system is investigated by solution state UV-visible spectroscopy.

Chapter five reports the synthesis and characterisation of a series of platinum complexes of the form $PhPt(PEt_3)_2C{\equiv}C\text{-}R\text{-}C{\equiv}CPt(PEt_3)_2Ph$ where R = $-(C_6H_4)C_6F_4(C_6H_4)-$, $-C_6F_4-$, and $-(C_6H_4)C_6(CH_3)_4(C_6H_4)-$. The synthesis and characterisation of a series of new di-yne ligands containing aza-cyclic rings $Me_3SiC{\equiv}C\text{-}(C_6H_4)C_4N_2H_2(C_6H_4)\text{-}C{\equiv}CSiMe_3$ and $Me_3SiC{\equiv}C\text{-}(C_6H_4)C_4N_4(C_6H_4)\text{-}C{\equiv}CSiMe_3$ is also reported. These new compounds are investigated by solution state UV-visible spectroscopy with conclusions drawn on the effects of inherent twist angles in these systems on their photophysical properties.

Chapter six reports the experimental details of the synthesis and characterisation of all the compounds described in previous Chapters.

Abbreviations used in the Text

Å	angstrom
^{n}Bu	*n*-butyl
^{t}Bu	*tert*-butyl
CT	charge transfer
DCM	dichloromethane
DMF	dimethylformamide
dppe	*bis*-(diphenylphosphino)ethane
dppm	*bis*-(diphenylphosphino)methane
EI/MS	electron ionisation mass spectrometry
ε	molar extinction coefficient
Et	ethyl
h	hour(s)
IR	infra-red
Me	methyl
MLCT	metal to ligand charge transfer
MS	mass spectrometry
NLO	non-linear optics
NMR	nuclear magnetic resonance
Ph	phenyl
^{i}Pr	*iso*-propyl
R	alkyl group
R_f	retardation factor (chromatography)
THF	tetrahydrofuran
TLC	thin layer chromatography
TMS	trimethylsilyl
TMSA	trimethylsilylacetylene
UV	ultra-violet
XRD	X-ray diffraction

w.r.t. NMR spectroscopy

s	singlet
d	doublet
t	triplet
t_{ps}	pseudo triplet
q	quartet

Chapter 1

Introduction

1. Introduction

The generation of light has changed much throughout the ages, from the flaming torch or campfire of early man's first use of 'artificial' lighting, to today's world dependence on electric lighting available at the flick of a switch. Irrespective of the circumstances, visible light is always produced by the emission of radiation in the form of electromagnetic waves, corresponding to wavelengths from about $7x10^{-7}$ m (red) to $4x10^{-7}$ m (violet). The full electromagnetic spectrum is shown in Figure 1.1.

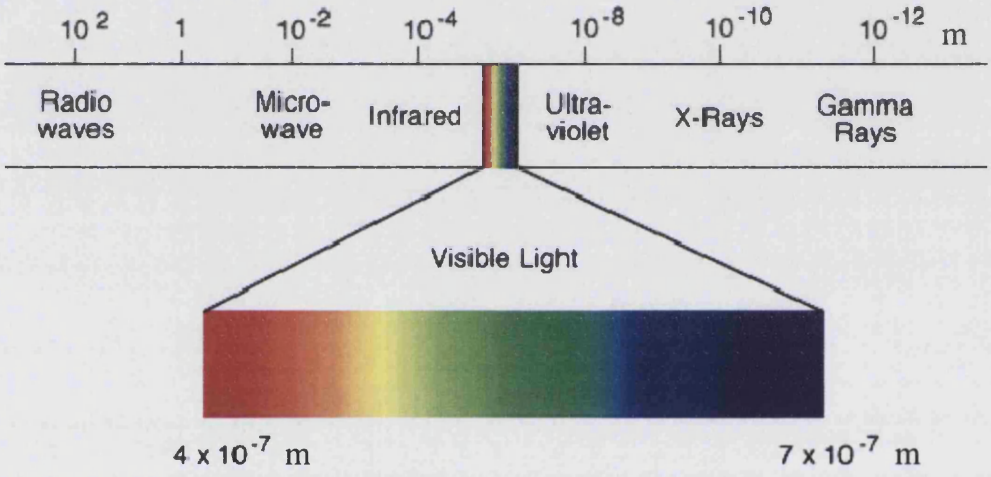

Figure 1.1 The Electromagnetic Spectrum.

Electric lighting was first demonstrated by Edison in 1879. Edison used the phenomenon of incandescence to generate light; utilising high electrical currents, which are passed through a material causing it to glow, with the emission of light as it gets hot.

The incandescent light bulb consists of a glass enclosure which either contains a vacuum or is filled with a low-pressure noble gas. Inside the bulb there is a filament of tungsten wire, through which an electrical current is passed, and as the filament resists the electron flow it becomes very hot. This excites electrons in the filament material to a higher atomic orbital and subsequently releases a photon when they fall back to their original orbits. A great deal of energy, however, is released as lower energy, infrared radiation. In fact, more infrared

radiation is released than visible light, which manifests itself as heat. This is wasted energy, and can account for upto 90% of the input electrical energy.

In the current climate of environmental awareness and energy conservation, there is clearly much room for improvement for the supply of lighting for everyday applications, and this problem has been the focus of much scientific research over recent years.

1.1 Luminescence and Light Emitting Diodes (LEDs)

Luminescence is light not generated by high temperatures alone. It is a different process from incandescence, and can occur at room temperature. For a material to be luminescent, it must emit light after it has been energetically excited. There are two distinct types of luminescence: fluorescence and phosphorescence.[1]

Fluorescence occurs when an excited state with the same multiplicity as the ground state decays radiatively to the ground state, as shown below in Figure 1.2.

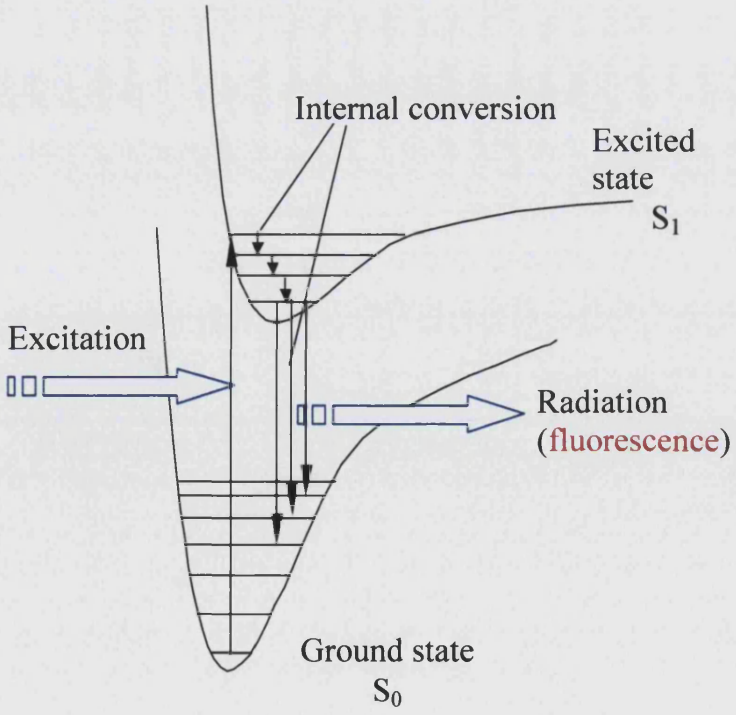

Figure 1.2 The process of fluorescence.

The process is spin allowed and is usually fast at room temperature, therefore the emission occurs immediately after absorption and decays rapidly. All transitions are vertical, in accordance with the Franck-Condon principle.

Phosphorescence involves a non radiative conversion, or intersystem crossing to a state of different multiplicity (for example from a singlet to a triplet) and slower radiative decay to the ground state from this "reservoir" state (Figure 1.3). Phosphorescence is therefore a longer lived effect and may persist long after the excitation process ceases.

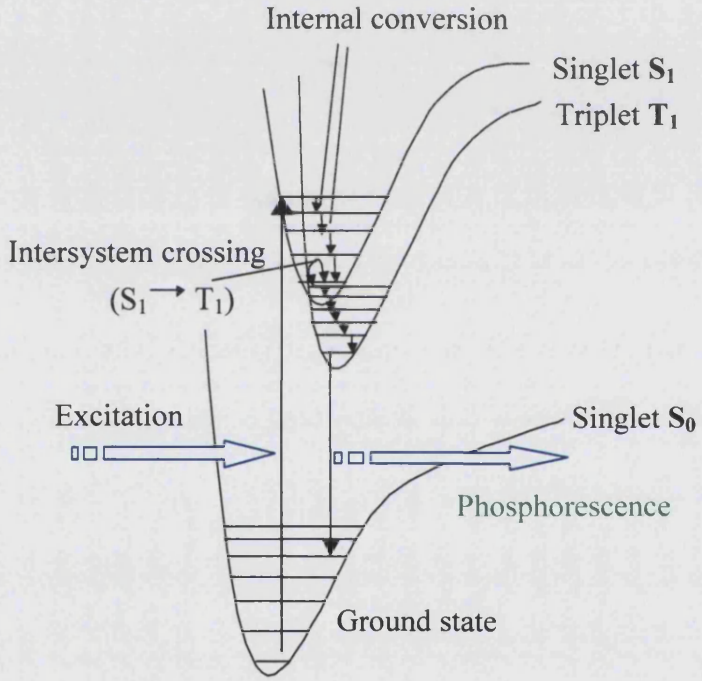

Figure 1.3 The process of phosphorescence.

Although this intersystem crossing process is forbidden as governed by the spin selection rule, i.e. $\Delta S = 0$ for an allowed transition, the rule may be relaxed by a process known as spin-orbit coupling. Spin-orbit coupling allows intersystem crossing by mixing the spin angular and orbital angular momenta, therefore allowing radiative decay to the ground state. Complexes containing heavier transition metal elements with larger spin-orbit coupling constants may therefore exhibit this phenomenon. Both types of luminescence show an emission red-shift to longer wavelengths than the exciting radiation. This is

evident from the two diagrams above as some of the vibrational energy has been dissipated by radiationless decay into the surrounding medium.

There are many ways in which the excited state needed for luminescence can be accessed. These are discussed in the following section.

⇨ *Chemiluminescence* is the emission of light as a result of a chemical reaction.

An example of this is the use of light sticks for emergency lighting. The light stick contains a glass ampoule, which typically contains hydrogen peroxide, suspended in phathalic ester. The hydrogen peroxide mix is stored inside the glass ampoule in order to keep it from mixing with the phenyl oxalate ester and starting the light producing chemical reaction. When the glow product is activated by bending it, the thin-walled glass ampoule breaks and its contents mix with the solution outside. Then, the hydrogen peroxide reacts with the phenyl oxalate ester, as shown in Figure 1.4.

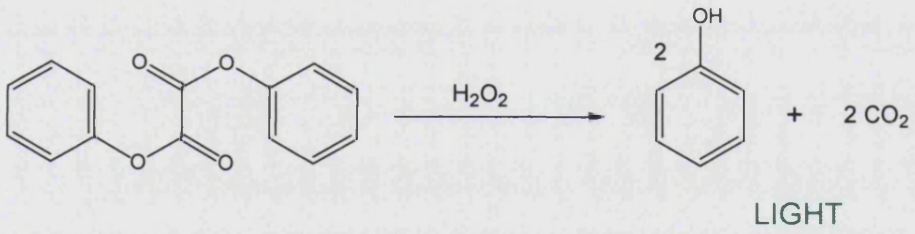

Figure 1.4 Example of light generated by chemiluminescence.

Chemiluminescence can also be observed in nature, for example in fireflies and glow worms. The firefly contains the enzyme luciferase, which triggers the oxidation reaction of luciferin in the presence of the phosphate adenosine triphosphate (ATP), Figure 1.5,[2] to give the corresponding ketone, with the total energy of the system being balanced by the release of a photon of light.

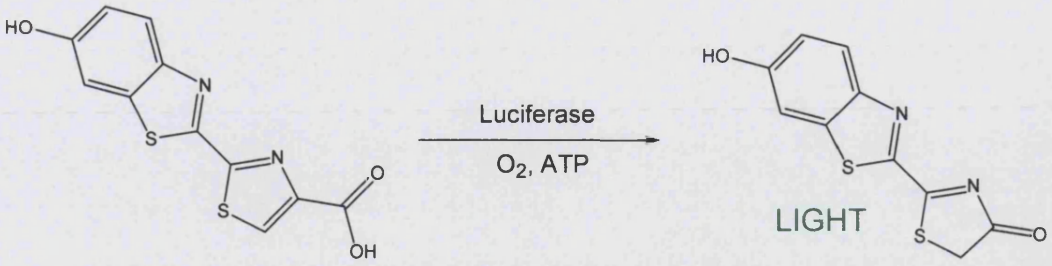

Figure 1.5 An example of bioluminescence. Oxidation of luciferase to generate light in fireflies.

⇨ *Radioluminescence* is produced in a material by the bombardment of ionizing radiation such as beta particles.

Self-luminous paints, such as ones used for dial markings for watches and other instruments, owe their behaviour to radioluminescence. These paints consist of a phosphor and a radioactive substance, for example, tritium or radium. Another example is the now-disused mixture of radium and copper-doped zinc sulfide paint used historically to paint clock dials.

⇨ *Sonoluminescence* is the emission of short bursts of light from imploding bubbles in a liquid when excited by sound.

The wavelength of the emitted light from sonoluminescence is very short - the spectrum extends well into the ultraviolet. The high energy waves produced indicate a temperature in the bubble of at least 10,000 °C. Such a high temperature makes the study of sonoluminescence especially interesting for the possibility that it might be a means to achieve thermonuclear fusion.[3] If the bubble is hot enough, and the pressures in it high enough, fusion reactions like those that occur in the Sun could be produced within these tiny bubbles.

⇨ *Crystalloluminescence* is the effect of luminescence produced during crystallisation.

There is a theory that the light is produced through the micro-fracture of growing crystallites. Separation of electrical charges may occur on the fracture

facets on the surface of micro-fracture and their following recombination. Crystalloluminescence effect is used to determine the critical size of the crystal nucleus[4].

⇨ *Photoluminescence* is the process in which a molecule absorbs a photon of visible electromagnetic radiation, there is a transition to a higher electronic energy state, followed by radiation of a photon back out of lower energy.

This is the most common type of luminescence studied in the scientific community. Photoluminescence spectroscopy is a non-destructive method of probing the electronic structure of materials. The intensity and spectral content of this photoluminescence is a direct measure of various important material properties.

⇨ *Triboluminescence* is the process in which light is generated *via* the breaking of asymmetric interactions in a crystal when that material is scratched, crushed, or rubbed.

Researchers have not yet arrived at a full understanding of the effect but the current theory of triboluminescence, which is supported by crystallographic,[5] spectroscopic,[6] and other experimental evidence, suggests that upon fracture of asymmetrical materials, charge is separated and when the charges recombine a flash of light is seen as a result of the electric discharge ionising the surrounding air. Further research suggests that crystals which display triboluminescene must lack symmetry (in order to permit charge separation) and be poor conductors.

⇨ *Electroluminescence* is the emission of light in response to an electric current passed through a substance, or to a strong electric field.

Generally, electroluminescence proceeds by the process outlined in Figure 1.6.

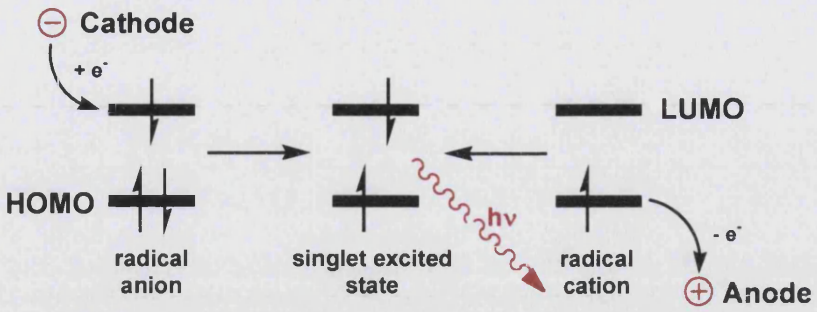

Figure 1.6 The process of electroluminescence.

When a potential difference is applied between two ends of an appropriate material several physical processes can occur to generate light by electroluminescence. Firstly, a charge carrier from the cathode injects an electron into the LUMO (Lowest Unoccupied Molecular Orbital) of a molecule, generating a radical anion. At the same time an electron is removed from a neighbouring molecule's HOMO (Highest Occupied Molecular Orbital) at the anode to generate a radical cation. These two species can meet, or migration of the electron and the hole can occur through the species under the influence of the field generated by the current. The rate of migration of the electrons and the holes is dependent upon the material. When the two species combine, an exciton is formed. The exciton can be treated in the same way as the two excited states seen in the Jablonski Schemes, Figures 1.2 and 1.3, and will decay back down to the ground state following the same pathways as shown for photoluminescence. The main difference between electrochemically excited species and photochemically excited species is the ratio of singlet and triplet species generated. This is discussed in more detail later in this section.

In 1936 Destriau first published the process of electroluminescence using zinc sulphide phosphor.[7] Much work then followed on the production of Light Emitting Diodes (LEDs) utilising this phenomenon, up until the 1960's when the first commercially usable devices were developed by General Electric. Figure 1.7 shows a basic schematic of a LED device.

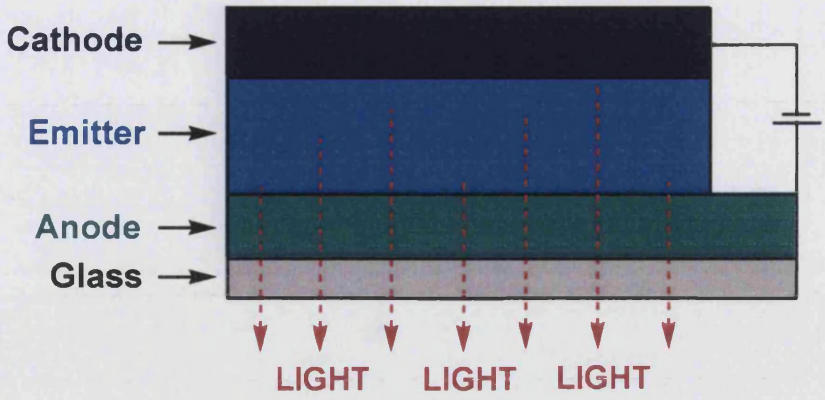

Figure 1.7 Schematic of a LED set-up.

The cathode is made up of a low work function metal such as Al, Mg, Ag or Au. These metals are chosen to ease the injection of electrons into the emitter layer. The anode is made up of a high work function material, which needs to be transparent to allow light to pass through. Indium Tin Oxide (ITO) is usually used for this purpose. The emitter layer, which is sandwiched between the anode and cathode, is a specifically designed material to generate luminescence of the desired wavelength. To produce an efficient device a good conducting material is required with high electron/hole mobilities. It is investigation into the emitter layer that has generated vast amount of scientific research over the last 70 years.

Arsenic, gallium and phosphorus were combined by Bevacqua[8] to obtain a red light source with an emission of 655 nm. The intensity of the device produced was poor and further work was conducted using gallium phosphide to produce a device emitting red light with much improved intensities over GaAsP.[9] Improvements in manufacturing techniques and increased understanding led to additional coloured LEDs being prepared in the 1970s, including oranges, yellows and greens from doping with GaAs and GaP.[10]

More recently organic light emitting diodes (OLEDs) have been produced which utilise the conjugation of aromatic molecules for the production of light. OLEDs work by sandwiching several layers of conjugated polymeric materials between two electrodes, one of which is transparent and allows light to pass out

the device. The first observation of luminescence from an organic molecule was reported in a paper by Pope *et al*,[11] on luminescence of anthracene.

Research however, remained largely focused on inorganic materials due to the low efficiency of organic light emitters. Organic dyes as light emitters regained popularity in the late 1980s but these systems required expensive vapour deposition. This problem was overcome by Friend *et al*,[12] when they published a paper revealing a solution to this problem by using the conjugated polymer poly(p-phenylenevinylene) (PPV). Friend's group, based in physics in Cambridge UK, and a group in chemistry, led by Holmes, were collaborating to research PPV. They were able to develop a simple device using a spin-coating process to produce the first OLED.

Further research followed from many groups using PPV based molecules that incorporate side chains and heteroatoms to tune the band gap of the materials and therefore the colour of the emitted light. Figure 1.8 shows some of the examples of the PPV derived polymers which have been reported.

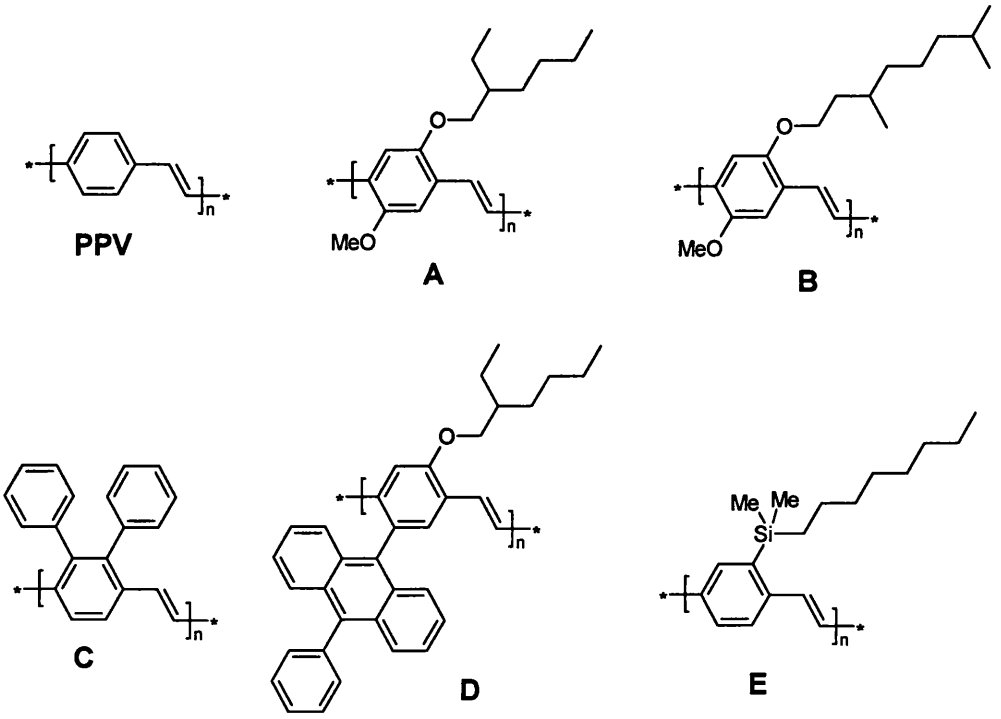

Figure 1.8 PPV and derivative polymers.

The red-orange emission of polymer **A** poly[2-methoxy-5-(2-ethylhexyloxy)-p-phenylenevinylene] (MEH-PPV), was reported by Braun *et al.*[13] Polymer **B** was synthesised in 1996 by Phillips, and led to multilayer OLEDs that were more efficient due to improved hole injection. The phenyl groups observed in polymer **C** poly(2,3-diphenylenevinylene) serve to increase the solubility of the polymer and therefore increase its processability, but the electroluminescent efficiency of this molecule as a single layer device is relatively low, although it was found that the introduction of pendant groups such as that in polymer **D** behave as inter-chain spacers and delay the excited state decay, thereby increasing the electroluminescent efficiency. The silicon atoms in polymer **E** served to increase the solubility of the polymer and increased the band gap, allowing access to green photo-emissions.

The downfall of OLED devices arises because of their poor efficiency. The ratio of singlet to triplet states generated in conventional OLED devices has been determined as 1:3, which in turn limits the maximum efficiency to 25%.[14] The efficiency of OLEDs is limited by the statistics of singlet states recombining. Triplet states can emit photons but the probability of this is quite small and energy loss from the triplet state usually occurs by intersystem crossing, followed by internal conversion to the ground state. To overcome this problem the triplet state needs to be accessed. As mentioned in the description of luminescence earlier in this section, decay from the triplet excited state back to the singlet ground state is spin forbidden, as governed by the selection rules. This governing physical law can be relaxed by the inclusion of heavy atoms.

In very heavy atoms, relativistic shifting of the energies of the electron energy levels accentuates the spin-orbit coupling effect. In typical organic molecules with weak spin-orbit coupling and highly forbidden triplet-singlet transitions, triplet state population is transferred into heat. Only the singlet state can emit radiatively (fluorescence). On the other hand, in organo-transition-metal compounds, fast intersystem crossing induced by spin-orbit coupling effectively depopulating the excited singlet into the lowest triplet state. Again due to spin-orbit coupling, the triplet can decay radiatively as phosphorescence even with high emission quantum yield at ambient temperature. In case of validity of spin

statistics only 25% of the excitons can be exploited by organic emitters, while for triplet emitters additional 75% of the excitons may be harvested. Thus, the efficiency of light emission in an electro-luminescent device with triplet emitters can be up to a factor of four higher than with singlet emitters.[15]

To combine the properties of the highly conjugated aromatic compounds as exploited in OLEDs, with the spin-orbit coupling properties of transition metals, a method was needed for the synthesis of these new "organo-transition-metal compounds". One such method is the use of alkynes as a bridging unit between the metal centre and the aromatic system. The sp-hybridised carbons of the alkynes allow for good orbital overlap with the d-orbital of transition metals, the chemistry of a variety of transition metal σ-acetylide complexes is discussed in the following section. Emphasis is given on the synthesis and photophysical properties of these systems.

1.2 Transition Metal σ-Acetylide Complexes

Transition metal σ-acetylide complexes (Figure 1.9) have been studied extensively due to their many interesting chemical and physical properties.

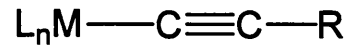

Figure 1.9 Transition Metal σ-Acetylide Complexes.

These properties find many valuable potential applications in modern technology, from light-emitting diodes, [16] liquid-crystalline materials [17] to materials with non-linear optical properties[18] and one-dimensional conductors.[19] Monomeric, oligomeric and polymeric compounds are all known and their properties studied.[20,21]

The properties of these materials can be tuned by the adjustment of both the alkyne ligand and the metal environment. Functional groups on the alkyne ligands (**R**) can alter the electronic properties of complex as well as their solubility. The auxiliary ligands ($\mathbf{L_n}$) (i.e. spectator ligands, other than the

acetylides), coordination geometry and oxidation state of the metal (**M**) have all been varied to investigate the effects on the properties of the acetylide complexes.[22]

It is well recognised that the metal to carbon bond, in metal σ-acetylide complexes, is generally thermally stable due to stabilisation through a $d\pi$-$p\pi$ interaction. The absence of β-hydrogen atoms on the alkyne ligand removes the possibility of decomposition of these compounds by β-hydride elimination. Photoelectron spectroscopy and calculations indicate a significant overlap between the filled metal d-orbitals and the filled π-system of the alkynyl moiety.[23] The energy difference between the HOMO metal d orbitals and the LUMO π^* alkynyl orbitals appears to be too large (*ca* 15 eV) for π-accepting behaviour.

The metal geometry is an important factor in the control of the properties of the acetylide complexes. Pt(II) and Pd(II) exhibit well defined square planar geometries with *cis/trans* isomers possible, therefore if linear rigid-rod complexes are desired, the *trans* geometry is employed and if 'angular' materials are required then the *cis* geometry is used. Ru(II) and Rh(III), showing octahedral geometry, may also be used to make *trans* linear rod complexes, or *cis* angular complexes. Chelating ligands such as diphosphines and diimines can be used to control stereochemistry in these compounds. Ag(I) and Au(I) are both generally limited to linear, two-coordinate geometry and are therefore employed in the synthesis of linear rigid rod acetylide complexes. The choice of metal centre can have a significant effect on the band gap, with four coordinate d^8 square planar metal centres favoured over six coordinate d^6 octahedral units, because of the greater optical gap energy of the latter (*ca* 0.4 eV).[24]

The chemistry of these various transition metal alkynes are discussed in more detail in the following sections, with particular emphasis on their synthesis and photophysical properties.

1.2.1 Platinum and Palladium

The square planar geometries along with the kinetic inertness of Pt(II) and Pd(II) gives rise to linear and stable alkynyl complexes. Platinum(II) acetylide complexes were first synthesised by Hagihara *et al*,[17] using the condensation reaction between terminal or di-terminal alkynes and platinum chlorides. Subsequently this method was adapted,[25] for example as shown in Figure 1.10.

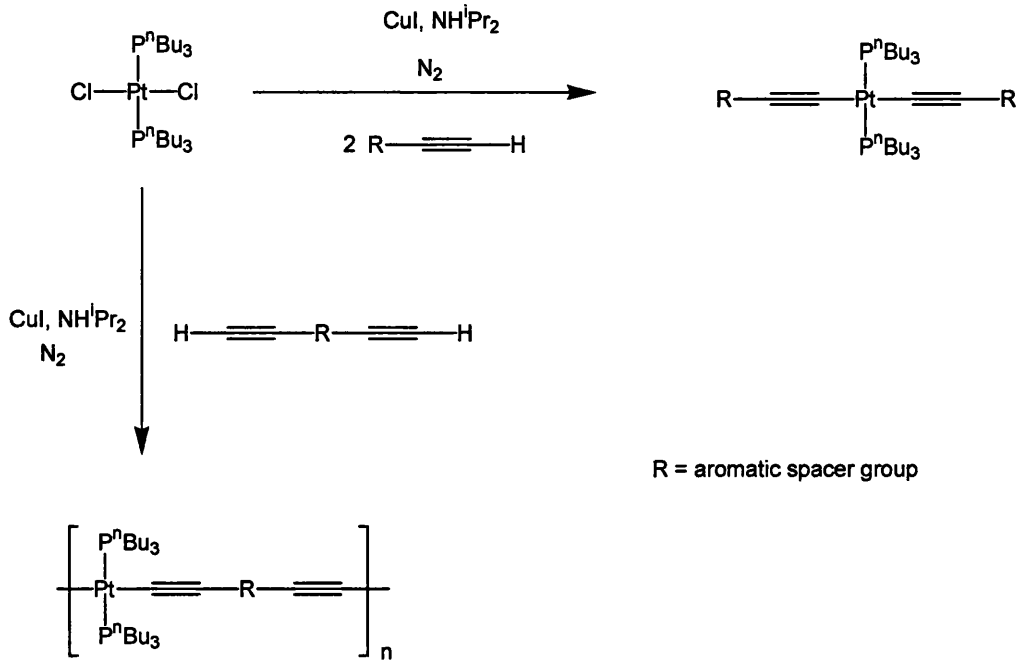

Figure 1.10 Synthesis of Pt(II) di-ynes and poly-ynes.

The copper(I) iodide in the scheme is used as a catalyst, and it is thought that a copper(I) acetylide intermediate is formed during the reaction. The copper(I) acetylide is a highly reactive species, and the alkyne is readily able to transmetalate to the platinum starting material to produce the desired product. The diisopropylamine is used as the solvent and also acts as a base to accept excess protons. This route has only been successfully used for the Group 10 metals palladium and platinum. It is unsuccessful with elements earlier in the transition series, including nickel since they tend to react with the basic amine solvent to form amine complexes.

Alternative synthetic routes have also been reported, involving the use of trimethylstannyl alkynyl derivatives,[26] for example as shown in Figure 1.11. The trimethylstannyl derivatives have been shown to be more stable than the free alkynes,[27] although concerns about the health implication of Sn(IV) have made this route less popular. An extra step is also required in the synthesis of the final compound; this involves the treatment of the alkyne with ^{n}BuLi followed by Me_3SnCl.[28]

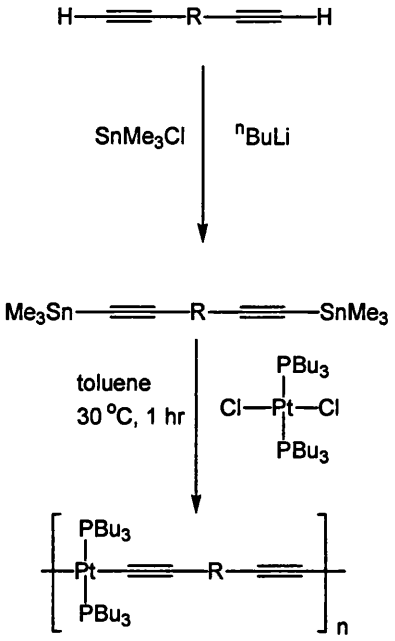

Figure 1.11 Synthesis of a platinum acetylide polymer *via* trimethylstannyl alkynyl derivatives.

This method does have some advantages, namely the avoidance of amine solvents, allowing the synthesis of nickel analogues. Stoichiometric treatment of *bis*(trimethylstannyl)alkynes with *trans*-$[MCl_2(PBu_3)_2]$ affords polymers in excellent yield. In the case of M = Pt average molecular weights up to M_w = 210,000 were observed,[29] which is on average 30,000 Daltons higher than the dehydrohalogenation route of Hagihara *et al.*

A variety of platinum(II) and palladium(II) species have been investigated with respect to their photoluminescence properties. The monomeric complexes *trans*-$[Pt(C{\equiv}CH)_2(PEt_3)_2]$ and *trans*-$[Pt(C{\equiv}CPh)_2(PEt_3)_2]$ gave intense vibronically structured emission in rigid glasses at 77 K.[20] The emissive state has been assigned as Pt 6d to $\pi^*(C{\equiv}C)$ MLCT in character upon excitation into

the low-energy MLCT absorption bands. Polymeric metal acetylide complexes have also been studied such as the materials shown in Figure 1.12.

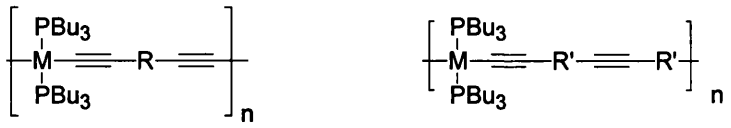

where M = Pt (II) or Pd (II); R and R' are aryl spacer groups, as shown below

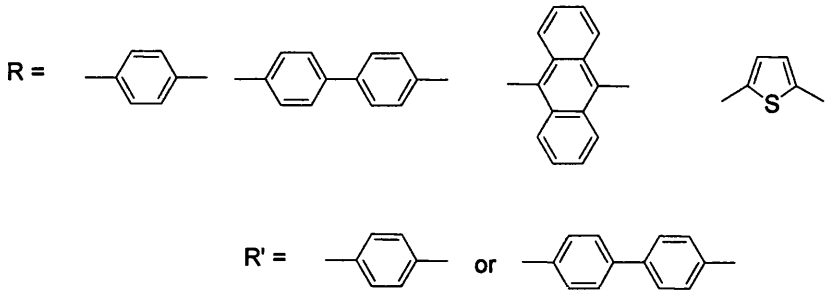

Figure 1.12 Pt(II) and Pd(II) polyynes investigated for photoluminescent behaviour.

Studies on thin films at liquid helium temperatures have shown long-lived phosphorescence, assigned to a triplet-singlet transition. The platinum species have much longer phosphorescence lifetimes than isostructural palladium species and this is likely to be due to the greater effect of spin-orbit coupling for platinum.[24]

The polymeric metal acetylide complexes, with their extended conjugation lengths have shown low energies of absorption. The polymeric systems, however, are difficult to study due to their relatively large size and molecular weights. Di-yne complexes have been synthesised as dimeric models for the polyyne systems, as they are easier to study and establish structure-property relationships for the systems. Examples of such di-ynes in the literature are given in Figure 1.13 along with the general synthetic route to the complexes. The same dehydrohalogenation reaction is employed in the synthesis of the dimeric system as for the polyyne analogues, but using a different platinum starting material. *Trans*-$Pt(PBu_3)_2Cl_2$ is used for the synthesis of the polymeric systems, where the two chlorides offer two active sites leading to polymerisation. The butyl phosphines are employed to aid solubility leading to extensive degrees of polymerisation. The di-yne complexes are synthesised

using *trans*-$Pt(PEt_3)_2(Ph)Cl$, this starting material only contains one chloride and therefore one reactive site towards the alkyne ligand. The phenyl group effectively "caps off" one site of the platinum centre forcing the synthesis of the discrete di-platinum di-yne complex.

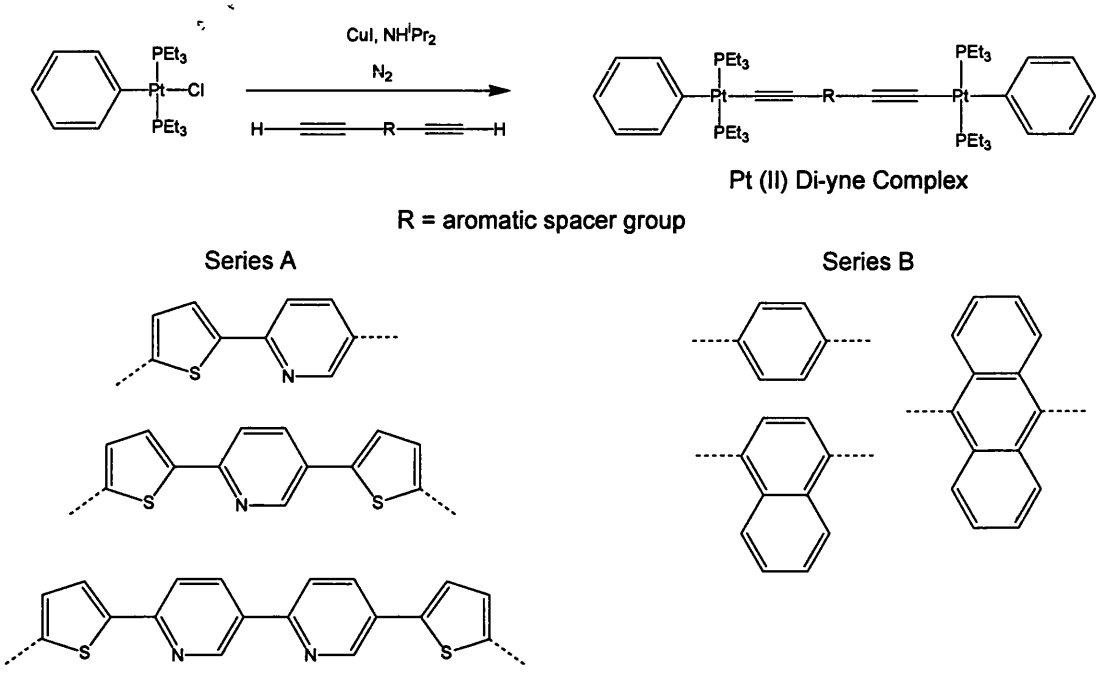

Figure 1.13 Synthesis of platinum di-yne complexes

Raithby and co-workers investigated a series of systems containing thienyl-pyridine rings, with adjacent electron donating and accepting units as the aromatic spacer groups (Series A, Figure 1.13).[30] The aim of the investigation was to establish the affect of the donor-acceptor unit of the energies of the singlet and triplet excited states. Absorption spectra were shown to be dominated by π-π^* transitions, with the platinum fragments acting as net electron donors to the electron withdrawing spacer groups. The pyridine rings in the systems were thought to withdraw electron density toward the lone pair, away from the system backbone. This reduction in electron density was rationalised as the reason for the higher optical gaps as compared to the purely thiophene-containing systems.

The use of fused ring spacers has been found to be a powerful approach to the production of some low band gap conjugated organic polymers.[31] The Raithby group took inspiration from this, and designed a series of fused ring spacers

platinum acetylide complexes (Figure 1.13, Series B).[32] Optical spectroscopic measurements showed that the electron-rich naphthalene and anthracene spacers create strong donor–acceptor interactions between the Pt(II) centres and conjugated ligands along the rigid backbone of the polymers. The band gaps decrease as the size of the aromatic linker group increases, consistent with there being greater delocalisation within the anthracene linker group compared to the benzene linker group.

The lowest band gap observed for a Pt(II) complex was reported by Wong and co-workers, Figure 1.14.[33] The group synthesised a Pt(II) polyyne with a 9-dicyanomethylenefluorene-2,7-diyl as a donor–acceptor spacer with a band gap of 1.58 eV. The authors suggest that electron-withdrawing groups at the periphery exert a more pronounced influence on narrowing the band gaps of these polymers than electron-donating substituents.

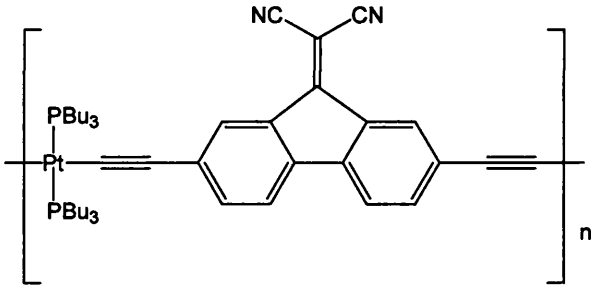

Figure 1.14 Low band gap Pt(II) polyyne containing 9-dicyanomethylenefluorene-2,7-diyl spacer group.

1.3.1 Gold and Silver

Ethynyl compounds are amongst the most stable gold(I) organometallic compounds known.[34] The preference of gold(I) for two-coordinate, linear coordination makes it ideal for the synthesis of rigid-rod materials with ethynyl ligands. Several linear complexes [Au(C≡CR)L] have been synthesised (L = tertiary phosphine[35], arsine[36], isocyanide[37] or amine[38]) either from the polymeric [{Au(C≡CR)}$_n$] or by the reaction of [LAuCl] with Grignard reagents. A more convenient synthesis of gold(I) ethynyls makes use of the simple reaction

between [Au(PR$_3$)Cl] and terminal alkynes in basic alcoholic solution,[39] as shown in Figure 1.15.

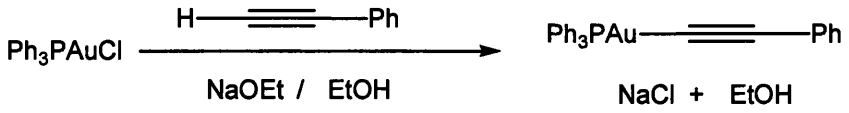

Figure 1.15 Synthesis of gold alkynyl complex under basic ethanolic conditions.

This method is generally applicable to a wide range of terminal alkynes, easily precipitating the sparingly soluble gold(I) ethynyl in high yield. Methanolic solutions also prove to be effective using either Na(OMe) or KOH as the base.[40] This approach has been used to synthesise a range of ethynyl complexes.

Many gold(I) complexes exhibit short Au···Au contacts between 2.7 – 3.5 Å. This tendency to aggregate was termed aurophilicity by Schmidbaur *et al*,[41] and is a consequence of relativistic effects of the heavy atom d^{10} system. The aurophilic effect can lead to long-chain arrangements of gold(I) complexes in the solid state – if these complexes are already rigid-rod linear structures, then this motif will be extended throughout the crystalline material to give linear polymers.

The photoluminescence of gold(I) complexes has been widely studied in the last decade. The first luminescent gold(I) acetylide reported was [Au$_2$(μ-dppe)$_2$(C≡C-Ph)$_2$],[42] Figure 1.16, which shows intermolecular (but no intramolecular) Au···Au interaction between two units leading to an Au···Au separation of 3.153(2) Å.

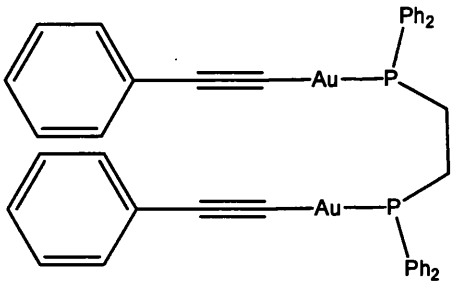

Figure 1.16 The first luminescent Au(I) acetylide complex reported, [Au$_2$(μ-dppe)$_2$(C≡C-Ph)$_2$].

The complex displays a ligand-centred emission at 420 nm in dichloromethane solution at 298 K, and the solid sample emits at 550 nm at 298 K. It was suggested that the Au···Au interactions may influence the photoluminescence of these gold(I) complexes. Mononuclear, dinuclear and polymeric rigid-rod gold(I) acetylide containing complexes have also been synthesised and investigated for their luminescence properties with examples shown in Figure 1.17.[37]

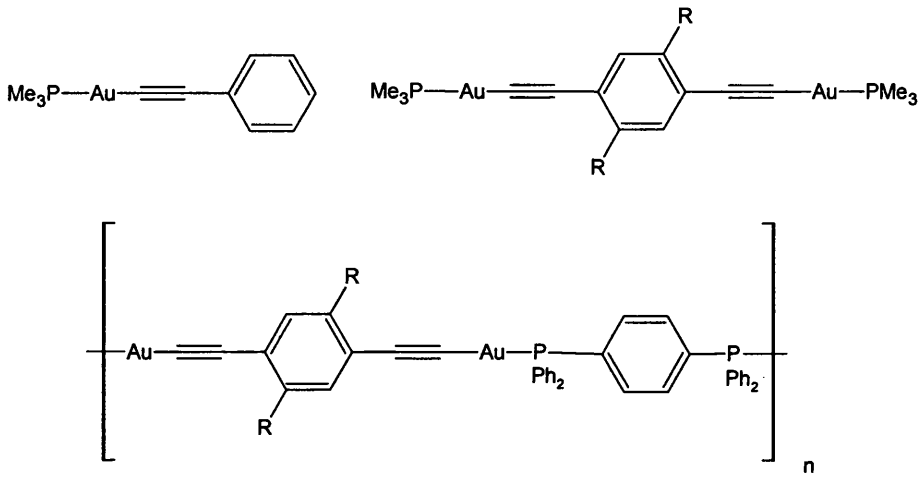

Figure 1.17 Gold(I) alkynyl compounds studied for their luminescent properties by Puddephatt *et al*, where R = H or Me.

The compounds all show strong emission on excitation (λ_{ex} > 350nm). The mono and dinuclear complexes are soluble in dichloromethane and emit at 424-504nm and 415nm, respectively. These emissions have been assigned as π–π^* or σ–π^* transitions. The dinuclear complex emits at 540 nm in the solid state, strongly red-shifted compared to the solution emission. This is suggested to be due to short Au···Au contacts (3.163(1) Å) in the solid state. The polymeric complexes are insoluble and can only be investigated in the solid state; they show broad emission at 600 nm. This low energy emission can be attributed to extensive delocalised π-conjugation along the polymer chain, as well as the short Au···Au contacts in the solid state.

The Yam group have extensively studied the photophysical properties of a large series of gold(I) alkynyl complexes.[43] A series of mono-, di- and trinuclear gold(I) phosphine alkynyl complexes have been synthesised and structurally characterised. In general, they assigned the intense absorption spectra as high-

energy absorptions due to Intra-Ligand (IL) phosphine-centred and π-π^*(C≡C) transitions, and the low-energy absorptions were assigned as metal perturbed IL π-π^*(C≡C) transitions mixed with metal-to-alkynyl MLCT transitions. Both the electronic absorption and emission energies are found to depend on the nature of the alkynyl ligands. The nuclearity of the metal complexes also has an influence on the electronic absorption as well as emission behaviour. The emission energies are generally found to be lowest in the trinuclear complexes, attributed to the presence of weak Au···Au interactions.

Silver acetylides are much less well known and studied although examples have been reported.[44] A series of trinuclear Ag complexes were synthesised by the Che[45] and Yam groups.[46] The groups reported Ag(I) alkynyl complexes $[Ag_3(\mu\text{-dppm})_3(\mu_3\text{-}\eta^1\text{-C}\equiv\text{C-R})]^{2+}$ and studied their luminescence. Ag···Ag interactions were also shown to influence the photoluminescent properties.

1.3.2 Ruthenium and Osmium

Ruthenium and osmium alkynyl complexes have been extensively investigated by Lewis and co-workers utilising trimethylstannylalkynes. Incorporation of Ru(II),[47] and Os(II)[48] metal centres into mono-, di- and polymeric alkynyl systems were studied. Synthetic methods were found to be particularly reliable for the synthesis of *trans*-oriented di- and polyalkynyl Ru(II) complexes (with stabilising dppe and dppm ligands), the synthesis of the monomeric and polymeric Ru alkynyl is shown in Figure 1.18. Similar schemes have also been reported for Os(II) (with dppm).

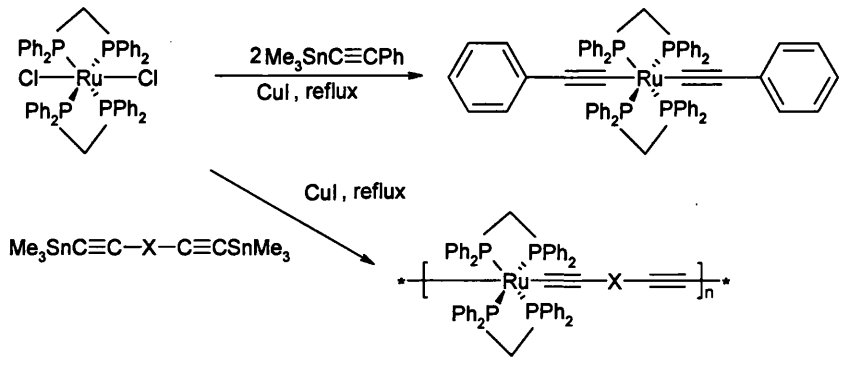

Figure 1.18 Synthesis of Ru alkynyls using trimethylstannyl reagents.

Dixneuf and co-workers developed a synthetic strategy to mono- and unsymmetrical dialkynyl ruthenium compounds *via* a vinylidene intermediate.[49] Initial findings by the group showed that *cis*- $[RuCl_2(Ph_2PCH_2PPh_2)_2]$ readily activates terminal alkynes to produce stable and isolable vinylidene complexes in excellent yields. Sodium hexafluoro phosphate is used for the production of a 16 electron Ru intermediate by the displacement of a chloride ligand. The vinylidene species is then deprotonated by the addition of one molar equivalent of DBU (1,8-diazabicyclo[5.4.0]undec-7-ene) in dichloromethane. The reaction is carried out at room temperature, and gives the *trans*-chloro alkynyl metal derivative, the general reaction scheme is illustrated in Figure 1.19.

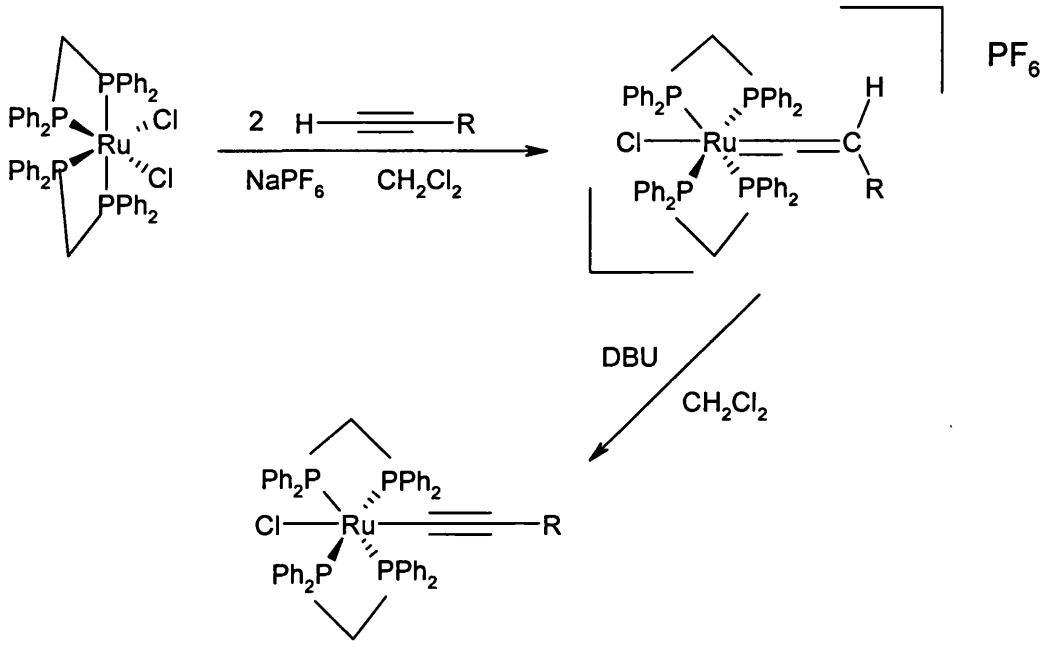

Figure 1.19 Formation of vinylidene intermediates in the synthesis of ruthenium alkynyl complexes.

1.3 Properties of Transition Metal σ-Acetylide Complexes

Transition metal σ-acetylide complexes have been suggested to be good materials for potential use in Light Emitting Diode (LED) technology. The conjugated aromatic systems linked to the metal centres *via* the acetylene groups have been used to tune the optical gaps of these materials. Whilst the heavy metal centres provide a route into efficient radiative use of triplet excited state, *via* spin orbit coupling. The complexes possess other interesting physical and electronic properties which may have applications in modern technology, such as nonlinear optics and liquid crystalline phases.

1.3.1 Nonlinear Optics

As light travels through a material a variety of nonlinear optical effects may occur. The interaction of light with such a material will cause its properties to change. As light travels through the material, its electric field interacts with charges in the material. The time dependent electron density distribution in the material resulting from this interaction can affect the propagation of subsequent light waves travelling through the material. These interactions can cause the original optical beam to have its frequency, phase, polarisation, or path changed significantly. The study of these changes is termed Nonlinear Optics (NLO) since it describes the deviations of behaviour away from classical optics.

This ability to manipulate light has many important technological applications in optical signal processing, generation of variable frequency laser light, tuneable filters, and optical data storage. In order to control the properties of light, chemists must design and synthesise molecules within which the combination of photons can take place, and in which both the magnitude and response time of these optical processes can be controlled.[50]

Organometallic compounds provide new opportunities for engineering materials with nonlinear optical properties. It is possible to change the transition metal element, its oxidation state and hence the number of d-electrons, examine the difference between diamagnetic and paramagnetic complexes and the effect of

novel bonding geometries and coordination patterns with a view to altering the non linear properties of the material.

In particular, transition metal acetylides are exceptionally useful for nonlinear optical studies due to the following reasons:

- ⇨ Metal to ligand or ligand to metal charge transfer bands are often observed in the UV to visible region of the spectrum. These optical absorption bands are often associated with large optical nonlinearities.
- ⇨ Chromophores containing metals are among the most intensely coloured materials known. The intensity of the optical absorption band is related to its transition dipole moment. Large optical nonlinearities are associated with such strongly allowed transitions.[51]
- ⇨ The presence of electron density away from the nuclei within a molecule increases its polarisability, and therefore its potential for nonlinear optical behaviour, hence systems with extensive π-conjugation are ideal.

Interest in nonlinear optics of square-planar metal aromatic complexes arose from the knowledge that the fragments, $MX_2(PEt_3)_2$, where M=Ni, Pd, and Pt; X=I, Br and Cl, are good electron donors. Experiments revealed that this class of compounds substituted with various aromatic acceptors could exhibit relatively large nonlinear optical behaviour.[52]

More recently rigid rod polymers have been used to study their nonlinear optical behaviour. The presence of low energy MLCT transitions and the possibility of extended delocalisation through the polymer chain provide the rationale for studying these materials for NLO applications.[53] The susceptibilities of the polyacetylide organometallic polymers are greater than those of the equivalent organic polyacetylide. A strong dependence between NLO response and metal employed (Ni, Pd, Pt) is seen. The nickel monomers and polymers tend to give larger hyperpolarisabilities than the platinum complexes. The full involvement of the metal in the polarisability of the polymer electron backbone is not yet known.[54]

A recent review by Humphrey and Cifuentes summarises the studies of the NLO properties of metal alkynyl complexes.[55] The review focuses on the synthesis and structure property relationship of Ru, Ni and Au complexes. The paper also reviews the recent progress with switching the nonlinearity of alkynyl complexes using protonation/deprotonation and, particularly, oxidation/reduction processes. This area in which alkynyl complexes may well prove superior to organic molecules, and has been seen as a niche for organometallics in nonlinear optics. An example of a switchable NLO system is given in Figure 1.20.

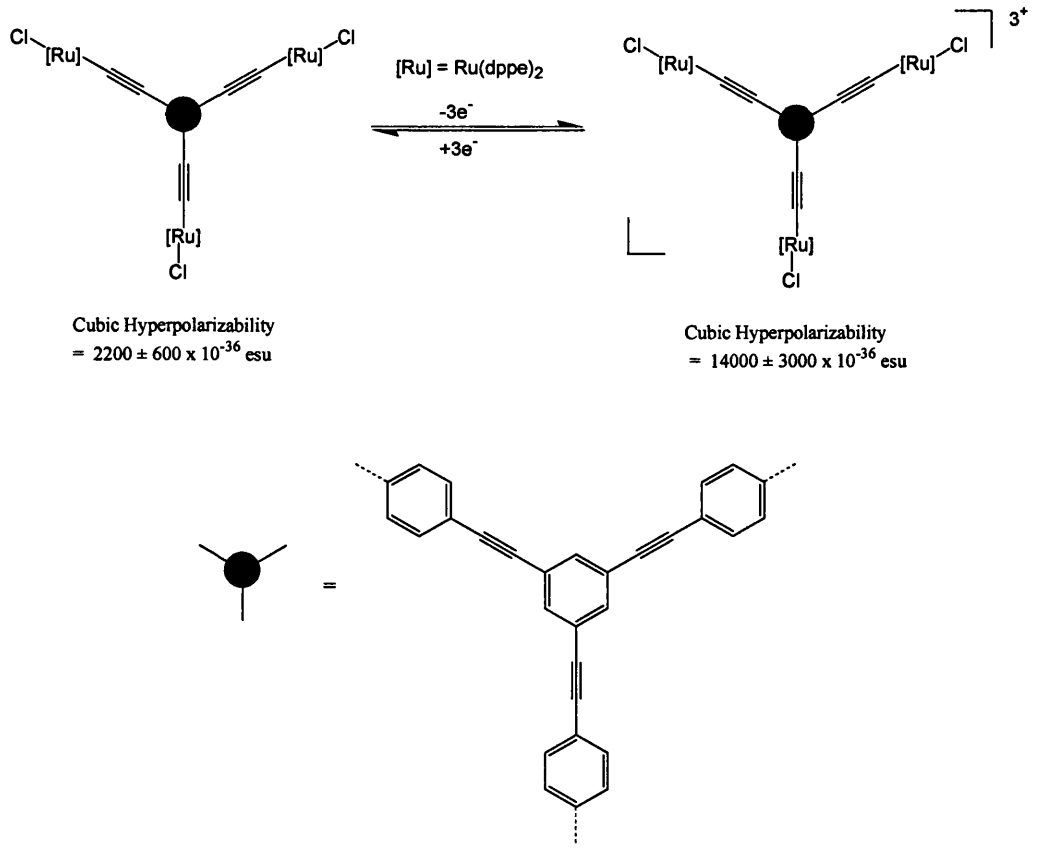

Figure 1.20 Switchable NLO system based on Ru alkynyl complexes.

1.3.2 Liquid Crystal Phases

Liquid crystalline compounds demonstrate molecular order between that of an ordered solid and a disordered liquid or solution. These intermediate phases are referred to as mesophases and can be split into two subdivisions (Figure 1.21).

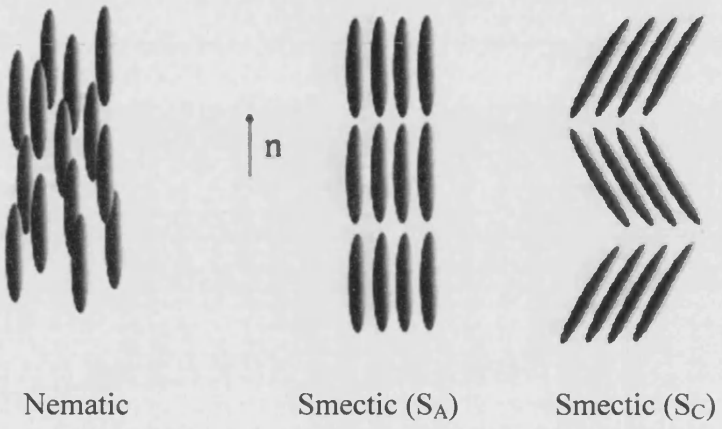

Figure 1.21 Liquid Crystalline phases.

- *Nematic* – the molecules align parallel in the direction *n*, but can move within the N phase and rotate freely around the long molecular axis. There is orientational, but no positional order.
- *Smectic* – this phase has a higher degree of order. Molecules are arranged in layers and are parallel within the layers. The S_A phase has molecules aligned parallel to the layer normal, but with no positional order within the layer. Other Smectic phases include S_C, where the molecules are arranged as in the S_A phase but with the layers tilted relative to each other.

The Liquid crystal state was recognised in the middle of the 19th century in nerve myelin.[56] Since then the area of liquid crystals has become a major, multidisciplinary field of research. Following the pioneering work of Gray and co-workers in the early 1970s with correct properties and sufficient stability to be used widely in commercial applications.[57] This has resulted in a multimillion-pound industry devoted to liquid crystal displays (LCDs). This is all down to the way liquid crystals are affected by electric current. A particular type of liquid crystal, called twisted nematics (TN), is naturally twisted.

Applying an electric current to these liquid crystals will untwist them to varying degrees, depending on the voltage. Liquid Crystal Displays (LCDs) use these liquid crystals because they react predictably to electric current in such a way as to control light passage.

Studies on homometallic (Figure 1.22) and heterometallic rigid rod polymers (Figure 1.22) by ^{31}P NMR spectroscopic techniques showed that all those investigated possessed a negative diamagnetic anisotropy, that is, they were shown to align with their long molecular axes perpendicular to the applied magnetic field. This was interpreted in terms of the negative diamagnetic anisotropy of the carbon-carbon triple bond.[58]

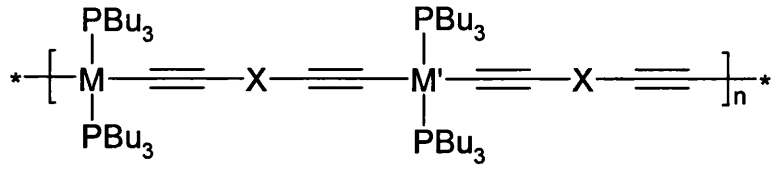

Figure 1.22 Rigid rod polymers, where M'=Pd or Ni; M=Pd, M'=Ni, and X=aromatic spacer group.

This work with polymeric acetylides prompted studies of related low molar mass compounds, and the Pt(II) complex in Figure 1.23 was found to possess two types of liquid crystalline phases.[59]

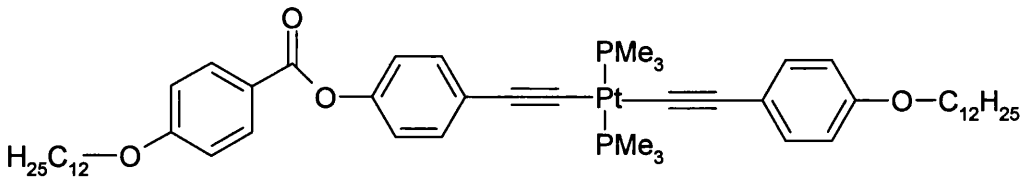

Figure 1.23 Pt(II) complex, which was found to posses liquid crystalline phases.

Particular attention has recently been directed towards a better understanding of the relationships between the shape and nature of a complex and the structure of the liquid crystal phase. Bruce *et al* have studied a series of complexes of palladium(II) and platinum(II) based on trialkoxystilbazole esters and showed how varying the ligand bulk effects the various liquid crystal phases, Figure 1.24.[60]

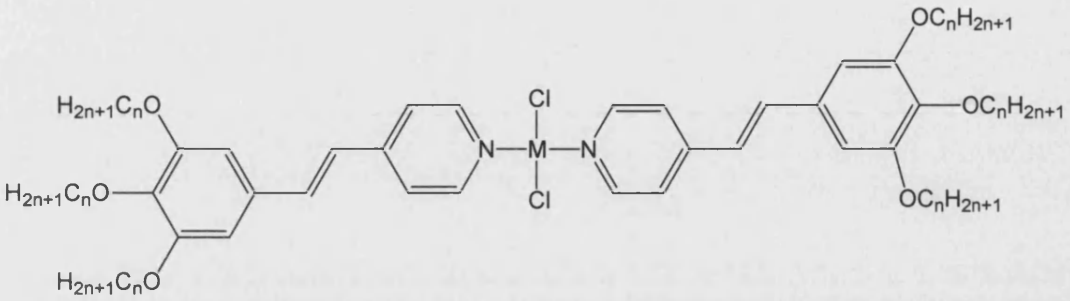

Figure 1.24 Complexes of Pd(II) and Pt(II) based on trialkoxystilbazole esters. M = Pd(II) or Pt(II), n = 6, 8, 10, 12, or 14.

The linear Au(I) alkynyl complexes of the type in Figure 1.25 have been shown to form nematic and smectic A phases without decomposition.[61]

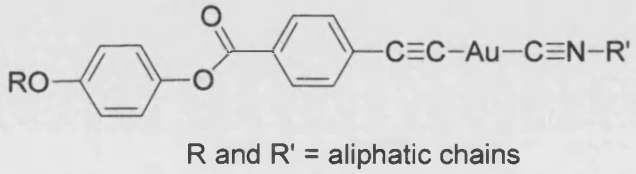

Figure 1.25 Gold(I) alkynyl complex studied for liquid crystalline behaviour.

The isonitrile ligand is used in preference to much more sterically bulky phosphines for stabilization of the gold acetylide. The molecules therefore, have a more rod-like structure and are more suitable for the formation of liquid crystal mesophases. A representative crystal packing diagram for the di-alkynyl Au(I) complexes with the following R Groups is given in Figure 1.26.

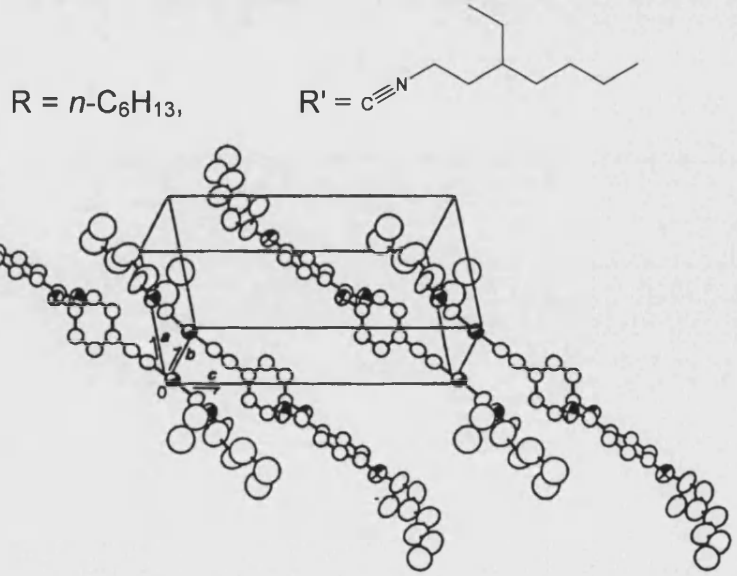

Figure 1.26 Crystal packing diagram of a Au(I) alkynyl complex.

It is clear to see how these linear rigid-rod gold(I) complexes order in the solid state as parallel rows. As the crystal melts some order is retained within the plane so as to give liquid crystalline states.

1.5 Summary and Thesis Aims

The issue of providing energy efficient lighting is becoming ever more imperative in today's energy consuming world. Organic Light Emitting Diodes (OLED)s have already entered the market place as replacement lighting to the traditional incandescent bulbs. The luminescence efficiency of the organic polymers used in OLEDs are limited to a maximum of 25%, due to the physical laws governed by the spin selection laws. There has been a rapid expansion over recent years in the incorporation of metals into these organic polymers, due to the numerous properties that metals can bring to these systems, such as spin-orbit coupling. The spin-orbit coupling properties of these heavy atoms can give rise to a greater luminescent efficiency, by allowing the efficient radiative use of the triplet state.

A successful method of incorporating metals into the conjugated polymeric systems is the use of alkynes as a bridging unit between the metal centre and the organic π- system. Transition metal σ-acetylide complexes and polymers have been extensively studied in the literature for their luminescent properties. Dinuclear metal acetylides complexes have in the past been studied within the Group as model systems for the polymeric analogues. These dinuclear complexes have been exploited to establish structure-property relationships for the polymeric systems, and to gain better understanding on how the π- systems of the spacer groups effect the photophysical properties of the complexes.

The aim of the work described in this Thesis has been to design a series of new di-yne ligands in order to study the effects of the incorporation of various heteroatoms and functional groups within the dinuclear metal complexes, on their luminescent properties. Chapters 2 to 5 describe the synthesis of these new di-yne ligands and the study of the photophysical properties of their corresponding Pt(II) complexes by solution UV-visible Spectroscopy.

1.6 Referenences

[1] P.W. Atkins, *Physical Chemistry*, Oxford, 4th Ed.

[2] C. E.Wayne, R. P. Wayne, *Photochemistry*, Oxford, University Press. 2001

[3] B. Barber, C. C. Wu, R. Lofstedt, P. Roberts, and S. Putterman, *Phys. Rev. Lett.*, 1994, **72**, 1380

[4] B. P. Chandra, P K Verma, M. H. Ansari *J. Phys. Condens. Matter.*, 1997, **9** 7675

[5] J. M. Cole, *Chem. Soc. Rev.*, 2004, **33**, 501

[6] Z. V. Todres, *J. Chem. Res.* 2004, **2**, 89

[7] S. Destriau, *J. Chim. Phys.*, 1936, **33**, 587

[8] N. Holonyak, S. F Bevacqua, *Appl. Phys. Lett.,* 1962, **4**, 82-83

[9] Y. Yamamoto, S. Somani, *Nonclassical Light from Semiconductor Lasers and LEDs*, Springer Series in Photonics

[10] G. H. White, R. A. Logan, *Appl. Phys. Lett.*, 1968, **13**, 139

[11] M. Pope, H. P. Kallman, P. Magnante, *J. Chem. Phys.*, 1963, **38**, 2042

[12] J. H. Burroughes, D. D. C. Bradley, A. R. Brown, R. N. Marks, K. Mackay, R. H. Friend, P. L. Burn, A. B. Holmes. *Nature,* 1990, **347,** 539

[13] D. Braun, A. J. Heeger, 1991, *Appl. Phys. Lett.*, **58**, 1982.

[14] J. Ho, (2002) *Improving the External Extraction Efficiency of Organic LEDs [WWW]* http://www.mtl.mit.edu/researchgroups/MEngTP/John_Ho_Proposal.pdf (January 17th 2006)

[15] J. Brooks, Y. Babayan, S. Lamansky, P. I. Djurovich, I. Tsyba, R. Bau, M. E. Thompson, *Inorg. Chem.*, 2002, **41**, 3055

[16] N. Chawdhury, M. Younus, P. R. Raithby, J. Lewis, R. H. Friend, *Opt. Mater.*, 1998, **9**, 498

[17] S. Takahashi, M. Kariya, T. Yatake, K. Sonogashira, N. Hagihara, *Macromolecules*, 1978, **11**, 1063

[18] W. J. Blau, H. J. Byrne, D. J. Cardin, A. P. Davey, *J. Mater. Chem.*, 1991, **1**, 245

[19] O. Lhost, J. M. Toussaint, J. L. Brédas, H. F. Wittmann, K. Fuhrmann, R. H. Friend, M. S. Khan, J. Lewis, *Synth. Met.*, 1993, **55-57**, 56

[20] N.J. Long, C. K. Williams,; *Angew. Chem. Int. Ed. Engl.*, 2003, **42** 2586.

[21] P. Nguyen, P. Gómez-Elipe, I. Manners, *Chem. Rev.*, 1999, **99**, 1515

[22] V. W.-W. Yam, K. K.-W. Lo, K. M.-C. Wong, *J. Organomet. Chem.*, 1999, **578**, 3

[23] J. Manna, K.J John. M.D. Hopkins, *Adv. Organomet. Chem. 1996*, **38**, 79

[24] G. Frapper, M. Kertz, *Inorg. Chem. 1993*, **32**, 732

[25] M. S. Khan, A. K. Kakkar, N. J. Long, J. Lewis, P. R. Raithby, P. Nguyen, T. B. Marder, F. Wittmann, R. H. Friend, *J. Mater. Chem.*, 1994, **4**, 1227

[26] B. Cetinkaya, M. F. Lappert, J. McMeeking, D. E. Palmer, *J. Chem. Soc. Dalton Trans.* 1973, 1202.

[27] B. F. G. Johnson, A. K. Kakkar, M. S. Khan, J. Lewis, A. E. Dray, R. H. Friend, F. Wittmann, *J. Mater. Chem.*, 1991, **1**, 485

[28] M. E. Wright, *Macromolecules*, 1989, **22**, 3256

[29] S. J. Davies, B. F. G. Johnson, M. S. Khan, J. Lewis, *J. Chem. Soc. Chem. Commun.*, 1991, 187.

[30] M. S. Khan, M. R. A. Al-Mandhary, M. K. Al-Suti, N. Feeder, S. Nahar, A. Köhler, R. H. Friend, P. J. Wilson, P. R. Raithby, *J. Chem. Soc. Dalton Trans.* 2002, 2441.

[31] K. Ogawa, S. Rasmussen, *J. Org. Chem.*, 2003, **68**, 2921

[32] M. S. Khan, M. R. A. Al-Mandhary, M. K. Al-Suti, F.R. Al-Battashi, S. Al-Saadi, B. Ahrens, J. K. Bjernemose, M. F. Mahon, P. R. Raithby, M. Younus, N. Chawdhury, A. Köhler, E. A. Marseglia, E. Tedesco, N. Feeder, S. J. Teat, *Dalton Trans.*, 2004, **15**, 2377

[33] W.-Y.Wong, K. -H. Choi, G.-L. Lu, J. -X. Shi, *Macromol. Rapid Commun.*, 2001, **22**, 461.

[34] G. K. Anderson, *Adv. Organomet. Chem.*, 1982, **20**, 39

[35] H. Lang, S. Koecher, S. Back, G. Rheinwald, G. Van Koten, *Organometallics*, 2001, **20**, 1968

[36] Abu-Salah, Omar M., *J. Organomet. Chem.*, 1990, **387**, 123

[37] M. J. Irwin, J. J. Vittal, R. J. Puddephatt, *Organometallics*, 1997, **16**, 3541

[38] J. Vicente, M. T. Chicote, M. M. Alvarez-Falcon, P. G. Jones, *Organometallics*, 2005, **24**, 4666

[39] R. J. Cross, M. F. Davidson, *J. Chem. Soc., Dalton Trans.*, 1986, 411

[40] M. I. Bruce, E. Horn, J. G. Matisons, M. R. Snow, *Aust. J. Chem.*, 1984, **37**, 1163

[41] F. Sherbaum, A. Grohmann, B. Huber, C. Krüger, H. Schmidbaur, *Angew. Chem., Int. Ed.*, 1988, **27**, 1544

[42] D. Li, X. Hong, C. M. Che, W. C. Lo, S. M. Peng, *J. Chem. Soc., Dalton Trans.*, 1993, 2929

[43] V. W. W. Yam, C. K. Li, C. L. Chan, *Angew. Chem., Int. Ed.*, 1998, **37**, 2857

[44] R. J. Lancashire, *Comprehensive Coordination Chemistry*, 1987, **5**, Pergamon, Oxford, 861

[45] C. F. Wang, C.M. Chan, C.M. Che, *Polyhedron*, 1996, **15**, 1853

[46] V. W. W Yam, W. K. M. Fung, K. K. Cheung, *Organometallics*, 1997, **16**, 2032

[47] A. J. Hodge, S. L. Ingham, A. K. Kakkar, M. S Khan, J. Lewis, N. J. Long, D. G. Parker, P. R. Raithby, *J. Organomet. Chem.* 1995, **488**, 205

[48] M. Younus, N.J. Long, P.R. Raithby, J. Lewis, *J. Organomet. Chem.* 1998, **570**, 55

[49] O. Lavastre, J. Plass, P. Bachmann, P.H. Dixneuf, *Organometallics*, 1997, **16**, 184

[50] D. W. Bruce, D. O'Hare, *Inorganic Materials*, 2nd Edition, Wiley, 1997, 122

[51] G. L. Geoffroy, M. S. Wrighton, *Organometallic Photochemistry*, Academic Press, New York, 1979

[52] W. Tam, J. C. Calabrese, *Chem. Phys. Lett.* 1988, **144**, 79

[53] L. Plasseraud, L. Gonzalez Cuervo, D. Guillon, G. Suss-Fink, R. Deschenaux, D. W. Bruce, B. J. Donnio, *Mater. Chem.* 2002, **12**, 2653

[54] N. Chawdhury, M. Younus, P. R. Raithby, J. Lewis, R. H. Friend, *Opt. Mater.*, 1998, **9**, 498

[55] M. P. Cifuentes, M. G. Humphrey, *J. Organomet. Chem.*, 2004, **689**, 3968

[56] R. Virchow, *Virchows Arch*, 1854, **6**, 571

[57] G. W. Gray, K. J Harrison. J.A. Nash, *Electron Lett.* 1973, **9**, 130

[58] S. Takahashi, Y. Takai, H. Morimoto, K. Sonogashira, N. Hagihara, *Mol. Cryst. Liq. Cryst.* 1982, **82**, 139

[59] T. Kaharu, H. Matsubara, S. Takahashi, *J. Mater. Chem.*, 1992, **2**, 43

[60] L. Plasseraud, L. Gonzalez Cuervo, D. Guillon, G. Suss-Fink, R. Deschenaux, D. W. Bruce, B. J Donnio, *J. Mater. Chem.* 2002, **12**, 2653

[61] T. Kaharu, R. Ishii, T. Adachi, T. Yoshida, S. Takahashi, *J. Mater. Chem.*, 1995, **5**, 687

Compound Naming and Numbering

Chapter 2

1,4-*Bis*-trimethylsilylethynyl-benzene
(1)

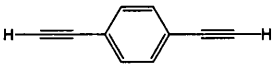

1,4-Diethynyl-benzene
(2)

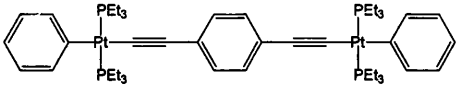

1,4-*Di*-(*trans*-(phenyl,*bis*-triethylphosphine)platinum) ethynyl-benzene
(3)

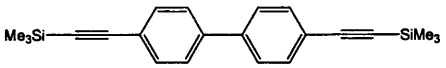

4,4'-*Bis*-trimethylsilylethynyl-biphenyl
(4)

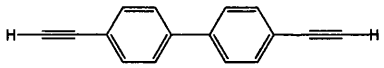

4,4'-Diethynyl-biphenyl
(5)

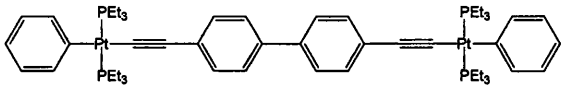

4,4'-*Di*-(*trans*-(phenyl,*bis*-triethylphosphine)platinum) ethynyl-biphenyl
(6)

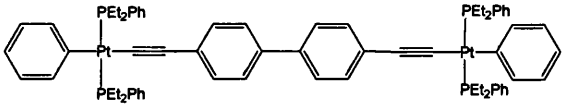

4,4"-*Di*-(*trans*-(phenyl,*bis*-(diethyl)(phenyl)phosphine)platinum) ethynyl-biphenyl
(7)

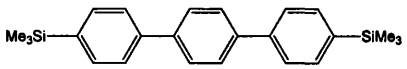

4,4"-*Bis*-trimethylsilyl-terphenyl
(8)

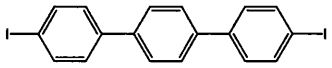

4,4"-Diiodo-terphenyl
(9)

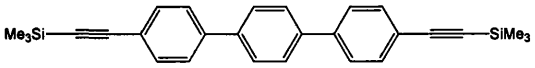

4,4"-*Bis*-trimethylsilylethynyl-terphenyl
(10)

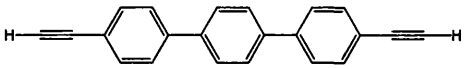

4,4"-Diethynyl-terphenyl
(11)

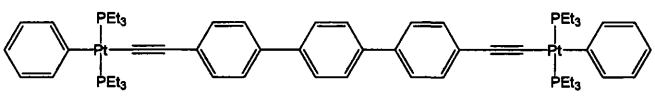

4,4"-*Di*-(*trans*-(phenyl,*bis*-triethylphosphine)platinum) ethynyl-terphenyl
(12)

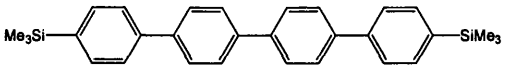

4,4'''-*Bis*-trimethylsilyl-quaterphenyl
(13)

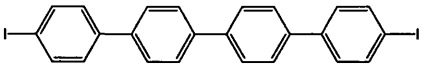

4,4'''-Diiodo-quaterphenyl
(14)

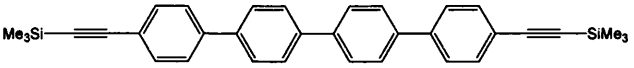

4,4'''-*Bis*-trimethylsilylethynyl-quaterphenyl
(15)

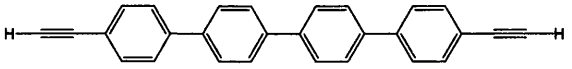

4,4'''-Diethynyl-quaterphenyl
(16)

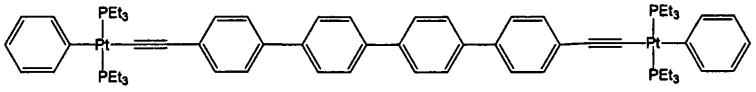

4,4'''-*Di*-(*trans*-(phenyl,*bis*-triethylphosphine)platinum) ethynyl-tetraphenyl
(17)

Chapter 3

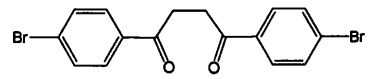

1,4-*Di*-(4-bromo-phenyl)-butane-1,4-dione
(18)

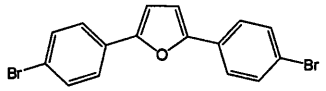

2,5-*Di*-(4-bromo-phenyl)-furan
(19)

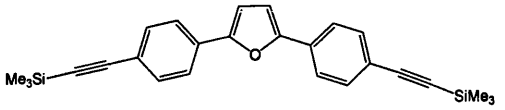

2,5-*Bis*-(4-trimethylsilylethynyl-phenyl)-furan
(20)

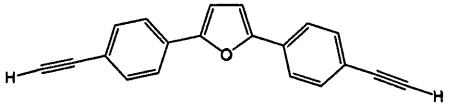

2,5-*Di*-(4-ethynyl-phenyl)-furan
(21)

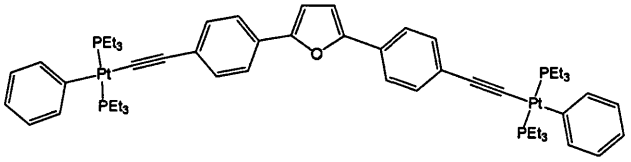

2,5-*Di*-(4-(*trans*-(phenyl,*bis*-triethylphosphine)platinum ethynyl))phenyl)-furan
(22)

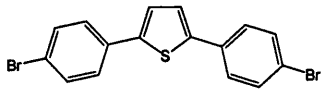

2,5-*Di*-(4-bromo-phenyl)-thiophene
(23)

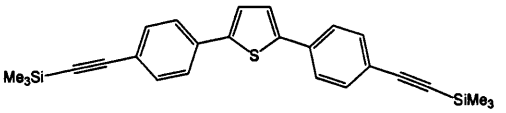

2,5-*Bis*-(4-trimethylsilylethynyl-phenyl)-thiophene
(24)

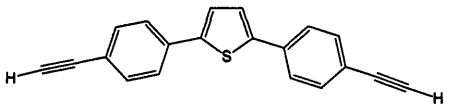

2,5-*Di*-(4-ethynyl-phenyl)-thiophene
(25)

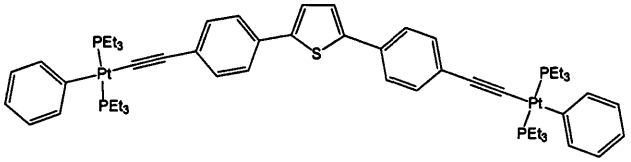

2,5-*Di*-(4-(*trans*-(phenyl,*bis*-triethylphosphine)platinum ethynyl)phenyl)-thiophene
(26)

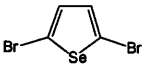

2,5-Dibromo-selenophene
(27)

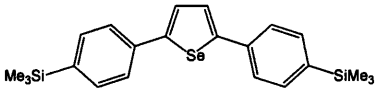

2,5-*Bis*-(4-trimethylsilyl-phenyl)-selenophene
(28)

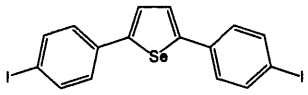

2,5-*Di*-(4-iodo-phenyl)-selenophene
(29)

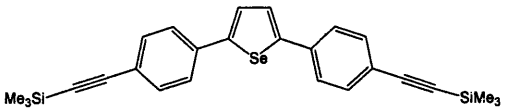

2,5-*Bis*-(4-trimethylsilylethynyl-phenyl)-selenophene
(30)

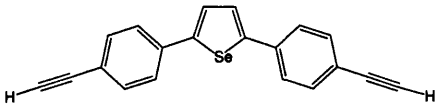

2,5-*Di*-(4-ethynyl-phenyl)-selenophene
(31)

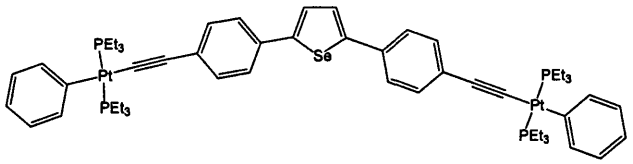

2,5-*Di*-(4-(*trans*-(phenyl,*bis*-triethylphosphine)platinum ethynyl)phenyl)-selenophene
(32)

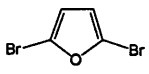

2,5-Dibromo-furan
(33)

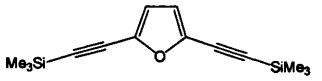

2,5-*Bis*-trimethylsilylethynyl-furan
(34)

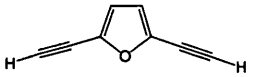

2,5-Diethynyl-furan
(35)

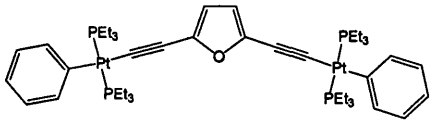

2,5-*Di*-(*trans*-(phenyl,*bis*-triethylphosphine)platinum ethynyl)-furan
(36)

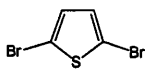

2,5-Dibromo-thiophene
(37)

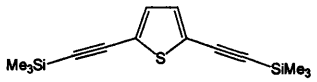

2,5-*Bis*-trimethylsilylethynyl-thiophene
(38)

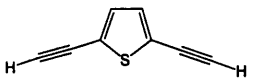

2,5-Diethynyl-thiophene
(39)

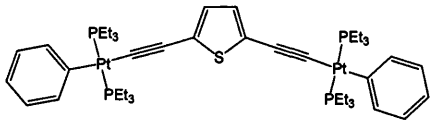

2,5-*Di*-(*trans*-(phenyl,*bis*-triethylphosphine)platinum ethynyl)-thiophene
(40)

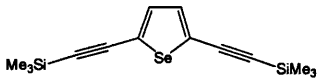

2,5-*Bis*-trimethylsilylethynyl-selenophene
(41)

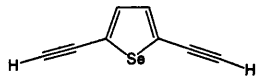

2,5-Diethynyl-selenophene
(42)

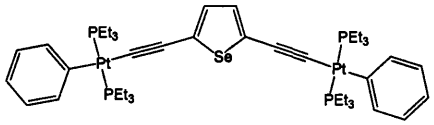

2,5-*Di*-(*trans*-(phenyl,*bis*-triethylphosphine)platinum ethynyl)-selenophene
(43)

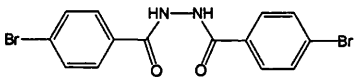

4-Bromo-benzoic acid *N'*-(4-bromo-benzoyl)-hydrazide
(44)

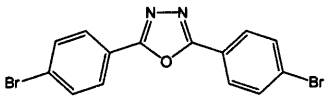

2,5-*Di*-(4-bromo-phenyl)-[1,3,4]oxadiazole
(45)

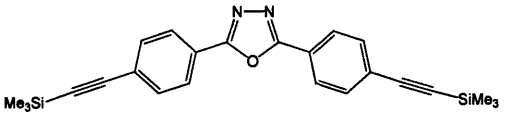

2,5-*Bis*-(4-trimethylsilylethynyl-phenyl)-[1,3,4]oxadiazole
(46)

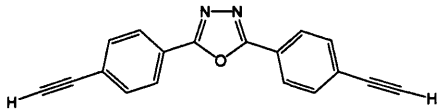

2,5-*Di*-(4-ethynyl-phenyl)-[1,3,4]oxadiazole
(47)

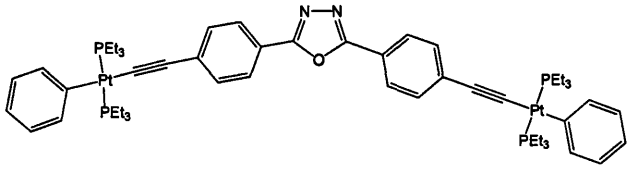

2,5-*Di*-(4-(*trans*-(phenyl,*bis*-triethylphosphine)platinum ethynyl))phenyl)-[1,3,4]oxadiazole
(48)

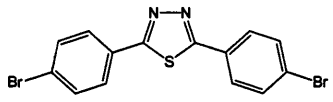

2,5-*Di*-(4-bromo-phenyl)-[1,3,4]thiadiazole
(49)

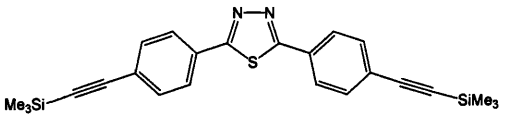

2,5-*Bis*-(4-trimethylsilylethynyl-phenyl)-[1,3,4]thiadiazole
(50)

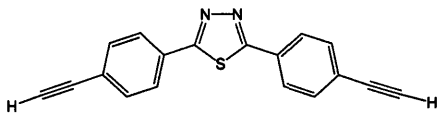

2,5-*Di*-(4-ethynyl-phenyl)-[1,3,4]thiadiazole
(51)

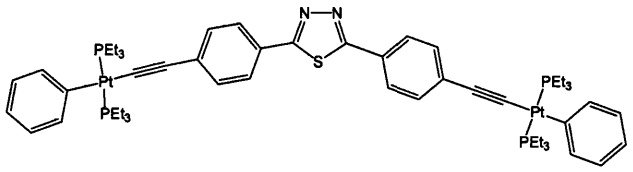

2,5-*Di*-(4-(*trans*-(phenyl,*bis*-triethylphosphine)platinum ethynyl))phenyl)-[1,3,4]thiadiazole
(52)

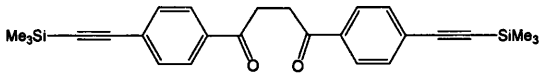

1,4-*Bis*-(4-trimethylsilylethynyl-phenyl)-butane-1,4-dione
(53)

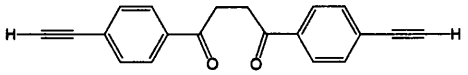

1,4-*Di*-(4-ethynyl-phenyl)-butane-1,4-dione
(54)

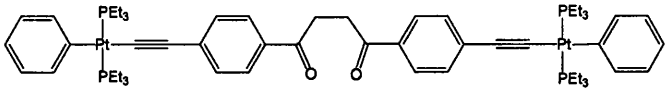

1,4-*Di*-(4-(*trans*-(phenyl,*bis*-triethylphosphine)platinum ethynyl))phenyl)-butane-1,4-dione
(55)

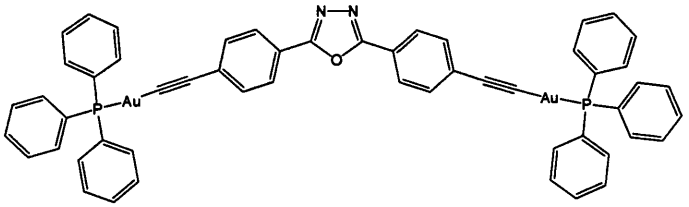

2,5-*Bis*-(4-((triphenylphosphine) gold ethynyl)phenyl)-[1,3,4]oxadiazole
(56)

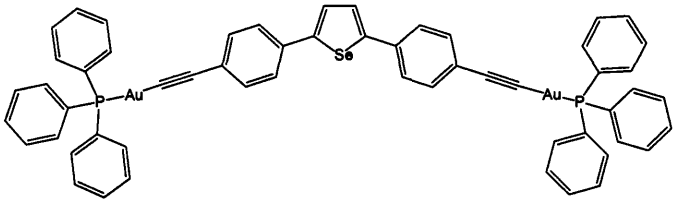

2,5-*Bis*-(4-((triphenylphosphine) gold ethynyl)phenyl)-selenophene
(57)

Chapter 4

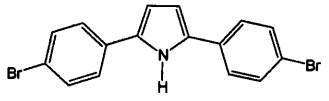

2,5-*Di*-(4-bromo-phenyl)-1*H*-pyrrole
(58)

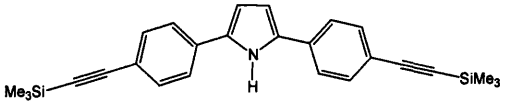

2,5-*Bis*-(4-trimethylsilylethynyl-phenyl)-1*H*-pyrrole
(59)

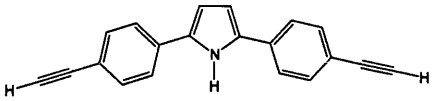

2,5-*Di*-(4-ethynyl-phenyl)-1*H*-pyrrole
(60)

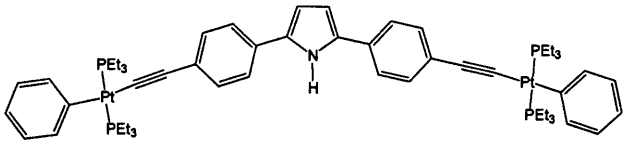

2,5-*Di*-(4-(*trans*-(phenyl,*bis*-triethylphosphine)platinum ethynyl)phenyl)-1*H*-pyrrole
(61)

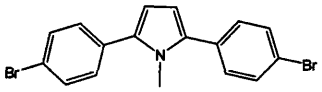

2,5-*Di*-(4-bromo-phenyl)-1-methyl-1*H*-pyrrole
(62)

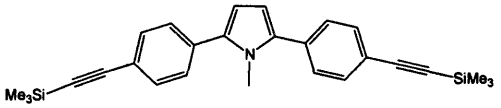

1-Methyl-2,5-*bis*-(4-trimethylsilylethynyl-phenyl)-1*H*-pyrrole
(63)

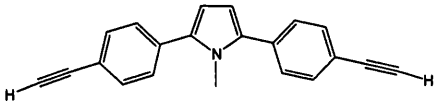

1-Methyl-2,5-*di*-(4-ethynyl-phenyl)-1*H*-pyrrole
(64)

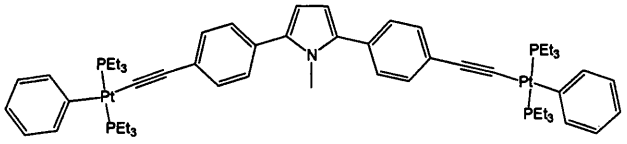

1-Methyl-2,5-*di*-(4-(*trans*-(phenyl,*bis*-triethylphosphine)platinum ethynyl)phenyl)-1*H*-pyrrole
(65)

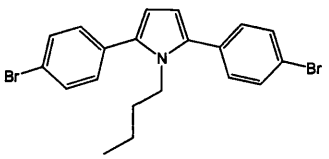

1-Butyl-2,5-*di*-(4-bromo-phenyl)-1*H*-pyrrole
(66)

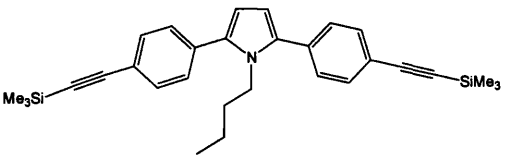

1-Butyl-2,5-*bis*-(4-trimethylsilylethynyl-phenyl)-1*H*-pyrrole
(67)

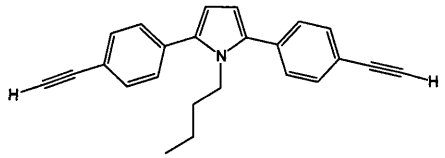

1-Butyl-2,5-*di*-(4-ethynyl-phenyl)-1*H*-pyrrole
(68)

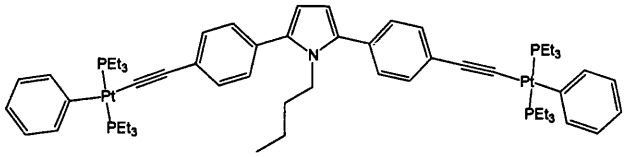

1-Butyl-2,5-*di*-(4-(*trans*-(phenyl,*bis*-triethylphosphine)platinum ethynyl))phenyl)-1*H*-pyrrole
(69)

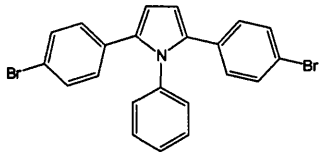

1-Phenyl-2,5-*di*-(4-bromo-phenyl)-1*H*-pyrrole
(70)

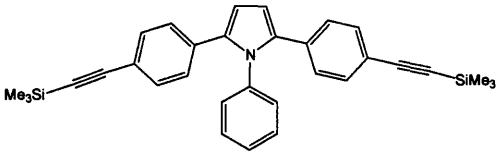

1-Phenyl-2,5-*bis*-(4-trimethylsilylethynyl-phenyl)-1*H*-pyrrole
(71)

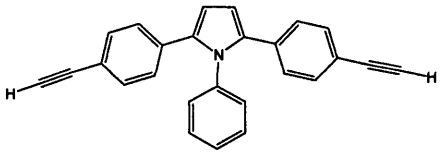

1-Phenyl-2,5-*di*-(4-ethynyl-phenyl)-1*H*-pyrrole
(72)

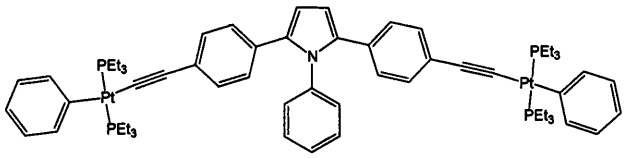

1-Phenyl-2,5-*di*-(4-(*trans*-(phenyl,*bis*-triethylphosphine)platinum ethynyl)phenyl)-1*H*-pyrrole
(73)

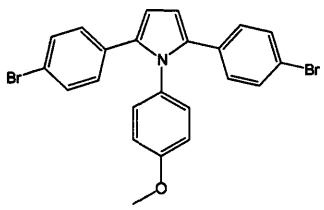

1-(4-methoxy-phenyl)-
2,5-*di*-(4-bromo-phenyl)-1*H*-pyrrole
(74)

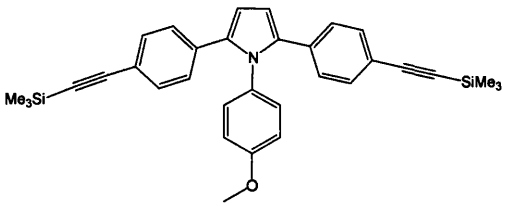

1-(4-Methoxy-phenyl)-2,5-*bis*-(4-trimethylsilylethynyl-phenyl)-1*H*-pyrrole
(75)

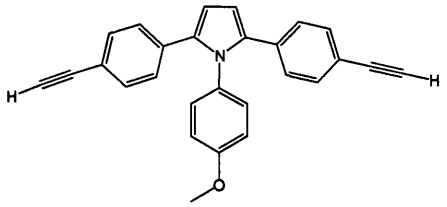

1-(4-methoxy-phenyl)-2,5-*di*-(4-ethynyl-phenyl)-1*H*-pyrrole
(76)

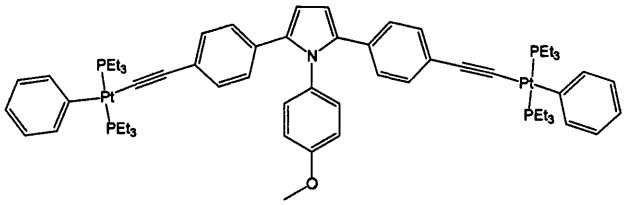

1-(4-methoxy-phenyl)-2,5-*di*-(4-(*trans*-(phenyl, *bis*-triethylphosphine)platinum ethynyl)phenyl)-1*H*-pyrrole
(77)

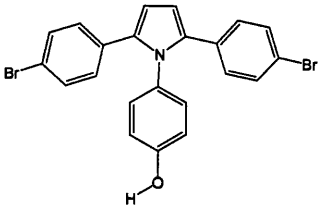

4-[2,5-di-(4-bromo-phenyl)-pyrrol-1-yl]-phenol
(78)

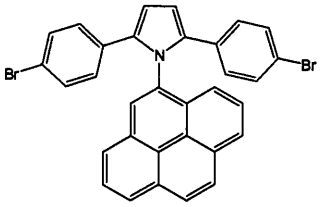

1-pyrenyl-2,5-*di*-(4-bromo-phenyl)-1*H*-pyrrole
(79)

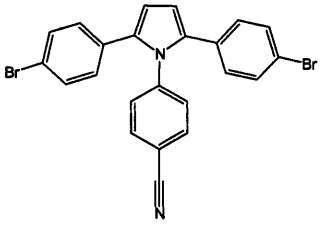

4-[2,5-*Di*-(4-bromo-phenyl)-pyrrol-1-yl]-benzonitrile
(80)

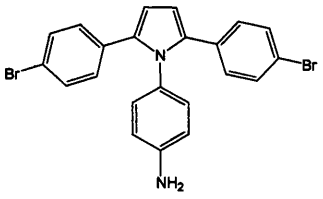

4-[2,5-*Di*-(4-bromo-phenyl)-pyrrol-1-yl]-phenylamine
(81)

Chapter 5

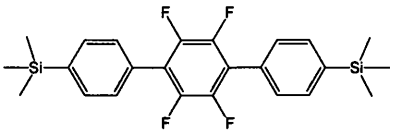

2',3',5',6'-Tetrafluoro-4,4"-*bis*-trimethylsilyl-terphenyl
(82)

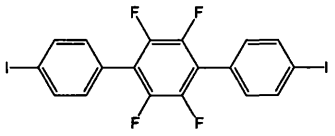

2',3',5',6'-Tetrafluoro-4,4"-diiodo-terphenyl
(83)

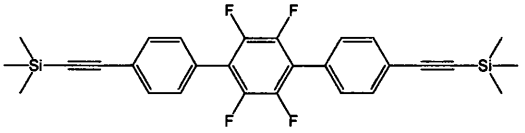

2',3',5',6'-Tetrafluoro-4,4"-*bis*-trimethylsilylethynyl-terphenyl
(84)

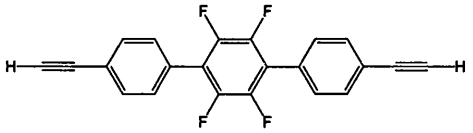

2',3',5',6'-tetrafluoro-4,4"-diethynyl-terphenyl
(85)

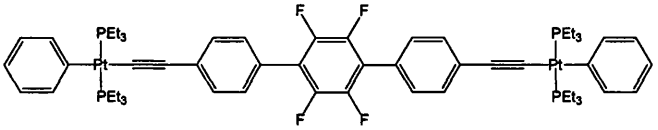

2',3',5',6'-tetrafluoro-4,4"-*Di*-((*trans*-(phenyl,*bis*-triethylphosphine)platinum) ethynyl)-terphenyl
(86)

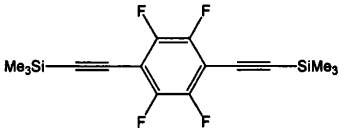

1,2,4,5-Tetrafluoro-3,6-*bis*-trimethylsilylethynyl-benzene
(87)

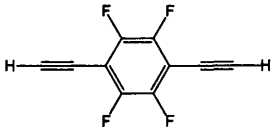

1,4-Diethynyl-2,3,5,6-tetrafluoro-benzene
(88)

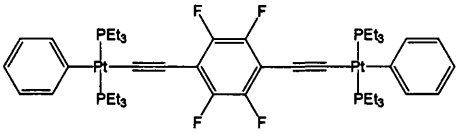

1,4-*Di*-((*trans*-(phenyl,*bis*-triethylphosphine)platinum) ethynyl) 2,3,5,6-tetrafluoro-benzene
(89)

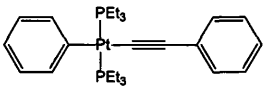

(trans-(phenyl,*bis*-triethylphosphine)platinum)) ethynyl-benzene
(90)

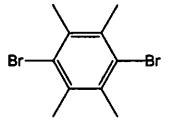

1,4-Dibromo-2,3,5,6-tetramethyl-benzene
(91)

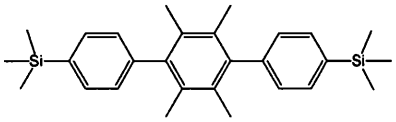

2',3',5',6'-Tetramethyl-4,4"-*bis*-trimethylsilyl-terphenyl
(92)

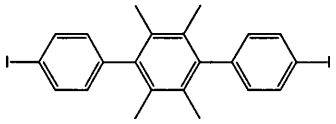

2',3',5',6'-Tetramethyl-4,4"-diiodo-terphenyl
(93)

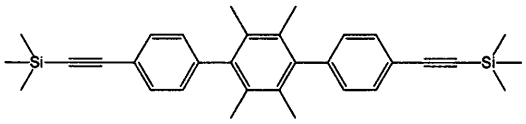

2',3',5',6'-Tetramethyl-4,4"-*bis*-trimethylsilylethynyl-terphenyl
(94)

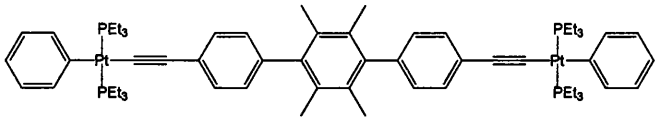

2',3',5',6'-tetramethyl-4,4"-*Di*-((*trans*-(phenyl,*bis*-triethylphosphine)platinum)ethynyl)-terphenyl
(95)

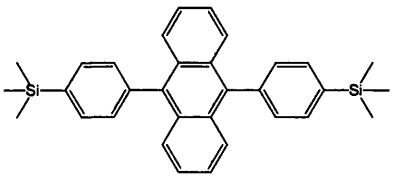

9,10-*Bis*-(4-trimethylsilyl-phenyl)-anthracene
(96)

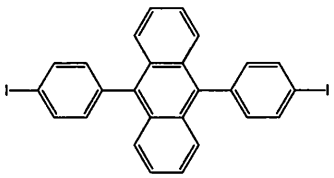

9,10-*Di*-(4-iodo-phenyl)-anthracene
(97)

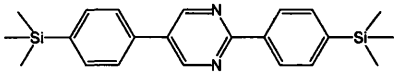

2,5-*Bis*-(4-trimethylsilyl-phenyl)-pyrimidine
(98)

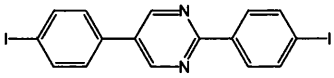

2,5-*Di*-(4-iodo-phenyl)-pyrimidine
(99)

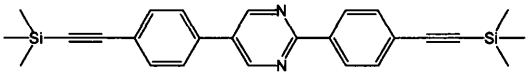

2,5-*Bis*-(4-trimethylsilylethynyl-phenyl)-pyrimidine
(100)

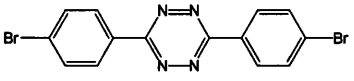

3,6-*Di*-(4-bromo-phenyl)-[1,2,4,5]tetrazine
(101)

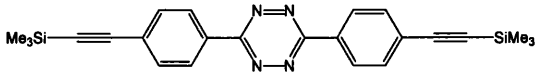

3,6-*Bis*-(4-trimethylsilylethynyl-phenyl)-[1,2,4,5]tetrazine
(102)

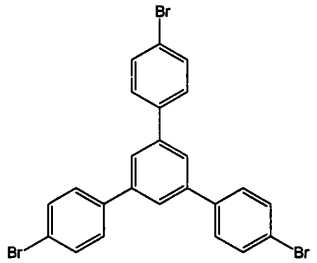

1,3,5-*Tri*-(4-bromo-phenyl)-benzene
(103)

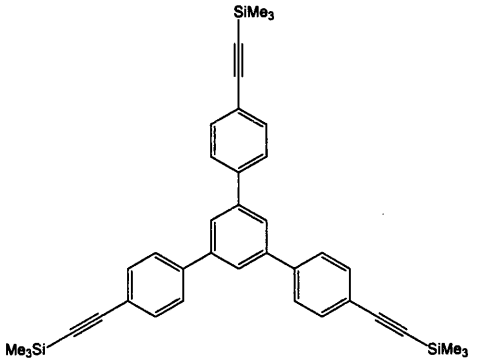

1,3,5-*Tris*-(4-trimethylsilylethynyl-phenyl)-benzene
(104)

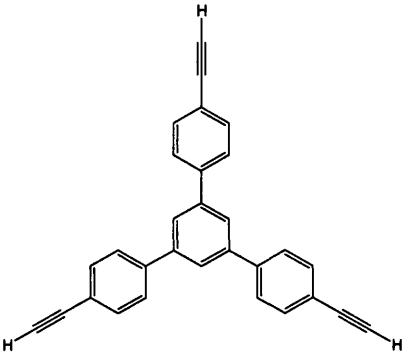

1,3,5-Tri-(4-ethynyl-phenyl)-benzene
(105)

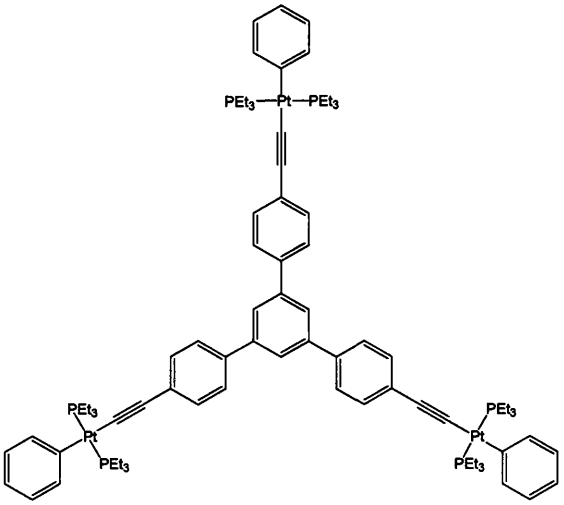

1,3,5-Tri-(4-(*trans*-(phenyl,*bis*-triethylphosphine)platinum ethynyl)phenyl)-benzene
(106)

Chapter 2

Oligophenylene Systems

2. Oligophenylene Systems

2.1 Introduction

2.1.1 Background

An electronically conjugated system is a series of atoms covalently bonded with alternating single and multiple bonds in a molecule. This system allows for the delocalisation of electron density, which increases stability and thereby lowers the overall energy of the molecule. Conjugated systems often have unusual properties, such as β-carotene's extended conjugated hydrocarbon chain resulting in its strong orange colour, see Figure 2.1.[1]

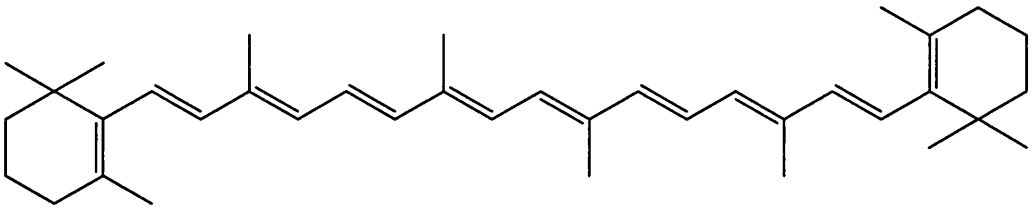

Figure 2.1 Structure of beta-carotene with ten conjugated double bonds.

The colour is determined by the "length" of the conjugated system, since the electron can travel the whole length of the chain. A simple way to visualise this is by thinking of the molecule as a real-world example of the "particle-in-a-box" solution to the Schrödinger equation. Where $E=hf \sim 1/L^2$, so the frequency, and thus colour, of emitted light is proportional to $1/L^2$.

In Chapter 1 conjugated organic compounds were discussed and their use in organic light emitting diodes (OLEDs) was highlighted. One particular conjugated system with linked arene rings, poly(*p*-phenylene) (PPP) (Figure 2.2a), has attracted considerable interest over the last decade since it acts as an excellent organic conductor upon doping. Doping with I_2 or AsF_5 raises its conductivity from 10^{-12} S cm^{-1}, in its neutral form into the metallic region with values around 500 S cm^{-1}.[2] Polymers with PPP in the backbone have been used as the active component in blue light-emitting diodes,[3] and this area of research has become widely investigated as highlighted in a number of review articles.[4,5]

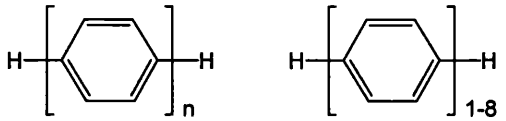

PPP OPP

Figure 2.2 (a) Poly(*p*-phenylene) (PPP) and (b) oligo-(*p*-phenylene)s (OPP).

PPP is a highly insoluble polymer, and thus is difficult to characterise and study. Oligo-(*p*-phenylene)s (OPP) have been extensively studied and reported in the literature for their spectroscopic behaviour.[2] The solubility of the polymers rapidly decreases with increasing chain length but the addition of substituents along the conjugated backbone greatly improves this.

The development of refined models to accurately predict absorption and emission spectra of well-defined oligo(phenylene) systems is ongoing.[6] Determining the maximum effective conjugation length requires the synthesis of regioregular PPPs of defined length. The electronic absorption band in the visible region is increasingly red-shifted as the conjugation length increases, and the maximum effective conjugation length is calculated as the saturation point of the red-shift. Early studies by Hoeve *et al* estimated that the effective conjugation extended over 11 phenylene units,[7] while later studies increased this estimate to 20 units.[8]

More recently, Otsubo *et al* synthesised 48-, 72-[9] and 96-*mer*[10] oligothiophenes, and found that the red-shift, while small (a difference of 0.1 nm between the 72- and the 96-mer), does not saturate, meaning that the effective conjugation length may be even longer than 96 units.

2.1.2 Objectives

The aim of this section of research was to study the effect of increasing the conjugation length of the π- system spacer bridging the two platinum centres of the model compound shown in Figure 2.3, and to study the effect of the any inherent twist angles between adjacent arene rings, by introducing a series of oligo-*p*-phenylene spacers. As discussed in Chapter 1, much of the published work has focused on the effects of changing the conjugated spacer group, X. The first compound of this class to be reported was the 1,4-diethynyl benzene derivative, where X is *para*-C_6H_4.[11]

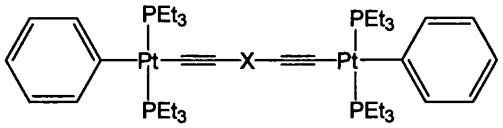

Figure 2.3 Model compound under investigation, where X is an aromatic spacer group.

Since publication of this compound, no studies have focused on systematically extending the number of π bonds bridging the two platinum centres. It was proposed to base this study on this archetypal compound and design analogues based upon it to extend the conjugation length of the chromophore. By doing this it was hoped to investigate the concept of conjugation within the model compound shown in Figure 2.3.

2.2 Results and Discussion

2.2.1 Synthetic Strategy

The general synthetic strategy towards the oligo-*p*-phenylene systems is shown in Figure 2.4.

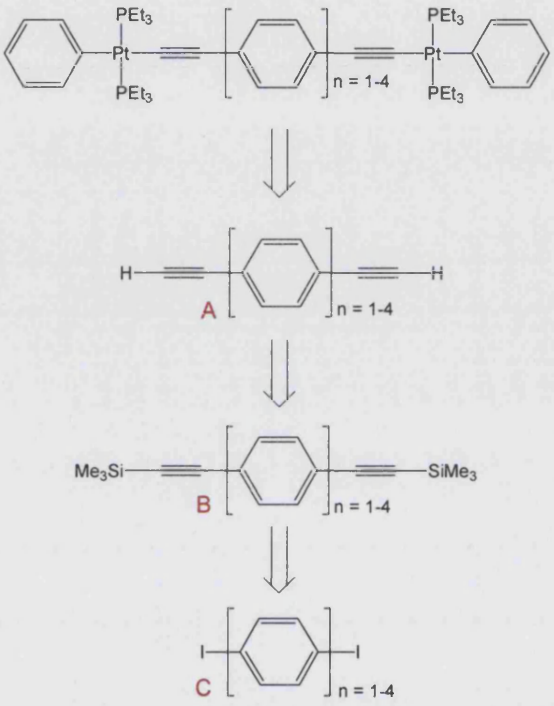

Figure 2.4 General synthetic scheme for linear polyphenyl systems.

The synthetic route to the desired complexes can be broken down to into three retrosynthetic steps. The three synthons making up the series are the terminal diethynyl species **(A)**, the *bis*-trimethylsilylethynyl species **(B)**, and the di-iodo species **(C)**.

2.2.2 Ligand Synthesis

The 1,4-diiodobenzene and 4,4'-diiodo-biphenyl required in the synthetic strategy as outlined in Figure 2.5, were commercially available. The 4,4''-diiodo-terphenyl and 4,4'''-diiodo-quaterphenyl were not commercially available, therefore, the scheme outlined in Figure 2.5 was devised for their synthesis.

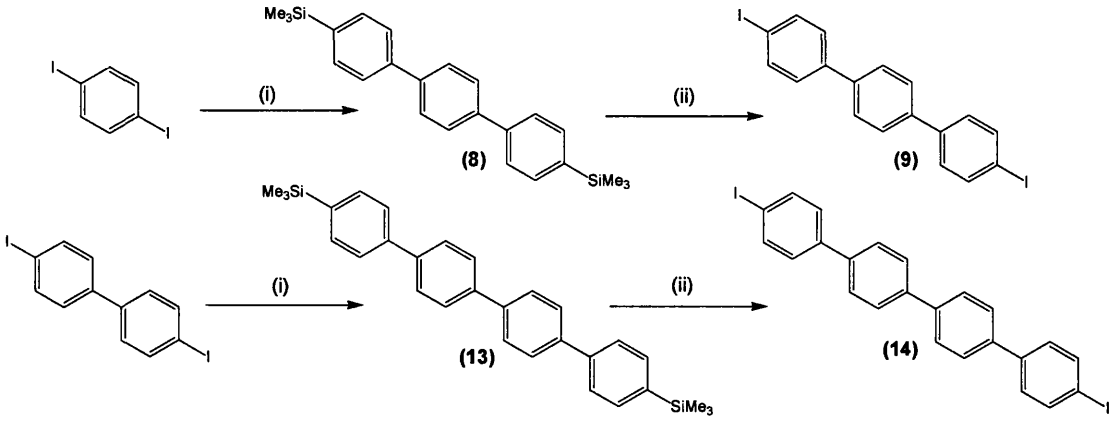

Figure 2.5 Synthesis of 4,4''-diiodo-terphenyl and 4,4'''-diiodo-quaterphenyl. (i) *p*-$Me_3Si(C_6H_4)B(OH)_2$, $Pd(PPh_3)_4$, $NaHCO_{3(aq)}$, toluene, Δ (ii) ICl, $CHCl_3$.

4,4''-*Bis*-(trimethylsilyl)-terphenyl **(8)** was synthesised by a Suzuki coupling[12] *via* the reaction of 4-trimethylsilyl phenylboronic acid with 1,4-diiodobenzene in the presence of tetrakis(triphenylphosphine)palladium(0) catalyst and aqueous sodium hydrogen carbonate. The reaction was carried out under reflux in toluene and after 48 h the reaction was complete, as confirmed by TLC. The crude product was purified using standard aqueous extraction techniques to yield an analytically pure product in a yield of 68%. 4,4'''-*Bis*-(trimethylsilyl)-quaterphenyl **(13)** was prepared under the same conditions using 4-trimethylsilyl phenylboronic acid and 4,4'-diiodo-biphenyl as the starting materials. On completion of the reaction the solution was evaporated to low volume which precipitated the product from solution. The solid was collected by filtration and recrystallised from chloroform to yield the pure product, in a yield of 59%. Both **(8)** and **(13)** were fully characterised by ^1H and ^{13}C NMR and IR spectroscopies and elemental analyses were found to be in agreement with the calculated values.

Removal of the trimethylsilyl groups of 4,4''-*bis*-(trimethylsilyl)-terphenyl **(8)** was achieved by the addition of iodine monochloride in chloroform. After a short period of time the product was formed as a precipitate. The product was collected by

filtration and washed with cold chloroform to remove impurities. The product, 4,4''-diiodo-terphenyl **(9)**, was obtained with a yield of 62% and was characterised by mass spectrometry, elemental analysis and NMR spectroscopy. The most indicative feature of the spectroscopic data for this compound was the absence of the single peak in the ^{1}H NMR spectrum at 0.32 ppm. Synthesis of 4,4'''-diiodo-quaterphenyl **(14)** was obtained in a similar manner, to yield the analytically pure product in 48% yield. No NMR spectroscopic analyses were carried out on this product due to its insolubility in all common organic solvents. Characterisation was achieved by mass spectrometry and elemental analysis.

Syntheses of the trimethylsilyl protected diynes were achieved by employing the Sonogashira Coupling reaction.[13] Reaction of the corresponding aryl diiodide with trimethylsilyl acetylene *via* catalytic (CuI and $Pd(PPh_3)_2Cl_2$ catalyst) cross-coupling lead to the formation of the desired products. The synthetic scheme for this set of reactions is shown in Figure 2.6.

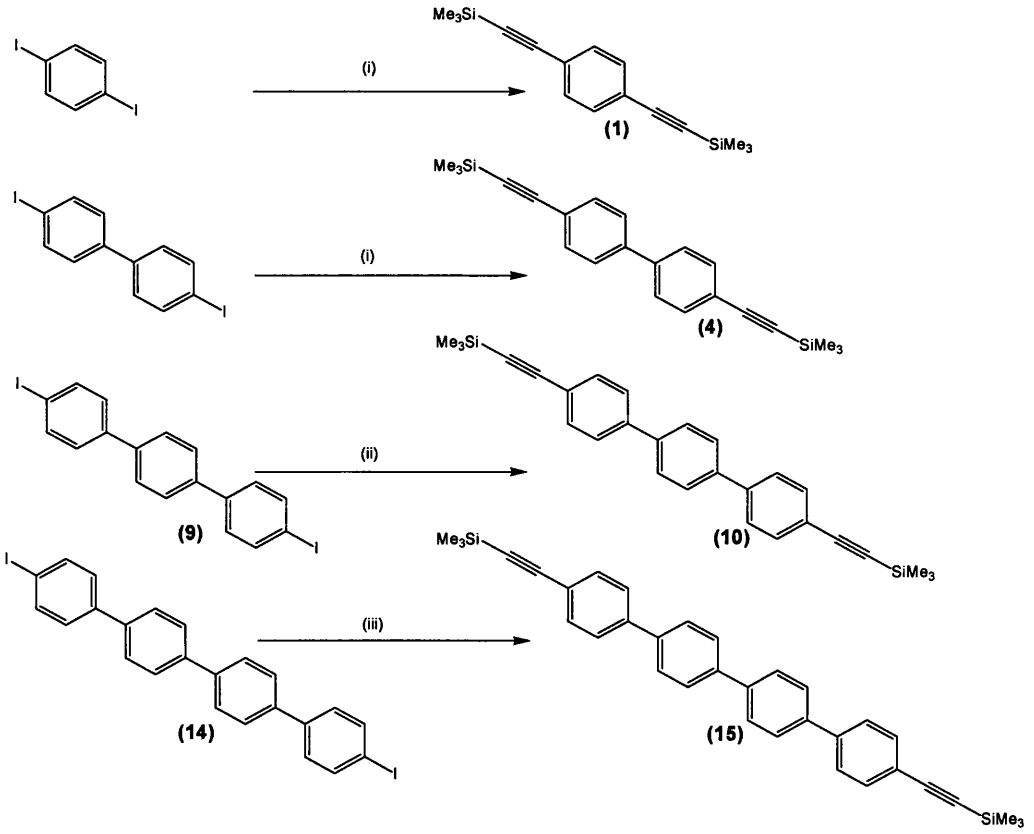

Figure 2.6 Synthesis of trimethylsilyl protected diyne ligands.

(i) Me_3SiCCH, $Pd(PPh_3)_2Cl$, CuI, $^iPr_2NH$, CH_2Cl_2 (ii) Me_3SiCCH, $Pd(PPh_3)_2Cl_2$, CuI, $^iPr_2NH$, THF (iii) Me_3SiCCH, $Pd(PPh_3)_2Cl_2$, CuI, $^iPr_2NH$, DMF, Δ.

Sonogashira coupling reactions of the four aryl diiodides varied only in the solvent used in the reaction. The solvent was chosen to aid the solubility of the starting material, hence for 1,4-diiodobenzene and 4,4'-diiodo-biphenyl, dichloromethane was employed, for 4,4''-diiodo-terphenyl tetrahydrofuran was used, and for 4,4'''-diiodo-quaterphenyl, hot dimethylformamide was required to solublise the starting material. ^{1}H NMR spectroscopy provided evidence of the formation of the *bis*-trimethylsilyethynyl products (**(1)**, **(4)**, **(10)** and **(15)**). The aromatic proton resonances of the C_6H_4 units gave simple resonances due to the symmetry of the compounds. A singlet resonance was also present at around 0 ppm in each case with an integral corresponding to 18 protons of the trimethylsilyl groups. IR spectroscopic data supported the NMR spectroscopy showing characteristic ν(C≡C) stretches with a range of 2100-2130 cm^{-1} for all four diynes. Bands at 1250 cm^{-1} were also observed corresponding to the Si-C stretches. The spectroscopic data for all new compounds was found to be similar to that in previously reported compounds.[14]

2.2.3 Complex Synthesis

The synthesis of the desired platinum complexes of the polyaryl diynes firstly required the deprotection of the ligand to yield the terminal alkyne ready to be attached to the metal, shown in Figure 2.7.

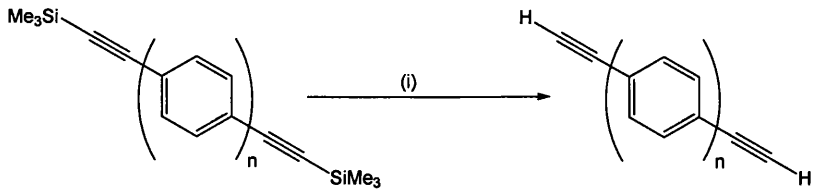

Figure 2.7 Synthesis of terminal diyne ligands.
(i) KOH(aq), MeOH/CH_2Cl_2 (1:1 v/v), n = 1-4.

These reactions were carried out in the presence of potassium hydroxide in a mixture of dichloromethane and methanol. The reaction of potassium hydroxide with methanol produces the methoxide anion, which acts as a nucleophile and attacks the silicon centre. It is the strong silicon-oxygen bond in the by-product (methoxy-trimethylsilane) which drives the reaction to completion.[15] The volatile by-product is removed on drying and the terminal alkyne is extracted *via* a water/dichloromethane mixture to give the terminal alkynes in high yields. Synthesis of 1,4-diethynyl benzene **(2)** required particular care due to the volatility of the compound. Work up of this compound was handled in an ice-bath whenever possible. 4,4'-diethynyl

biphenyl **(5)** and 4,4"-diethynyl terphenyl **(11)** were both synthesised under the same conditions to give analytically pure products in yields of 89 and 72%, respectively.

All terminal alkynes in this Chapter were characterised by NMR and IR spectroscopy, and displayed a characteristic ^{1}H NMR spectra resonance at *ca* 3 ppm corresponding to the proton on the alkyne. The absence of the Si-C stretch in the IR spectra at around 1250 cm^{-1} was also noted. Due to the instability of the terminal alkynes, deprotection reactions were only carried out on small quantities to yield merely sufficient ligand required for the next step. Yields for the synthesis of terminal alkynes, **(2)**, **(5)** and **(11)**, were all > 70%.

The final steps of the reaction scheme for the synthesis of the four platinum complexes **(3)**, **(6)**, **(8)** and **(17)** involved dehydrohalogenation, this process was achieved by reacting the terminal alkyne ligands with the platinum starting material *trans*-Pt(Ph)(PEt$_3$)$_2$Cl. The platinum precursor was synthesised by adapted literature methods *via* the synthesis of *cis*-Pt(PEt$_3$)$_2$Cl$_2$ from PtCl$_2$,[16] followed by the phenylation of this product to give *trans*-Pt(Ph)(PEt$_3$)$_2$Cl.[17] This scheme is shown in Figure 2.8.

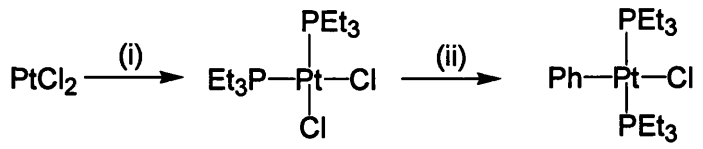

Figure 2.8 Synthesis of the platinum starting material *trans*-Pt(Ph)(PEt$_3$)$_2$Cl. (i) Me$_2$S, CH$_2$Cl$_2$, PEt$_3$, (ii) AgSO$_3$CF$_4$, MeOH, NaBPh$_4$, CH$_2$Cl$_2$, LiCl.

Platinum dichloride was suspended in dichloromethane and dimethylsulphide was added, the reaction was stirred at room temperature, for 1h. Triethyl phosphine was then added to the mixture which was left to stir for a further 2h. The reaction mixture was then evaporated to low volume and the product was triturated using pentane. Recrystallisation from ethanol afforded the pure *cis-bis*-triethylphosphine platinum dichloride with a yield of 85%. The second reaction in this scheme was the substitution of one of the chlorides with a phenyl group, which would act as a capping unit once the ligand was attached, preventing further ligand substitution leading to polymer formation. *Cis-bis*-triethylphosphine platinum dichloride was dissolved in methanol, and two molar equivalents of silver triflate were added, in order to abstract

the chloride ligands. The silver chloride was removed by filtration. Phenylation of the complex was achieved by the addition of one molar equivalent of sodium tetraphenylborate. Lithium chloride was added to re-insert a single chloride onto the final complex. The product was collected *via* a dichloromethane/water liquid extraction. The organic phase was evaporated to dryness to yield the crude product which was recrystallised from methanol in a yield of 68%.

The syntheses of the desired platinum complexes **(3)**, **(6)** and **(12)** were achieved by the dehydrohalogenation reaction shown in Figure 2.9. The reactions were carried out in dichloromethane and diisopropylamine, with a catalytic amount of copper iodide. The amine acts as a base in the reaction, deprotonating the alkyne, which then coordinates to the copper forming a more reactive species [18] which is able to transmetalate with $Pt(Ph)(PEt_3)_2Cl$ – forming the desired product.

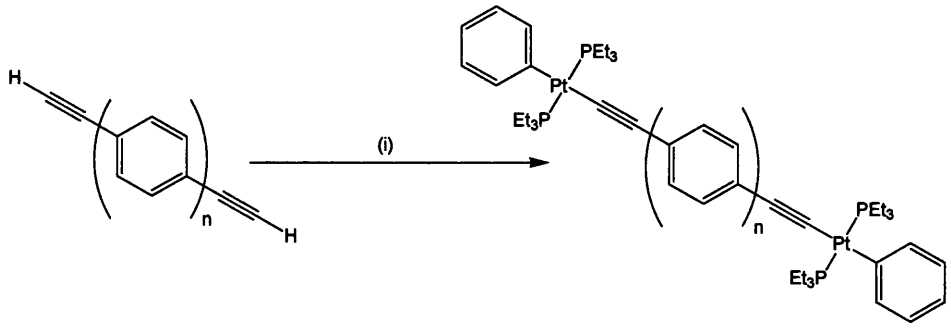

Figure 2.9 Dehydrohalogenation reaction for the synthesis of (3), (6) and (12).
(i) *trans*-$Pt(Ph)(PEt_3)_2Cl$, CuI, $^iPr_2NH$, CH_2Cl_2.

Work up of the reactions comprised of the removal of the volatile components followed by the elution of the reaction mixture through a silica gel plug with ethyl acetate/hexane mixtures. This process removed the binary salts and copper catalyst residues. Further purification of the complexes was achieved by recrystallisation from ethanol. Yields of 62-75 % were achieved for the synthesis of these complexes. Synthesis of the tetraphenyl platinum complex **(17)** was attempted by a different route due to problems with the solubility and low yielding reactions for the corresponding ligand **(15)**. At the time this synthetic work was being conducted for this Chapter a new synthetic route was being developed by our Group towards the formation of platinum acetylide complexes. This involved the *in situ* deprotection and dehydrohalogenation in one step and is shown in Figure 2.10.

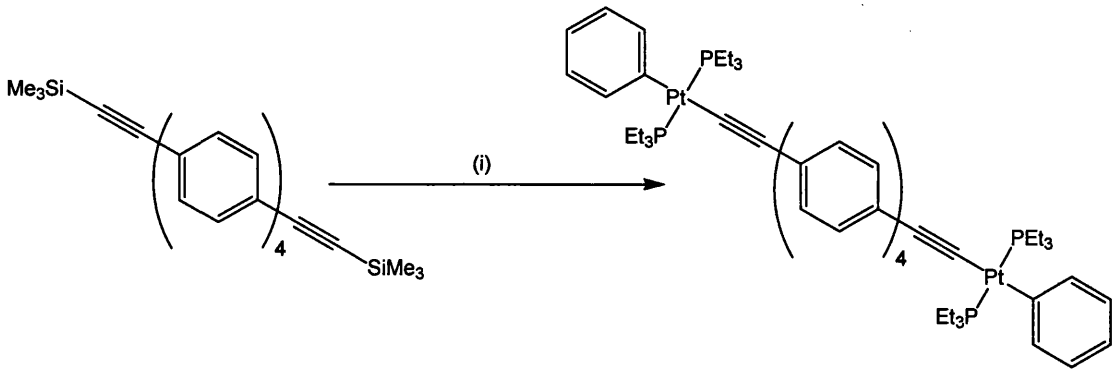

Figure 2.10 Synthesis of (17).
(i) *trans*-Pt(Ph)(PEt_3)$_2$Cl, CuI, $^iPr_2NH$, CH_2Cl_2, NaOMe, MeOH.

The trimethylsilyl protected ligand **(15)** was charged into a Schlenk tube along with the platinum starting material *trans*-Pt(Ph)(PEt_3)$_2$Cl, copper iodide catalyst and sodium methoxide. The solids were then dissolved in an equal mixture of methanol and dichloromethane. It was found from previous studies within the group that methanol was required as a proton source in the deprotection step. After a few minutes of stirring diisopropyl amine was added to the solution and the reaction was left to stir for 18 hours. TLC analysis of the reaction mixture showed no starting materials to be present therefore the reaction was worked up using the same procedure as for all the other platinum complexes in this Chapter.

The NMR spectroscopic data suggests the formation of the desired complex **(17)**. These results were supported by TLC experiments, revealing a single spot at a different R_f value to the starting materials.

During the synthetic work carried out for this Chapter, a second platinum complex was synthesised using the 4,4'-diethynylbiphenyl ligand. Complex **(7)** was made in the same manner as **(6)** but with a different platinum starting material, containing diethylphenyl phosphine ligands rather than the triethyl phosphines for all other complexes in this Chapter. This was designed to investigate role of the phosphines ligands in these systems, and their resultant effects on the electronic properties of the complexes.

2.3 Molecular Structures

In order to further characterise the new platinum di-ynes, and to gain useful information about the twist angles in the poly-*p*-phenylene spacer groups, crystal structure determinations were undertaken on all the systems for which suitable crystals could be obtained. The structure solutions of all the solid state structures presented in this Thesis were carried out by either Dr. Mary Mahon or Dr. Gabriele Kociok-Köhn. The molecular structure of **(6)** was determined by X-ray crystallography using single crystals grown from an ethanol solution and is shown in Figure 2.11. Selected bond lengths and angles are shown in Table 2.1, full crystallographic data is given in Appendix 1.

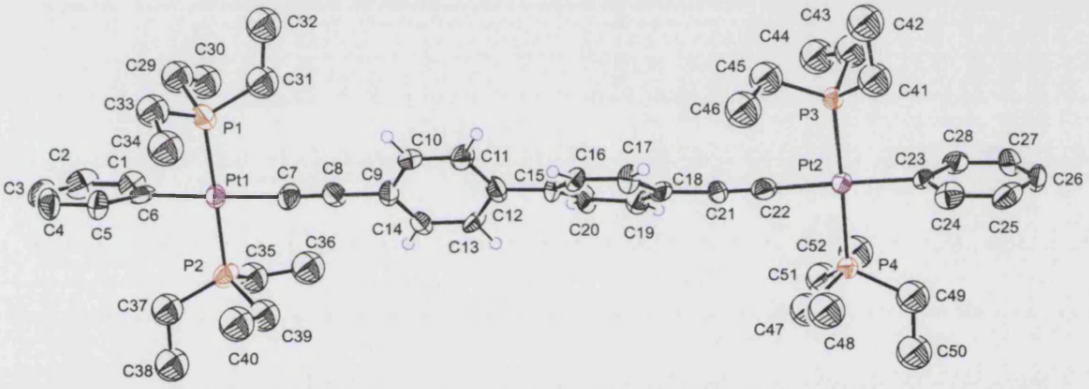

Figure 2.11 Molecular structure of (6) depicted with a 50% ellipsoid probability. Hydrogen atoms have been omitted for clarity, except for those on the biphenyl ligand shown in blue.

Bond Lengths (Å)		Bond Angles (°)	
Pt_1-C_7	2.010(17)	Pt_1-C_7-C_8	176.0(16)
Pt_2-C_{22}	2.014(18)	Pt_2-C_{22}-C_{21}	179.6(16)
Pt_1-C_6	2.070(17)	P_1-Pt_1-P_2	178.11(18)
Pt_2-C_{23}	2.066(15)	P_3-Pt_2-P_4	177.14(14)
Pt_1-P_1	2.267(5)	C_6-Pt_1-C_7	178.1(7)
C_{12}-C_{15}	1.47(2)	C_{22}-Pt_2-C_{23}	177.5(6)
C_7-C_8	1.22(2)	Dihedral C_9-C_{14} /C_{15}-C_{18}	31.1(5)
C_{21}-C_{22}	1.20(2)		

Table 2.1 Table of selected bond lengths and bond angles of the molecular structure of (6).

The Pt_1-C_7 and Pt_2-C_{22} bonds at 2.010(17) Å and 2.014(18) Å, respectively, are similar to the values in the range of di-platinum di-yne complexes characterised

previously in the Group (1.96(2)-2.09(3) Å). The Pt-P distances (av. 2.267 Å) lie in the expected range, 2.27(6)-2.32(8) Å, by comparison to other structurally characterised systems. The Pt-C_6 and Pt-C_{23} distances of 2.070(17) and 2.066(15) Å, fall in the previously determined range of 2.05(2)-2.09(3) Å.[14]

As expected, the alkynylic units are essentially linear, with Pt-C≡C and C≡C-C angles are close to the 180° angle (see Table 2.1). P-Pt-P angles are also close to the 180° angle confirming the square planar geometry at the platinum centre. The square plane of the Pt_1 makes a 24.3(5)° angle with the plane of the central phenyl ring (C_9-C_{14}) on one side of the molecule and an angle of 58.3(5)° between Pt_2 and (C_{15}-C_{20}). Angles of 80.8(5)° and 87.2(5)° are observed with the square plane platinum and the terminal phenyl ring at each end, respectively. The terminal and central arene rings then make angles of 57.6(5)° and 34.5(5)° with each other.

Figure 2.12 shows the molecular structure of **(6)** with the di-yne ligand in the space-filling format. The plot highlights the ortho-ortho proton interactions on the central rings, which force the rings to twist relative to each other with a dihedral angle of 31.1(5)°.

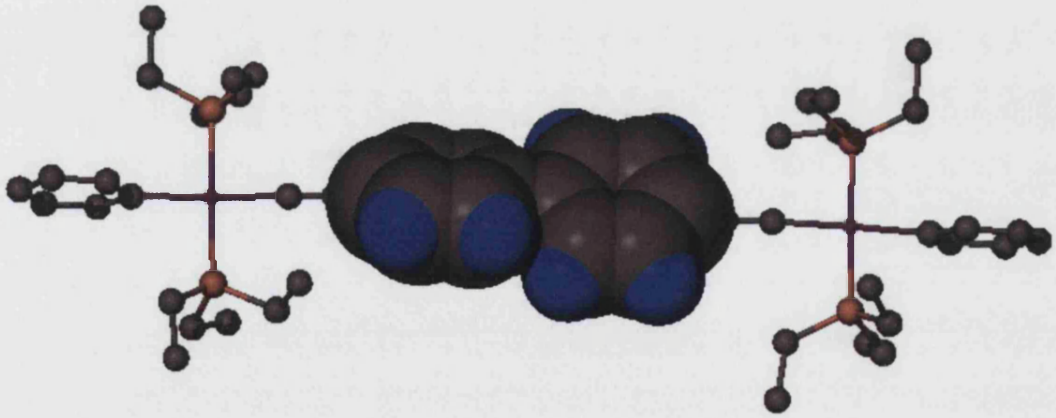

Figure 2.12 Molecular structure of (6) depicted in ball and stick form with the biphenyl group shown in space-fill format.

The molecular structure of **(7)** was confirmed by X-ray crystallography using single crystals grown from ethanol and is shown in Figure 2.13, with selected bond lengths and angles shown in Table 2.2, full crystallographic data given in Appendix 1.

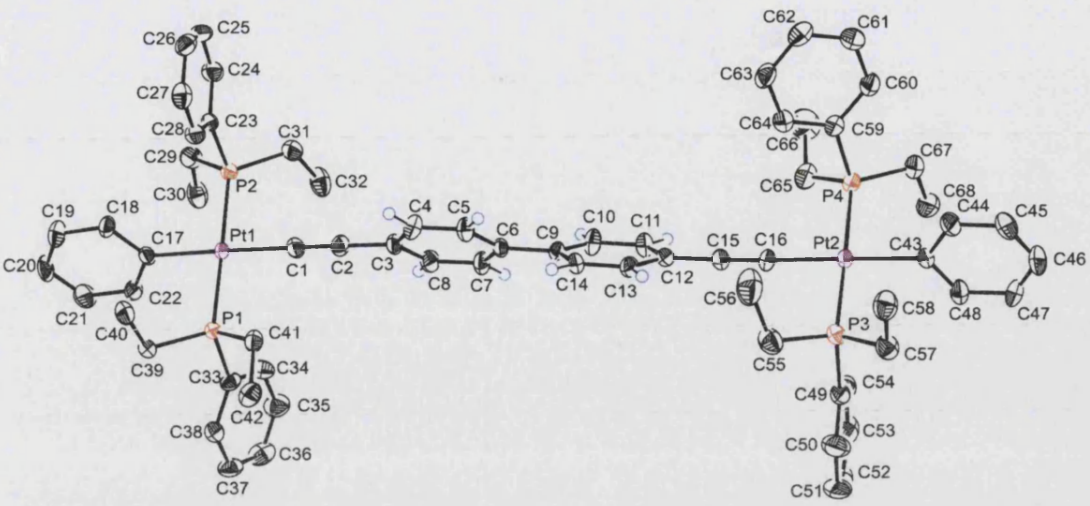

Figure 2.13 Molecular structure of (7) depicted with a 50% ellipsoid probability. Hydrogen atoms have been omitted for clarity, except for those on the biphenyl ligand shown in blue.

Bond Lengths (Å)		Bond Angles (°)	
Pt_1-C_1	2.023(5)	Pt_1-C_1-C_2	178.0(5)
Pt_2-C_{16}	2.020(4)	Pt_2-C_{16}-C_{15}	177.1(5)
Pt_1-C_{17}	2.076(4)	P_1-Pt_1-P_2	177.18(5)
Pt_2-C_{43}	2.064(4)	P_3-Pt_2-P_4	176.55(5)
Pt_1-P_1	2.3053(12)	C_{17}-Pt_1-C_1	178.30(19)
C_6-C_9	1.487(6)	C_{16}-Pt_2-C_{43}	178.83(19)
C_1-C_2	1.208(6)	Dihedral C_3-C_8 /C_9-C_{14}	31.3(5)
C_{15}-C_{16}	1.208(6)		

Table 2.2 Table of selected bond lengths and bond angles of the molecular structure of (7).

The structure of **(7)** is closely related to that of **(6)**. All bond lengths and bond angles are similar and may be considered to be essentially equivalent with the exception of the Pt-P bonds. The molecular structure of **(7)** exhibits slightly elongated Pt-P bond distances (2.3053(12) Å) compared to the structure of **(6)** (2.267(5) Å). This is due to the change in phosphine ligand on the platinum centre, with triethyl phosphine present in **(6)** and diethylphenyl phosphine in **(7)**. The phenyl group on the phosphine ligand set induces an electron withdrawing effect, pulling electron density away from the phosphorus thus weakening the Pt-P bond. The dihedral angle between the two central arene rings remains at 31.3(5)° as compared to 31.1(5)° that of **(6)**.

The molecular structure of **(12)** was determined by X-ray crystallography using a single crystal grown from ethanol and is shown in Figure 2.14, with selected bond lengths and angles shown in Table 2.3, full crystallographic data given in appendix 1.

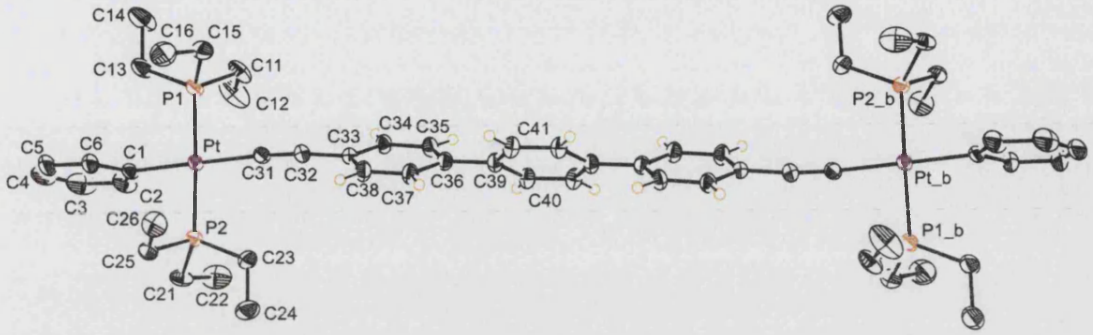

Figure 2.14 Molecular structure of (12) depicted with a 50% ellipsoid probability. Hydrogen atoms have been omitted for clarity except for hydrogens on the terphenyl ligand, shown as blue spheres.

Bond Lengths (Å)		Bond Angles (°)	
Pt-C_{31}	2.023(4)	Pt-C_{31}-C_{32}	175.5(4)
Pt-C_1	2.062(4)	C_{31}-C_{32}-C_{33}	174.6(4)
Pt-P_1	2.2921(11)	P_1-Pt-P_2	176.45(4)
Pt-P_2	2.2973(10)	C_1-Pt-C_{31}	176.84(16)
C_{31}-C_{32}	1.211(6)	Dihedral C_{33}-C_{38} /C_{39}-C_{41}	34.4(3)
C_{36}-C_{39}	1.486(6)		

Table 2.3 Table of selected bond lengths and bond angles of the molecular structure of (12)

The asymmetric unit consists of half a molecule of **(12)** with the remainder of the molecule generated by a centre of inversion present in the middle of the central arene ring. The symmetry transformations used to generate equivalent atoms are 1 -x+1,-y+2,-z+1 and are labelled as "atom"_b.

The molecular geometry of **(12)** is similar to that of **(6)**. The terminal phenyl ring (C_1-C_6) makes an angle of 83.6(3)° with the platinum-centred square plane, and the outer phenyl ring of the terphenyl (C_{33}-C_{38}) makes an angle of 21.9(3)° to the same platinum-centred square plane. Rings (C_{33}-C_{38}) and (C_{39}-C_{41}) are related by a dihedral angle of 34.4(3)°, this is highlighted in Figure 2.15.

Figure 2.15 Molecular structure of (12) depicted in ball and stick form with the central arene rings shown in space-fill format.

It has not been possible to obtain crystals of the platinum complex containing the tetra arene ring spacer.

The molecular structures of **(6)**, **(7)** and **(12)** have shown that the central arene rings in the spacer ligands are twisted relative to each other. This twist is due to the unfavourable ortho-ortho proton interactions, and is expected to have an effect on the photophysical properties of the system. The comparison of the molecular structures of **(6)** and **(7)** has shown that the change in phosphine ligand has no effect on the overall geometry of the system, other than the slight change in the Pt-P bond length.

2.4 UV-visible Spectroscopic Studies

The UV-visible spectra for all terminal alkyne ligands and their corresponding platinum complexes in this chapter were determined. All measurements were carried out in dichloromethane at 0.01 mM concentrations. Specific details of instrumentation and method of data collection is given in the general Experimental Section 6.1.

Figure 2.16 shows both the UV-visible absorption and emission spectra of 1,4-diethynylbenzene. The absorption spectrum exhibits intense absorption bands at 260 and 273 nm with extinction coefficients (ε) in the order of 10^4 $dm^{-3}mol^{-1}cm^{-1}$. These can be assigned to $\pi \rightarrow \pi^*$ transitions, corresponding to the movement of electrons from the highest occupied to the Lowest Unoccupied Molecular Orbitals (LUMO). The band at 273 nm is believed to correspond to a transition from the ground state of both the electronic and vibrational states of the molecule to the excited electronic state in its vibronic ground state (0→0). The second peak at 260 nm corresponds to a transition to the same electronic excited state but now a higher energy, excited vibrational state within it (0→1). The difference between these two energies corresponds to an energetic spacing of around 1830 cm^{-1}. It is worth noting that this vibrational spacing corresponds to vibrational data in the excited state. The energy corresponds to the IR section of the electromagnetic spectrum and more precisely lies in between the stretching frequency of a C≡C bond (*ca* 2100-2250 cm^{-1}) and a C=C bond (*ca* 1630-1680 cm^{-1}).

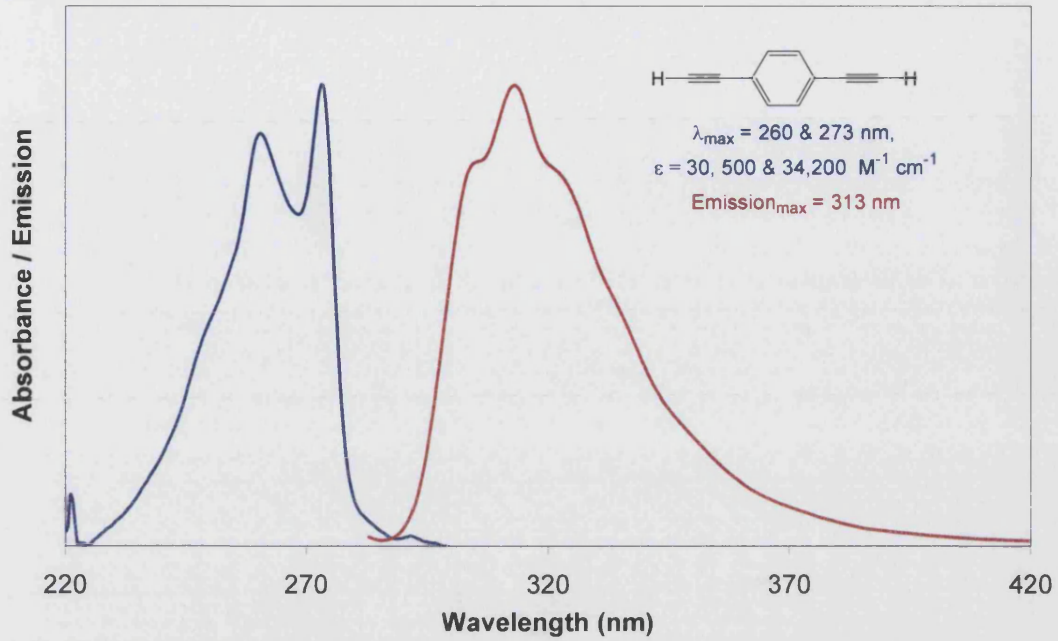

Figure 2.16 UV-visible spectra of 1,4-diethynylbenzene, absorption is shown in blue and emission in red.

The emission spectrum was collected after exciting the sample at 273 nm. The emission band exhibits a maxima at 313 nm with two shoulder peaks at 305 and 322 nm. The energetic spacing of these peaks is at 840 cm^{-1} and 860 cm^{-1}. This can be tentatively assigned to the out-of-plane C-H bending vibrations of the two adjacent protons on the arene ring (reference values[19] – 860-800 cm^{-1}). Excitation at the second wavelength of 260 nm gave the essentially identical spectrum as excitation at 273 nm but with a slight drop in intensity. This is consistent with a pure substance existing in solution in a unique form and supports the notion that the 260 nm peak is a vibrational peak of the 273 nm band.

The UV-visible absorption and emission spectra of the di-platinum complex **(3)** were measured and are shown in Figure 2.17. The absorbance spectrum consists of one main peak with a λ_{max} value of 349 nm and a side shoulder peak at 333 nm. These can be assigned to a $\pi \rightarrow \pi^*$ transition. The energy spacing of these peaks with a value of 1380 cm^{-1} can be assigned to the aromatic vibrational mode of the arene spacer ligand. There are also two further peaks present at 301 nm and 271 nm. The energy spacing of these peaks corresponds to a value of 3680 cm^{-1}.

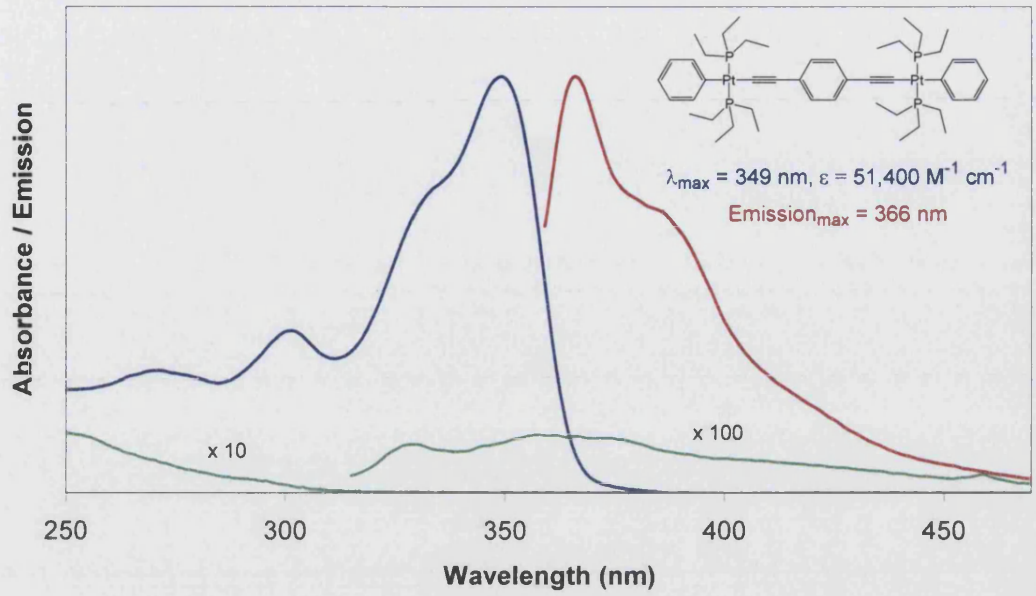

Figure 2.17 UV-visible spectra of $Ph(PEt_3)_2PtCC(C_6H_4)CCPt(PEt_3)_2Ph$ (3), absorption is shown in blue and emission in red. $PhPt(PEt_3)_2Cl$ is shown in green, measured at the same concentration.

The UV-visible spectra of the platinum starting material $PhPt(PEt_3)_2Cl$ is also shown in Figure 2.17. The absorption spectrum has been amplified ten fold and the emission spectrum by one hundred times. As the two sets of data were collected at the same concentration, the low intensity of the spectra for the platinum starting material suggests that none of peaks observed for **(3)** can be assigned as metal based.

A large shift is evident in the absorption λ_{max} from 273 nm for the free ligand to 349 nm for the corresponding di-platinum complex. This shift is due to the extension of the chromophore length, the 6d orbitals on the platinum centres are able to interact with the π orbitals of the alkyne ligand thus extending the conjugation length of the system.

The emission spectrum of complex **(3)** was collected after exciting the sample at 349 nm and is shown in red in Figure 2.17. The band exhibits a maximum at 366 nm with a shoulder peak at 386 nm, this corresponds to an energy spacing of ca. 1420 cm^{-1}.

Further spectral data was collected for the 4,4'-diethynylbiphenyl ligand as shown in Figure 2.17. The absorption spectrum of this ligand gave a much broader peak shape

than the monophenyl analogue in Figure 2.16. This can be attributed to the extra degrees of freedom in the biphenyl analogue giving rise to many more possible vibrational states. No vibronic structure was evident in the absorbance spectra of this ligand. The increase in λ_{max} values for the absorbance spectra of the mono-phenyl ligand to the biphenyl ligand, from 273 nm to 289 nm, is consistent with the drop in energy of the electronic transition due to the increase in conjugation length of the chromophore.

The emission spectrum, with some vibronic structure, exhibits two main bands at 326 and 340 nm and a shoulder peak at 355 nm. The progressional spacings corresponding to these peaks come at *ca* 1250 cm^{-1}.

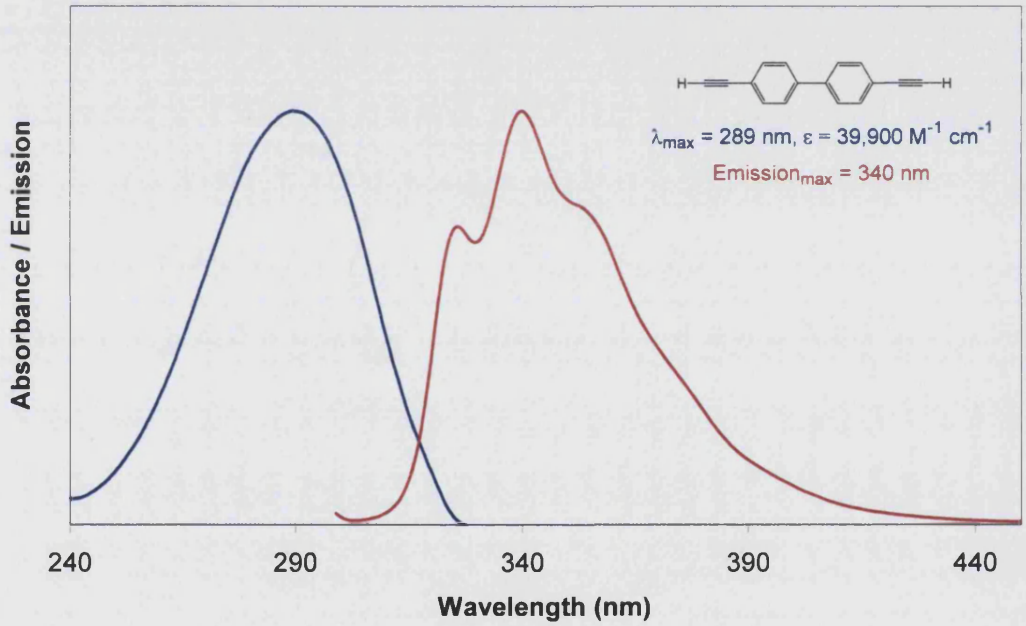

Figure 2.18 UV-visible spectra of 4,4'-diethynylbiphenyl, absorption is shown in blue and emission in red.

UV-visible spectra of complex **(6)**, as shown in Figure 2.19 have similar characteristics as complex **(3)** in Figure 2.17. The λ_{max} value of the absorbance spectrum comes at the same value as for complex **(3)**. However, the absorption peak is broader and the onset of absorption is shifted to a higher wavelength.

The emission spectrum mirrors the absorption with the main band appearing at 387 nm with a side shoulder peak at 403 nm, giving an energy spacing of *ca* 1030 cm^{-1}.

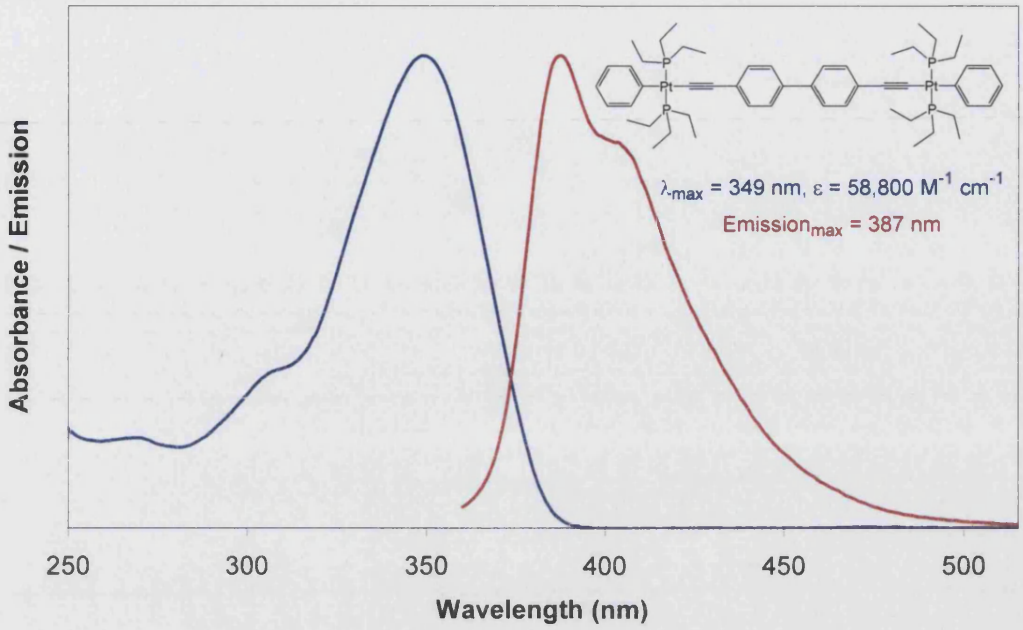

Figure 2.19 UV-visible spectra of $PhPt(PEt_3)_2CC(C_6H_4)_2CCPt(PEt_3)_2Ph$ (6), absortion is shown in blue and emission in red.

The UV-visible spectra of complex **(7)** are shown in Figure 2.20. No change in peak shape, peak position or onset of absorption was found as compared to that of complex **(6)**. The small change of ε value is within the experimental error, 58,800 dm^3 mol^{-1} cm^{-1} for **(6)** and 58,200 dm^3 mol^{-1} cm^{-1} for **(7)**.

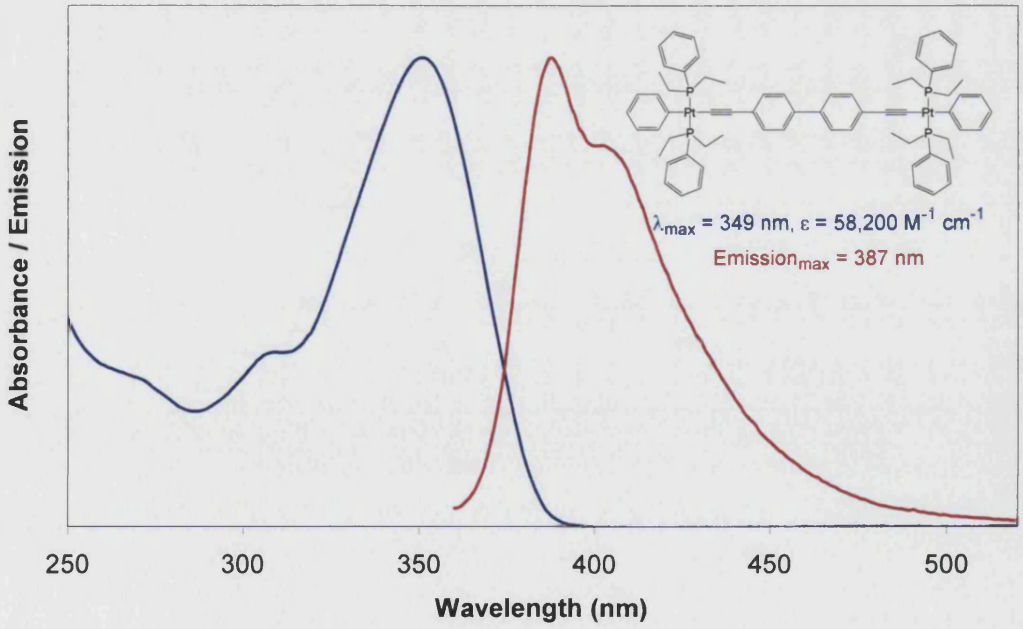

Figure 2.20 UV-visible spectra of $PhPt(P(Ph)Et_2)_2CC(C_6H_4)_2CCPt(P(Ph)Et_2)_2Ph$ (7), absorption is shown in blue and emission in red.

The UV-visible spectra of 4,4''-diethynylterphenyl **(11)** are shown in Figure 2.21. The broadness of the absorbance band has increased compared to that of 4,4'-diethynylbiphenyl with no vibronic structure observed. There is also an increase in the wavelength of the onset of absorption. The emission spectrum gives rise to two main peaks at 354 and 372 nm with a shoulder peak at 387 nm. These peaks correspond to energy spacings of *ca* 1370 which is clearly visible and 1040 cm^{-1} which is tentatively assigned to the shoulder peak.

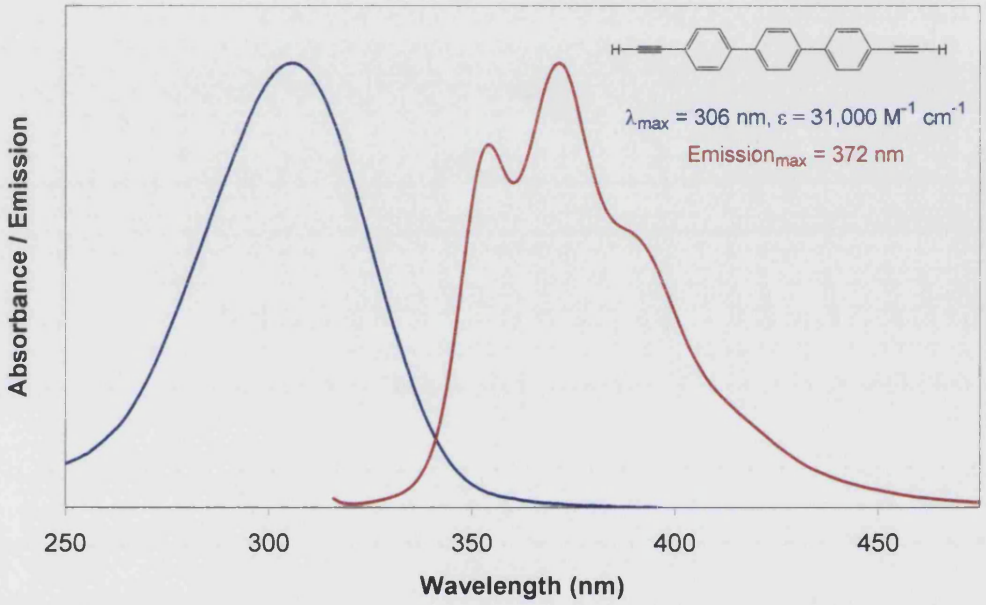

Figure 2.21 UV-visible spectra 4,4''-*bis* ethynylterphenyl (11), absorbance is shown in blue and emission in red.

The UV-visible spectra of complex **(12)** are given in Figure 2.22. The broad absorbance peak exhibits a maximum at 350 nm, which is essentially the same for all the platinum complexes of this series. The onset of absorption does follow the trend of shifting to a higher wavelength, lower energy compared to the biphenyl analogue **(6)**. No vibronic structure is observed in the absorbance spectrum.

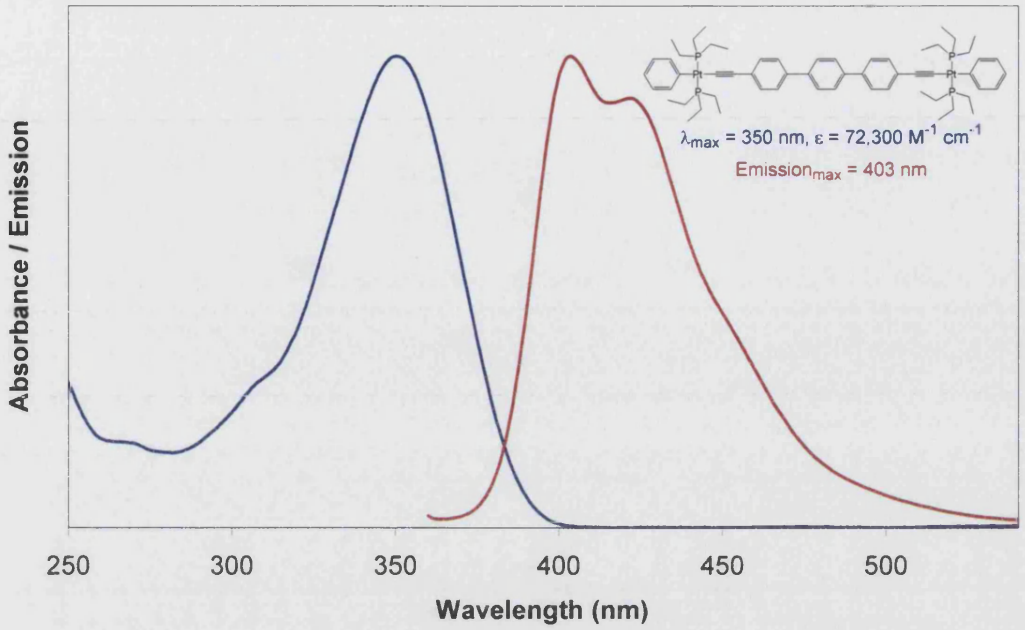

Figure 2.22 UV-visible spectra of $Ph(PEt_3)_2PtCC(C_6H_4)_3CCPt(PEt_3)_2Ph$ (12), absorbance is shown in blue and emission in red.

The emission spectrum of **(12)** exhibits a broad peak maximising at 403 and 422 nm. The difference in energy of these two peaks corresponds to an energy spacing of *ca* 1,120 cm^{-1}.

An important feature of the UV-visible absorption spectra collected for this study is the onset of absorption, as this is directly analogous to the optical gap energy of the system. The Stokes shift is the difference in the wavelengths of the absorption maxima and emission maxima. It is associated with the difference in molecular geometry between ground and excited states. The larger the change in geometry the greater the Stokes shift observed in the spectra. The optical gaps and Stokes shifts of the di-yne ligands and Pt(II) complexes are summarised in Table 2.4.

As the number of rings increases in the systems for both the terminal alkynes and the corresponding complexes, the Stokes shift increases. The optical gap of the system is shown to decrease with an increasing number of phenylene rings, consistent with the increase in the size of the chromophore.

Compound	Onset of absorption (nm)	Optical gap (eV)	Stokes shift (nm)
1,4-diethynylbenzene **(2)**	300	4.14	40
4,4'-diethynylbiphenyl **(5)**	330	3.76	51
4,4"-diethynylterphenyl **(11)**	386	3.22	66
(3)	388	3.20	17
(6)	397	3.13	38
(12)	409	3.04	72

Table 2.4 Table of UV-visible data for polyphenyl ligands and complexes.

In parallel studies to this chapter of work, other members of the group were studying the oligothiophene analogues (Figure 2.23) to the polyphenyl compounds. Some of the preliminary results have been reported.[20] Analyses were carried out on the oligothiophenyl complexes by UV-visible spectroscopy to compare with the complexes reported in this Chapter.

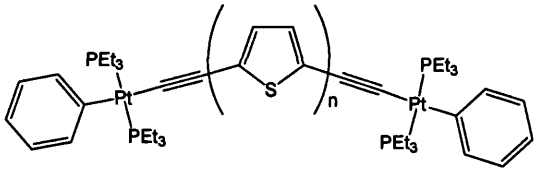

Figure 2.23 Oligothienyl complexes, where n = 1 thienyl, n = 2 bithienyl, n = 3 terthienyl.

Figure 2.24 shows the optical gap energies of complexes shown in Figure 2.23 along with the oligophenyl ligands and complexes. All three series show a drop in optical gap energy as the number of rings is increased. The thienyl analogues show the lowest energy optical gaps, with the terthienyl complex showing an optical gap of 2.46 eV compared to 3.04 eV for the terphenyl complex.

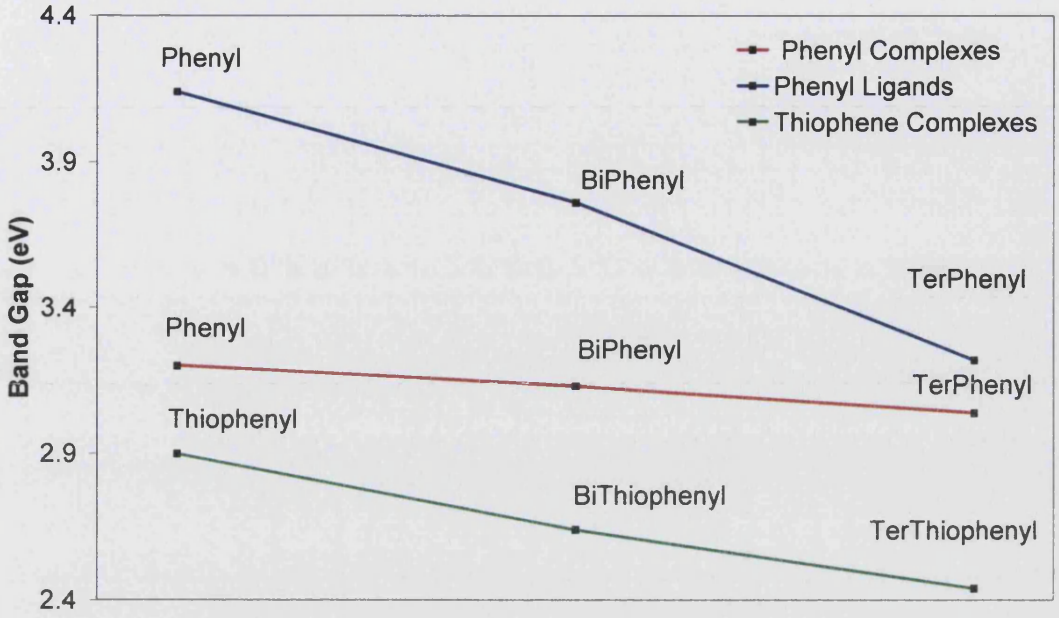

Figure 2.24 Optical gap energies of oligophenyls and oligothiophenyl compounds.

As the number of thiophene units increases the optical gap decreases, the same is true for the phenyl equivalents, but the drop in energy is less pronounced. This is because the phenylene groups do not line up in a planar nature as they do in the thienyl series, as seen in the dihedral angles in the solid state structures of **(6)** and **(12)**. The twist angle between the adjacent arene rings counteracts the drop in energy, which is observed due to the extension of the length of the conjugated system.

2.5 Density functional theory (DFT) calculational studies

In order to further understand the electronic structures of the bridging ligands **(2)**, **(5)**, **(11)** and **(16)**, and the properties they invoke on the corresponding metal complexes, Density Functional Theory (DFT) calculations, using the Gaussian03 program,[21] employing the B3LYP functional[22,23,24] in conjunction with the 6–31G* basis set[25] were carried out under D_{2h} symmetry. The calculated energies of the p_z orbitals that comprise the π- system of the ligands for fully optimised geometries are plotted in Figure 2.26. Molecular orbitals with orbital character concentrated on the alkynes, i.e. perpendicular to the p_z direction, are shown in red on the diagram. The calculated optical gap energies are shown in blue. The energies calculated for the alkyne π-orbitals for where n = 0 were calculated under $D_{\infty h}$ symmetry.

A decrease in the energy (stabilisation) of the LUMO is clearly observed as the number of arene rings increases from 1 through to 4. The HOMO energy is also seen to increase (destabilised) in line with increasing number arene rings. Consequently there is an overall decrease in the HOMO-LUMO energy gap from n = 1 through to 4. This decrease clearly correlates with the optical gap trend seen in the UV-visible spectra of **(2)**, **(5)** and **(11)** as discussed in Section 2.4.

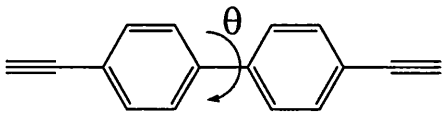

Figure 2.25 Variable "twist angle" of the biphenyl ligand (5). θ = dihedral angle.

Further calculations were carried out on the biphenyl ligand **(5)**, Figure 2.25, with orbital energies calculated under the 3 symmetry groups D_{2h} (θ = 0°), D_2 (rigid symmetry broken, to allow the structure to relax and find its energy minimum and therefore its optimal θ value) and D_{2d} (θ = 90°). The motivation for this part of the study was to investigate how the dihedral angle between the two adjacent arene rings affects the energies of the molecular orbitals of the system and to predict the extent of the minimum twist required to avoid the ortho-ortho interactions of adjacent rings. The results of these calculations are summarised in Figure 2.27.

Firstly, it should be noted that under the D_2 symmetry calculation the ligand was found to adopt a "twisted" structure with an optimal θ value at ~36.5°. The results also show an increase in the HOMO-LUMO energy gap of the biphenyl system under D_2 symmetry at 4.39 eV compared to that of the system under D_{2h} symmetry at 4.13 eV. A larger increase is observed for the system under D_{2d} symmetry. With the two rings at right angles to each other, the overlap of the "p_z" orbitals of one ring and the next is lost and consequently the LUMO energy increases and the HOMO energy decreases leading to an elevated HOMO-LUMO energy gap of 5.43 eV.

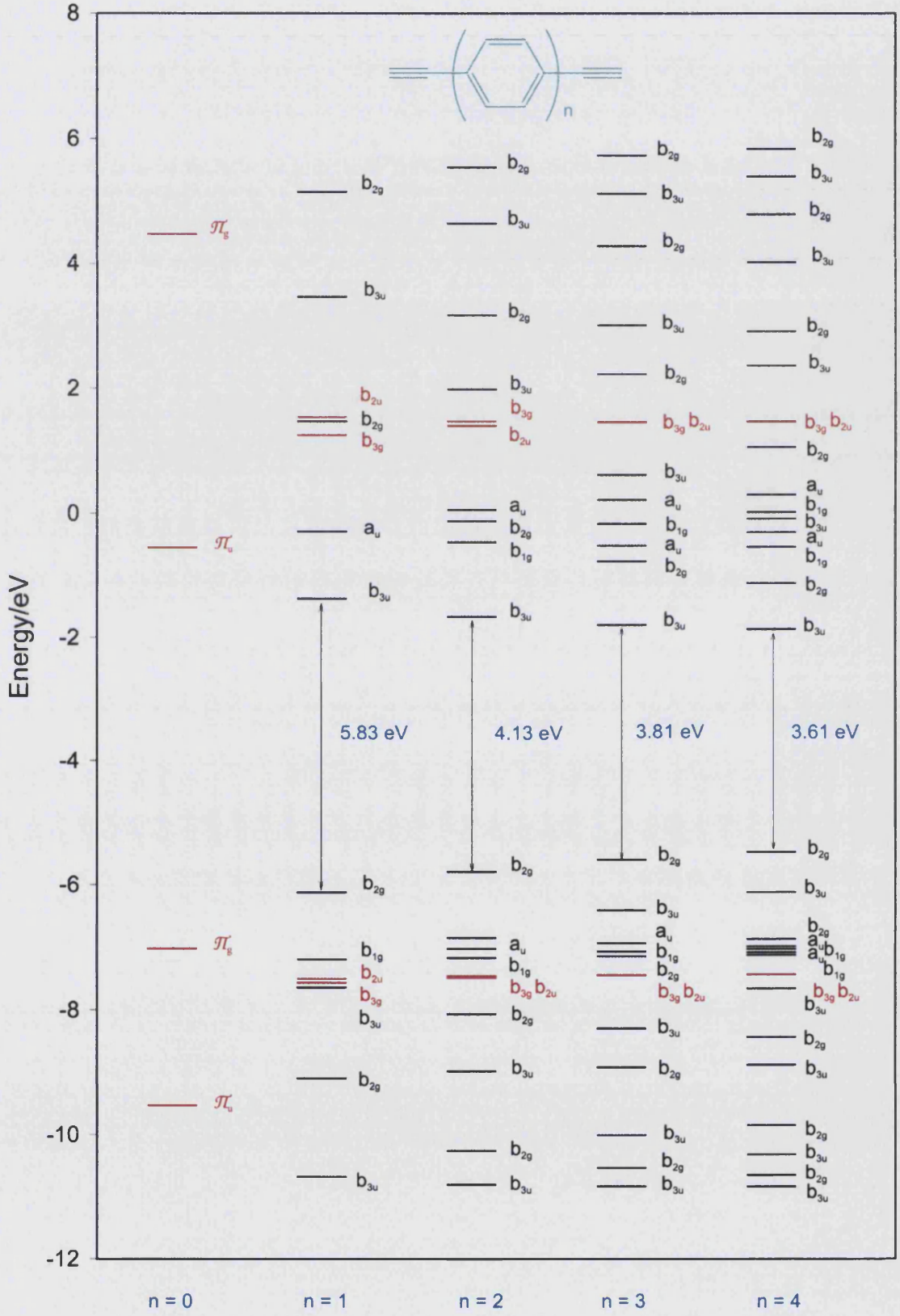

Figure 2.26 Orbital energies of the oligophenyl ligands as calculated using the Gaussian03 program under D_{2h} symmetry.

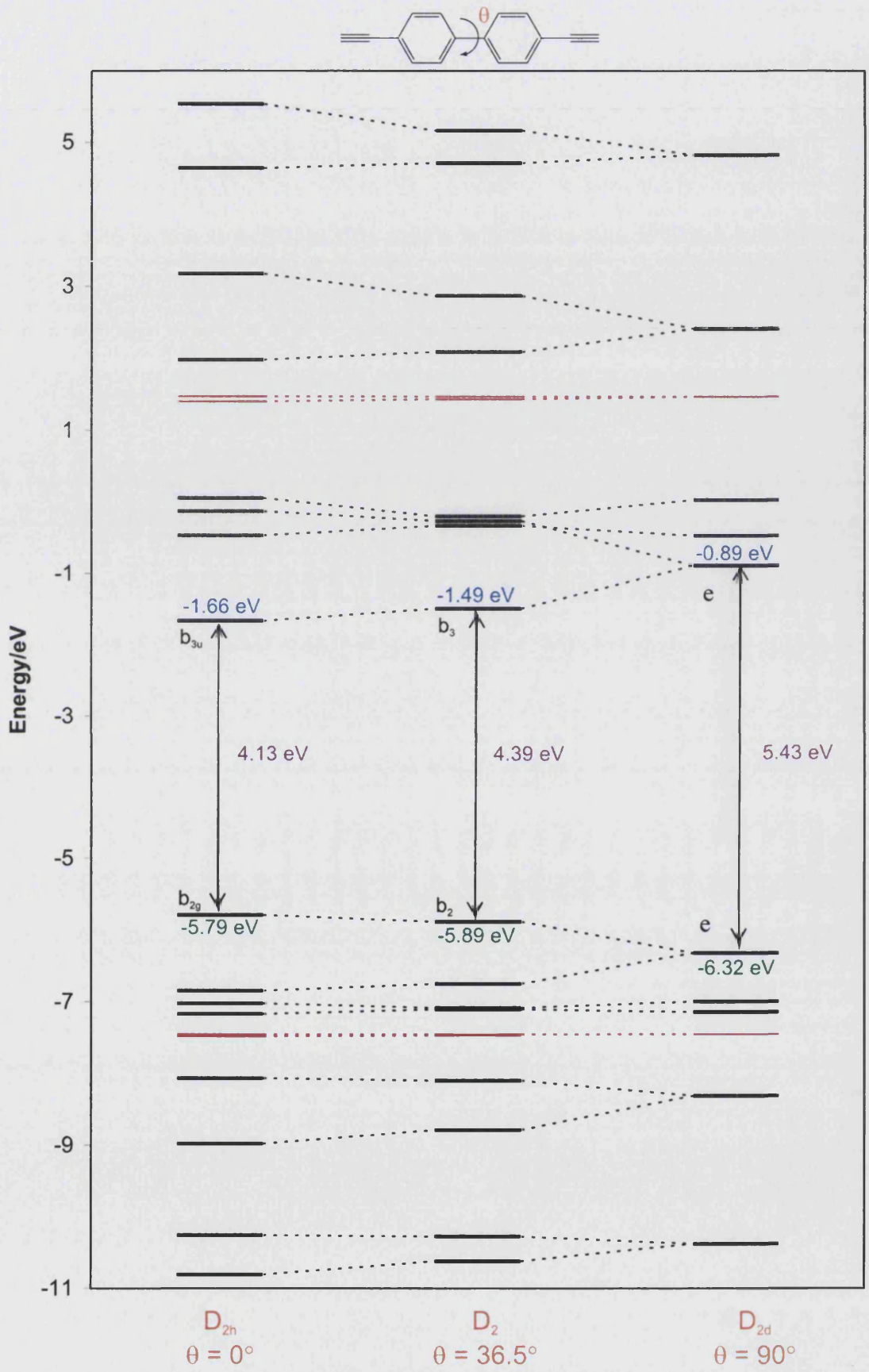

Figure 2.27 Orbital energies of the biphenyl ligand (5) as calculated using the Gaussian03 program under D_{2h}, D_2 and D_{2d} symmetries. The energies of the orthogonal orbitals are shown in red.

2.6 Conclusions

A series of oligophenyl containing ligands and corresponding Pt(II) complexes have been successfully synthesised and fully characterised in good to high yields. Their UV-visible spectra have been investigated and the optical gaps of the systems calculated.

The absorption spectra of complexes **(3)**, **(6)** and **(12)** have shown that the values of λ_{max} remain constant at 349 nm. The onsets of absorptions, however, are influenced by the number of arene rings in the central spacer ligand. The optical gaps of the systems decrease as the number of rings increases. The phosphine ligands on the platinum centre have been shown to have little effect on the UV-visible spectra of systems. This shows that the orbitals on the phosphine ligands do not contribute to the molecular frontier orbitals of the system.

Comparison of the oligophenyl complexes with the oligothienyl complexes has shown that both systems follow the same trend, with the thiophene analogues displaying lower optical gaps in every case. The drop in optical gap energy with increasing arene rings is more pronounced in the thienyl series due to the planar nature of the rings. The increase of phenylene rings does cause a drop in optical gap energy, but this is offset to some extent due to the twist angles between the adjacent rings.

Single crystal structures of complexes **(6)** and **(12)** have shown the dihedral angles between the central arene rings of the spacer groups to be 31.1(5)° and 34.4(3)°, respectively. This inherent twist angle is thought to be partly responsible for the higher optical gap of the phenyl analogues compared to the thiophenyl systems. The electronic factors imposed by the incorporation of the heteroatom are also thought to be responsible for the lower optical gaps of the thiophenyl systems. These two factors are the purpose for the investigation in Chapter 3, i.e. the twist angles of adjacent arene rings in the spacer ligand and the electronic effects of heteroatoms in the system.

2.7 References

[1] J. D. Coyle, *Introduction to Organic Photochemistry*, 1986, Chichester : John Wiley

[2] J. M. Tour, *Adv. Mat.*, 1994, **6**, 190

[3] F. Hide, *Acc. Chem. Res.*, 1997, **30**, 430

[4] P. Novak, K. Miller, K. S. V. Santhanam, O. Haas, *Chem. Rev.* 1997, **97**, 207

[5] R. E. Martin, F. Diederich, *Angew. Chem. Int. Ed.*, 1999, **38**, 1350

[6] H. Bässler, *Electronic Materials: The Oligomer Approach*; Müllen, K.; Wegner, G., Eds.; Wiley-VCH: Weinheim, Germany 1998

[7] W. Hoeve, H. Wynberg, E. E. Havinga, E. W. Meijer, *J. Am. Chem. Soc.* 1991, **113**, 5887

[8] H. Meier, U. Stalmach, H. Kolshorn, *Acta Polym.*, 1993, **48**, 379

[9] H. Nakanishi, N. Sumi, Y. Aso, T. Otsubo, *J. Org. Chem.*, 1998, **63**, 8632

[10] T. Izumi, S. Kobashi, K. Takimiya, Y. Aso, T. Otsubo, *J. Am. Chem. Soc.*, 2003, **125**, 5286

[11] M. S. Khan, M. R. A. Al-Mandhary, M. K. Al-Suti, F. R. Al-Battashi, S. Al-Saadi, B. Ahrens, J. K. Bjernemose, M. F. Mahon, P. R. Raithby, M. Younus, N. Chawdhury, A. Kohler, E. A. Marseglia, E. Tedesco, N. Feeder, S. J. Teat, *Dalton Trans.*, 2004, **15**, 2377

[12] N. Miyaura, T. Yanagi, A. Suzuki., *Synth. Commun.*, 1981, **11**, 513

[13] K. Sonogashira, Y. Tohda, N. Hagihara, *Tetrahedron Lett.*, 1975, 4467

[14] M. S. Khan, M. R. A. Al-Mandhary, M. K. Al-Suti, B. Ahrens, M.F. Mahon, L. Male, P.R. Raithby, C.E. Boothby, A. Kohler, *Dalton Trans.*, 2003, **1**, 74

[15] S. E. Thomas, *Organic Synthesis: The Roles of Boron and Silicon*, 1992, Oxford University Press

[16] M. Younus, *PhD Thesis*, Cambridge, 1999

[17] K. Siegmann, *Organometallics*, 1989, **8**, 2659

[18] K. Sonogashira, Y. Tohda, N. Hagihara, *Tetrahedron Lett.*, 1975, **16**, 4467

[19] D. H. Williams, I. Fleming, *Spectroscopic methods in organic chemistry*, 1989, 4th Edition, McGraw-Hill

[20] J. Lewis, N. J. Long, P. R. Raithby, G. P. Shields, W. Y. Wong, M. Younus, *J. Chem. Soc. Dalton Trans.*, 1997, **22**, 4283

[21] B. Schlegel, G. E. Scuseria, M. A. Robb, J. R. Cheeseman, V. G. Zakrzewski, J. A. J. Montgomery, R. E. Stratmann, J. C. Burant, S. Dapprich, J. M. Millam, A. D. Daniels, K. N. Kudin, M. C. Strain, O. Farkas, J. Tomasi, V. Barone, M. Cossi, R. Cammi, B. Mennucci, C. Pomelli, C. Adamo, S. Clifford, J. Ochterski, G. A. Petersson, P. Y. Ayala, Q. Cui, K. Morokuma, D. K. Malick, A. D. Rabuck, K. Raghavachari, J. B. Foresman, J. Cioslowski, J. V. Ortiz, A. G. Baboul, B. B. Stefanov, G. Liu, A. Liashenko, P. Piskorz, I. Komaromi, R. J. Gomperts, R. L. Martin, D. J. Fox, T. Keith, M. A. Al-Laham, C. Y. Peng, A. Nanayakkara, M. Challacombe, P. M. W. Gill, B. Johnson, W. Chen, M. W. Wong, J. L. Andres, C. Gonzalez, M. Head-Gordon, E. S. Replogle and J. A. Pople, *Gaussian 03 Version A9*, Gaussian Inc., Pittsburgh, PA, 2003

[22] A. D. Becke, *Phys. Rev. A: Gen. Phys.*, 1988, **38**, 3098

[23] A. D. Becke, *J. Chem. Phys.*, 1993, **98**, 5648

[24] C. Lee, W. Yang, R. G. Parr, *Phys. Rev. B: Condens. Matter*, 1988, **37**, 785

[25] W. J. Hehre, L. Radom, P. v. R. Schleyer, J. A. Pople, *Ab initio Molecular Orbital Theory*, John Wiley & Sons, New York, 1986

Chapter 3

Chalcogenophene Systems

3. Chalcogenophene Systems

3.1 Introduction

3.1.1 Background

The chalcogenophene systems shown in Figure 3.1 derive their aromatic character through the delocalisation of a lone pair of electrons on the heteroatom into the π-system of the ring.

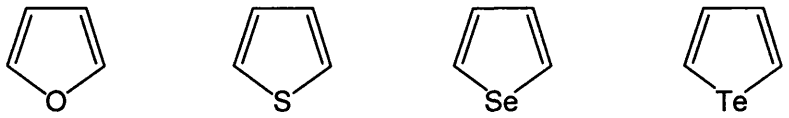

Furan Thiophene Selenophene Tellurophene

Figure 3.1 Heterocycles containing Group 16 elements.

In each heterocycle delocalisation results in the loss of electron density from the heteroatom, with the extent of the delocalisation, and hence the aromaticity influenced by the electronegativity of the heteroatom. Table 3.1 shows the Pauling Electronegativities of the Group 16 elements discussed in this Chapter.[1] In the case of furan, the highly electronegative oxygen centre holds on tightly to its electron density, hence the lone pair of electrons cannot delocalise easily. As Group 16 is descended the electronegativity of the heteroatom reduces and it is potentially easier for the lone pair of electrons to delocalise into the ring system. However, concurrently the orbitals become more mis-matched and the interactions are less effective.

Heteroatom	Pauling Electronegativity
O	3.5
S	2.5
Se	2.4
Te	2.1

Table 3.1 Pauling Electronegativity values for the Group 16 elements.

It is clear that both the electronegativity and the size of the frontier orbitals of the heteroatom are important in determining the degree of aromaticity of the heterocycle.

A comparative study of the aromatic character of furan, thiophene, selenophene, and tellurophene was carried out by Marino *et al.*[2] The ground state aromaticities of the chalcogenophenes were compared using several different criteria; NMR dilution shift, the difference in chemical shifts of the α- and β-protons, the effect of a 2-methyl substitution on the ring proton chemical shifts, the diamagnetic susceptibility exaltation, the sum of the bond orders, and the mesomeric dipole moment. The agreement among the results obtained was remarkably good and the following order of decreasing aromaticity was established: benzene > thiophene > selenophene > tellurophene > furan.

Chalcogenophenes have been incorporated into a variety of π-conjugated organic systems and their luminescent properties studied. The Yu group utilised the Stille coupling reaction (Figure 3.2) to synthesise polyphenylene-*co*-furan (PPF) and polyphenylene-*co*-thiophene (PPT), and have subsequently characterised each compounds luminescent properties.[4]

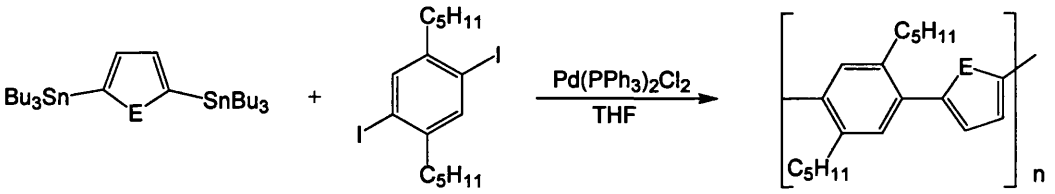

Figure 3.2 Synthesis of polyphenylene-*co*-furan (E = O) and polyphenylene-*co*-thiophene (E = S).

Both polymeric compounds showed similar photoluminescent spectra. PPF was found to have a larger quantum efficiency for emission than PPT, although PPF was found to be photochemically unstable due to photooxidation.

A recent publication by Humphrey *et al* reported the synthesis of and crystallographic and electrochemical studies on alkyne-coordinated Group 6-Iridium clusters linked by heterocyclic groups.[5] The report describes the synthesis of a series of silyl-protected 2,5-diethynyl thiophene and selenophene derivates and their use as ligands for the synthesis of a series of dinuclear compounds containing Iridium clusters, the paper

also discusses comparisons with the previously reported phenyl-based analogous compounds.[6,7] The photophysical properties of these systems were not investigated, however, cyclic voltammetric scans for these complexes all showed reversible oxidation processes.

Chalcogenophenes have been studied extensively in their polymeric forms. Polythiophene (PTh), Figure 3.3, is one of the most widely studied conjugated organic polymers both experimentally[8] and theoretically,[9] as demonstrated by Schopf and Koßmehl's comprehensive review of the literature published on the compound between 1990 and 1994.[10] In addition, Roncali surveyed electrochemical synthesis in 1992, [11] and the electronic properties of substituted PThs in 1997,[8] while McCullough's review focussed on the chemical synthesis of conducting PThs.[12] Conversely, the other polymers depicted in Figure 3.3 have only been investigated to a much lesser extent.

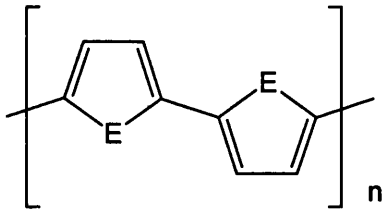

Figure 3.3 Polyheterocyclic compounds where E = O - Polyfuran (PF), E = S – Polythiophene (PTh), E = Se – Polyselenophene (PSe), E = Te – Polytellurophene (PTe).

Experimental investigation of polyfuran (PF) has been hindered by the difficult conditions necessary to polymerise furan.[13] The band gap for PF was determined to be 2.35 eV, 0.35 eV larger than that found for PTh. Theoretical calculations of band gaps have differed from the experimental observations, due to the ring opening of the polymers and limited conjugation lengths, these complications have resulted in PF being the least studied of the heterocyclic polymers.

The band gap for polyselenophene (PSe) was determined electrochemically to be 2.0 eV, very similar to that found for PTh. A series of oligoselenophenes up to hexamers were synthesised and their absorption spectra measured.[14] As the selenophene oligomers absorb at wavelengths about 0.2-0.3 eV longer than the corresponding

thiophene oligomers, one would expect a slightly smaller band gap for PSe than for PTh.

Polytellurophene (PTe) has been obtained by electropolymerisation of bitellurophene.[15] The black film obtained was tested for its conductivity but no band gap values were determined. Theoretical results predict a PTe band gap that is 0.34 eV smaller than for PTh. Although no reasons are given in the literature for lack of experimental data on PTe, the ease of oxidation of the tellurium could be responsible.

3.1.2 Objectives

The aim of this section of research was to study the effect of incorporating some chalcogenophenes into the systems studied in Chapter 2. The initial work was to modify complex **(12)** (Figure 3.4a) by removing the central arene ring and replacing it with a heterocycle (Figure 3.4b) and to investigate the steric and electronic effects of this substitution. The investigations into oligophenyl rings detailed in Chapter 2, showed that the adjacent arene rings were twisted relative to each other, with dihedral angles of around 34° observed in the solid state. This twist occurs to minimise the *ortho* proton-proton interactions, and is responsible for the disruption of optimal orbital overlap between the rings, leading to a lowering of the conjugation in the system.

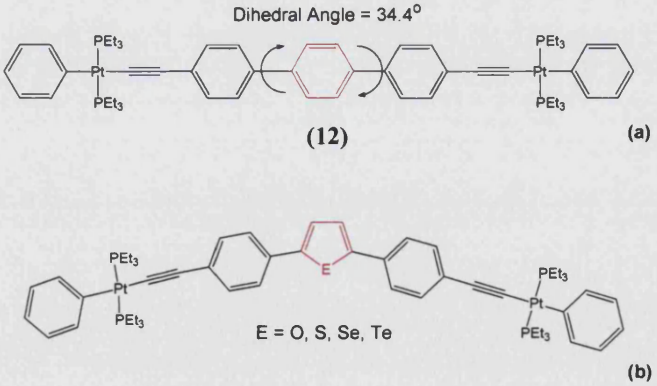

Figure 3.4 Compound (12) (a) and heterocyclic analogues (b).

Substitution of the central arene ring for a chalcogenophene should lead to a more planar system, through the reduction of these proton-proton contacts, and give rise to better delocalisation across the compound, and changing the chalcogen ought to induce different degrees of steric and electronic effects in the system.

3.2 Results and Discussion

3.2.1 Synthesis of Chalcogenophene- Containing Ligands

This section details the synthesis of the heterocyclic ligands required in order to investigate the objectives of this Chapter. The first such ligand necessary for this study was the furan- containing di-yne **(20)**, Figure 3.5.

The synthetic route to compound **(20)** was based on the compound 1,4-*bis*-(4-bromo-phenyl)-butane-1,4-dione **(18)**, which could be used as a reagent in a Paal-Knorr ring closing reaction to form a furan precursor molecule.

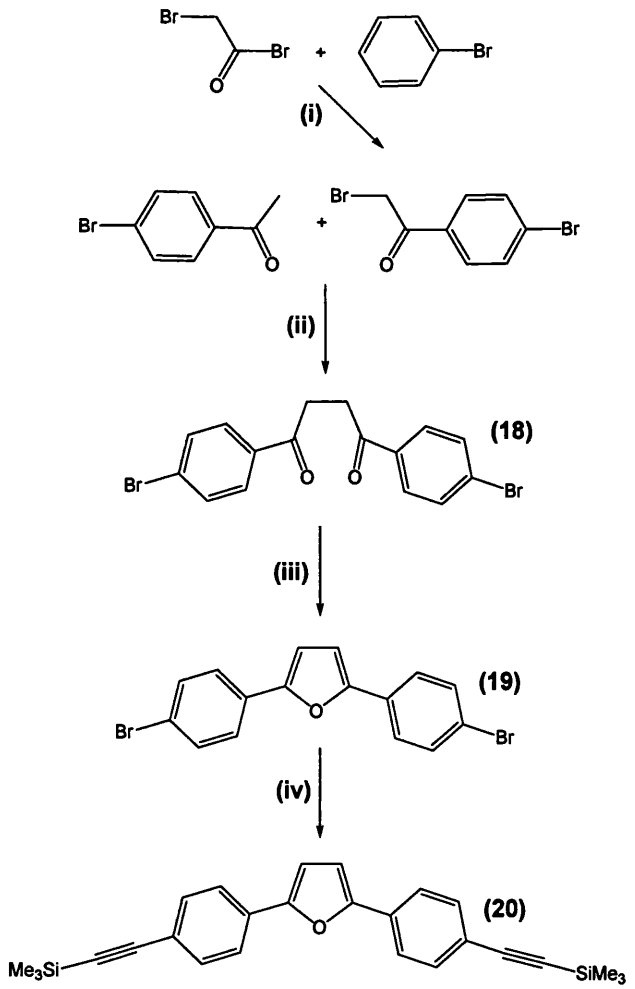

Figure 3.5 Synthetic scheme employed for (20).

Reagents and conditions; (i) $AlCl_3$, CH_2Cl_2, 0-10 °C (ii) $ZnCl_2$, Et_2NH, ^tBuOH, C_6H_6 (iii) P_2O_5, xylene, Δ (iv) Me_3SiCCH, $Pd(PPh_3)_2Cl_2$, CuI, $^iPr_2NH$, CH_2Cl_2.

The 1,4-diketone **(18)** was synthesised by a two step reaction (Figure 3.5). Aluminium trichloride was used as the catalyst in the Friedel-Crafts acylation reaction of bromobenzene with bromo-acetylbromide to form 2-bromo-1-(4-bromo-phenyl)-ethanone.[16] This was then reacted with 1-(4-bromo-phenyl)-ethanone to give **(18)**, using zinc chloride in the presence of diethylamine and *tert*-butanol forming a zinc chloride-amine-*tert*-butyl alcohol complex as a condensation reagent in accordance with the published method.[17] The reaction was left to stir for 7 days after which time TLC revealed that the reaction had reached completion. The mixture was evaporated to low volume in order to precipitate the product from solution. This was then collected by filtration and washed with cold benzene affording an analytically pure product in 85% yield.

Phosphorus pentoxide was employed as the ring closing reagent in the synthesis of 2,5-*di*-(4-bromo-phenyl)-furan **(19)**. The pentoxide was refluxed with 1,4-*di*-(4-bromo-phenyl)-butane-1,4-dione **(18)** in xylene for 2 h. The reaction mixture was allowed to cool before water was added and the mixture heated to 80 °C to quench any excess pentoxide. After heating the xylene was removed under reduced pressure and the product extracted into dichloromethane. Methanol was added to the solution and the dichloromethane removed under reduced pressure precipitating the product from solution. This was collected by filtration and characterised by ^{1}H and ^{13}C NMR spectroscopy. The ^{1}H NMR spectrum showed a singlet at 6.74 ppm corresponding to the C*H* resonance on the furan ring. The compound was further characterised by elemental analysis and mass spectrometry.

A Sonogashira coupling reaction (see Chapter 2, Section 2.2.2) was used for the synthesis of the trimethylsilyl protected alkyne ligand **(20)**. The existence of a singlet in the ^{1}H NMR spectrum at 0.27 ppm with an integral of 18 protons confirmed the formation of the *bis*trimethylsilylethynyl product. This was verified with the observation of a characteristic $\upsilon(C\equiv C)$ stretching frequency in the IR spectrum at 2158 cm^{-1}. The protected ligand **(20)** is air stable but degrades with time in the presence of light. Therefore the compound was stored in the absence of light.

The thiophene containing ligand **(24)** was synthesised from compound **(18)** *via* reaction scheme shown in Figure 3.6.

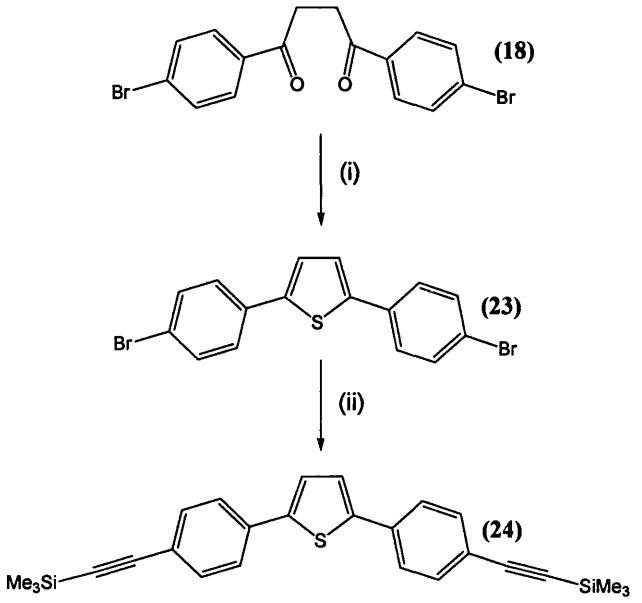

Figure 3.6 Synthesis of (24). Reagents and conditions: (i) Lawesson's Reagent, xylene, Δ (ii) Me_3SiCCH, CuI, $Pd(PPh_3)_2Cl_2$, $^iPr_2NH$, CH_2Cl_2.

Synthesis of the thiophene containing compound **(23)** utilised a similar strategy as adopted for the furan analogue **(19)**, with the starting material 1,4-*di*-(4-bromo-phenyl)-butane-1,4-dione **(18)** being used in a Paal-Knorr ring closing reaction.

The first attempts to synthesise 2,5-*di*-(4-bromo-phenyl)-thiophene **(23)** employed phosphorus pentasulphide as the ring closing reagent, refluxing five molar equivalents of P_2S_5 with **(18)** in xylene. The reaction produced a mixture of two products, namely the desired product 2,5-*di*-(4-bromo-phenyl)-thiophene **(23)** and the furan analogue 2,5-*di*-(4-bromo-phenyl)-furan **(19)**. This was evident in the ^1H NMR spectrum of the product obtained, with two singlets observed corresponding to C*H* resonances of two different heterocycles. The C*H* resonance positions on the furan and thiophene rings were observed at 6.74 ppm and 7.27 ppm, respectively. Attempts to separate these two compounds by chromatography proved unsuccessful as both compounds ran at very similar R_f values on silica and alumina TLC plates in various solvent combinations. It is believed that the presence of water in the reaction solvent was responsible for the formation of the furan product.

Lawesson's reagent (2,4-*bis*(4-methoxyphenyl)-1,3,2,4-dithiadiphosphetane 2,4-disulfide), was used in a subsequent attempt at ring closure under the same conditions, and proved to be successful in converting the ketone to the thioketone. The 1,4-dithioketone was then ring closed forming the thiophene through the loss of hydrogen sulphide,[18] by refluxing for 18 hours in xylene. The reaction was deemed complete by TLC, and then quenched with water. The product was extracted *via* a dichloromethane/water extraction, and the analytically pure product **(23)** was obtained in 83% yield, and fully characterised by ^{1}H and ^{13}C NMR spectroscopy, elemental analysis and mass spectrometry.

The synthesis of the *di*-alkynyl species **(24)** was carried out in a similar manner to that of the furan derivative **(19)**. The main difference was that the thiophene derivative was more stable than the furan. The di-yne **(24)** was achieved in 83% yield and was characterised by ^{1}H and ^{13}C NMR and IR spectroscopies and elemental analysis.

No selenophene ring closing reagents were found in the literature; therefore a different synthetic strategy was used for the synthesis of the selenophene containing ligand **(30)**. It was decided to utilise a similar scheme to the one employed in the synthesis of the oligophenyl systems in Chapter 2, i.e. to utilise the Suzuki Coupling reaction. The selenophene- containing ligand **(30)** was synthesised *via* the four step reaction scheme shown in Figure 3.7.

2,5-dibromoselenophene **(27)** was synthesised by adapting the published method for the synthesis of 2,5-dibromothiophene.[19] The commercially available selenophene was brominated using two equivalents of bromine in hydrobromic acid and diethyl ether. After 2 hours a ^{1}H NMR spectrum of the crude reaction mixture revealed a 90% yield of di-substituted product and 10% of the mono-substituted product (2-bromoselenophene). A saturated solution of sodium thiosulphate was added to quench the excess bromine in the reaction mixture and the organic phase was separated and dried. Removal of the solvent afforded a brown oil which was purified by vacuum distillation. An isolated yield of 64% was obtained for this product and characterised using multinuclear NMR spectroscopy.

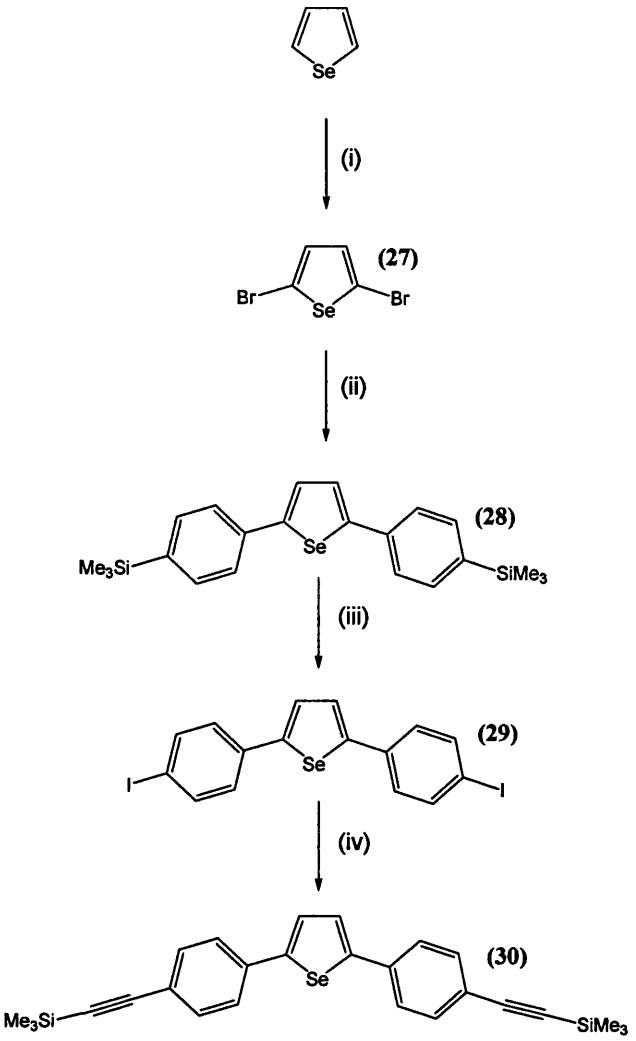

Figure 3.7 Synthesis of the selenophenyl ligand (30). Reagents and conditions: (i) Br_2, HBr, Et_2O (ii) *p*-$Me_3Si(C_6H_4)B(OH)_2$, $Pd(PPh_3)_4$, $NaHCO_{3(aq)}$, toluene, Δ (iii) ICl, $CHCl_3$ (iv) Me_3SiCCH, $Pd(PPh_3)_2Cl_2$, CuI, $^iPr_2NH$, CH_2Cl_2.

2,5-*bis*-(4-trimethylsilyl-phenyl)-selenophene **(28)** was synthesised by a Suzuki coupling of the 2,5-dibromoselenophene and 4-trimethylsilyl phenylboronic acid. The two starting materials were refluxed in toluene in the presence of tetrakis triphenylphosphine palladium as catalyst and aqueous sodium hydrogen carbonate. After refluxing for 76 hours TLC revealed that the reaction had reached completion and the organic phase was decanted and evaporated to dryness to afford a brown oil. The crude product was purified by column chromatography, then recrystallisation. The analytically pure product was obtained with a yield of 64% and characterised using multinuclear NMR spectroscopy, elemental analysis and IR spectroscopy.

The trimethylsilyl groups of compound **(28)** were then removed, using iodine monochloride in dichloromethane solution to afford the di-aryl iodide product **(29)**, 2,5-*di*-(4-iodo-phenyl)selenophene. After a few minutes a yellow precipitate formed, and the reaction was left to stir for a further 15 hours. The solid was then filtered off and washed with cold ethanol. The conversion was confirmed by the absence of the singlet resonance at 0.29 ppm in the ^{1}H NMR spectrum, corresponding to the loss of the trimethylsilyl group, and was further characterised by ^{13}C and ^{77}Se NMR spectroscopy and elemental analysis.

The Sonogashira reaction of the aryl iodide **(29)** with trimethylsilylacetylene was observed at a faster rate than the aryl bromides **(19)** and **(23)**. The reaction was complete in 4 hours, compared to that of the furan **(19)** and thiophene analogues **(23)** which took 18 and 26 hours, respectively. This is due to the increased reactivity of aryl iodides over aryl bromides during palladium catalysis.[21] The reaction was carried out in dichloromethane and diisopropylamine in the presence of *bis*(triphenylphosphine)palladium(II) chloride and copper iodide catalysts. On completion, the volatiles were removed under reduced pressure and the crude product passed through a silica plug with ethyl acetate/hexane eluent. The highly soluble compound was purified by column chromatography to give the analytically pure compound **(34)** in a 68% yield. This was confirmed by multinuclear NMR spectroscopy, elemental analysis and IR spectroscopy.

A similar approach was attempted in the synthesis of the tellurophene analogue as adopted for the lighter period analogues. Tellurophene itself is not commercially available; therefore it was prepared using literature procedures outlined in Figure 3.8.

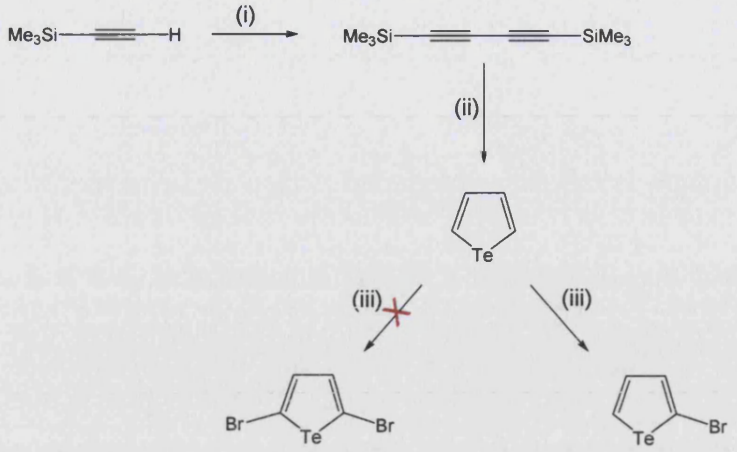

Figure 3.8 Attempted synthesis of 2,5-dibromotellurophene. Reagents and conditions: (i) O_2, CuCl,[22] (ii) Na_2Te, MeOH,[23] (iii) BuLi, Et_2O, 1,2-dibromo-tetrachloroethane, -78 °C.[24]

Direct bromination of tellurophene, using Br_2 as was achieved with the furan analogue, was not attempted. This is because the literature suggests that the tellurium itself is brominated rather than the 2- and 5- positions of the tellurophene ring.[23] Several attempts were made using an alternative literature preparation.[24] This reaction involved the use of *n*-butyl lithium in diethyl ether to produce the di-lithium salt, followed by the reaction with 1,2-dibromo-tetrachloroethane to give 2,5-dibromotellurophene. Every time this reaction was attempted the 2-bromotellurophene was obtained as the single product. The reaction was repeated using *tert*-butyl lithium, but these "harsher" conditions were found to decompose the product. Work is currently ongoing within the group investigating alternative routes to the desired product.

The spectroscopic characterisation of the ligands in this section all give spectra which could be assigned to the expected products. Some of the more interesting features and trends will be discussed in Section 3.4.

3.2.2 Synthesis of di-platinum complexes (22), (26) and (32)

Figure 3.9 illustrates the deprotection and dehydrohalogenation steps utilised for the synthesis of complexes **(22)**, **(26)** and **(32)**.

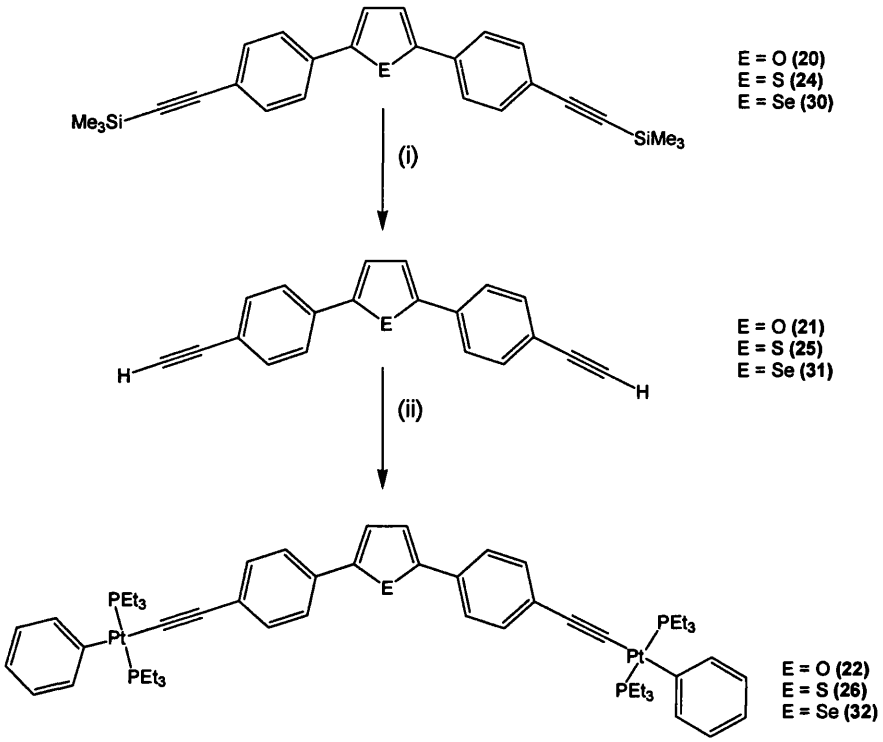

Figure 3.9 Synthesis of complexes (22), (26) and (32) where E = O, S and Se. Reagents and conditions: (i) $KOH_{(aq)}$, $MeOH/CH_2Cl_2$ (ii) $PhPt(PEt_3)_2Cl$, CuI, $^iPr_2NH$, CH_2Cl_2.

Attempted syntheses of complexes **(22)**, **(26)** and **(32)** were carried out as outlined in Figure 3.9 with work-up of reactions carried out using the same method of complex synthesis as discussed in Chapter 2, Section 2.2.3. The thiophene and selenophene analogues both gave good results, with near quantitative yields for the deprotection step. The existence of a singlet in the ^1H NMR spectra for **(21)**, **(25)** and **(31)** at 3.15 ppm, 3.09 ppm and 3.16 ppm, respectively indicated the presence of a free alkyne proton. The compounds were further characterised by ^{13}C NMR and IR spectroscopy. The dehydrohalogenation steps towards **(26)** and **(32)** gave good yields of 66% and 82%, respectively. The ^{31}P NMR spectra showed a single resonance with Pt satellites for the thiophenyl and selenophenyl complexes at 10.00 ppm ($^1J_{PtP}$ = 2638 Hz) and 10.01 ppm ($^1J_{PtP}$ = 2639 Hz), respectively.

The synthesis of the furan analogue proved to be more problematic, giving a low yield and requiring further purification. This was believed to be due to the instability of the furan heterocycle in the system, under the reaction conditions. It was thought that the copper iodide could have a role in ring-opening the furan ring, or decomposing the complex into other side products. A second attempt to synthesis the furan complex **(22)** in the absence of copper iodide and at an elevated temperature, proved to be successful. Using the same work-up conditions as for **(26)** and **(32)**, **(22)** was obtained as an analytically pure product in a yield of 61%. A singlet was observed for **(22)** in the ^{31}P NMR spectrum at 10.20 ppm with Pt satellites corresponding to a coupling constant of $^{1}J_{PtP} = 2641$ Hz.

As for all the ligands in this section, the platinum complexes all gave spectroscopic data which could be assigned to the desired products. Some of the more important features and trends will be discussed in Section 3.4.

3.2.3 UV-visible spectroscopic studies of complexes (22), (26) and (32)

The purified and fully characterised complexes **(22)**, **(26)** and **(32)** were then studied for their photophysical properties by undertaking UV-visible absorption studies in dichloromethane solutions at room temperature. Figure 3.10 shows the UV-visible absorption spectra of the di-platinum complexes **(22)**, **(26)** and **(32)**. The furan derivative **(22)** exhibits two main absorbance bands at 357 and 375 nm, with a shoulder band also present at 393 nm. The energy spacings between these bands correspond to energies of ~1350 cm^{-1} and ~1220 cm^{-1}. The onset of absorption is observed at 439 nm corresponding to an energy of 2.83 eV. The thiophene complex **(26)** exhibits a broad absorbance band with a maxima at ~388 nm, with the onset of absorption occurring at 462 nm, which equates to an energy of 2.69 eV. The selenophene analogue **(32)** also exhibits a broad absorbance band, with a maxima at 397 nm. The onset of absorption is observed at 467 nm, corresponding to an energy of 2.66 eV.

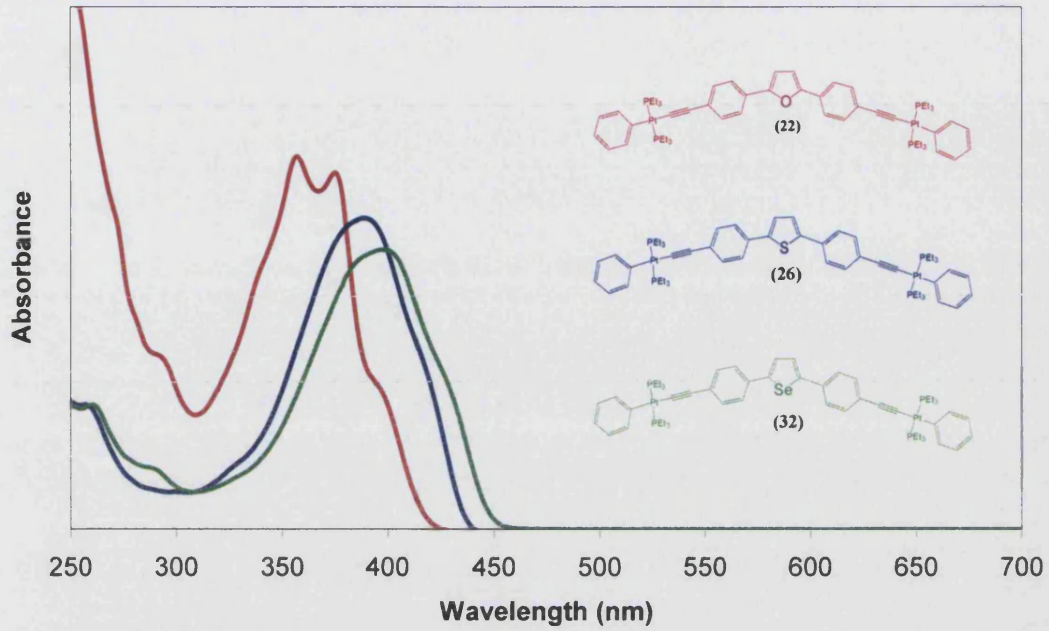

Figure 3.10 UV-visible spectra of the platinum complexes (22), (26) and (32) in CH_2Cl_2 solution at RT.

It is clear from Figure 3.10 that there is a definite shift of λ_{max} values for the complexes as the heteroatom changes from oxygen to sulphur and then to selenium. In addition, the onset of absorption shifts to higher wavelength, lower energy, as the heteroatom changes down Group 16.

Table 3.2 summarises the UV-visible data obtained from the spectroscopic measurements on compounds **(22)**, **(26)** and **(32)**, along with the arene derivative for comparison. The results clearly indicate a decrease in band gap energy of the system as the central arene ring of the terphenyl complex **(12)** is replaced by a Group 16 heterocycle. A further drop in energy is observed as the chalcogen changes from oxygen to selenium down Group 16. The coefficients of absorption values (ε), however, do not change significantly and all lie within experimental error.

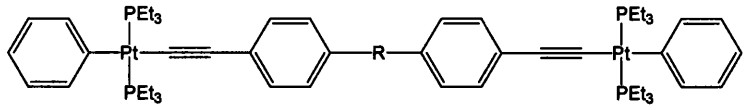

R=	Onset of absorption (nm)	(eV)	λ_{max} (nm)	ε ($dm^3mol^{-1}cm^{-1}$)
	409	3.04	350	72,300
	439	2.83	375	75,300
	462	2.69	388	77,300
	467	2.66	397	69,700

Table 3.2 Table of spectroscopic data of complexes (12), (22), (26) and (32).

The emission spectra for complexes **(22)**, **(26)** and **(32)** are shown along with their corresponding absorption spectra in Figure 3.11. All three spectra exhibit strong emission bands with two main maxima. The furan analogue displays two emission bands at 396 and 419 nm, with the energy spacing between these two bands equating to 1390 cm^{-1}, while the thiophene analogue emits at 438 and 463 nm, with an energy spacing corresponding to 1230 cm^{-1}. Similarly, the selenophene analogue exhibits two bands, at 451 and 475 nm, with an energy separation of 1120 cm^{-1}.

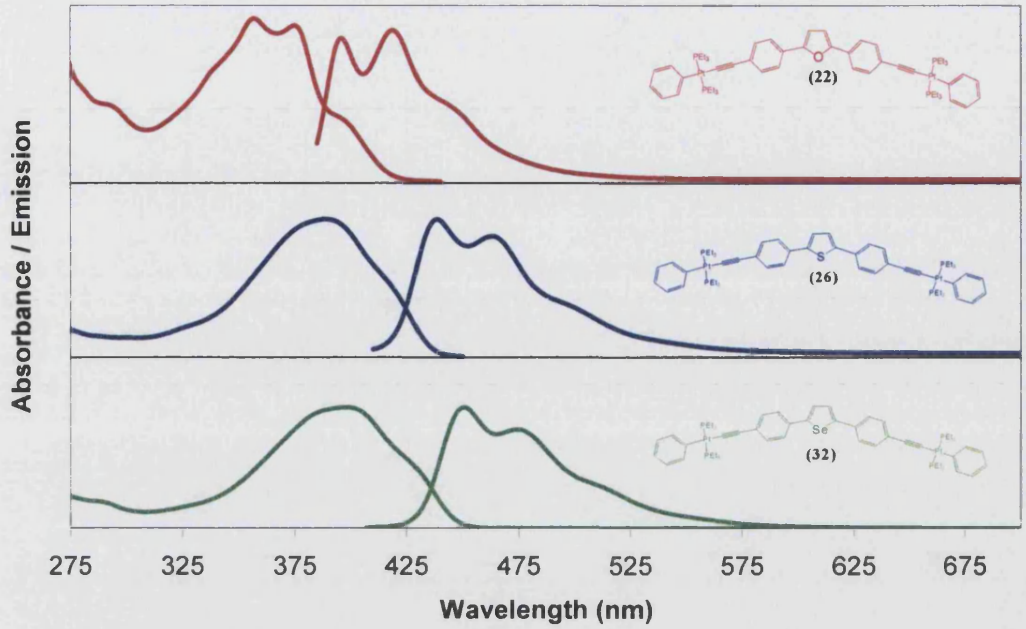

Figure 3.11 UV-visible absorption and emission spectra of the platinum complexes (22), (26) and (32) in CH_2Cl_2 solution at RT.

3.2.4 DFT calculational studies of compounds (21), (25) and (31)

To understand and explain the spectroscopic behaviour in Section 3.2.3, electronic structure calculations of the systems were undertaken. Density Functional Theory (DFT) calculations, using the Gaussian03 program,[28] employing the B3LYP functional[29,30,31] in conjunction with the 6–31G* and SDD basis sets[32,25] were carried out, initially under C_{2v} symmetry. The thiophene- and selenophene- containing ligands were recalculated under C_2 symmetry to check for a global minimum energy under a relaxed geometry. This was carried out after imaginary frequencies were observed in the results for **(25)** and **(31)**, indicating the global minimum was not reached in both cases. Geometry optimisations were carried out to locate the lowest energy molecular structure for all the terminal alkyne ligands **(21)**, **(25)** and **(31)**. The energies of the molecular orbitals were also calculated with the energies of frontier orbitals given in Table 3.3.

Compound	Symmetry	HOMO (eV)	LUMO (eV)	Optical Gap (eV)	Dihedral Angle (°)
(21)	C_{2v}	-5.28	-1.74	3.33	0
(25)	C_{2v}	-5.39	-1.94	3.23	0
(25)	C_2	-5.46	-1.83	3.36	22.4
(31)	C_{2v}	-5.40	-2.04	3.14	0
(31)	C_2	-5.49	-1.91	3.29	24.9

Table 3.3 DFT calculational results obtained for ligands (21), (25) and (31).

The first significant result to note from the DFT calculations is the preferred geometry of the arene rings in the di-yne ligands. All the systems were allowed to undergo optimum geometry calculations under both C_{2v} and C_2 enforced symmetry, Figure 3.12. The furan- containing ligand **(21)** was found to observe no change in the total energy of the molecule under the lower symmetry group C_2 when compared to calculation under the higher symmetry group C_{2v}. This suggests that the compound chooses to adopt a planar structure, and does not observe a drop in energy by twisting the adjacent arene rings relative to the central furan ring.

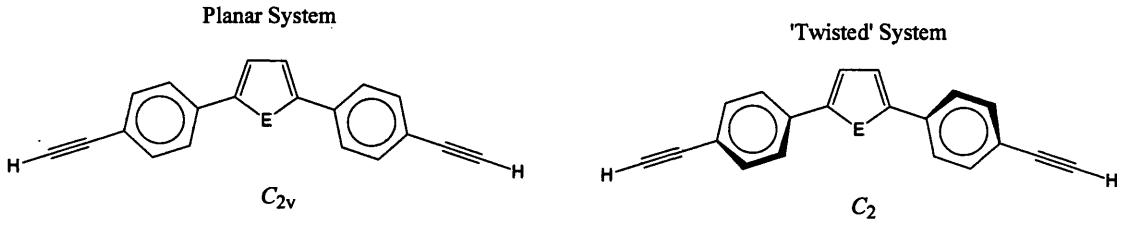

Figure 3.12 The two symmetry groups under which DFT calculations were undertaken. E = O (21), S (25) Se (31).

The thiophene- containing ligand **(25)** does show a difference in energy under the two different symmetry groups. A drop in the total energy minima of 1.55 kJ mol^{-1} is observed under the C_2 when compared to C_{2v} calculations. This drop in energy coincides with a twist of the arene rings relative to the thiophene ring with a calculated dihedral angle of 22.4°. Under the C_2 symmetry restrictions the energies of the frontier orbitals change as outlined in Table 3.3. This effect can be explained by the development of greater steric effects due to the larger heteroatom. The larger atomic size of the sulphur atom enforces the *ortho-* hydrogens on the adjacent arene ring closer to the thiophene. This gives rise to unfavourable interactions and the system twists away from planarity to minimise this. The selenophene- containing

ligand was also found to decrease in total energy under C_2 when compared to C_{2v} calculations by 2.18 kJ mol^{-1}. This drop in energy coincides with a twist of the arene rings relative to the selenophene ring with a calculated dihedral angle of 24.9°. The same effect is not observed for the furan as the smaller atomic size of the oxygen allows enough space between the hydrogens on the furan and the ortho- hydrogens on the adjacent ring.

The predicted optical energy gap of **(21)** and **(25)** under the same symmetry (C_{2v}) suggests a drop in energy for the thiophene- containing ligand when compared to the furan- containing ligand by 0.1 eV. These two results suggest that the increase in the size of the chalcogen within the heterocycle has an electronic effect on the system causing a drop in the optical energy gap and a steric effect on the system by forcing an increase in the optical energy gap.

3.2.5 Synthetic details for the platinum complexes (36), (40) and (43)

It is clear from the calculational data in Section 3.2.4, that the chalcogen in the heterocyclic systems imposes both electronic and steric factors. To investigate purely the electronic influence of the chalcogen, it was decided to synthesise simpler chalcogenophene systems in which the adjacent arene rings were "removed" thus eliminating any steric influences of the heteroatom on the system. The synthesis of these simpler single ring di-yne complexes is discussed in this section.

The strategy employed in the synthesis of the furan- containing complex **(36)** is illustrated in Figure 3.13.

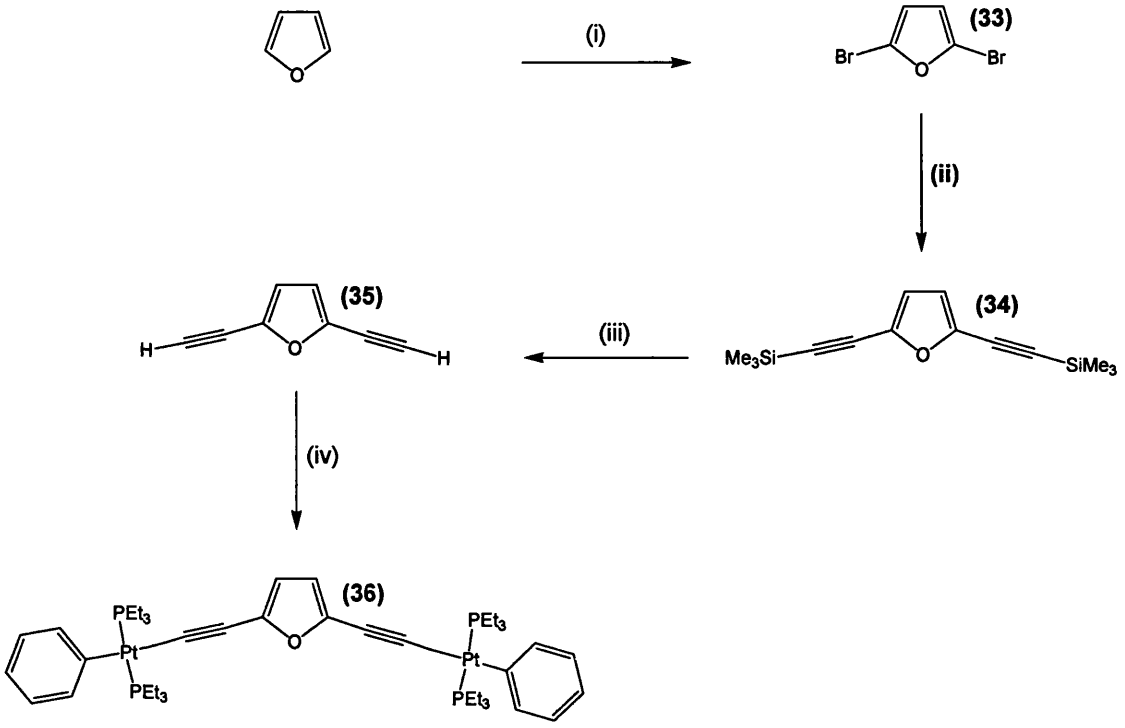

Figure 3.13 Synthesis of the platinum complex (36). Reagents and conditions: (i) Br_2, HBr, Et_2O (ii) Me_3SiCCH, $Pd(PPh_3)_2Cl_2$, CuI, $^iPr_2NH$, CH_2Cl_2 (iii) $KOH_{(aq)}$, MeOH, CH_2Cl_2 (iv) $PhPt(PEt_3)_2Cl$, CuI, $^iPr_2NH$, CH_2Cl_2.

In the first stage, furan was brominated using bromine in chloroform to yield 2,5-dibromofuran **(33)** as a yellow oil (Figure 3.13), which was purified by chromatography to give the analytically pure product in a 60% yield.

(33) was then used in a Sonogashira coupling reaction with trimethylsilylacetylene to synthesise 2,5-di(trimethylsilylethynyl)furan **(34)**. The reaction was achieved under standard conditions already discussed in this Thesis (Section 3.2.1). However, purification was carried out by sublimation of the crude product to yield **(34)** as an analytically pure pale yellow solid, which was characterised by ^1H and ^{13}C NMR and IR spectroscopy.

Deprotection of **(34)** to synthesise 2,5-di(ethynyl)furan **(35)** was carefully carried out in the absence of light. The work up of the reaction was adapted from the standard deprotection conditions used for other compounds in this Thesis due to the high volatility of the product. An aqueous extraction was carried out using diethyl ether as the organic solvent, since this was more easily removed than other solvents, allowing

the work up to be carried out in an ice bath wherever possible. The product was found to be relatively unstable and degraded rapidly, within hours, to give a dark brown oil. For this reason full characterisation was not possible and the product was used in the next step of the reaction scheme as soon as its identity and purity had been confirmed by ^{1}H and ^{13}C NMR spectroscopy.

The synthesis of the platinum complex **(36)** was carried out by a dehydrohalogenation reaction between 2,5-diethynyl furan **(35)** and the platinum starting material *trans-bis*(triethylphosphine)(phenyl)platinum(II) chloride. The reaction was carried out as for all other platinum complexes in this Chapter, with extra care taken due to the volatility of 2,5-diethynyl furan **(35)**.

The thienyl **(40)** and selenienyl **(43)** analogues of complex **(36)** were synthesised in a similar manner, see Figure 3.14. The thiophenyl complex has been reported previously,[26] therefore this section of work can be seen as an extension of this complex into the furan and selenophene analogues.

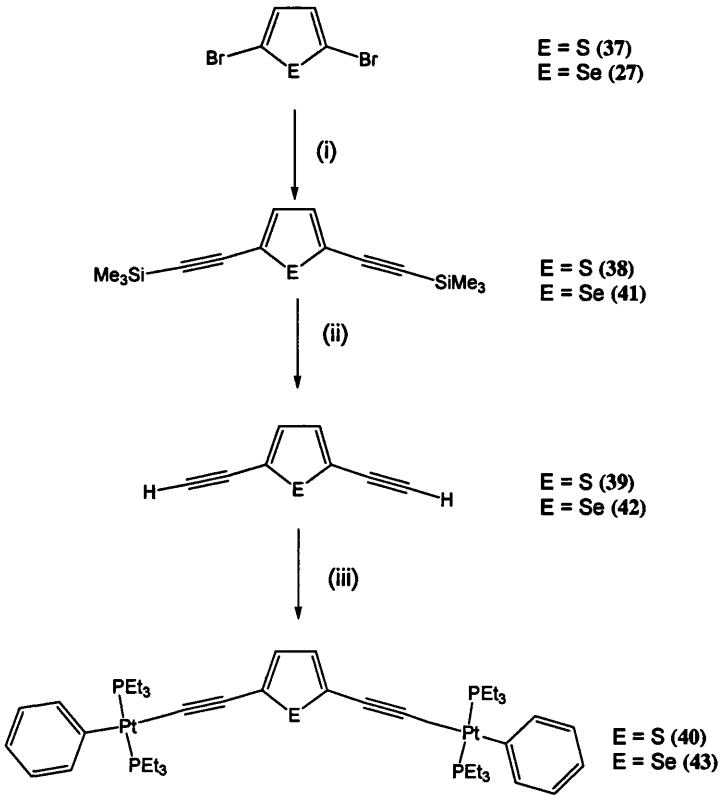

Figure 3.14 Synthesis of the platinum complexes (40) and (43).

Reagents and conditions: (i) Me_3SiCCH, $Pd(PPh_3)_2Cl_2$, CuI, $^{i}Pr_2NH$, CH_2Cl_2 (ii) $KOH_{(aq)}$, MeOH, CH_2Cl_2 (iii) $PhPt(PEt_3)_2Cl$, CuI, $^{i}Pr_2NH$, CH_2Cl_2.

The 2,5-dibromothiophene **(37)** employed in a Sonogashira coupling with trimethylsilylacetylene was commercially available, while 2,5-dibromoselenophene **(27)** was synthesised as highlighted in Section 3.2.2. The trimethylsilylethynyl analogues **(38)** and **(41)** were obtained with yields of 82% and 76%, respectively, with both compounds exhibiting the characteristic 18 proton singlet at 0.24 ppm in the ^{1}H NMR spectrum for the trimethylsilyl groups. Compounds **(39)** and **(42)** were then synthesised using the standard aqueous KOH conditions outlined for the furan derivative **(35)**. A yield of 75% was achieved for **(39)** and 62% for **(42)**. The slightly low yields are due to the high volatility and low stability of the compounds.

The platinum complexes **(40)** and **(43)** were synthesised using a dehydrohalogenation reaction as for the furan analogue **(36)**, with a yield of 70% achieved for both the thiophenyl and selenophenyl complexes.

3.2.6 UV-visible spectroscopic studies of complexes (36), (40) and (43)

Figure 3.15 shows the UV-visible absorption spectra of the di-platinum complexes **(36)**, **(40)** and **(43)**. The spectra were collected at room temperature in a dichloromethane solution at 0.01 mM concentration. The furan derivative **(36)** exhibits two main absorbance bands with maxima at ~358 and ~347 nm. The energy spacing between these bands corresponds to an energy of ~885 cm^{-1}, with the onset of absorption observed at 413 nm, corresponding to an energy of 3.01 eV. The thiophene derivative **(40)** exhibits absorbance band maxima at 377 and 362 nm. The energy difference between these two bands equates to 1100 cm^{-1}, with the onset of absorption at 469 nm, equating to an energy of 2.65 eV. The selenophene analogue **(43)** exhibits an absorbance band with maxima at 391 and 373 nm, corresponding to an energy spacing of 1230 cm^{-1} with the onset of absorption observed at 480 nm (2.58 eV).

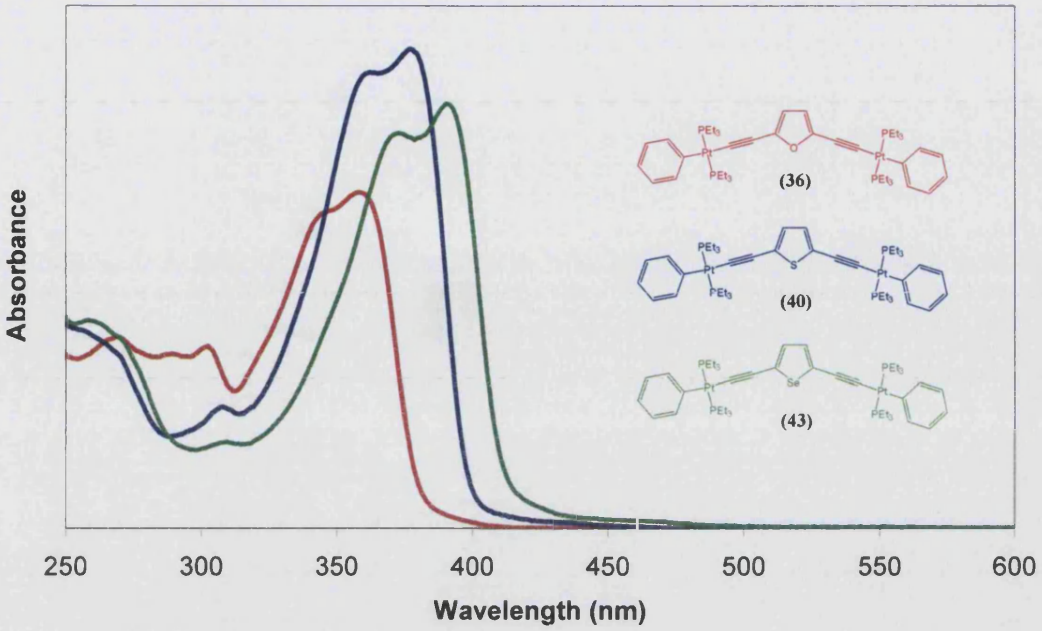

Figure 3.15 Absorption spectra of (36), (40) and (43) in CH_2Cl_2 at RT.

Table 3.4 compares the UV-visible data for the heterocycle complexes and the corresponding arene analogue. The results clearly indicate a drop in the band gap energy of the system when the central arene ring of the phenyl complex **(3)** is replaced by furan, with a further decrease being observed upon moving down the Group 16 heterocycles.

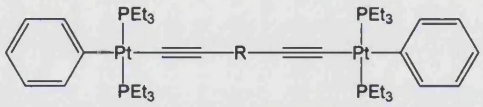

R=	Onset of absorption (nm)	(eV)	λ_{max} (nm)	ε ($dm^3mol^{-1}cm^{-1}$)
	388	3.20	349	51,400
	413	3.01	358	32,100
	469	2.65	377	45,800
	480	2.58	391	40,500

Table 3.4 Table of spectroscopic data of complexes (36), (40) and (43).

The emission spectra of complexes **(36)**, **(40)** and **(43)** are shown along with their corresponding absorption spectra in Figure 3.16. Each emission spectrum was collected after exciting the corresponding sample at its absorption maxima wavelength, 358, 377 and 391 nm for **(36)**, **(40)** and **(43),** respectively.

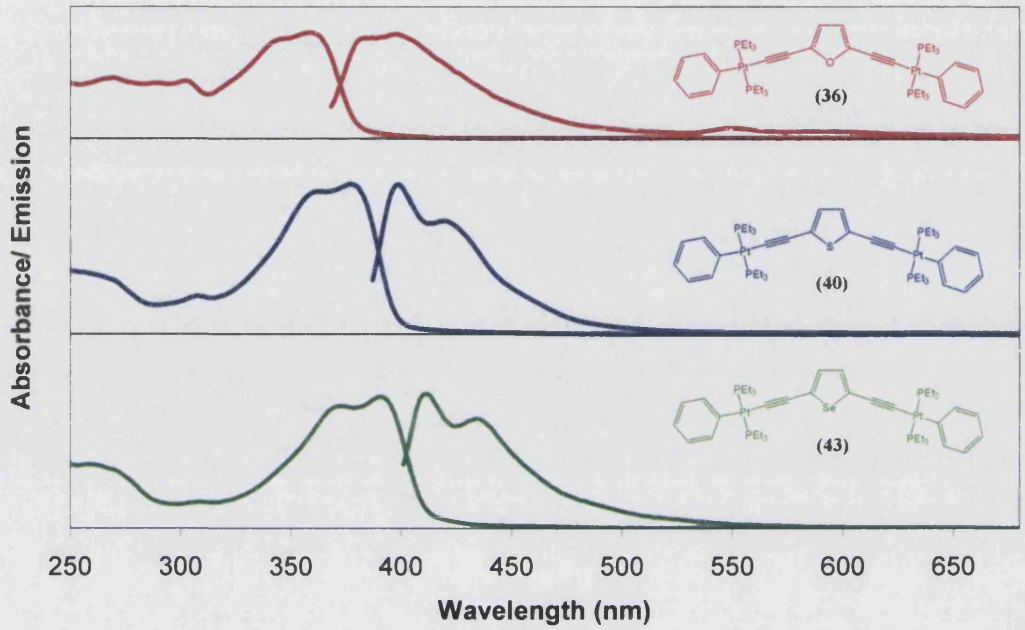

Figure 3.16 UV-visible absorption and emission spectra of (36), (40) and (43) in CH_2Cl_2 at RT.

All three spectra exhibit strong emission bands with two main maxima. In the furan analogue, the two emission bands are at 384 and 398 nm, in which the energy spacing between these two bands equates to ~910 cm^{-1}. This energy is associated with ground state vibrational data, and lies within the literature range of the υ(C=C) within a furan ring.[27] For the thiophene analogue, the emission bands are at 399 and 419 nm, with an energy spacing corresponding to ~1200 cm^{-1}, which can be equated to the υ(C=C) within a thiophene ring.[27] While the selenophene analogue exhibits two bands at 410 and 434 nm, with an energy separation equating to ~1350 cm^{-1} between them, which is associated within the literature range of the υ(C=C) in a selenophene ring.[27]

3.2.7 DFT calculational studies of compounds (35), (39) and (42)

In order to further understand the electronic structures of the bridging ligands **(35)**, **(39)** and **(42)**, DFT calculations, using the Gaussian03 program,[28] employing the B3LYP functional[29,30,31] in conjunction with the 6–31G* basis set[32] were carried out under C_{2v} symmetry.

The energies of the molecular orbitals of the π- system of the ligands **(35)**, **(39)** and **(42)** along with the tellurophene analogue are plotted in Figure 3.17. Each non-hydrogen atom in these systems contributes one "p_z" orbital to give nine π- molecular orbitals, occupied by a total of 10 π electrons. The energies of the LUMO orbitals are given in blue, the HOMO orbitals in green and the optical gaps in red. The figure clearly shows the trend of decreasing optical gap as the size of the chalcogen is increased. The energy of the LUMO orbitals decrease steadily (stabilise) through the series of the chalcogenophenes (furan through to tellurophene), and this can be explained in terms of molecular orbital character of the LUMO being centred over the heteroatom thus effecting the energy of that orbital. The HOMO energies however, remain fairly constant with the molecular orbitals displaying a nodal plane through the centre of the heteroatom, therefore the heteroatom does not contribute to the HOMO and does not affect its energy, beyond its influences on molecular geometry.

These results show that the heteroatoms are involved in the frontier molecular orbitals of these systems, with the energy of the HOMO affected by the chalcogen. The electronic effects of the different chalcogens can therefore be used to tune the optical gap of the system. The same decreasing optical energy gap trend is also observed in the experimental results obtained from the UV-visible spectroscopic studies in Section 3.2.6. The calculational results therefore show an excellent agreement with experimental data, showing that the models used in these calculations work well to give credible qualitative results. Although the tellurophene analogue ligand was not synthesised, the DFT results predict a further small decrease in optical energy gap from the selenophene ligand.

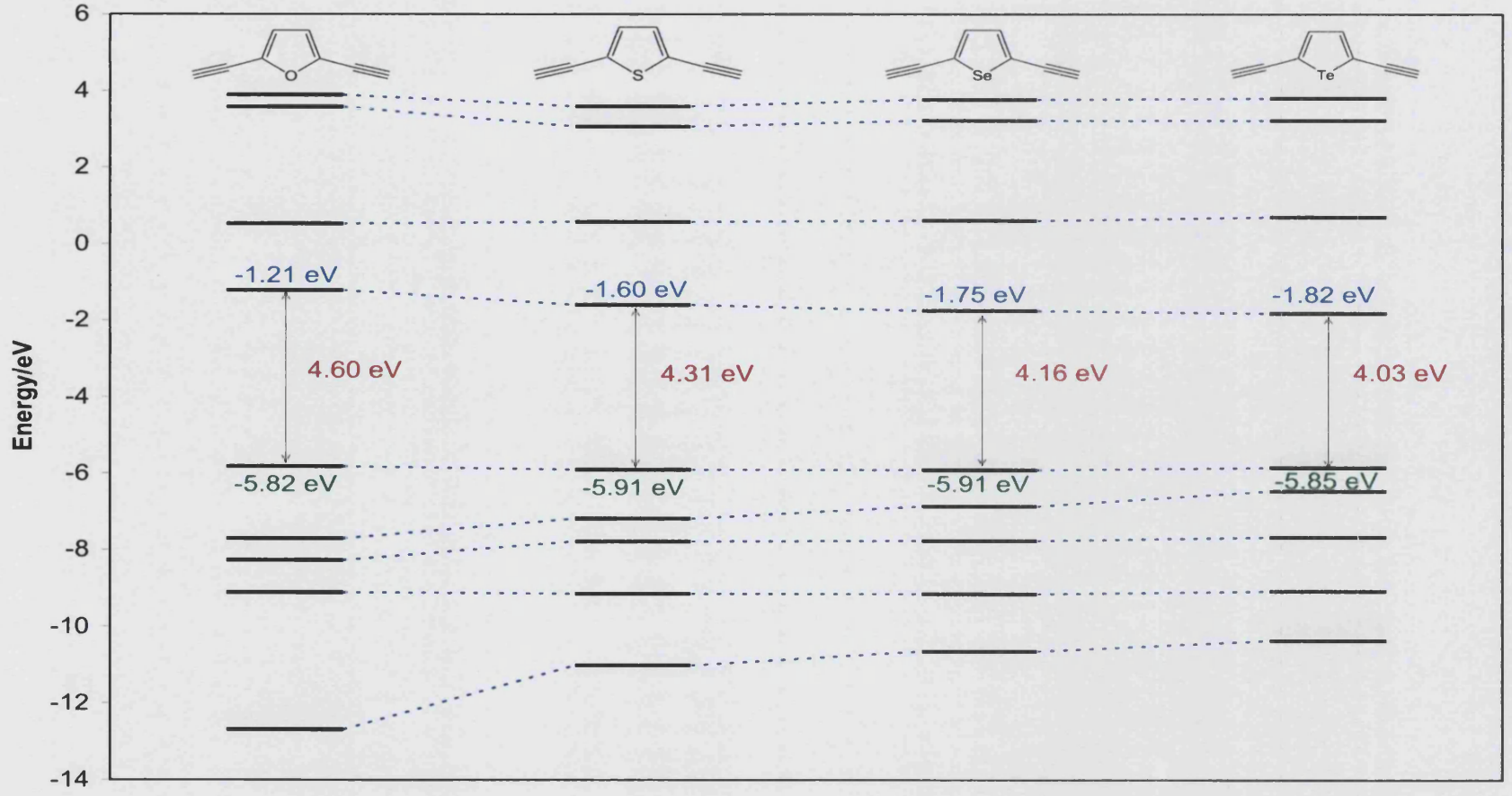

Figure 3.17 Molecular orbital energies of the chalcogenophene ligands as calculated using the Gaussian03 program under D_{2h} symmetry.

3.2.8 Synthetic details for the diazole containing compounds

One method of eliminating the steric effects of the heterocycle on the system is to "remove" all the protons on the central heterocycle. This can be achieved by replacing the CH groups with two N atoms, making a diazole heterocycle. This would eliminate the possibility of ortho-ortho proton interactions forcing the rings to twist relative to each other, and therefore allowing the possibility of a planar system. The synthesis of these compounds will be discussed in this section. The author wishes to acknowledge that the synthesis of the diazole compounds were carried out jointly with Claire Lock as part of a final year research project towards a MChem degree entitled "Luminescent organometallic materials for novel inorganic light emitting diodes".

The synthetic strategy employed in the synthesis of the oxadiazole- containing ligand is shown in Figure 3.18.

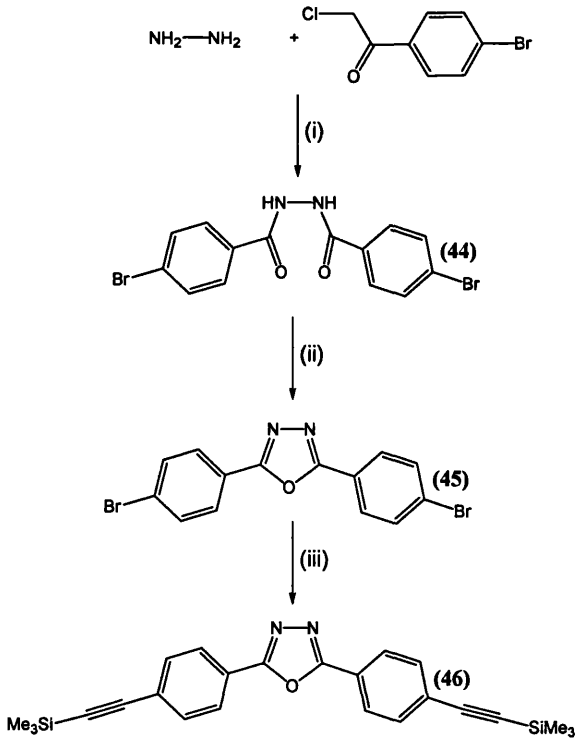

Figure 3.18 Synthesis of (46). Reagents and conditions: (i) pyridine, Δ (ii) $POCl_3$, Δ (iii) Me_3SiCCH, $^iPr_2NH$, $Pd(PPh_3)_2Cl_2$, CuI, THF.

4-Bromobenzoyl chloride was reacted with hydrazine hydrate in pyridine under reflux for 1 hour. The reaction was then cooled and treated with water to precipitate the by-products, and the filtrate evaporated to low volume to give a white crude product which was recrystallised from toluene to give a translucent white solid.[33] A yield of 60% was achieved and the product was analytically pure and subsequently characterised by ^{1}H NMR spectroscopy and elemental analysis.

The next step in the reaction scheme was to form the central oxadiazole ring. This was achieved by heating **(44)** with phosphorus oxychloride under reflux overnight. The excess phosphorus oxychloride was then removed by distillation, and the remaining sample was treated with water to decay any remaining phosphorous oxychloride. The organic phase was then separated and dried giving the crude product which was recrystallised from ethanol to give **(45)** as colourless crystals (94%).

(45) was then reacted to replace the terminal bromides with trimethylsilylacetylene groups. This reaction process follows that previously described (see Figure 3.6), using the palladium catalysed cycle, and was determined complete after 24 hours by TLC. A standard Sonogashira coupling reaction work-up, followed by washing the crude product with ethyl acetate, produced **(46)** in 93% yield.

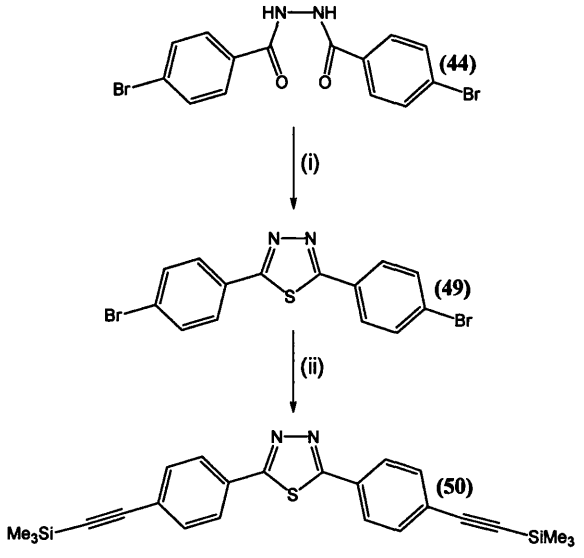

Figure 3.19 Synthesis of the thiadiazole ligand (50).

Reagents and conditions: (i) P_4S_{10}, xylene, Δ (ii) Me_3SiCCH, $^iPr_2NH$, $Pd(PPh_3)_2Cl_2$, CuI, THF.

The cyclisation was carried out in accordance with the method described by Stolle *et al*, whereby the 1-benoyl-2(4-bromobenzoyl)hydrazine was reacted with phosphorus pentasulphide in xylene under reflux.[34] After 14 hours the solution was cooled to room temperature and water added dropwise before the solution was reheated. The solution was then allowed to cool to room temperature again and its pH neutralised using sodium hydrogen carbonate. The volatiles were then removed to yield a brown solid which was recrystallised from xylene to give the pure product as a white powder. A yield of 76% was achieved for **(49)** and the product was characterised by NMR spectroscopy and elemental analysis.

The next step of the sequence was achieved using the palladium catalysed method described previously to give **(50)**. Work up of the product was carried out in the same manner as employed for the oxadiazole analogue. A yield of 76% was achieved and the product was characterised by NMR and IR spectroscopy in addition to elemental analysis.

Synthesis of the selenadiazole compound was attempted following the reported literature preparation,[35] shown in Figure 3.20.

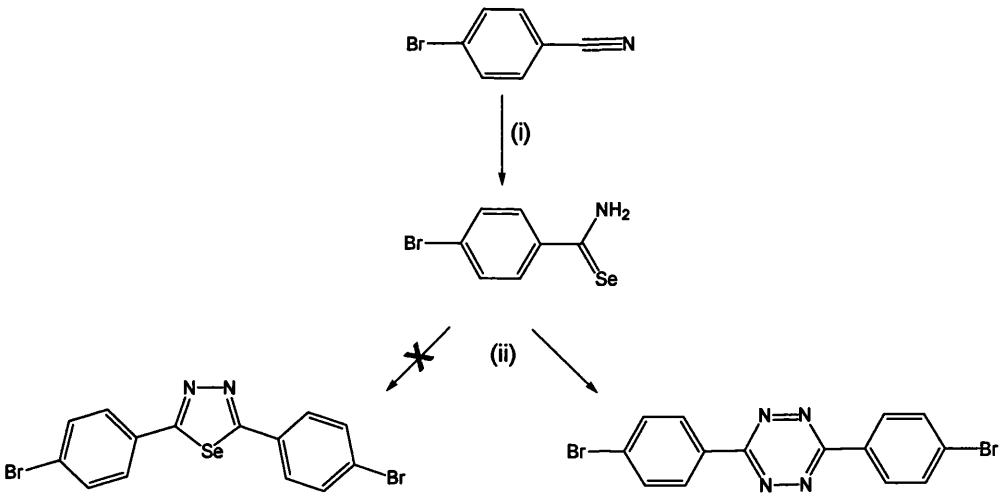

Figure 3.20 Attempted synthesis of 2,5-*Bis*-(4-bromo-phenyl)-[1,3,4]selenadiazole
Reagents and conditions: (i) Se, $NaBH_4$, pyridine, 2M HCl (ii) N_2H_4, MeOH.

The reaction of 4-bromobenzonitrile to 4-bromo-selenobenzamide proceeded well, using published methods.[36] However, the cyclisation of this product to form the selenadiazole compound did not proceed as expected, with the reaction of 4-bromo-

selenobenzamide with hydrazine in methanol at room temperature, giving an insoluble pink solid, believed to be 3,6-*bis*-(4-bromo-phenyl)-[1,2,4,5]tetrazine.

The oxadiazole and thiadiazole ligands were converted to their corresponding platinum complexes as outlined in Figure 3.21. The method for synthesising the terminal alkynes **(47)** and **(51)** and the platinum complexes **(48)** and **(52)** were the same as previously discussed in this Chapter.

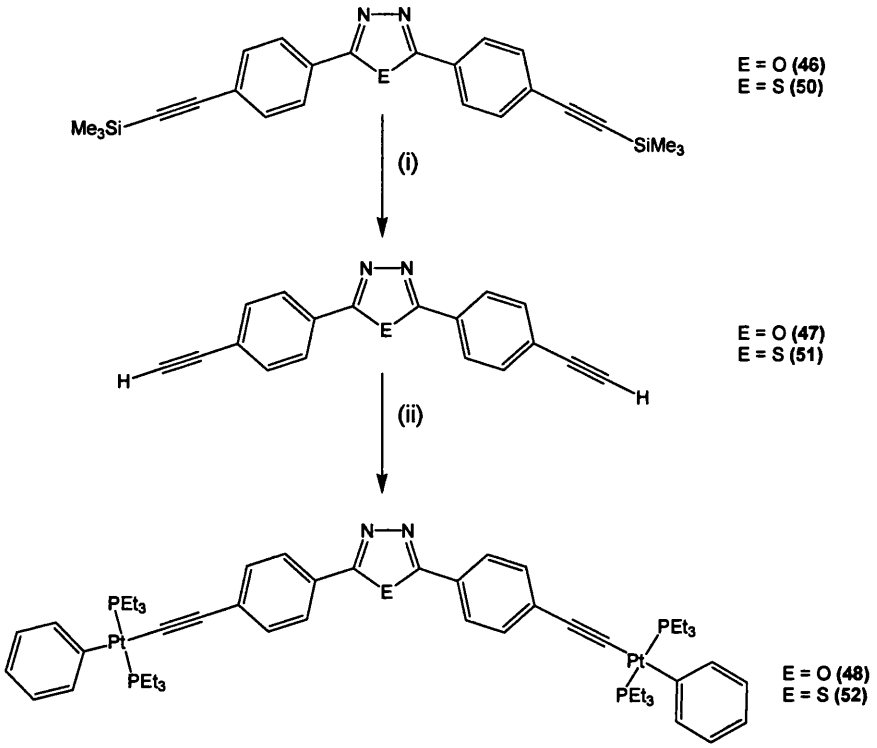

Figure 3.21 Synthesis of (48) and (52) where E = O or S.
Reagents and conditions: (i) $KOH_{(aq)}$, $MeOH/CH_2Cl_2$ (ii) $PhPt(PEt_3)_2Cl$, CuI, $^iPr_2NH$, CH_2Cl_2.

3.2.9 UV-visible spectroscopic studies of complexes (48) and (52)

The solution phase photophysical properties of **(48)** and **(52)** were investigated as 0.01 mM dichloromethane solutions at room temperature. The electronic absorption spectra were first determined, followed by emission spectra after exciting the corresponding sample at its absorption maxima wavelength, 366 and 384 nm for **(48)** and **(52)**, respectively. Figure 3.22 shows the UV-visible absorption and emission spectra of the di-platinum complexes **(48)** and **(52)**. The oxadiazole complex **(48)** displays one main absorbance band at 366 nm, with an onset of absorption at 432 nm

(2.88 eV). The thiadiazole complex **(52)** exhibits a maxima at 384 nm, with an onset of absorption at 458 nm (2.71 eV).

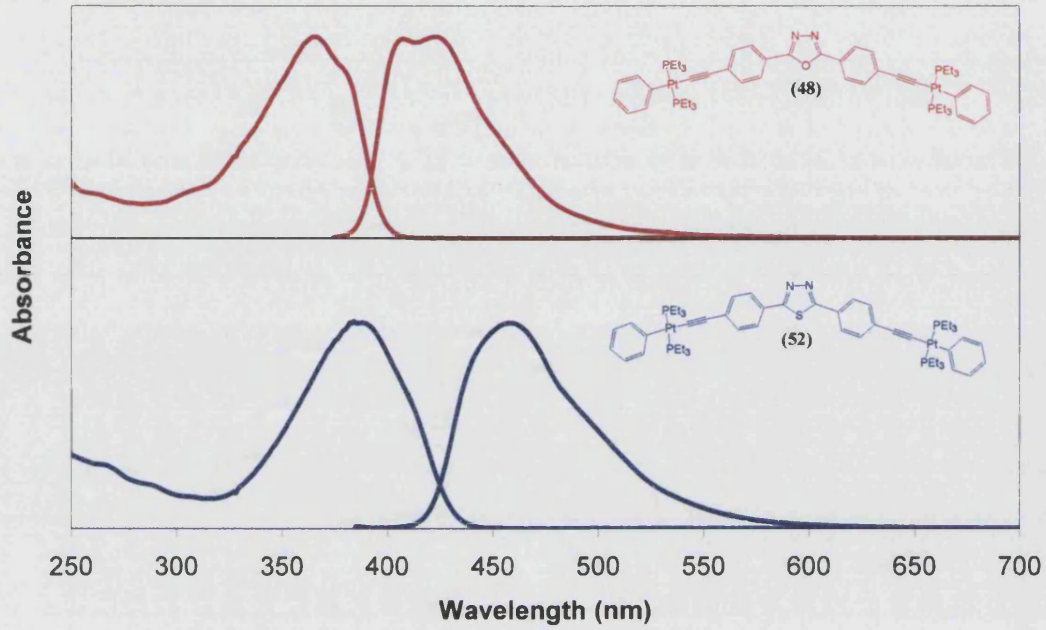

Figure 3.22 UV-visible absorption and emission spectra of platinum complexes (48) and (52).

The emission spectra for complexes **(48)** and **(52)** both show strong emission bands, with the oxadiazole complex **(48)** displaying two maxima at 407 and 423 nm, while complex **(52)** displays a broader emission spectrum with a maximum around 458 nm.

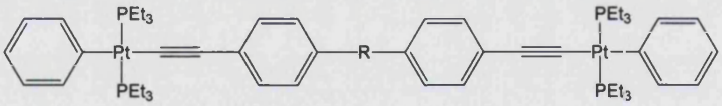

R=	Onset of absorption (nm) (eV)	λ_{max} (nm)	ε ($dm^3mol^{-1}cm^{-1}$)
	439 2.83	375	75,300
	462 2.69	388	77,300
	432 2.88	366	95,000
	458 2.71	384	94,000

Table 3.5 Table of UV-visible data for (22), (26), (48) and (52).

The spectroscopic data is summarised in Table 3.5 along with the data for the furan and thiophene analogues for comparison.

3.2.10 DFT calculational studies of compounds (47) and (51)

To investigate further the electronic structures of the diazole- containing ligands **(47)** and **(51)**, DFT calculations were carried out as previously seen in Section 3.2.4. The Gaussian03 program was used,[28] employing the B3LYP functional[29,30,31] in conjunction with the 6–31G* basis set.[32] The energies of the HOMOs and LUMOs are given in Table 3.6 along with the previously discussed values for the furan and thiophene analogues.

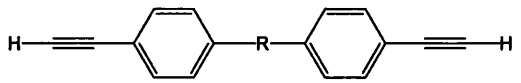

R=	Symmetry	HOMO (eV)	LUMO (eV)	Optical Gap (eV)	Dihedral Angle (°)
	C_{2v}	-5.28	-1.74	3.33	0
	C_{2v}	-5.39	-1.94	3.23	0
	C_2	-5.46	-1.83	3.36	22.4
	C_{2v}	-6.06	-2.08	3.66	0
	C_{2v}	-6.02	-2.29	3.42	0

Table 3.6 DFT calculational results obtained for ligands (21), (25) (47) and (51).

Firstly the geometry optimisation calculations showed that the thiadiazole- and oxadiazole- containing ligands choose to adopt a planar geometry (C_{2v} symmetry), with no further energy stabilisation gained from adopting a 'twisted' structure (C_2 symmetry) as was seen for the thiophene- containing analogue (Section 3.2.4). It is also worth noting that the calculations predict a higher optical gap for the diazole-containing ligands when compared to the chalcogenophene analogues. This was observed experimentally in the UV-visible studies of the corresponding Pt(II) complexes in Section 3.2.3.

3.2.11 Synthetic details for the dicarbonyl compounds (53) – (55) and UV-visible studies of (55)

During the synthesis of the furan complex **(22)** decomposition was observed for the platinum complex. It was proposed that one of the decomposition products was the ring opened furan, dicarbonyl complex **(55)**. To investigate this hypothesis the dicarbonyl complex was synthesised, as outlined in Figure 3.23. The product would also serve as a good comparison with the furan complex **(22)** in order to investigate how the loss in conjugation of the open system of **(55)** affects the photophysical properties.

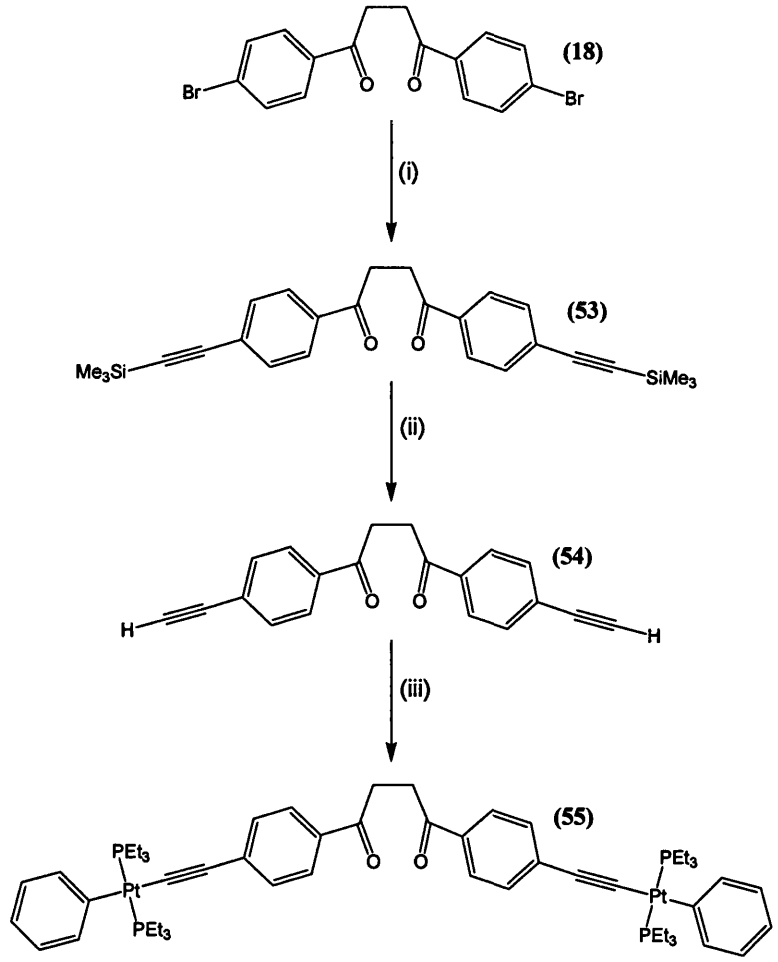

Figure 3.23 Synthesis of the platinum complex (55). Reagents and conditions: (i) Me_3SiCCH, $Pd(PPh_3)_2Cl_2$, CuI, $^iPr_2NH$, CH_2Cl_2 (ii) $KOH_{(aq)}$, $MeOH/CH_2Cl_2$ (iii) $PhPt(PEt_3)_2Cl$, CuI, $^iPr_2NH$, CH_2Cl_2.

Figure 3.24 displays the UV-visible absorption and emission spectra of complexes **(22)** and **(55)**. The di-carbonyl complex displays a broad absorption band commencing at 400 nm (3.11 eV), compared to the closed furan which commences at 439 nm (2.83

eV). The large difference in the onset of absorption is due to the loss of conjugation at the CH_2 position of the di-carbonyl. This results in a larger optical gap and, therefore, a shift to lower wavelength.

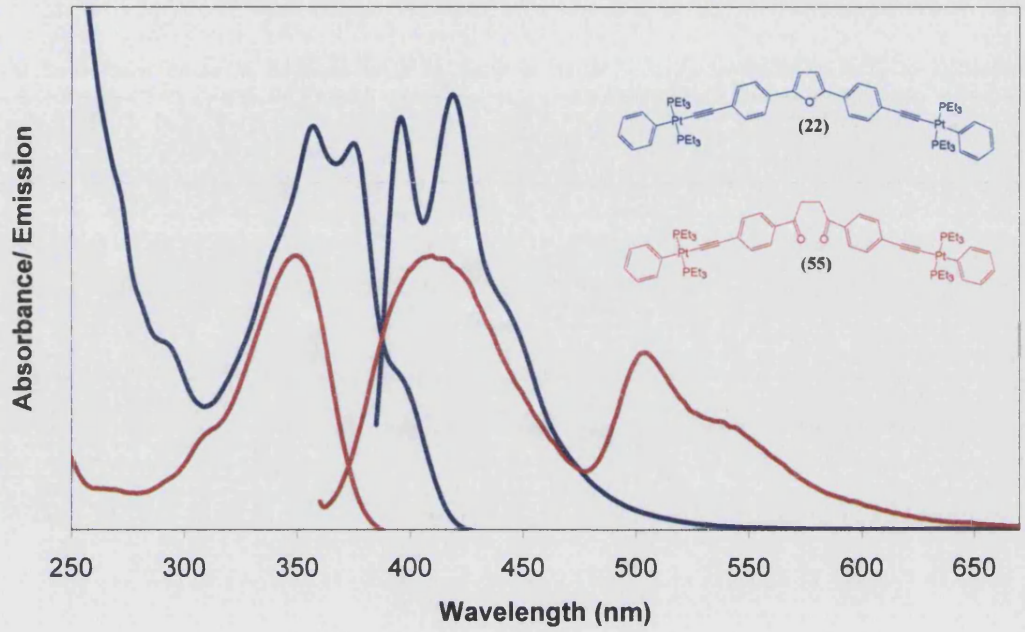

Figure 3.24 UV-visible absorption and emission spectra of platinum complexes (22) and (55).

The emission spectra are shown in Figure 3.24. Complex **(55)** displays a much broader spectrum with two distinct maxima at 409 and 504 nm, with an energy spacing between these two bands of 0.78 eV. The existence of the second band at 504 nm is tentatively assigned to the emission from an excimer formed in solution.[37]

3.2.12 Synthetic details for the gold(I) systems (56) and (57) and UV-visible spectroscopic studies

The effect of changing the metal centre on the photophysical properties of the system was the motivation for this section of research. Two di-ethynyl ligands were chosen, **(31)** and **(47),** which were previously complexed to Pt metal centres, to be used in the synthesis of gold(I) complexes. Ligand **(31)** 2,5-di-(4-ethynyl-phenyl)-selenophene was chosen because this is believed to have the greatest dihedral angle between adjacent rings, and ligand **(47)** was chosen as this is believed to have the most planar structure. Secondly, gold was the metal of choice as there is a possibility of an extended array or polymeric structure for the gold complexes *via* Au···Au interactions.[38]

The ligands were reacted with triphenylphosphine gold chloride in methanol and an excess of sodium methoxide. Both reactions produced a precipitate, which was the crude product and was filtered and washed with methanol, and the solid was recrystallised from ethanol/chloroform mixtures. The general reaction scheme is shown in Figure 3.25.

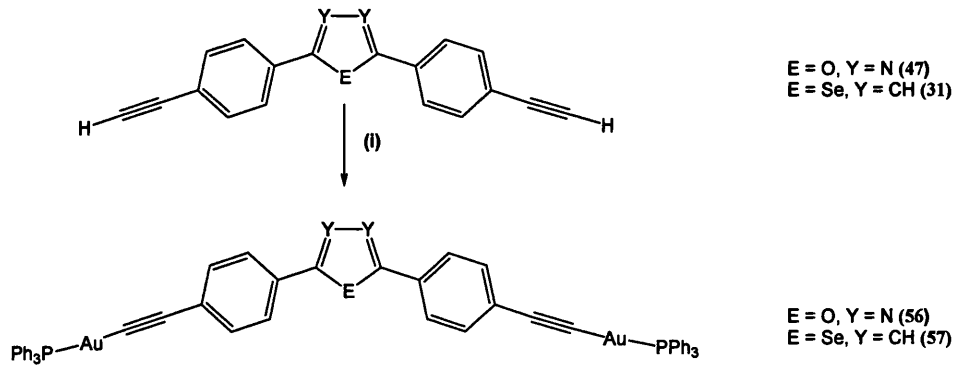

Figure 3.25 Synthesis of gold complexes (56) and (57). Reagents and conditions: (i) Ph_3PAuCl, NaOMe, MeOH.

Both gold(I) complexes were characterised by multinuclear NMR spectroscopy with ^{31}P NMR spectra exhibiting single resonances at 42.31 and 42.46 ppm for **(56)** and **(57),** respectively. This compares well with related alkynyl- triphenylphosphine gold (I) complexes in the literature.[39]

The UV-visible absorption and emission spectra of **(56)** and **(57)** were determined as 0.01 mM dichloromethane solutions. A comparison between the UV-visible spectra of the platinum and gold complexes of ligand **(31)** is provided in Figure 3.26. The spectra provide evidence that the absorbance and emission properties of these systems are ligand based, as both gold and platinum complexes display the same characteristics with an energy shift.

The absorption spectra of **(32)** and **(57)** show maxima at 397 nm and 376 nm, respectively. The onset of absorption has also shifted to lower energy for the platinum complex compared to the gold complex, with a value of 444 nm (2.80 eV) observed for the gold complex and 467 nm (2.66 eV) for the platinum complex. These wavelengths correspond to a drop in optical gap energy of 0.14 eV for the platinum complex when compared to that of the gold complex. This result suggests that there is a better degree of orbital interaction for the platinum orbitals with the alkynyl ligand orbitals, than found between the gold and the alkyne in the analogous complex. This increased interaction mediates a greater degree of delocalisation across the system and hence a drop in band gap energy.

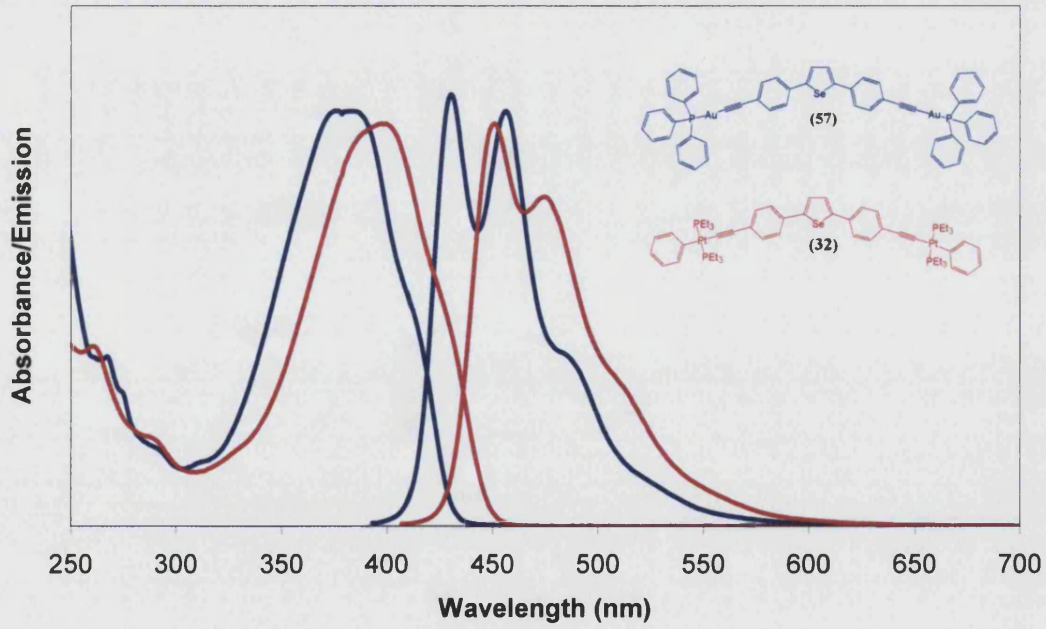

Figure 3.26 UV-visible absorption and emission spectra of the gold complex (57) and the platinum complex (32).

The emission spectra of **(32)** and **(57)** display strong vibronic structural bands. The platinum complex shows maxima at 451 and 475 nm, with an energy separation of ~1120 cm^{-1} between them, while the gold complex has maxima at 430 and 456 nm, with an energy separation of ~1330 cm^{-1} between them.

UV-visible absorption and emission spectra were collected for complex **(56)**, with an excitation wavelength of 341 nm for the emission spectrum. Similar behaviour was observed when comparing the gold complex with the analogous platinum complex **(48)** of the same ligand. The gold complex **(56)** displays an absorption band maximising at 341 nm, with absorption commencing at 381 nm corresponding to an optical gap energy of 3.26 eV. This optical gap energy is 0.38 eV higher than the related platinum complex, confirming the previously seen result of a better orbital interaction between the alkyne ligand and platinum, than found between the alkyne ligand and gold.

The solution phase photophysical properties of the terminal alkyne ligand **(47)** can also be compared with the gold(I) complex **(56)**, with the ligand absorption spectra maximising at 308 nm and the gold(I) complex at 341 nm.

The emission spectrum displays two main bands at 369 and 389 nm. The energy difference between these two bands equates to ~1390 cm^{-1}.

3.3 NMR Studies of Chalcogenophene- Containing Platinum(II) and Gold(I) Complexes

3.3.1 ^{1}H NMR Spectroscopy

For analogous ligands and complexes, where the chalcogen is the only variant in the system, the ^{1}H NMR spectra are very similar to each other, except that the C*H* resonance on the backbone of the heterocycle is observed to vary. Table 3.7 gives the CH resonances of these compounds.

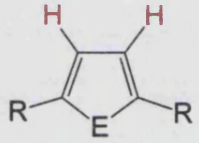

R =	E =	^{1}H NMR (ppm)
BrC_6H_4-	O	6.74
$TMSCCC_6H_4$-	O	6.77
$HCCC_6H_4$-	O	6.79
$PhPt(PEt_3)_2CCC_6H_4$-	O	6.77
$PhPt(PEt_3)_2CC$-	O	6.04
BrC_6H_4-	S	7.27
$TMSCCC_6H_4$-	S	7.31
$HCCC_6H_4$-	S	7.20
$PhPt(PEt_3)_2CCC_6H_4$-	S	7.21
$PhPt(PEt_3)_2CC$-	S	6.61
IC_6H_4-	Se	7.43
$TMSCCC_6H_4$-	Se	7.47
$HCCC_6H_4$-	Se	7.40
$PhPt(PEt_3)_2CCC_6H_4$-	Se	7.37
$PhPt(PEt_3)_2CC$-	Se	6.75

Table 3.7 Selected ^{1}H NMR spectroscopic data.

In all cases the heavier chalcogen containing compound displayed a higher ppm proton resonance on the backbone of the heterocycle. This is thought to be due to the change in the orientation of the chalcogenophene ring.

^{1}H NMR spectra of the platinum complexes, alkyl groups on the phosphines exhibit complex multiplets or broad resonances due to ^{1}H-^{1}H and ^{1}H-^{31}P coupling. In many

platinum complexes the *ortho* protons of the *Ph*-Pt groups were coupled not only to the *meta* protons on the arene ring but also to the spin active ^{195}Pt nuclei with a coupling constant of $^{3}J_{PtH} \approx 40$Hz.

3.3.2 ^{13}C NMR Spectroscopy

Assignment of ^{13}C resonance positions were aided by the use of PENDANT NMR experiments.

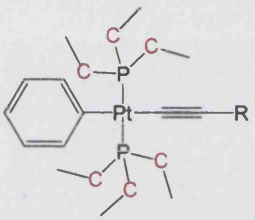

Spectral data for platinum complexes showed ^{31}P-^{13}C coupling in the CH_2 groups of the alkyl phosphine auxiliary ligands. This is a type of virtual coupling[40] which occurs when $^{2}J_{PP}$ is large relative to $^{1}J_{PC} + {}^{3}J_{PC}$, which is normally the case for *trans-bis*-phosphine complexes. The carbon nuclei then appear to be coupled equally to both phosphorus nuclei, and an apparent triplet is observed. The $^{1}J_{PC} + {}^{3}J_{PC}$ coupling constants for these complexes are all in the region of 30-35 Hz. However, when two phosphorus ligands are equivalent and are mutually *cis*, $^{2}J_{PP}$ is small and therefore only a doublet is observed. This behaviour has in the past proved to be a valuable tool in determining the stereochemistry of phosphorus complexes of Os^{II}, Ru^{II}, Rh^{II}, Ir^{II}, Pt^{II}, Pd^{II}, Pd^{IV}, and Pd^{IV}.[41]

The gold(I) complexes also exhibit ^{31}P-^{13}C coupling for all the CH carbons of the phenyl ring on the triphenyl phosphine auxiliary ligand. Typical values are shown for the selenophene containing gold complex **(57)** below.

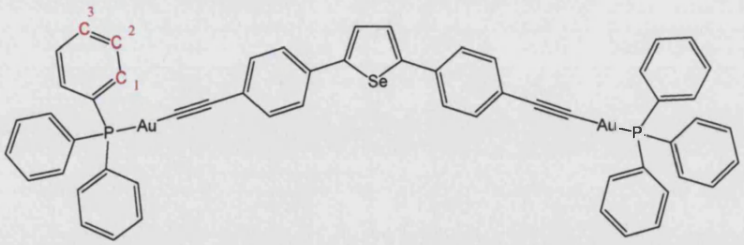

Carbon	^{13}C NMR resonance position (ppm)	Coupling Constant (Hz)
C_1	134.3	$^{2}J_{PC} = 14.1$
C_2	129.2	$^{3}J_{PC} = 11.1$
C_3	131.6	$^{4}J_{PC} = 2.1$

Table 3.8 Selected ^{13}C NMR spectroscopic data for (57).

Another important feature of the ^{13}C NMR spectral data collected for this series of compounds is the resonance positions of the *ipso* carbons on the heterocycles (given in Table 3.9).

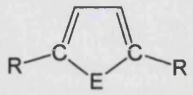

R =	E =	^{13}C NMR (ppm)
$TMSCCC_6H_4$-	O	153.50
$HCCC_6H_4$-	O	153.44
$PhPt(PEt_3)_2CCC_6H_4$-	O	153.21
$PhPt(PEt_3)_2CC$-	O	*absent*
$TMSCCC_6H_4$-	S	143.73
$HCCC_6H_4$-	S	134.75
$PhPt(PEt_3)_2CCC_6H_4$-	S	132.21
$PhPt(PEt_3)_2CC$-	S	126.80
$TMSCCC_6H_4$-	Se	136.08
$HCCC_6H_4$-	Se	136.42
$PhPt(PEt_3)_2CCC_6H_4$-	Se	132.54
$PhPt(PEt_3)_2CC$-	Se	131.52

Table 3.9 Selected ^{13}C NMR spectroscopic data.

The trend for each related compound in Table 3.9 shows that in all cases the heavier chalcogen containing compound displayed a higher ppm carbon resonance for the *ipso* carbon of the heterocycle. This is due to the greater electronegative heteroatoms, at the top of the group, inducing less of a shielding effect on the magnetic environment of the carbon being observed.

3.3.3 ^{31}P NMR Spectroscopy

The ^{31}P NMR spectral data of all the platinum complexes, shown in Table 3.10, show that the phosphines are in a *trans* arrangement around the platinum centre giving rise to a square planar geometry.[42,43] Due to the symmetry of the complexes all four phosphorus nuclei are equivalent giving rise to a single resonance. The presence of ^{195}Pt, which has a natural abundance of 33.8% and a spin quantum number of ½, gives rise to satellites around the central resonance. The $^{1}J_{PtP}$ coupling constants are quoted in Table 3.10. The values are all in the region of 2350-2650 Hz confirming

the *trans* arrangement. The values for the mono heterocyclic complexes are at the lower end of this range indicating the lower degree of conjugation through these systems.

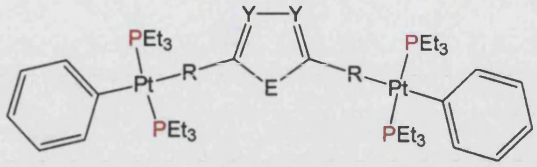

R =	E =	Y =	δ (^{31}P) (ppm)	$^{1}J_{PtP}$ (Hz)
-C≡C- **(36)**	O	CH	10.04	2361
-C≡C-C_6H_4- **(22)**	O	CH	9.99	2638
-C≡C-C_6H_4- **(48)**	O	N	10.20	2629
-C≡C- **(40)**	S	CH	10.09	2365
-C≡C-C_6H_4- **(26)**	S	CH	10.00	2638
-C≡C-C_6H_4- **(52)**	S	N	10.12	2630
-C≡C- **(43)**	Se	CH	10.13	2365
-C≡C-C_6H_4- **(32)**	Se	CH	10.01	2639

Table 3.10 Selected ^{31}P NMR spectroscopic data.

It can be noted that for all the "one- ring" chalcogenophene containing complexes (**(36)**, **(40)** and **(43)**) the $^{1}J_{PtP}$ coupling constants are in the range of 2361-2365 Hz. The "three- ring" chalcogenophene containing complexes (**(22)**, **(26)**, **(32)**, **(48)** and **(52)**) give rise higher $^{1}J_{PtP}$ coupling constants in the range of 2629-2639 Hz.

Changing the chalcogen down a series of analogous complexes has proved to have little effect on the phosphorus environment of the system.

3.3.4 Group 16 NMR Spectroscopy

To probe the nuclear environment of the new compounds synthesised in this Chapter it was decided to examine the NMR spectra of the spin active chalcogen within the molecules. The ^{17}O isotope of oxygen with a nuclear spin of 5/2 has an extremely low sensitivity of 1.10×10^{-5} (relative to ^{1}H = 1) and a low natural abundance of 0.037%.[41] For these reasons no ^{17}O NMR spectra were recorded. The low sensitivity (2.26×10^{-3}

– relative to ^{1}H = 1) and the resulting very broad signals due to the quadrupolar moment are the two main reasons why no ^{33}S NMR spectra were recorded.[41]

^{77}Se nuclei are of moderate NMR receptivity with relative natural abundances of 7.58%, meaning ^{77}Se NMR spectra were able to be collected for all Se containing compounds in this Chapter. It should be noted that variations up to *ca* 10 ppm with solvent and temperature can occur for ^{77}Se NMR and 20 ppm for ^{125}Te NMR. All ^{77}Se spectra were collected in deutero chloroform and at 298 K therefore all data are comparable.

The ^{77}Se NMR spectra proved to be extremely useful in the identification of the components of unseparated reaction mixtures for the ligands in this study. Much like ^{31}P NMR spectra were used in the identification of purified metal complexes containing phosphine ligands, a single signal in the $^{77}Se\{^{1}H\}$ NMR spectra indicated a pure single product for the selenophene containing ligands. The ^{77}Se NMR spectra were referenced to selenophene as an external standard (δ = 605.0 ppm) and the spectra were obtained at the operating frequency of 76.36 MHz; 30° pulses were used with an acquisition time of 0.85 s and a 5 s delay time.

Table 3.11 details the resonance positions and coupling constants obtained from the compounds synthesised for this study. All experiments were carried out in deutero-chloroform at 298 K. Coupling constants to nuclei such as proton, ^{13}C and ^{31}P are normally obtained from the positions of the satellites in the spectra of these nuclei. All selenium-proton coupling constants obtained for Table 3.9 were calculated from non-decoupled ^{77}Se NMR spectra.

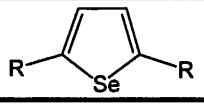

R	^{77}Se NMR (ppm)	$^{3}J_{SeH}$ (Hz)
-H	605.0	9.4
-Br	730.1	8.3
-C≡CSiMe$_3$	758.9	7.0
-C≡CH	761.2	8.3
-C≡CPt(PEt$_3$)$_2$(Ph)	709.0	7.5
-C$_6$H$_4$SiMe$_3$	572.6	8.5
-C$_6$H$_4$I	574.4	8.4
-C$_6$H$_4$C≡CSiMe$_3$	573.0	6.2
-C$_6$H$_4$C≡CH	574.8	5.9
-C$_6$H$_4$C≡CPt(PEt$_3$)$_2$(Ph)	563.2	6.0
-C$_6$H$_4$C≡CAu(PPh$_3$)	568.0	5.8

Table 3.11 Selected ^{77}Se NMR spectroscopic data.

The data shows a large shift in the resonance position of the ^{77}Se NMR from selenophene at 605.0 ppm to 761.2 ppm for the diethynyl-selenophene ligand **(42)**. It is also clear that for the compounds containing phenyl rings at the 2- and 5- positions on the selenophene a large upfield shift of over 100 ppm is observed when compared to the "one- ring" analogues. This is due to the extra shielding effects of the aromatic system.

3.4 Molecular structures determined by X-ray crystallography

Where suitable single crystals were obtained of X-ray diffraction quality, the molecular structures were determined. The solid state structures were sought after, so that the orientation of the arene rings in the central spacer ligand could be defined. The orientation of the rings in relation to the square planes of the platinum centres was also of interest, as this could have some correlation to the photophysical properties of the systems.

The molecular structure of **(36)** was determined by X-ray crystallography from a single crystal obtained from an ethanolic solution and is shown in Figure 3.27. Selected bond lengths and angles are provided in Table 3.12, with crystallographic data provided in Appendix 1.

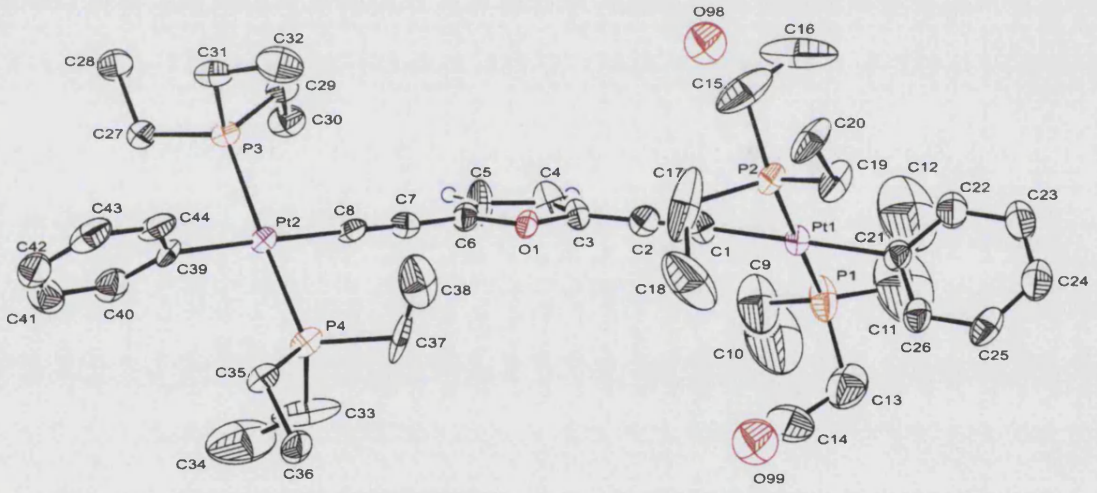

Figure 3.27 Molecular structure of (36) depicted with a 50% ellipsoid probability. Hydrogen atoms have been omitted for clarity, except for those on the furan ligand which are shown in blue.

The molecular structure of **(36)** consists of discrete di-nuclear molecules in which the platinum atoms are surrounded by four ligands in a square planar geometry with the two phosphines in a *trans* arrangement. The structure is disordered in the four ethyl groups, with occupancy distributed over two sites (60:40). Excess electron density was accounted for as partial oxygen atoms (O_{98} and O_{99}), this is believed to be water molecules which are present from the crystallisation solvent. The bond lengths and bond angles around the metal centre are comparable to similar di-platinum di-yne complexes characterised previously within the group and this Thesis. The plane of the furan ring (C_3, C_4, C_5, C_6, O_1) makes an angle of 42.99(12)° with the square plane

of the platinum centre (Pt_1, P_1, P_2, C_1, C_{21}) and an angle of 52.16(15)° with the square plane of the platinum centre (Pt_2, P_3, P_4, C_8, C_{39}).

Bond Lengths (Å)		Bond Angles (°)	
Pt_1-C_1	2.013(14)	Pt_1-C_1-C_2	177.8(13)
Pt_2-C_8	2.003(13)	Pt_2-C_8-C_7	177.5(14)
Pt_1-C_{21}	2.057(13)	P_1-Pt_1-P_2	179.40(15)
Pt_2-C_{39}	2.073(12)	P_3-Pt_2-P_4	174.26(13)
Pt_1-P_1	2.282(4)	C_1-Pt_1-C_{21}	179.3(6)
Pt_1-P_2	2.287(4)	C_{39}-Pt_2-C_8	178.6(5)
Pt_2-P_3	2.298(3)	C_6-O_1-C_3	108.5(11)
Pt_2-P_4	2.291(3)	Dihedral (C_3-C_6, O_1) /(Pt_1, P_1, P_2, C_2, C_{21})	42.99(12)
C_1-C_2	1.202(18)		
C_7-C_8	1.212(17)	Dihedral (C_3-C_6, O_1) /(Pt_2, P_3, P_4, C_8, C_{39})	52.16(15)

Table 3.12 Selected bond length and bond angle data for (36).

Single crystals of **(43)** grown from an ethanolic solution were subsequently used to obtain the X-ray structure shown in Figure 3.28. Selected bond lengths and angles are provided in Figure 3.13, with crystallographic data provided in Appendix 1.

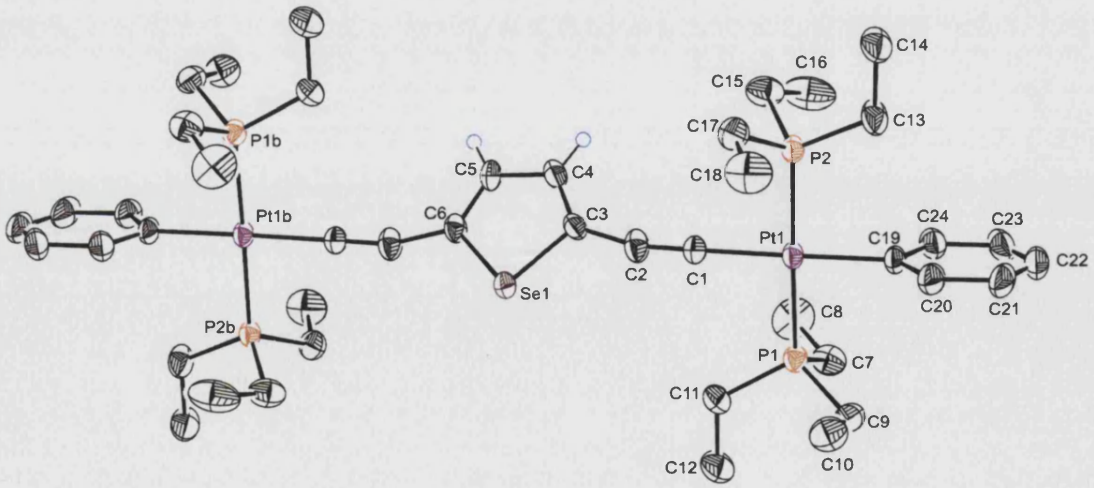

Figure 3.28 Molecular structure of (43) depicted with a 50% ellipsoid probability. Hydrogen atoms have been omitted for clarity, except for those on the selenophene ligand which are shown in blue.

The asymmetric unit contains one half of the dinuclear molecule in addition to one molecule of dichloromethane, which is omitted for clarity. The selenophene moiety straddles a crystallographic inversion centre, and hence is disordered over two sites. Only one representation is shown for clarity.

Bond Lengths (Å)		Bond Angles (°)	
Pt_1-C_1	2.010(4)	Pt_1-C_1-C_2	175.9(4)
Pt_1-C_{19}	2.057(4)	P_1-Pt_1-P_2	178.67(3)
Pt_1-P_1	2.2914(10)	C_6-Se_1-C_3	88.6(3)
Pt_1-P_2	2.2925(10)	C_1-Pt_1-C_{19}	176.75(15)
C_1-C_2	1.214(5)	Dihedral (C_3-C_6, Se_1) /(Pt_1, P_1, P_2, C_1, C_{19})	48.90(14)

Table 3.13 Selected bond length and bond angle data for (43).

The Pt_1-C_1 bond at 2.010(4) Å is similar to the values in the range of di-platinum di-yne complexes (1.96(2)-2.09(3) Å) characterised previously within the group.[44] The Pt-P distances (av. 2.29(10) Å) lie in the expected range, 2.27-2.32 Å, by comparison to other structurally characterised systems. The Pt-C_{19} distance of 2.057(4) Å falls in the previously determined range of 2.05(2)-2.09(3) Å. The plane of the selenophene ring (C_3, C_4, C_5, C_6, and Se_1) makes an angle of 48.90(14)° with the square plane of the platinum centre (Pt_1, P_1, P_2, C_1, and C_{19}).

The molecular structure of **(40)**, the thiophenyl analogue of the furyl **(36)** and selenophenyl **(43)** structures discussed in this section, has been previously reported by the Group.[26] Table 3.14 shows the bond angles of the heteroatoms in these related structures to the two adjacent carbon atoms of the heterocycles. The magnitude of the angle gives an indication of how far the heteroatom sits within the carbon framework of the heterocycle. In the furan structure **(36)** the largest angle is observed out of the three structures, this shows that the lighter chalcogen is able to sit the deepest in the heterocycle. The sulphur atom, with its larger atomic size, is pushed out further making a less obtuse angle of 95(1)° with the adjacent carbons. The selenium atom is pushed out further still, making and angle of 88.6(3)°.

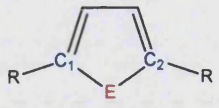

R = $CCPt(PEt_3)_2Ph$

E =	Angle (C_1-E-C_2)
O	107.2(9) °
S	95(1)°
Se	88.6(3)°

Table 3.14 Selected bond angles of complexes (36), (40) and (43).

The molecular structure of compound **(48)** is shown in Figure 3.29, which includes the atom numbering scheme. Selected bond lengths and angles shown in Figure 3.15, full crystallographic data given in Appendix 1.

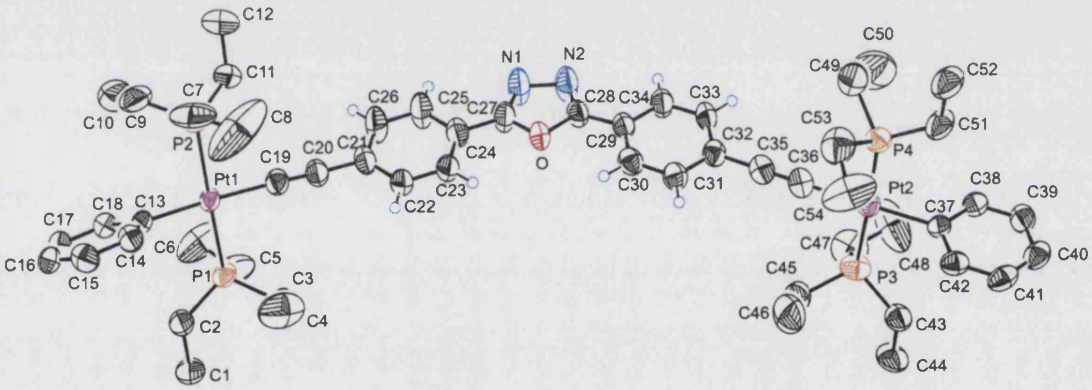

Figure 3.29 Molecular structure of (48) depicted with a 50% ellipsoid probability. Hydrogen atoms have been omitted for clarity, except for those on the di-yne ligand which are shown in blue.

The geometry around the metal centres of the molecular structure of **(48)** is closely related to the structures discussed in Chapter 2. The environment around the metal centre is essentially identical to all the other related Pt(II) complexes in this thesis, with all the bond lengths and bond angles lying in the range of previously characterised related complexes in the Group. The bond lengths and angles of the central di-yne ligand are of interest in this structure, as it is predicted that this oxadiazole ligand could give rise to the most planar molecular structure of all the related structures in this Chapter.

Bond Lengths (Å)		Bond Angles (°)	
Pt_1-C_{19}	2.022(7)	Pt_1-C_{19}-C_{20}	176.8(8)
Pt_2-C_{36}	2.015(8)	Pt_2-C_{36}-C_{35}	178.9(7)
Pt_1-P_1	2.2908(18)	P_1-Pt_1-P_2	175.13(8)
Pt_1-P_2	2.282(2)	P_3-Pt_2-P_4	176.82(8)
Pt_2-P_3	2.281(2)	C_{13}-Pt_1-C_{19}	176.2(3)
Pt_2-P_4	2.279(2)	C_{36}-Pt_2-C_{37}	178.13(8)
Pt_1-C_{13}	2.061(6)	C_{27}-O-C_{28}	102.8(6)
Pt_2-C_{37}	2.061(7)	**Dihedral Angles (°)**	
C_{19}-C_{20}	1.188(10)	$C_{21\text{-}26}$/C_{27},$N_{1\text{-}2}$,C_{28}, O	4.12(13)
C_{35}-C_{36}	1.182(10)	$C_{29\text{-}34}$/C_{27},$N_{1\text{-}2}$,C_{28}, O	5.25(13)
N_1-N_2	1.401(9)		
O-C_{27}	1.365(9)		
O-C_{28}	1.361(8)		
N_1-C_{27}	1.288(10)		
N_2-C_{28}	1.292(10)		

Table 3.15 Selected bond lengths and bond angles of complex (48).

The arene ring (C_{21}-C_{26}) and the square plane of Pt_1 metal centre is related by a dihedral angle of 64.86(10)°. The arene ring (C_{29}-C_{34}) and the square plane of Pt_2 metal centre is related by a dihedral angle of 81.35(11)°. The planar nature of the central di-yne ligand can be observed more clearly with an alternative view of the molecular structure as shown in Figure 3.30.

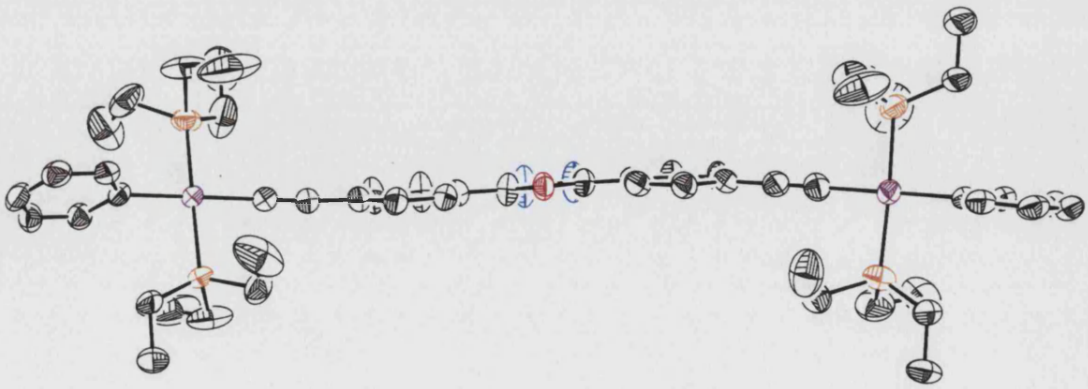

Figure 3.30 Molecular structure of (48), illustrating the near planar nature of the central di-yne ligand.

The central oxadiazole ring is related to its adjacent arene rings with angles of 4.12(13)° and 5.25(13)° for rings (C_{21}-C_{26}) and (C_{29}-C_{34}), respectively. This is the most planar structure that has been observed for all the related compounds structurally characterised in this Thesis. With this in mind, it would be expected that compound **(48)** should display the lowest optical gap energy in the UV-visible absorption spectrum. As this is not the case, one can conclude that the electronic effects of the heteroatoms in the central oxadiazole ring have a negative influence on the optical energy gap of the system.

X-ray crystallography was used to determine the molecular structure of **(52)** shown in Figure 3.31, also using single crystals obtained from an ethanolic solution. Selected bond lengths and angles are provided in Table 3.16 with crystallographic tables available in Appendix 1.

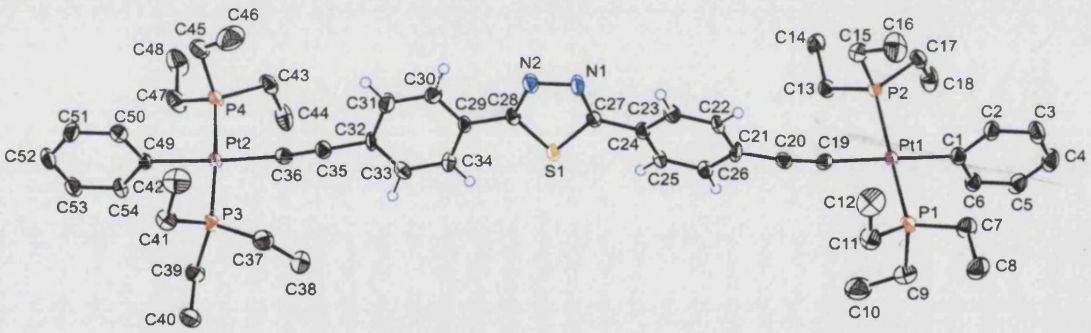

Figure 3.31 Molecular structure of (52) depicted with a 50% ellipsoid probability. Hydrogen atoms have been omitted for clarity, except for those on the di-yne ligand which are shown in blue.

The molecular structure of **(52)** is again closely related to the structures discussed in Chapter 2, with all the bond lengths and bond angles around the metal centre lying in the predetermined range as outlined in Chapter 2. The bond lengths and bond angles of the central di-yne ligand are of interest in this structure, so comparisons can be made with the analogous oxadiazole- containing complex **(48)**, and in particular how the chalcogen influences the sterics of the di-yne ligand.

Bond Lengths (Å)		Bond Angles (°)	
Pt_1-C_{19}	2.015(6)	Pt_1-C_{19}-C_{20}	173.6(5)
Pt_2-C_{36}	2.023(6)	Pt_2-C_{36}-C_{35}	174.4(6)
Pt_1-P_1	2.2863(17)	P_1-Pt_1-P_2	172.57(6)
Pt_1-P_2	2.2954(17)	P_3-Pt_2-P_4	176.89(6)
Pt_2-P_3	2.2937(16)	C_1-Pt_1-C_{19}	177.5(2)
Pt_2-P_4	2.2952(16)	C_{36}-Pt_2-C_{49}	175.3(2)
Pt_1-C_1	2.069(6)	C_{27}-S-C_{28}	87.1(3)
Pt_2-C_{49}	2.079(6)	**Dihedral Angles (°)**	
C_{19}-C_{20}	1.208(8)	$C_{21\text{-}26}$/C_{27},$N_{1\text{-}2}$,C_{28}, S	22.21(12)
C_{35}-C_{36}	1.198(8)	$C_{29\text{-}34}$/C_{27},$N_{1\text{-}2}$,C_{28}, S	6.55(11)
N_1-N_2	1.378(7)		
S_1-C_{27}	1.732(6)		
S_1-C_{28}	1.740(6)		
N_1-C_{27}	1.287(8)		
N_2-C_{28}	1.301(8)		

Table 3.16 Selected bond lengths and bond angles for complex (52)

Arene ring (C_{21}-C_{26}) and the square plane of Pt_1 metal centre is related by a dihedral angle of 83.08(15)°. Arene ring (C_{29}-C_{34}) and the square plane of Pt_2 metal centre is related by a dihedral angle of 66.96(13)°. The near planar nature of the central di-yne ligand can be observed more clearly with an alternative view of the molecular structure as shown in Figure 3.32.

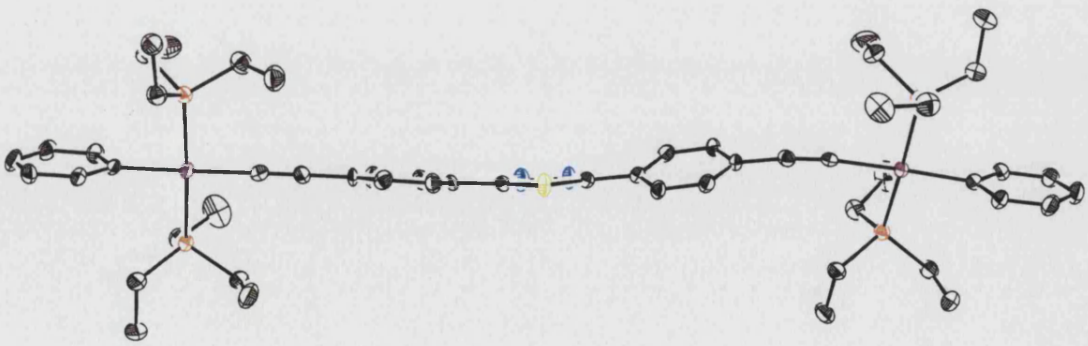

Figure 3.32 Molecular structure of (52), illustrating the near planar nature of the central di-yne ligand.

The central thiadiazole ring is related to its adjacent arene rings with angles of 22.21(12)° and 6.55(11)° for rings (C_{21}-C_{26}) and (C_{29}-C_{34}) respectively. These dihedral angles are clearly larger than the angles observed in oxadiazole- containing complex **(48)**. The larger sulphur atom is forcing the adjacent arene rings to twist slightly when compared to the oxygen derivative. This twist in the structure, however, does not influence the photophysical properties as much as the electronic effects of the heteroatom, as the optical energy gap of the thiadiazole complex is lower than the oxadiazole analogue even though it is less planar.

Single crystals of **(55)** grown from an ethanolic solution were subsequently used to obtain the X-ray structure shown in Figure 3.33. Selected bond lengths and angles are provided in Table 3.17, with the crystallographic tables presented in Appendix 1.

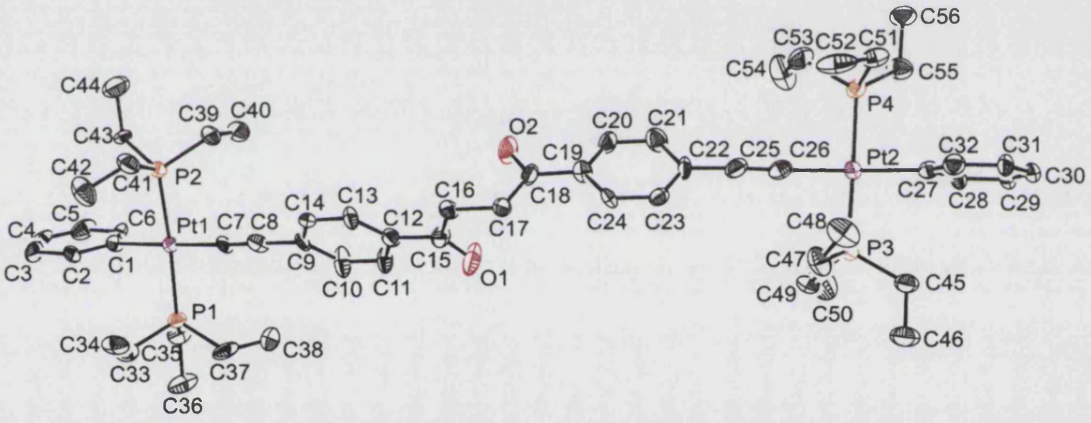

Figure 3.33 Molecular structure of (55) depicted with a 50% ellipsoid probability. Hydrogen atoms have been omitted for clarity.

All the bond lengths and bond angles around the metal centre were found to be within the range of similar structures as characterised by the Group. The bond lengths and angles of the central di-yne ligand are of interest in this structure, so the geometry of the system could be related back to the photophysical properties as studied by UV-visible spectroscopy in Section 3.2.11.

Bond Lengths (Å)		Bond Angles (°)	
Pt_1-C_7	2.026(11)	Pt_1-C_7-C_8	177.9(11)
Pt_2-C_{26}	2.006(14)	Pt_2-C_{26}-C_{25}	175.5(11)
Pt_1-P_1	2.289(3)	P_1-Pt_1-P_2	174.95(12)
Pt_1-P_2	2.286(3)	P_3-Pt_2-P_4	174.91(11)
Pt_2-P_3	2.291(3)	C_1-Pt_1-C_7	178.8(5)
Pt_2-P_4	2.296(3)	C_{26}-Pt_2-C_{27}	176.8(5)
Pt_1-C_1	2.083(11)	**Dihedral Angles (°)**	
Pt_2-C_{27}	2.066(12)	$C_{13,12,15,16}$/$C_{17,18,19,24}$	75.32(10)
C_7-C_8	1.195(16)	$C_{9\text{-}14}$/$C_{19\text{-}24}$	72.35(12)
C_{25}-C_{26}	1.212(18)		
C_{15}-O_1	1.204(15)		
C_{18}-O_2	1.230(15)		
C_{16}-C_{17}	1.513(16)		

Table 3.17 Selected bond lengths and bond angles for complex (55).

The arene ring (C_9-C_{14}) and the square plane of Pt_1 metal centre is related by a dihedral angle of 52.33(12)°. The arene ring (C_{19}-C_{24}) and the square plane of Pt_2 metal centre is related by a dihedral angle of 38.10(11)°. Arene rings (C_9-C_{14}) and (C_{19}-C_{24}) are related by a dihedral angle of 72.35(12)° which can be observed more clearly with an alternative view of the molecular structure in Figure 3.34.

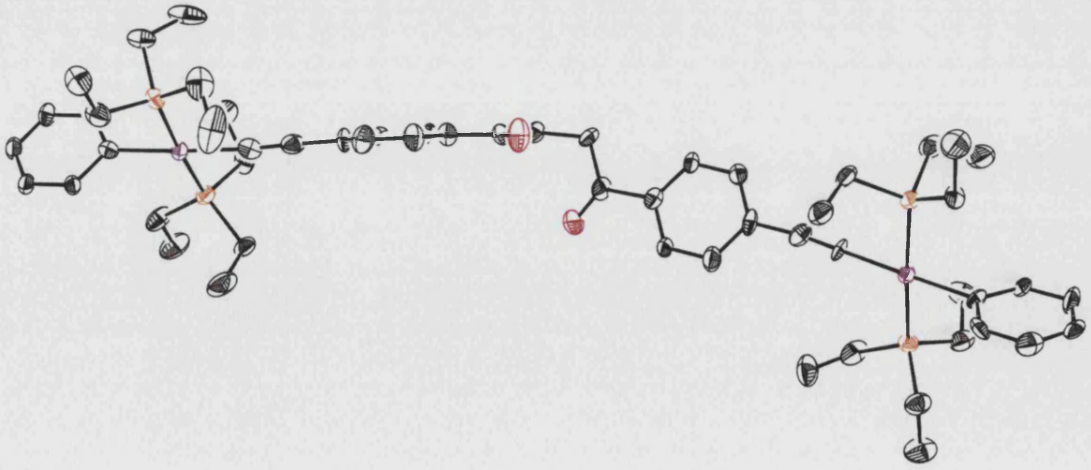

Figure 3.34 Alternative view of the molecular structure of (55).

The molecular structure of **(55)** clearly shows that the di-yne ligand is twisted by a large dihedral angle between the arene rings of the ligand. This means that the π-conjugation of the system is not possible through the entire length of molecule, and is reflected in the relatively high optical energy gap of the compound (Section 3.2.11).

The molecular structure of **(57)** is shown in Figure 3.35, which includes the atom numbering scheme. Selected bond lengths and angles shown in Table 3.18, full crystallographic data given in Appendix 1.

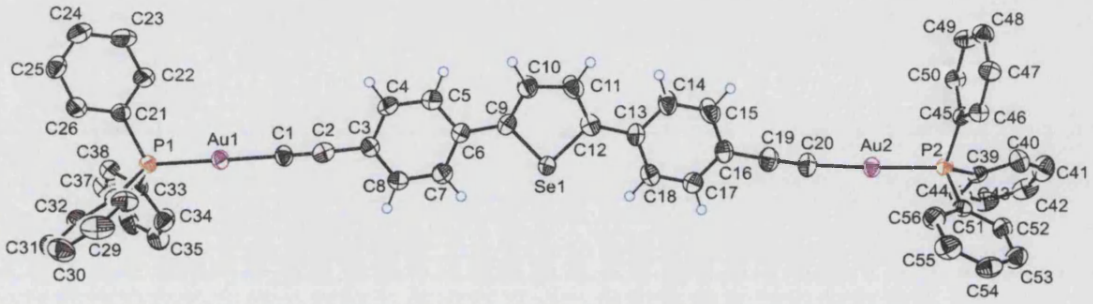

Figure 3.35 Molecular structure of (57) depicted with a 50% ellipsoid probability. Hydrogen atoms have been omitted for clarity, except for those on the di-yne ligand which are shown in blue.

Bond Lengths (Å)		**Bond Angles (°)**	
Au_1-P_1	2.2699(16)	P_1-Au_1-C_1	175.1(2)
Au_2-P_2	2.2749(16)	P_2-Au_2-C_{20}	172.9(2)
Au_1-C_1	1.969(6)	Au_1-C_1-C_2	174.8(6)
Au_2-C_{20}	2.000(9)	Au_2-C_{20}-C_{19}	170.3(6)
C_1-C_2	1.222(9)	C_9-Se-C_{12}	88.1(3)
C_{19}-C_{20}	1.214(9)	**Dihedral Angles (°)**	
		$C_{3\text{-}8}$/$C_{27\text{-}28}$,$N_{1\text{-}2}$, Se	7.61(10)
		$C_{13\text{-}18}$/$C_{27\text{-}28}$,$N_{1\text{-}2}$, Se	2.14(11)

Table 3.18 Selected bond lengths and bond angles of complex (57).

Arene ring (C_3-C_8) and the selenophene ring are related by a dihedral angle of 7.61(10)°. Arene ring (C_{13}-C_{18}) and the selenophene ring are related by a dihedral angle of 2.14(11)°. Arene rings (C_3-C_8) and (C_{13}-C_{18}) are related by a dihedral angle of 6.82(14)°. The relatively planar structure of **(57)** is some what surprising, considering the size of the heteroatom, as one would predict greater dihedral angles for the heavier chalcogenophene- containing systems.

In summary the molecular structures obtained in this Chapter have shown that the geometry of the di-yne spacer group does have an influence on the photophysical properties of the system, but this influence is far out weighed by the electronic influences of the heteroatoms within the heterocycles. For example the oxadiazole-containing complex **(48)** was shown to have the nearest to fully planar structure of the molecular structures obtained in the Chapter, but the thiadiazole- containing complex **(52)** exhibiting a less planar structure, gives rise to a lower optical energy gap than **(48)**.

3.5 Summary of Results and Conclusions

A series of new di-yne ligands incorporating chalcogenophene rings have been synthesised and characterised. All products were synthesised to moderate or high yields. The new ligands were complexed to a series of Pt(II) and Au(I) metal centres to afford dinuclear metal complexes.

The ligands and complexes synthesised within this Chapter have been characterised initially by multinuclear NMR spectroscopy followed by other analytical methods. The photophysical properties of the metal complexes in this Chapter have been investigated by solution state UV-visible absorption and emission spectroscopy. Some solid state structures, determined by single crystal X-ray diffraction, have been discussed here.

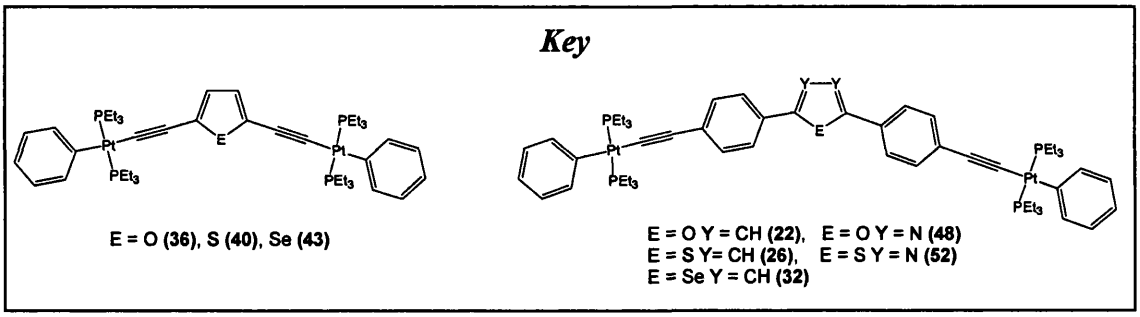

The UV-visible spectra of metal complexes **(22)**, **(26)** and **(32)** have shown that the band gaps decrease as Group 16 is descended. The difference is largest between the second and third periods, 0.14 eV, with only 0.03 eV being observed between third and fourth periods. This can be explained as second period elements have the ability to effectively hybridise s and p orbitals, unlike the remaining periods.[45] This trend is also observed for the complex series **(36)**, **(40)** and **(43)** with the difference between the second and third periods at 0.36 eV and 0.07 eV between third and fourth periods. Band gaps increase in the following order: selenophene<thiophene<furan, for the complex series [**(22)**, **(26)** and **(32)**] and [**(36)**, **(40)** and **(43)**]. This roughly reflects the trend in π-donor strengths. Weak π-donor strengths of the heteroatoms lead to small band gaps, which can be achieved by going to higher periods or to the left in the Periodic Table of a particular atom.[46]

Incorporating nitrogen into the system in the diazole complexes **(48)** (oxadiazole) and **(52)** (thiadiazole) was expected to give lower band gaps than the corresponding furan **(22)** and thiophene **(26)** complexes. This was predicted because of the planar nature of the di-yne ligands, as shown in the solid state structures reported in this Chapter. The planar structure leads to better delocalisation across the system and lowers the band gap. The nitrogen π-orbitals, however, do not interact with the system as well as the carbon π-orbitals in the furan and thiophene complexes. For this reason the optical gap of the system actually increases for the diazole systems in comparison with the furan and thiophene derivatives.

We have also shown in this Chapter how the open system of the dicarbonyl complex **(55)**, as observed in the molecular structure, gives a much broader UV-visible spectrum and higher band gap, compared with the "closed system" of the furan complex **(22)**.

The Au(I) complexes **(56)** and **(57)** have been compared to their Pt(II) analogue complexes **(48)** and **(32)** respectively. The UV-visible spectra showed that the Pt(II) complexes gave lower band gaps than the Au(I) complexes, as previously seen in the literature.[47]

3.6 References

[1] D. F. Shriver, P. W. Atkins, C. H. Langford, *Inorganic Chemistry*, Second Edition, 1998, Oxford University Press

[2] F. Fringuel, G. Marino, A. Taticchi, G. Grandoli, *J. Chem. Soc. Perkin Trans.*, 1974, **2**, 332

[4] H. Saadeh , T. Goodson , L.P. Yu, *Macromolecules*, 1997, **30**, 4608

[5] E. G. A. Notaras, N. T. Lucas, M. G. Humphrey, *Organometallics,* 2003, **22**, 3659

[6] N. T. Lucas, E. G. A. Notaras, S. Petrie, R. Stranger, M. G. Humphrey, *Organometallics,* 2003, **22**, 708

[7] N. T. Lucas, E. G. A. Notaras, M. P. Cifuentes, M. G. Humphrey, *Organometallics,* 2003, **22**, 284.

[8] J. Roncali, *Chem. Rev.*, 1997, **97**, 173

[9] G. Brocks, *J. Chem. Phys.*, 1996, **100**, 17327

[10] G. Schopf, G. Koßmehl, *Adv. Polym. Sci.*, 1997, **129**, 1

[11] J. Roncali, *Chem. Rev.*, 1992, **92**, 711

[12] R. D. McCullough, *Adv. Mater.* 1998, **10**, 93

[13] S. Glenis, M. Benz, E. LeGoff, J.L. Schindler, C.R. Kannewurf, M.G. Kanatzidis, *J. Am. Chem. Soc.*, 1993, **115**, 12519

[14] S. Inoue, H. Nakanishi, K. Takimiya, Y. Aso, T. Otsubo, *Synth. Met.*, 1997, **84**, 341

[15] T. Otsubo, S. Inoue, H. Nozoe, T. Jigami, F. Ogura, *Synth. Met.*, 1995, **69**, 537

[16] J. Stille, *Heterocycles*, 1997, **45**, 1363

[17] M. Ceylan, M. Guerdere, B. Burcu, K. Yakup, W. Secen, *Synthesis*, 2004, **11**, 1750

[18] Z. Kaleta, B. T Makowski, T. Soos, R. Dembinski, *Org. Lett.*, 2006, *8*, 1625

[19] M. A. Keegstra, L. Brandsma, *Synthesis*, 1988, **11**, 890

[21] J. Clayden, S. Warren, N. Greeves, P. Wothers, *Organic Chemistry*, 2000, Oxford University Press

[22] K. Stahl, K. Dehnicke, *J. Organomet. Chem.*, 1986, **316**, 85

[23] M. Mack, *Angew. Chem.*, 1966, **78**, 940

[24] S. Inoue, T. Jigami, H. Nozoe, T. Otsubo, F. Ogura, *Tetrahedron Lett.*, 1994, **35**, 8009

[25] M. Dolg, U. Wedig, H. Stoll, H. Preuss, *J. Chem. Phys.*,1997, **86**, 866

[26] J. Lewis, N. J. Long, P. R. Raithby, G. P. Shields, W. Y. Wong, M. Younus, *J. Chem. Soc. Dalton Trans.*, 1997, **22**, 4283

[27] D. H. Williams, I. Fleming, *Spectroscopic methods in organic chemistry*, 1989, 4th Edition, McGraw-Hill

[28] M. J. Frisch, G. W. Trucks, H. B. Schlegel, G. E. Scuseria, M. A. Robb, J. R. Cheeseman, V. G. Zakrzewski, J. A. J. Montgomery, R. E. Stratmann, J. C. Burant, S. Dapprich, J. M. Millam, A. D. Daniels, K. N. Kudin, M. C. Strain, O. Farkas, J. Tomasi, V. Barone, M. Cossi, R. Cammi, B. Mennucci, C. Pomelli, C. Adamo, S. Clifford, J. Ochterski, G. A. Petersson, P. Y. Ayala, Q. Cui, K. Morokuma, D. K. Malick, A. D. Rabuck, K. Raghavachari, J. B. Foresman, J. Cioslowski, J. V. Ortiz, A. G. Baboul, B. B. Stefanov, G. Liu, A. Liashenko, P. Piskorz, I. Komaromi, R. J. Gomperts, R. L. Martin, D. J. Fox, T. Keith, M. A. Al-Laham, C. Y. Peng, A. Nanayakkara, M. Challacombe, P. M. W. Gill, B. Johnson, W. Chen, M. W. Wong, J. L. Andres, C. Gonzalez, M. Head-Gordon, E. S. Replogle and J. A. Pople, *Gaussian 03 Version A9*, Gaussian Inc., Pittsburgh, PA, 2003

[29] A. D. Becke, *Phys. Rev. A: Gen. Phys.*, 1988, **38**, 3098

[30] A. D. Becke, *J. Chem. Phys.*, 1993, **98**, 5648

[31] C. Lee, W. Yang, R. G. Parr, *Phys. Rev. B: Condens. Matter*, 1988, **37**, 785

[32] W. J. Hehre, L. Radom, P. v. R. Schleyer, J. A. Pople, *Ab initio Molecular Orbital Theory*, John Wiley & Sons, New York, 1986

[33] L. Leonard, D. Locke, *J. Am. Chem. Soc.*, 1955, **77**, 1850

[34] S. Stolle, J. Johannissien, *J. Prakt. Chem.*, 1904, **69**, 477

[35] V. I. Cohen, *J. Heterocycl. Chem.*, 1979, **16**, 365

[36] A. Z. Al-Rubaie, L. Z. Yousif, A. J. H. Al-Hamad, *J. Organomet. Chem.*, 2002, **656**, 274

[37] C. E.Wayne, R. P. Wayne, *Photochemistry*, Oxford, University Press. 2001

[38] J. Li, P. Pyykko, *Chem. Phys. Lett.*, 1992, **197**, 586

[39] I. R. Whittall, M. G. Humprey, S. Houbrects, S. Persons, D. C. R. Hockless, *Organometallics*, 1996, **15**, 5738

[40] G. A. Morris, K. I. Smith, *J. Mag. Res.*, 1985, **65**, 506

[41] B.E. Mann, R. K. Harris, *NMR and the periodic table*, 1978

[42] S. O. Grim, R. L. Keiter,W. McFarlane, *Inorg. Chem.*, 1967, **6**, 1133

[43] B. Wrackmeyer, Z. Naturforsch., *B: Chem. Sci.*, 1991, **46**, 35.

[44] M. S. Khan, M. R. A. Al-Mandhary, M. K. Al-Suti, F. R. Al-Battashi, S. Al-Saadi, B. Ahrens, J. K. Bjernemose, M. F. Mahon, P. R. Raithby, M. Younus, N. Chawdhury, A. Kohler, E. A. Marseglia, E. Tedesco, N. Feeder, S. J. Teat, *Dalton Trans.*, 2004, **15**, 2377

[45] W Kutzelnigg. *Angew. Chem., Int. Ed. Engl.*, 1984, **23**, 272

[46] U. Salzner, J. B. Lagowski, P. G. Pickup, R. A. Poirier, *Synth. Metals*, 1998, **96**, 177

[47] J.S. Wilson, N. Chawdhury, M. R. A. Al-Mandhary, M. Younus, M. S. Khan, P. R. Raithby, A. Kohler, R. H. Friend, *J. Am. Chem. Soc.*, 2001, **123**, 9412

Chapter 4

Luminescent Pyrrole- Containing Systems

4. Luminescent Pyrrole- Containing Systems

4.1 Introduction

4.1.1 Background

The five-membered heterocyclic ring, pyrrole is shown with its numbering scheme in Figure 4.1.

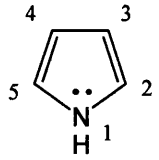

Figure 4.1 Pyrrole numbering scheme.

The nitrogen- containing heterocycle has very low basicity (pK_a = -4.2)[1] compared to amines and other aromatic compounds like pyridine (pK_a = 5.2),[2] where the ring nitrogen is not bonded to a hydrogen atom, due to the lone pair of electrons of the nitrogen atom becoming delocalised in the aromatic ring.[3]

Much like the polyphenylene systems (discussed in Chapter 2) and the polythiophene systems (discussed in Chapter 3), polypyrroles (PPy) have become widely studied as conductive polymers in the past decade.[4] Characteristics such as low oxidation potential, solubility in water of the pyrrole monomers,[5] high conductivity at room temperature,[6] as well as stability of charged samples under ambient conditions, make PPys both commercially and scientifically interesting. Conducting PPys have also shown tremendous technological potential and can be incorporated in electro-optical devices including molecular electronic devices,[7] electrocyclic capacitors,[8] actuators[9] and sensors.[10] However, the optical properties of substituted PPys, such as luminescence, decay time and quantum efficiency, have not been widely reported, perhaps due to their weak luminosity,[11] i.e poor density of luminous intensity in a given direction.

The Ono group have reported the only known pyrrole- containing di-yne as shown in Figure 4.2.[12]

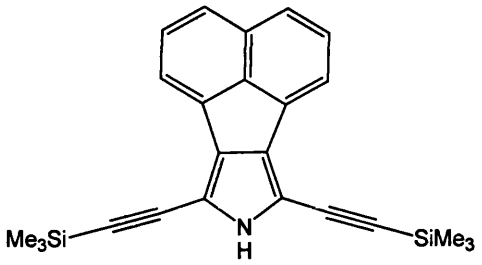

Figure 4.2 Structure of 7,9-bis-trimethylsilylethynyl-8H-acenaphtho[1,2-c]pyrrole.

This pyrrole- di-yne was used as a precursor to the synthesis of larger porphyrin-containing compounds which were studied for their luminescent properties. The electronic spectrum of the above di-yne was determined in dichloromethane solution and showed four maxima peaks at 316, 340, 390 and 416 nm. The optical gap energy of the complex was never reported.

Pyrroles have been extensively studied due to their luminescent properties as part of larger macrocyclic systems known as porphyrins. A porphyrin is a heterocyclic macrocycle made from 4 pyrrole subunits linked through 4 methine bridges, Figure 4.3.

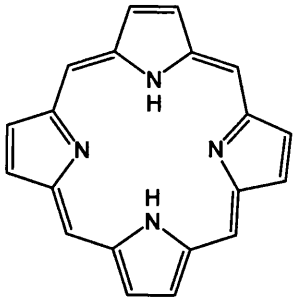

Figure 4.3 Porphyrin structure.

Porphyrins combine readily with metals, coordinating with them in the central cavity and are known collectively as metalloporphyrins. Iron- (heme), magnesium- (chlorophyll), zinc-, copper-, nickel-, and cobalt- (vitamin B12) containing porphyrins are known.[13]

The electronic spectra observed for metalloporphyrins originate from the aromatic tetrapyrrole- containing macrocycle.[14] However, the metal ion also plays a central role due to the heavy atom effect, i.e. spin-orbit coupling between the π-electrons of

the macrocycle and the electrons of the central atom.[15] The area of luminescent metalloporphyrins is very well documented, and applications of these materials include oxygen sensing,[16] and phosphoresent labelling in immunoassays.[17]

4.1.2 Objectives

The aim of this section of the research was to study the effect of incorporating a pyrrole ring into the central di-yne ligand and to make comparisons to the results obtained for the Group 16- containing heterocycles in Chapter 3. As there has been very little work published on pyrrole- containing di-ynes, and no subsequent metal complexes, this work was hoped to open up a new area of chemistry to be investigated.

A study of the effect of introducing further functional groups into the system by substituting the NH proton of the pyrrole ring with aliphatic and aromatic groups was also planned.

The drop in optical gap energy of the Group 16- containing heterocyclic systems, furan>thiophene>selenophene, in Chapter 3 was explained in terms of the trend in π-donor strengths.[18] The same theory also predicts a drop in optical gap energy as the heteroatoms are changed towards the left of the Periodic Table. It is therefore predicted that the pyrrole system will have a lower optical gap energy than its furan analogue. It should be noted, however, that this is not a direct comparison as the pyrrole ring is protonated at the 1- position, whereas the chalcogen- containing heterocycles simply have lone pairs on the heteroatoms.

4.2 Synthesis of the pyrrole containing ligands

The general syntheses of all the pyrrole- containing ligands within this Chapter were based on the Paal-Knorr synthesis of pyrroles. The Paal-Knorr Pyrrole Synthesis is the condensation of a 1,4-dicarbonyl compound with an excess of a primary amine or ammonia to give a pyrrole (Figure 4.4).[19]

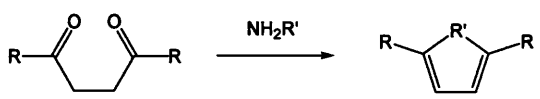

Figure 4.4 The Paal-Knorr Synthesis of Pyrroles.

To investigate how the pyrrole heterocycles affect the properties of our systems a series of pyrrole containing di-ynes were synthesised and characterised as described below. The series of ligands was designed as outlined in the retrosynthetic scheme shown in Figure 4.5.

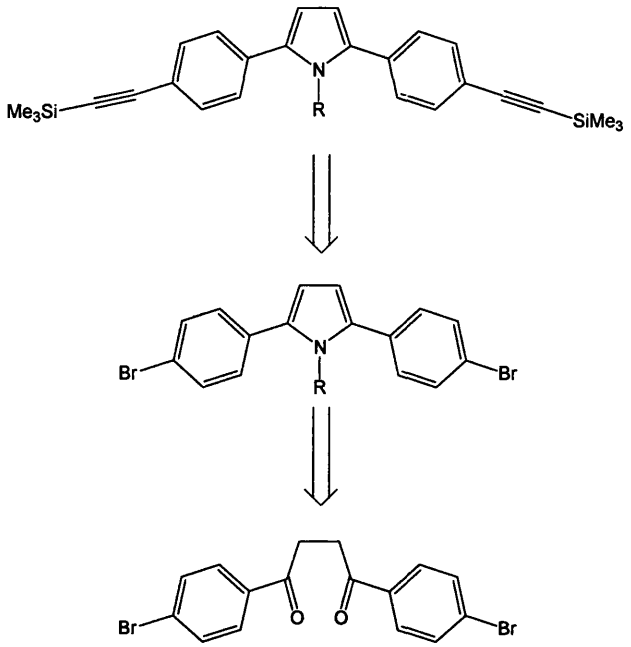

Figure 4.5 Retrosynthetic strategy towards Pyrrole- containing ligands. Where R = H, aliphatic, aromatic groups.

1,4-*di*-(4-bromo-phenyl)-butane-1,4-dione[20] **(18)** was used as the starting material for the synthesis of all the pyrroles in this Chapter. In first instance **(18)** was refluxed in an ethanolic solution of ammonium acetate for 3 h after which time the solution was concentrated to low volume to afford the pyrrole containing product, 2,5-*di*-(4-bromo-phenyl)-pyrrole **(58)** in a yield of 94%, Figure 4.6. The product has been previously reported, but was synthesised using 1,4-*bis*-(4-bromo-phenyl)-but-2-yne-1,4-dione as the starting material with a Pd/C catalyst under microwave irradiation.[21] A similar yield was reported for this synthetic route. The ^{1}H NMR spectrum of **(58)** showed a characteristic resonance at 6.57 ppm corresponding to the CH proton on the backbone of the pyrrole ring. This resonance was in fact split into a doublet by the NH proton at the 1-positon of the pyrrole, with a coupling constant of $^{4}J_{HH}$ = 2.5 Hz. Characterisation of **(58)** was supported by ^{13}C NMR spectroscopy, elemental analysis and mass spectrometry.

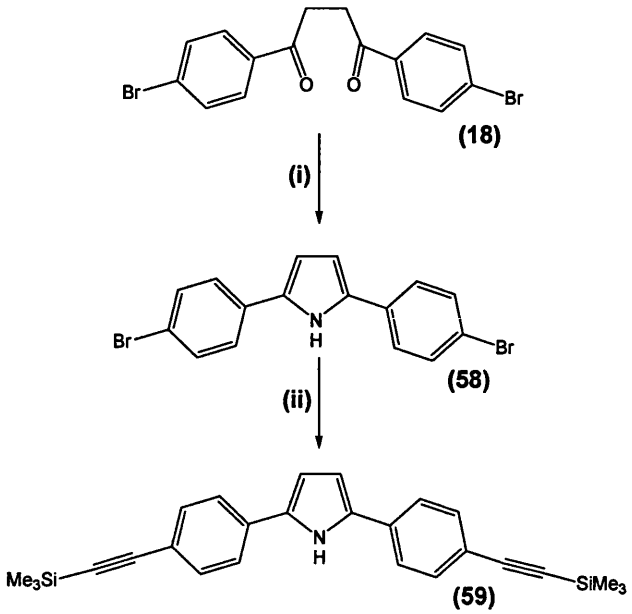

Figure 4.6 Synthesis of 2,5-*bis*-(4-trimethylsilylethynyl-phenyl)-pyrrole (59)
(i) CH_3COONH_4, EtOH, Δ (ii) Me_3SiCCH, $Pd(PPh_3)_2Cl_2$, CuI, $^iPr_2NH$, CH_2Cl_2.

Compound **(58)** was subsequently used to synthesise the dialkyne ligand **(59)** in the Sonogashira coupling reaction with trimethylsilyl acetylene, Figure 4.6. Standard conditions were used, as have already been outlined in previous Chapters. After work up, a yield of 84% was achieved for **(59)** with characterisation achieved by ^1H and ^{13}C NMR spectroscopy and elemental analysis.

Further pyrrole- containing ligands were synthesised using a similar method as for ligand **(59)**, see Figure 4.7. The methyl **(63)** and butyl **(67)** analogue ligands were synthesised to investigate how aliphatic substitution at the 1- position of the pyrrole effects the properties of the system. The synthesis of these ligands involved the Paal-Knorr reaction of 1,4-*bis*-(4-bromo-phenyl)-butane-1,4-dione **(18)** with methylamine in ethanol to form **(62)** and butylamine in ethanol to form **(66)**. Both dibromides were characterised by ^1H and ^{13}C NMR spectroscopy and by EI mass spectrometry. The CH resonances of the protons on the pyrrole ring were observed at 6.31 ppm and 6.34 ppm for **(62)** and **(66)**, respectively.

Compounds **(62)** and **(66)** were subsequently reacted with trimethylsilylacetylene in a Sonogashira reaction to form the desired di-yne ligands **(63)** and **(67)**, respectively. This method has been described previously in this Thesis. The di-yne ligands were characterised by ^1H and ^{13}C NMR and IR spectroscopies. The characteristic 18

proton singlet resonance was observed for both compounds in the ^1H NMR spectra, corresponding to the trimethylsilyl groups. The presence of the alkyne group was confirmed by the characteristic ν(C≡C) stretch at 2160 cm^{-1} for **(63)** and 2155 cm^{-1} for **(67)**, respectively.

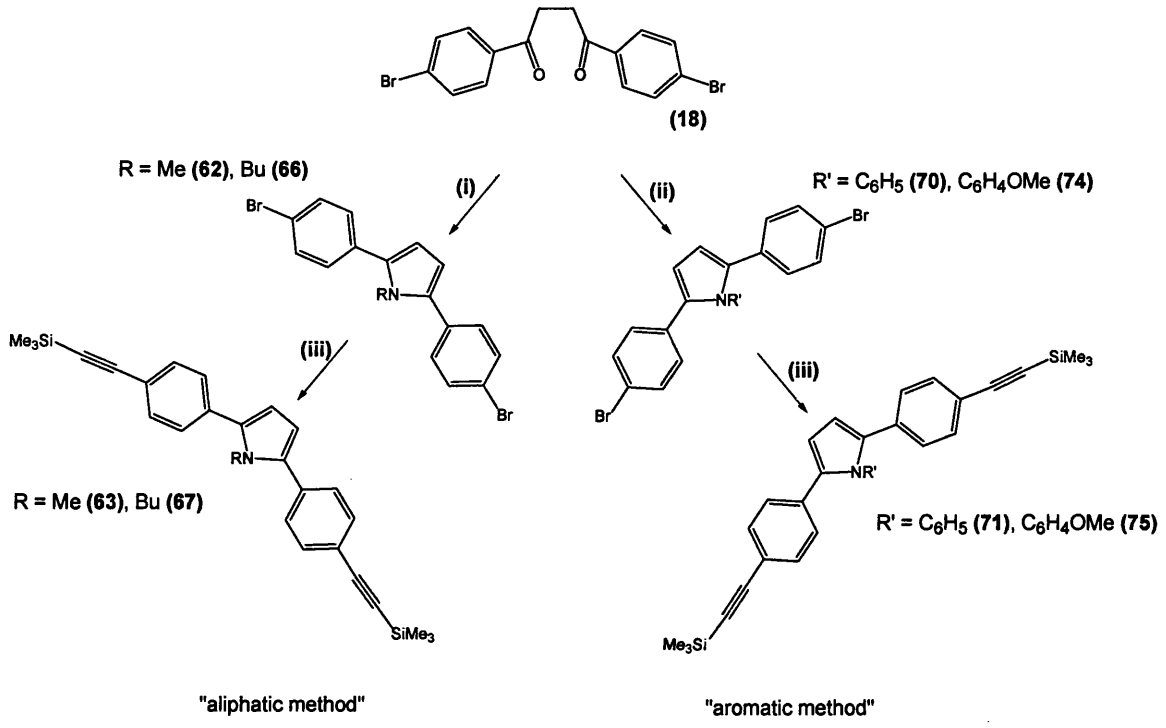

Figure 4.7 Synthesis of pyrrole containing ligands (i) xs. RNH_2, EtOH (ii) xs. $R'NH_2$, CH_3COOH, Δ (iii) Me_3SiCCH, $Pd(PPh_3)_2Cl_2$, CuI, $^iPr_2NH$, CH_2Cl_2.

Two more pyrrole containing ligands were synthesised, with aromatic functional groups at the 1- position of the pyrrole ring, Figure 4.7. These new compounds were designed to investigate if the chromophore of the di-yne spacer could be extended through the nitrogen of the pyrrole into a further conjugated functionality.

Initial attempts of the Paal-Knorr synthesis using amines containing aromatic groups proved to be unsuccessful using the same conditions as for the aliphatic amines. Refluxing of the 1,4-dicarbonyl **(18)** in an ethanolic solution of the aromatic amine failed to give any of the expected pyrrole containing product. After reviewing the literature, a preparation of a pyrrole with an aromatic group at the 1-position was found, Figure 4.8.[22]

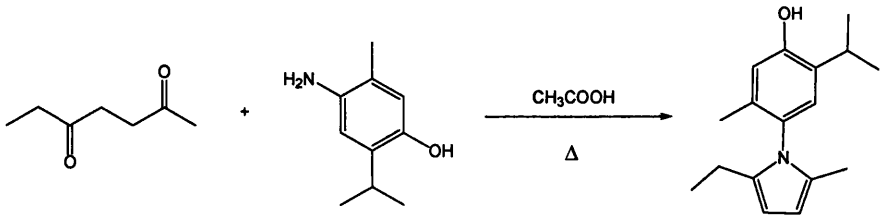

Figure 4.8 Synthesis of 4-(2-ethyl-5-methyl-pyrrol-1-yl)-2-isopropyl-5-methyl-phenol.

With this literature precedent in mind, a second attempt at the synthesis of the aromatic substituted pyrroles at the 1-position was carried out in acetic acid solution, Figure 4.7. The 1,4-dicarbonyl **(18)** and phenylamine were dissolved in acetic acid at 110 °C and after 3 hours of stirring a white precipitate was formed. The solid was collected and washed with acetic acid followed by ethanol to afford 2,5-*di*-(4-bromo-phenyl)-1-phenyl-pyrrole **(70)** in a yield of 80%. The use of acetic acid as the solvent is thought to accelerate the reaction, by acid catalysis.[23] The insolubility of the product in acetic acid also helps to drive the rate of reaction and gives rise to a simple work up of the product. The product was primarily characterised by ^{1}H NMR spectroscopy showing a singlet resonance at 6.47 ppm corresponding to the protons at the 3- and 4-position of the pyrrole. Characterisation was supported by ^{13}C NMR spectroscopy, EI mass spectrometry and elemental analysis.

The synthesis was repeated using 4-methoxyphenylamine as the ring closing reagent to produce 2,5-*di*-(4-bromo-phenyl)-1-methoxyphenyl-pyrrole **(74)** in a yield of 69%. The product was characterised by ^{1}H NMR spectroscopy showing a singlet resonance at 6.45 ppm, for the protons at the 3- and 4-positions of the pyrrole. ^{13}C NMR spectroscopy, EI mass spectrometry and elemental analysis of **(74)** all gave data to support the expected structure of the product.

Both dibromide products **(70)** and **(74)** were reacted with trimethylsilyl acetylene in a Sonogashira coupling reaction to produce the protected diyne ligands **(71)** and **(75)** in yields of 78% and 79%, respectively. Both products displayed the expected ^{1}H and ^{13}C NMR spectra for the desired product, with 18 proton integral singlet resonances at 0.22 ppm in the ^{1}H NMR spectra for the trimethylsilyl groups. This was supported by the IR spectra displaying $\nu(C{\equiv}C)$ at 2153 cm^{-1} for **(71)** and 2155 cm^{-1} for **(75)**, confirming the presence of the alkyne groups.

4.3 Synthesis of the pyrrole containing platinum (II) complexes

The trimethylsilyl protected diyne ligands in this Chapter were deprotected using an aqueous solution of potassium hydroxide solution to cleave the silyl group, generating the terminal alkyne. The yields obtained for this set of reactions, along with selected spectroscopic data, is given in Table 4.1.

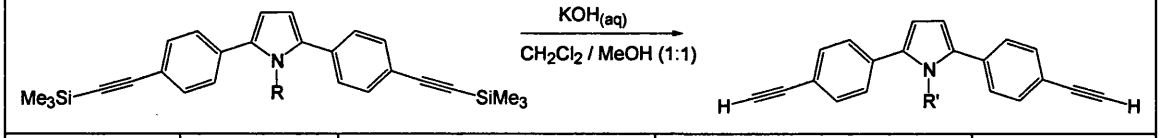

R' =	Yield (%)	^{1}H NMR (C≡C*H*)	^{1}H NMR (C*H*$_{pyrrole}$)	^{13}C NMR (C≡*C*H)	^{13}C NMR (*C*H$_{pyrrole}$)	IR ν(C≡C) (cm^{-1})
		(ppm)		(ppm)		
H **(60)**	98	3.13	6.63	77.78	109.21	1941
Me **(64)**	91	3.13	6.36	78.20	109.67	1943
^{n}Bu **(68)**	90	3.14	6.37	79.54	111.68	1944
C_6H_5 **(72)**	70	3.10	6.50	77.62	110.34	1943

Table 4.1 Selected spectroscopic data and yields of the terminal diyne ligands containing a pyrrole ring. ^{1}H NMR recorded at 400.13 MHz and ^{13}C NMR recorded at 100.61 MHz.

The terminal diynes were subsequently reacted with two molar equivalents of *trans-bis*(triethylphosphine)(phenyl)platinum(II) chloride, along with a copper iodide catalyst in a 1:1 mixture of triethylamine and dichloromethane to afford the dinuclear platinum complexes as discussed in previous Chapters. The yields of this set of reactions along with selected characterisation data is given in Table 4.2.

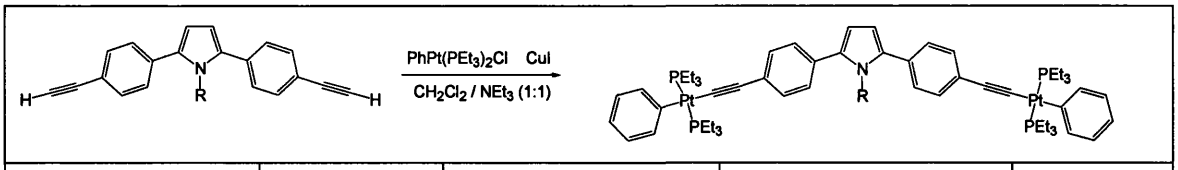

R =	Yield (%)	^{31}P NMR (ppm)	$^{1}J_{PtP}$(Hz)	Elemental Analysis Result % (calc. %)	IR ν(C≡C) (cm^{-1})
H **(61)**	77	9.99	2641	C = 52.4 (52.5) H = 6.39 (6.37) N = 0.94 (1.10)	2090
Me **(65)**	83	10.08	2639	C = 53.4 (52.8) H = 6.39 (6.45) N = 0.91 (1.08)	2089
^{n}Bu **(69)**	83	10.09	2639	C = 52.4 (53.8) H = 6.49 (6.70) N = 0.93 (1.05)	2091
C_6H_5 **(73)**	63	10.04	2633	C = 55.5 (54.8) H = 6.37 (6.31) N = 0.94 (1.03)	2096
*C_6H_4OMe **(77)**	53	10.10	2644	C = 55.7 (54.5) H = 6.27 (6.32) N = 0.92 (1.01)	2093

Table 4.2 Selected spectroscopic data and yields of the platinum (II) complexes of the pyrrole containing diyne ligands. *Synthesis of this compound was carried out by the *in situ* deprotection of the trimethylsilyl protected ligand (74), by the addition of sodium methoxide and methanol to the normal dehydrohalogenation reaction. ^{31}P NMR recorded at 161.97 MHz.

4.4 UV-visible spectroscopic studies of pyrrole containing platinum (II) complexes

The electronic absorption and emission spectra of the platinum(II) complexes **(61)**, **(65)**, **(69)**, **(73)** and **(77)** were determined as 0.01 mM concentration dichloromethane solutions, at room temperature. Figure 4.9 illustrates the absorption and emission (obtained by exciting the sample at 357 nm) spectra of complex **(61)** along with the spectra of the furan analogue **(22)** for comparison.

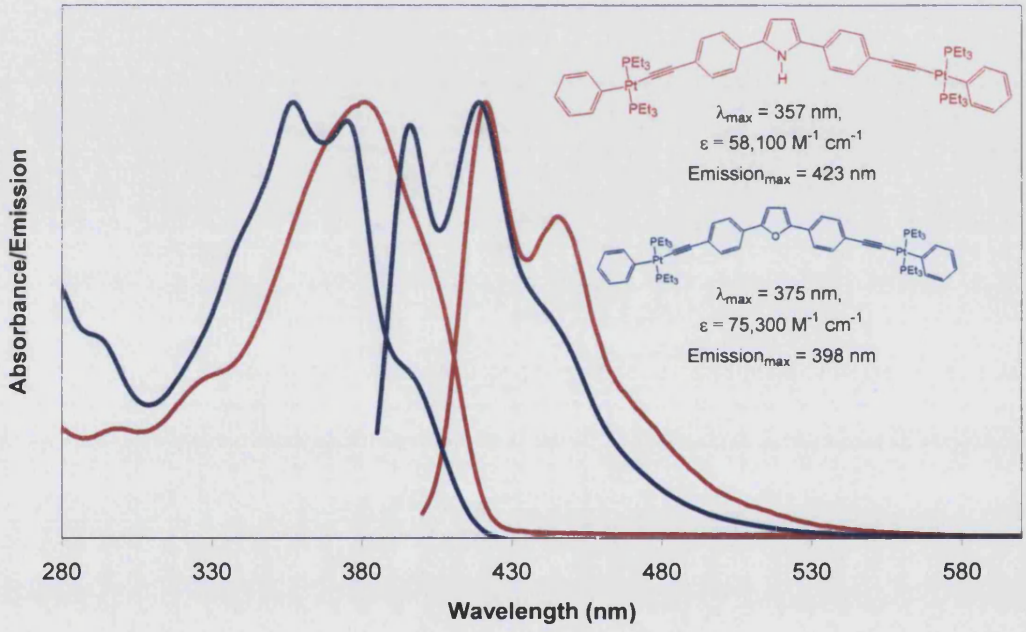

Figure 4.9 Absorption and emission spectra of (61) and (22) in CH_2Cl_2 solution at RT.

The pyrrole containing complex **(61)** exhibits one main absorbance peak at 357 nm. The onset of absorption is observed at 447 nm (2.77 eV). This corresponds to a bathochromic shift in energy, indicating a decrease in magnitude of the optical gap, as compared to the furan analogue **(22)** which absorbs from 2.83 eV. This trend was predicted in the objectives of this Chapter and can be explained in terms of the trend in π-donor strengths as the heteroatom in the central heterocyclic ring is replaced by an atom either further down the same group or by an element in a group to the left in the Periodic Table.[18] Both absorption and emission spectra are due to $\pi \rightarrow \pi^*$ transitions with some contribution from the metal centres as described previously.

The emission spectrum of **(61)** displays two main peaks at 421 and 445 nm, with the energy spacing between these two peaks corresponding to ~1280 cm^{-1}.

The electronic absorption and emission spectra of the platinum (II) complexes **(61)**, **(65)** and **(69)** are illustrated in Figure 4.10 for comparison.

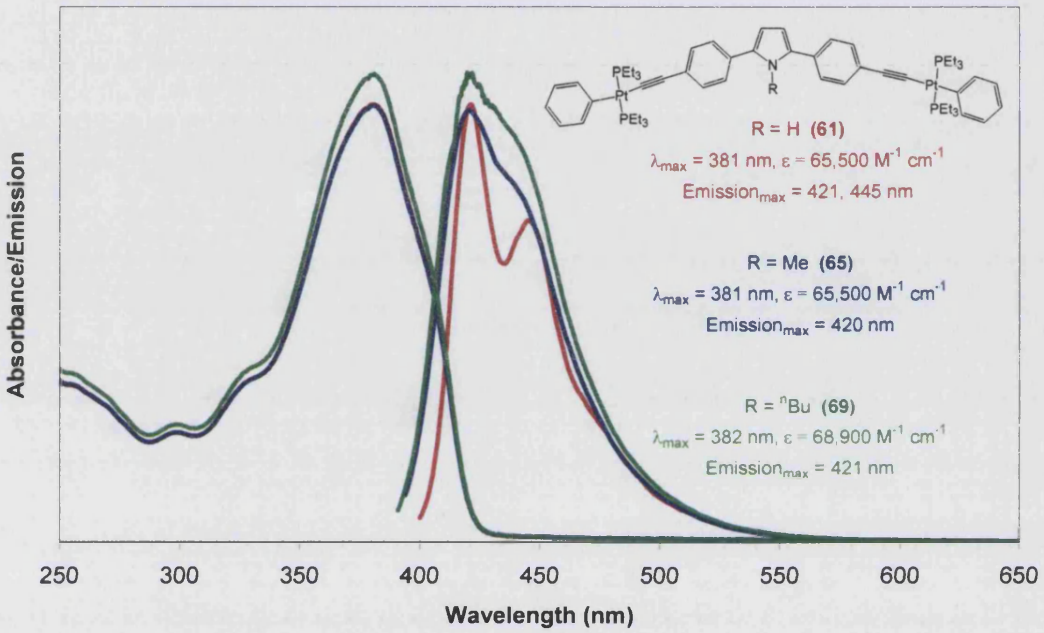

Figure 4.10 Absorption and emission spectra of (61), (65) and (69) in CH_2Cl_2 solution at RT.

The absorbance spectra of the platinum complexes shown in Figure 4.10 all show very similar characteristics. All three complexes **(61)**, **(65)** and **(69)** displayed an onset of absorption at 447 nm (2.77 eV). This suggests that substitution with alkyl chains at the 1-position of the pyrrole ring in these systems does not have a significant effect on the optical gap of the system, because the alkyl groups do not contribute to the molecular frontier orbitals.

The emission spectra of complexes **(61)**, **(65)** and **(69)** were collected after exciting the samples at 357 nm. The spectra again show very similar characteristics in terms of the position of the emission peak. The structure of the band, however, changes significantly with complex **(61)** showing two distinct bands at 421 and 445 nm, whilst complexes **(65)** and **(69)** display much broader bands with one main peak at 420 nm and both with shoulder peaks to higher wavelengths.

Figure 4.11 illustrates the absorption and emission of complexes **(73)** and **(77)**. The emission spectrum of **(73)** was obtained after exciting the sample at 342 nm and **(77)** after exciting at 345 nm. The figure also contains the spectra collected for complex **(61)** for comparison.

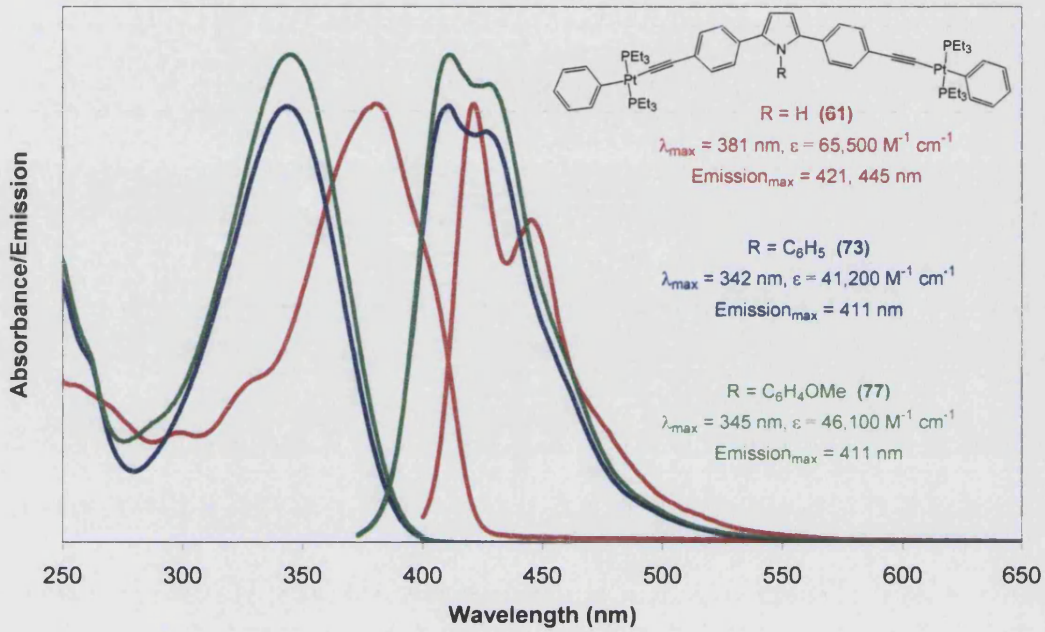

Figure 4.11 Absorption and emission spectra of (61), (73) and (77) in CH_2Cl_2 solution at RT.

The two spectra of **(73)** and **(77)** are of similar shape, with only small changes in the intensity of the peaks. Complex **(73)** maximises at 342 nm and complex **(77)** maximises at 345 nm. The onset of absorption is observed at 311 nm for **(73)** and 314 nm for **(77)**, this corresponds to optical gap energies of 3.01 eV and 3.00 eV, respectively.

Complexes **(73)** and **(77)**, however, display very different UV-visible spectra when compared to that of complex **(61)**. The aryl substituted pyrrole- containing complexes absorb at a lower wavelength, corresponding to a higher optical gap than the simpler 1-H pyrrole system. It was predicted that aryl substitution of the 1-position of the pyrrole ring would in fact extend size of the π-conjugated system, and therefore decrease the optical gap of the system. This is clearly not the case, and the optical gap is increased when compared to the 1-H pyrrole system. This may be explained in terms of steric crowding around the central ring of the di-yne ligand, and is illustrated in Figure 4.12.

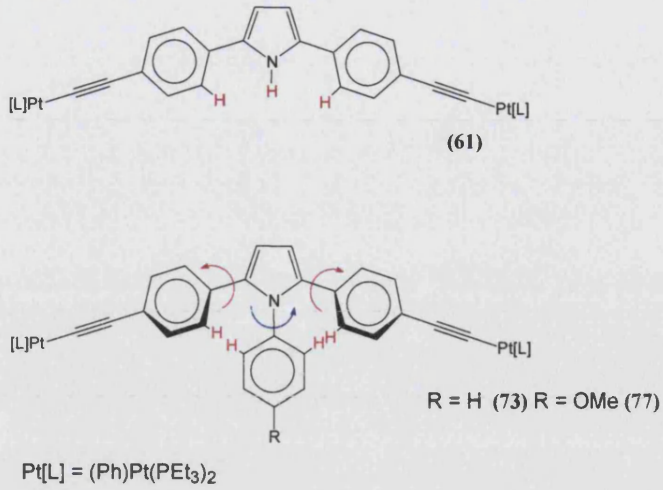

Figure 4.12 Steric crowding observed in complexes (73) and (77).

The proton on the nitrogen in complex **(61)** is relatively unhindered, and does not have much of an interaction with the nearest protons on the adjacent arene rings. In complexes **(73)** and **(77)** the aryl groups are far more sterically demanding than the proton, and are believed to have some effect on disrupting the effective length of the chromophore by forcing the $-C_6H_4-$ groups to twist, in order to minimise the proton-proton interactions (shown in red, Figure 4.12).

Table 4.3 summarises the photophysical data obtained from the absorption spectra of all the pyrrole containing Pt(II) complexes in this Chapter. It is clear to see that the substitution of alkyl groups at the 1-position of the pyrrole has no significant effect on the absorbance spectra observed. This suggests that the alkyl groups have no contribution to the molecular frontier orbitals of the system.

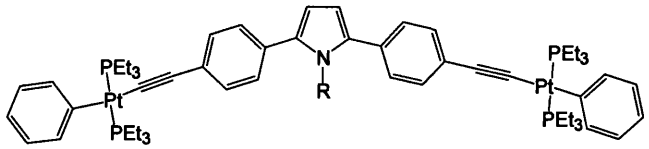

Compound	R =	Absorb. λ_{max} (nm)	Optical Gap (eV)
(61)	H	381	2.77
(65)	Me	381	2.77
(69)	^{n}Bu	382	2.77
(73)	C_6H_5	342	3.01
(77)	C_6H_4OMe	345	3.00

Table 4.3 Summary of photophysical data of complexes (61), (65), (69), (73) and (77).

Substitution of aryl groups at the 1-position of the pyrrole has shifted the spectra to higher energy. This is believed to be due to the inclusion of the sterically demanding groups at the 1- position, forcing the -C_6H_4- groups to twist relative to the pyrrole ring. This shift seems to be independent of the type of aryl group in question as the UV-visible spectra of complex **(73)** and **(77)** are similar with both complexes exhibiting optical gap energies within experimental error of each other.

4.4 Solid state X-ray structure of (61)

Suitable single crystals were obtained of X-ray diffraction quality of complex **(61)**, from ethanolic solution, and its molecular structure was determined. The relative orientation of the pyrrole ring to the adjacent arene rings was of interest. The most important bond lengths, bond angles and dihedral angles are discussed in this section as well as comparisons made with analogous molecular structures of complexes from Chapter 3.

Figure 4.13 illustrates the molecular structure of **(61)** as a thermal ellipsoid plot. Table 4.4 contains selected bond length, bond angle and dihedral angle data.

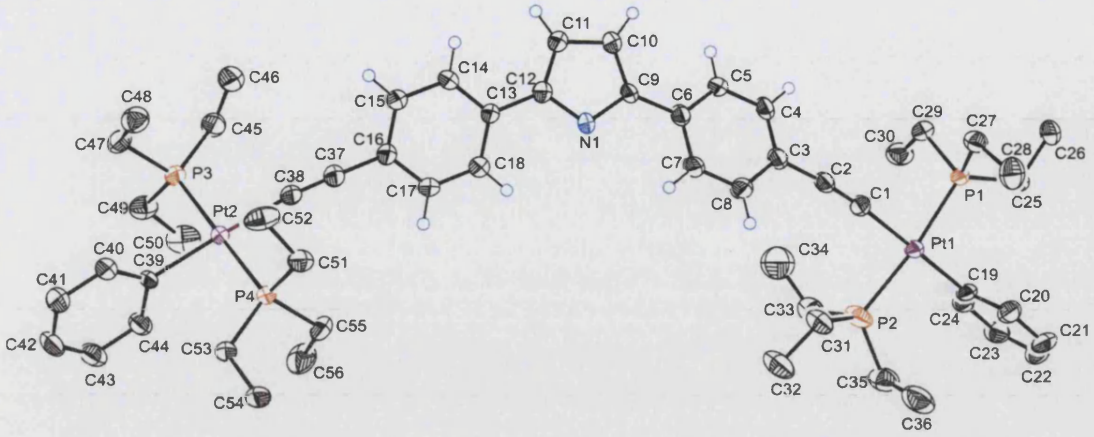

Figure 04.13 Molecular structure of (61) illustrated as a thermal ellipsoid plot at a 50% probability level. Hydrogen atoms have been omitted for clarity except on the central diyne ligand.

The ligands surround the platinum atoms in a square planar orientation with all bond lengths and bond angles falling in the same range as for all the analogous platinum(II) molecular structures in Chapters 2 and 3.

Bond Lengths (Å)		**Bond Angles (°)**	
Pt_1-C_1	2.031(6)	Pt_1-C_1-C_2	174.3(5)
Pt_2-C_{38}	2.037(6)	Pt_2-C_{38}-C_{37}	174.3(5)
Pt_1-P_1	2.2799(15)	P_1-Pt_1-P_2	171.33(8)
Pt_1-P_2	2.2980(18)	P_3-Pt_2-P_4	178.55(6)
Pt_2-P_3	2.2880(15)	C_1-Pt_1-C_{19}	179.4(3)
Pt_2-P_4	2.2855(15)	C_{39}-Pt_2-C_{38}	177.6(2)
Pt_1-C_{19}	2.060(6)	C_{12}-N-C_9	110.0(5)
Pt_2-C_{39}	2.070(5)	**Dihedral Angles (°)**	
C_1-C_2	1.205(8)	$C_{13\text{-}18}$/$C_{9\text{-}12}$,N	15.87(12)
C_{37}-C_{38}	1.185(8)	$C_{3\text{-}8}$/$C_{9\text{-}12}$,N	15.12(15)
C_9-N_1	1.389(7)	$C_{13\text{-}18}$/C_{38},C_{39},P_3,P_4,Pt_2	47.94(13)
C_{12}-N_1	1.380(7)	$C_{3\text{-}8}$/C_1,C_{19},P_1,P_2,Pt_1	30.59(15)
C_9-C_{10}	1.378(8)	C_1,C_{19},P_1,P_2,Pt_1/$C_{19\text{-}24}$	80.58(12)
C_{11}-C_{12}	1.379(8)	C_{38},C_{39},P_3,P_4,Pt_2/$C_{39\text{-}44}$	83.38(15)

Table 4.4 Selected bond length, bond angle and dihedral angle data from the molecular structure of complex (61).

The molecular structure of **(61)** bows round along the length of the complex, forming a 'crescent' structure. This bowing effect is not observed in analogous molecular structures of complexes of other heterocyclic systems in Chapter 3.

The pyrrole ring is twisted relative to its adjacent arene rings giving rise to dihedral angles of 15.87(12)° (relative to $C_{13\text{-}18}$) and 15.12(15)° (relative to $C_{3\text{-}8}$). This is the largest pair of dihedral angles observed from the series of three ring heterocyclic systems in this Thesis. It might be expected that the dihedral angle would be larger because of the presence of the proton on the pyrrole ring compared to the previously studied ring systems where there are only lone pairs on the heteroatom. The relative twist angles observed in the central di-yne ligand can be clearly seen in an alternative view of the molecular structure of **(61)** as shown in Figure 4.14.

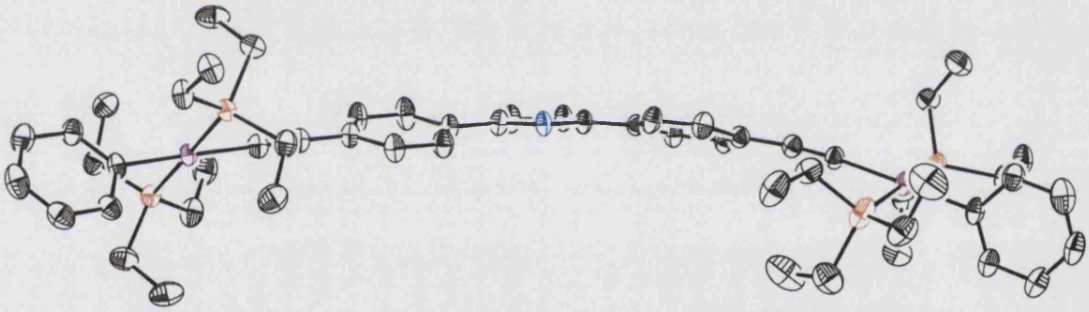

Figure 04.14 Alternative view of the molecular structure of complex (61).

Unfortunately, no other suitable single crystals of X-ray diffraction quality were obtained for the other pyrrole containing complexes within this Chapter, therefore the orientation of the substituted alkyl and aryl groups at the 1-position of the pyrrole could not be determined.

4.5 Summary and Conclusions

Novel synthetic routes towards a series of di-yne ligands incorporating pyrrole heterocycles have been developed. All products were synthesised in moderate or high yields. The new ligands were complexed to Pt(II) metal centres and fully characterised by multinuclear NMR and IR spectroscopies and by elemental analyses.

The structure of the pyrrole containing Pt(II) complex **(61)** has been confirmed by single crystal X-ray diffraction. The geometry around the metal centre is as expected, in a square planar arrangement, and the di-yne ligand shows a twisted structure with the pyrrole ring twisted to its adjacent arene rings by dihedral angles of 15.87(12)° and 15.12(15)°.

The solution state UV-visible spectra of the Pt(II) complexes were determined as dichloromethane solutions at room temperature. The 1-H pyrrole- containing Pt(II) complex **(61)** was compared to the furan- containing analogue **(22)**, with **(61)** showing a lower optical gap than **(22)**. The alkyl substituted pyrrole containing Pt(II) complexes, **(65)** and **(69)** were shown to have similar photophysical properties as complex **(61)**, suggesting the alkyl groups do not contribute to the molecular frontier orbitals.

Aryl substitution at the 1-position of the pyrrole ring was shown to increase the optical gap energy of the system by 0.24 eV. The shift was attributed to the steric effects of the aryl groups. Further substitution of the arene ring at the 1-position of the pyrrole was shown to have little effect on the photophysical properties of the system, as both complexes **(73)** and **(77)** gave almost identical UV-visible spectra.

4.6 References

[1] (Acidity in DMSO) M. Bordwell, *J. Am. Chem. Soc.*, 1981, **46**, 632

[2] E. P. Serjeant, B. Dempsey, *Ionisation Constants of Organic Acids in Aqueous Solution*, Oxford, 1979

[3] M. B. Smith, J. March, *March's Advanced Organic Chemistry: Reactions, Mechanisms, and Structure*, 5th Edition, Wiley-Interscience, 2001

[4] T. A. Skotheim, R. L. Elsenbaumer, J. R. Reynolds, *Handbook of Conducting Polymers,* 2nd edition, New York, 1998.

[5] J. Simonet, J. R Berthelot, *Prog. Solid State Chem.,* 1991, **21**, 1.

[6] K. Sato, M. Yamamura, T. Hagiwara, K. Murata, M. Tokumoto, M. *Synth. Met.* 1991, **40**, 35.

[7] G. P. Kittlesen, H. S. White, M. S. Wrighton, *J. Am. Chem. Soc.*, 1984, **106**, 7389

[8] L. H. Krings, E. E. Havinga, J. J. T. M. Donkers, F. T. A. Vork, *Synth. Met.*, 1993, **54**, 453

[9] E. Smela, O. Inganas, I. Lundstrom, *Science*, 1995, **268**, 1735

[10] I. T. Kim, R. L. Elsenbaumer, *Chem. Commun.*, 1998, 327

[11] K. Jun-Gill, K. Tack-Jin, P. Changmoon, W. Lee Sang, K. In Tae, *Bull. Korean Chem. Soc.*, 2004, **25**, 704

[12] N. Ono, T. Yamamoto, N. Shimada, K. Kuroki, M. Wada, R. Utsunomiya, T. Yano, H. Uno, T. Murashima, *Heterocycles*, 2003, **61**, 433

[13] F. R. Longo, *Porphyrin Chemistry Advances*, Ann Arbor Sci. Pub., 1979,

[14] A. Harriman, *J. Chem. Soc. Faraday Trans. II*, 1981, **77**, 1281

[15] M. Kaska, *J. Chem. Phys.*, 1952, **20**, 71

[16] D. B. Papkovsky, G. V. Ponomarev, W. Trettnak, P. O'Leary, *Anal. Chem.*, 1995, **67**, 4112

[17] E. Y. Mantrova, M. V. Demcheva, A. P. Stavitsky, *Anal. Biochem.*, 1994, **219**, 109

[18] U. Salzner, J. B. Lagowski, P. G. Pickup, R. A. Poirier, *Synth. Metals*, 1998, **96**, 177

[19] R. U. Braum, K. Zeitler, T. J. J. Muller, *Org. Lett.*, 2001, **3**, 3297

[20] M. Ceylan, M. Guerdere, B. Burcu, K. Yakup, W. Secen, *Synthesis*, 2004, **11**, 1750

[21] H. Rao, P. Surya, S. Jothilingam, H. W. Scheeren, *Tetrahedron*, 2004, **60**, 1625

[22] S. Raynard, *Ann. Inst. Pasteur*, 1957, **92**, 618

[23] G. Minetto, L. F. Raveglia, A. Sega, M. Taddei, *Eur. J. Org. Chem.*, 2005, 5277

Chapter 5

Tuneable "Twisted" Systems

5. Tuneable 'Twisted' Systems

5.1 Introduction

5.1.1 Background

An ability to control the optical and electronic properties of luminescent oligomers or polymers is currently an important issue in the design of new materials for organic light emitting diodes.[1,2]

Recently, there has been a large amount of research targeted at preparing and exploiting "planarised" poly(*p*-phenylene) (PPP) systems to maximise the extent of conjugation. Oligomers and polymers with 5,6-dihydrophenanthrecene-3,8-diyl repeat units (poly(phenanthrecene)s), (PPT) Figure 5.1a, and 4,5,9,10-tetrahydropyrene-2,7-diyl sub-structures (poly(tetrahydropyrene)s (PTHP)), Figure 5.1b, have been used as "planarised" PPP analogues".[3] These systems with their ethane-1,2-diyl bridges between adjacent phenylene rings maintain inherent flexibility and are not fully planarised. However, UV-visible spectroscopic studies of these systems showed a degree of conjugation nearly twice as high as those of the parent PPPs and OPPs.

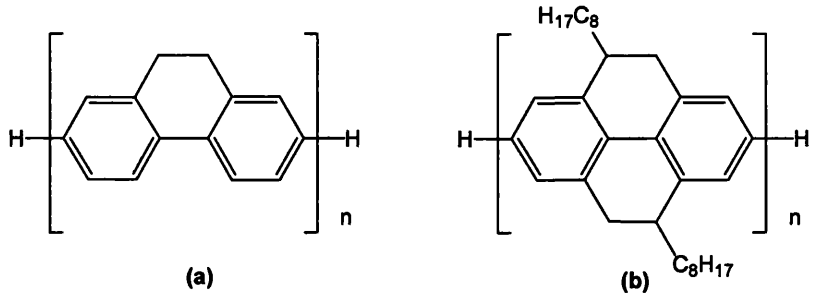

Figure 5.1 Planarised PPP models (a) poly(phenanthrecene) (PPT), (b) poly(tetrahydropyrene) (PTHP).

Tour *et al* reported a fully planarised polymer with a PPP-type backbone using an imine bridge, Figure 5.2.[4] The main PPP backbone was synthesised via a Suzuki Coupling of an arylbis(boronic ester) with an aryl dibromide. The imine

bridges were then formed by exposing the polymer to trifluoroacetic acid forcing the consecutive units into planarity.

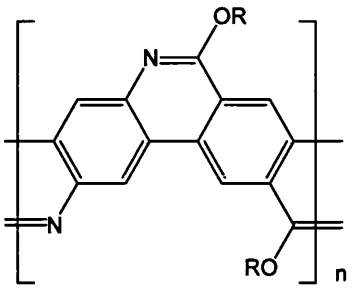

Figure 5.2 Imine bridged PPP planarised analogue.

5.1.2 Objectives

The aim of this Chapter of work was to study the effects of the steric interactions within the di-nuclear Pt(II) systems utilised in previous Chapters. For this purpose a series of new di-yne ligands and Pt(II) complexes were synthesised and fully characterised. The new compounds, and particularly the organic spacer groups, were designed to attempt to enforce a range of twist angles between adjacent arene rings in the spacer by replacing the protons on the spacer ligands with larger sterically demanding groups, or by altering the ring substituents from electron donating to electron withdrawing groups, thus fine tuning the size and properties of the central chromophore. The strategy for the design of further new ligands in which the steric interactions were minimised by replacing the CH groups on the spacer ligand with nitrogen atoms. It was hoped that this would planarise the systems and would maximise the extent of conjugation, mirroring the work of Tour.[4]

The final aim of this section of work was to move from linear di-yne spacer units to those based on trisubstituted arene ring systems and thus investigate the effect of incorporation of a third metal centre into the system.

5.2 Synthesis of 4,4''-*bis*-(*trans*-(phenyl,*bis*-triethylphosphine) platinum) ethynyl-2',3',5',6'-tetrafluoro-terphenyl (86)

The first system in which sterically demanding groups were used to attempt to enforce a twist due to steric interactions was the tetrafluoro complex **(86)**. The synthesis of complex **(86)** was achieved *via* a 5 step reaction scheme shown in Figure 5.3.

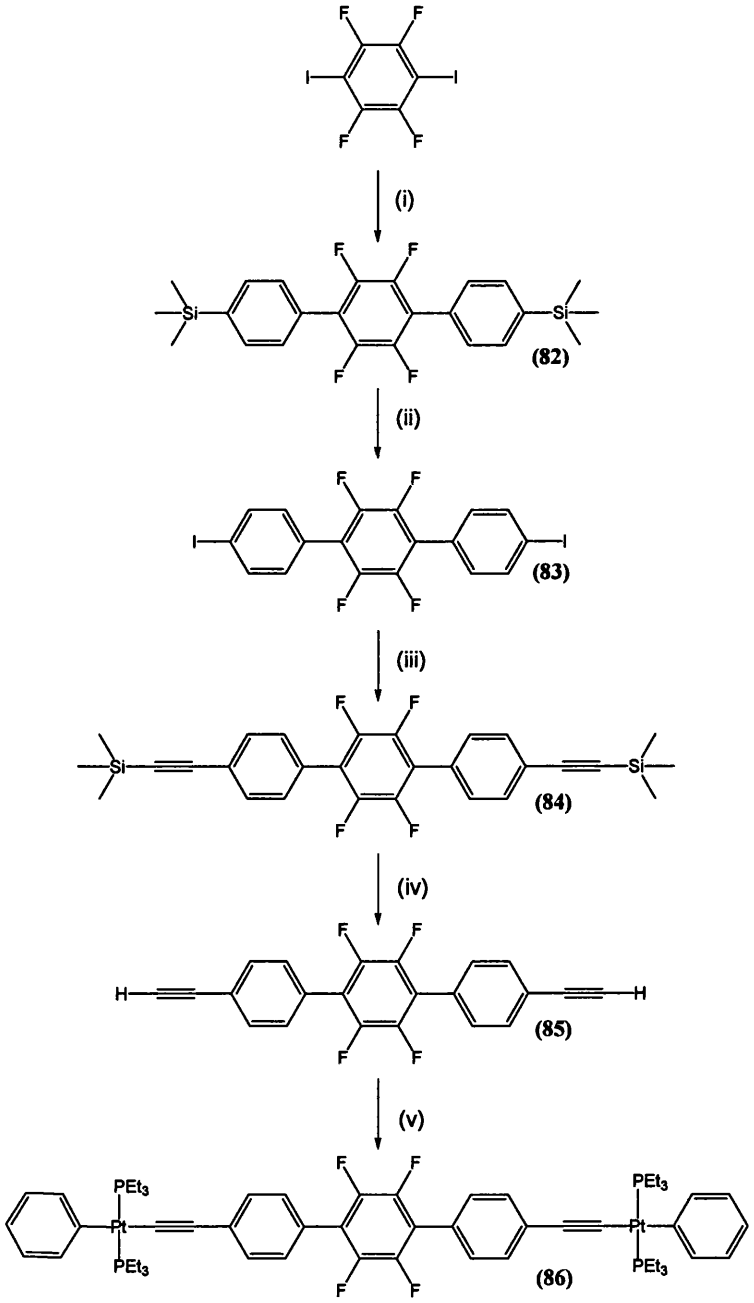

Figure 5.3 Synthetic route towards complex (86) (i) *p*-$Me_3Si(C_6H_4)B(OH)_2$, $Pd(PPh_3)_4$, $NaHCO_{3(aq)}$, toluene, Δ (ii) ICl, $CHCl_3$, (iii) Me_3SiCCH, $Pd(PPh_3)_2Cl_2$, CuI, $^iPr_2NH$, CH_2Cl_2 (iv) $KOH_{(aq)}$, $MeOH/CH_2Cl_2$ (v) $PhPt(PEt_3)_2Cl$, CuI, $^iPr_2NH$, CH_2Cl_2.

The commercially available 1,2,4,5-tetrabromo-3,6-diiodo-benzene was reacted with *p*-trimethylsilyl-phenyl boronic acid in a Suzuki coupling reaction under standard conditions.[5] Analytically pure **(82)** was achieved after purification by chromatography and recrystallisation in a yield of 82%. The product was characterised by ^{1}H, ^{13}C and ^{19}F NMR spectroscopy, with the proton NMR spectrum showing the characteristic singlet resonance at 0.32 ppm corresponding to the 18 protons of the trimethylsilyl groups. The ^{13}C NMR spectrum was assigned to all the carbon environments with a coupling constant of $^{1}J_{FC}$ = 246 Hz observed for the *ipso*-carbon directly bonded to the fluoride on the central arene ring. The elemental analysis confirmed the expected molecular formula ($C_{24}H_{26}Si_2F_4$).

Compound **(82)** was subsequently reacted with iodine monochloride in a chloroform solution affording the di-iodide compound **(83)** in a yield of 80%. The cleavage of the trimethylsilyl groups was confirmed by the absence of the singlet at 0.32 ppm. The ^{13}C NMR spectrum showed only 5 of the 6 expected resonances due to poor solubility of the compound. Further analysis by EI mass spectrometry and elemental analysis confirmed the molecular formula of **(83)** to be $C_{18}H_8F_4I_2$.

Compound **(83)** was then used in the Sonogashira coupling reaction with trimethylsilyl acetylene to give the protected di-yne ligand **(84)**. The reaction was carried out in the presence of *bis*(triphenylphosphine)palladium(II)chloride and copper iodide catalysts, in diisopropyl amine and dichloromethane solution. After 4 hrs the volatiles were removed and the crude product was purified by chromatography to afford **(84)** in a yield of 68%. The product was characterised by ^{1}H, ^{13}C and ^{19}F NMR spectroscopy, supported by elemental analysis. The 18 proton resonance at 0.28 ppm in the ^{1}H NMR spectrum, along with quaternary carbon resonances at 96.05 and 104.30 ppm in the ^{13}C NMR spectra were the most indicative features in the NMR spectra obtained.

The di-yne compound **(84)** was then deprotected using an aqueous solution of potassium hydroxide in a methanol solution. The volatiles were then removed

after 1 h and extracted from water into dichloromethane. The solvent was removed to afford the terminal alkyne **(85)** in a yield of 85%. Characterisation was achieved by multinuclear NMR spectroscopy, showing the appearance of a singlet resonance in the ^{1}H NMR spectrum at 3.17 ppm which corresponds to the terminal alkyne proton.

The terminal alkyne **(85)** was reacted with half an equivalent of *trans-bis*(triethylphosphine)(phenyl) platinum(II)chloride to give the Pt (II) dinuclear complex **(86)**. The reaction was carried out in a dichloromethane solution with a copper iodide catalyst and di-isopropylamine. The product was purified by chromatography and recrystallisation to afford **(86)** in a yield of 90%. Characterisation was achieved by multinuclear NMR spectroscopy. This includes ^{1}H NMR spectroscopy showing multiplet resonances at 1.07-1.15 ppm and 1.74-1.81 ppm for the CH_3 and CH_2 groups of the alkyl phosphine, respectively. The ^{13}C NMR spectrum exhibits all 14 expected resonances, with coupling seen to phosphorus ($^{1}J_{PC}+^{3}J_{PC}$ = 34 Hz) and fluorine ($^{1}J_{FC}$ = 247 Hz). The ^{19}F NMR spectrum shows a single resonance at -145.1 ppm. The ^{31}P NMR spectrum exhibits a singlet with platinum-195 satellites and a coupling constant of $^{1}J_{PtP}$ = 2636 Hz. This confirms the *trans-* arrangement at the platinum centre.

5.3 Synthesis of 1,4-*di*-((*trans*-(phenyl,*bis*-triethylphosphine) platinum)ethynyl)-2,3,5,6-tetrafluoro-benzene (89)

To eliminate the steric effects of the fluorides in complex **(86)** on the adjacent arene rings, a second tetrafluoro-benzene complex was synthesised to investigate purely the electronic effects of the incorporation of fluorine into the system.

The terminal di-yne ligand 1,2,4,5-tetrafluoro-3,6-*di*-ethynyl-benzene **(88)** was synthesised by adapting a literature preparation.[6] Although the ligand has been reported in the literature since 1972[7] only two metal complexes of the ligand are known. The first is a Rh(II) complex[8] and the second is a Pt(II) organometallic

polymer.[6] The synthetic route to the Pt(II) complex **(89)** is outlined in Figure 5.4.

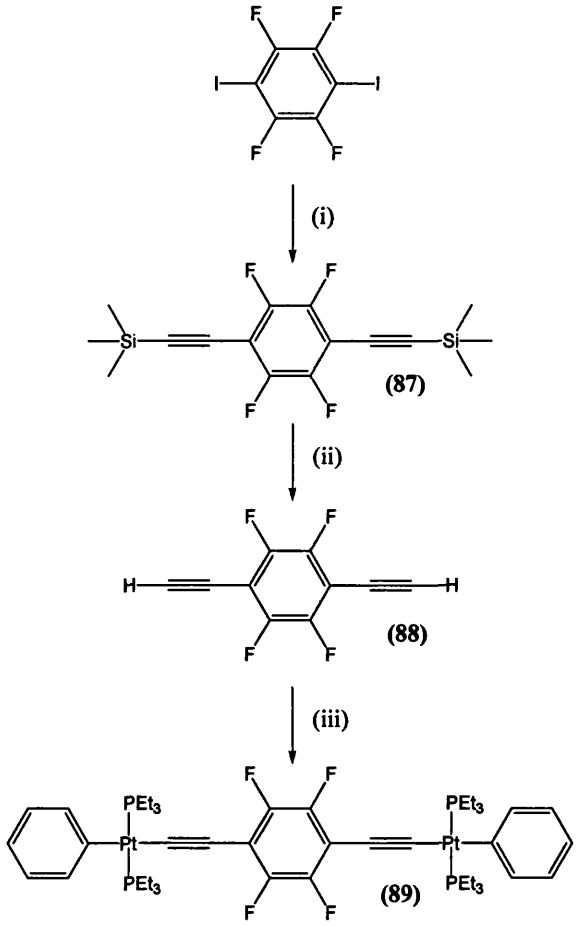

Figure 5.4 Synthesis of complex (89).
(i) Me_3SiCCH, $Pd(PPh_3)_2Cl_2$, CuI, $^iPr_2NH$, CH_2Cl_2 (ii) $KOH_{(aq)}$, $MeOH/CH_2Cl_2$
(iii) $PhPt(PEt_3)_2Cl$, CuI, $^iPr_2NH$, CH_2Cl_2.

Complex **(89)** was synthesised by the reaction of the terminal di-yne ligand **(88)** with half an equivalent *trans-bis*(triethylphosphine)(phenyl)platinum(II)chloride, with a copper iodide catalyst in dichloromethane and diisopropyl amine. The pure product was obtained after purification by chromatography and recrystallisation in a yield of 79%. The complex was characterised by ^1H, ^{13}C, ^{19}F, ^{31}P NMR spectroscopies. The ^1H and ^{13}C NMR spectra both showed the expected resonances consistent with the expected molecular structure. The ^{19}F NMR spectrum exhibited a singlet resonance at -144.0 ppm, and the ^{31}P NMR spectrum showed a singlet at 10.28 ppm with coupling observed to ^{195}Pt in the form of satellites corresponding to a coupling constant of $^1J_{PtP}$ = 2613 Hz. The

elemental analysis results were consistent with the molecular formula $C_{46}H_{70}F_4P_4Pt_2$.

Compound	(82)	(83)	(84)	(85)	(86)	(87)	(88)	(89)
^{19}F NMR (ppm)	-144.3	-143.7	-145.1	-145.0	-145.1	-136.7	-137.6	-144.0

Table 5.1 ^{19}F NMR data of compounds (82) – (89). Spectra were recorded at 376.5 MHz.

Table 5.1 displays the ^{19}F NMR data of the tetrafluoro- compounds **(82)** – **(89)**. It is clear to see that the chemical shift of the resonances observed do not significantly alter on substitution of the 1,4- positions of the central arene ring.

5.4 UV-visible studies of the tetra-fluoride containing complexes (86) and (89)

The purified and fully characterised complexes **(86)** and **(89)** were studied for their photophysical properties by obtaining UV-visible absorption spectra as 0.01 mM dichloromethane solutions at room temperature. Figure 5.5 shows the UV-visible absorption and emission spectra of the di-platinum complex **(86)** and the non-fluorinated analogue **(12)** for comparison.

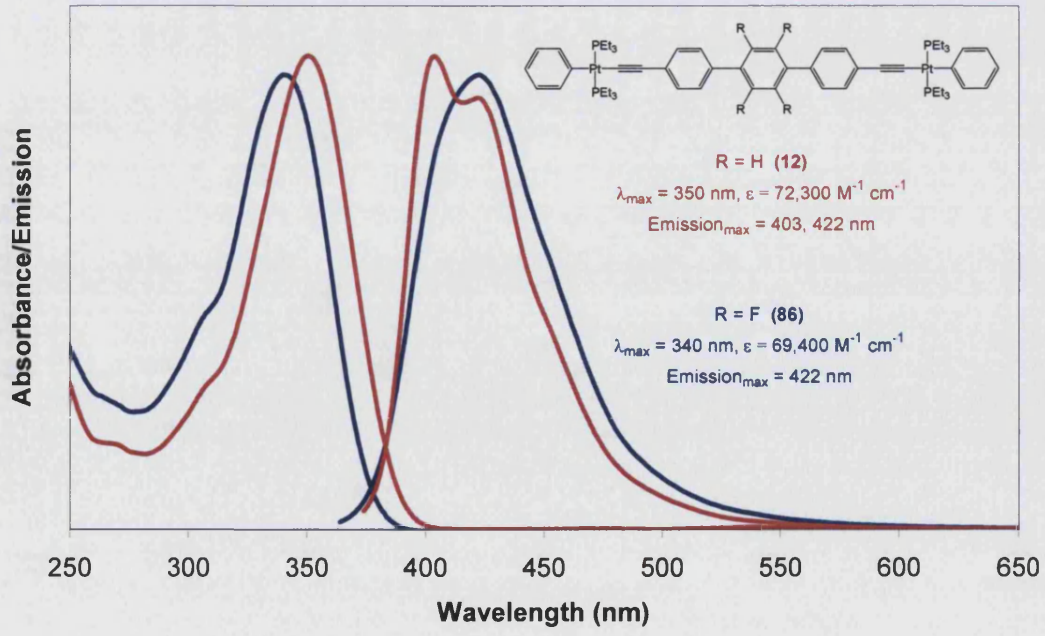

Figure 5.5 Absorption and emission spectra of (12) and (86) in CH_2Cl_2 at RT.

The absorption spectrum of **(86)** displays a maxima 340 nm and an onset of absorption at 392 nm (3.16 eV). The emission spectrum of **(86)** displays a maxima at 422 nm.

Figure 5.6 displays the UV-visible absorption and emission spectra of the di-platinum complex **(89)** and the non-fluorinated analogue **(3)** for comparison.

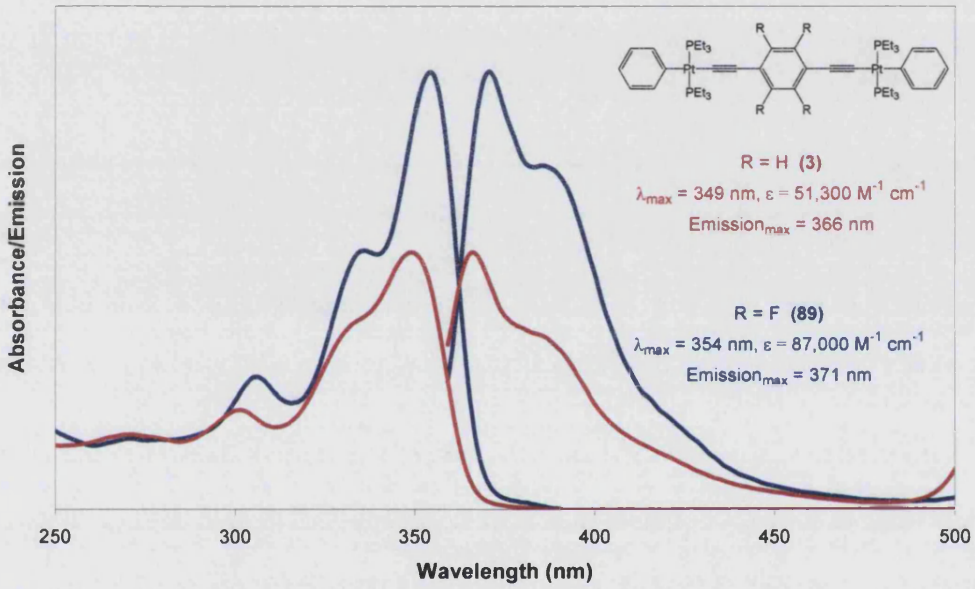

Figure 5.6 Absorption and emission spectra of (3) and (89) in CH_2Cl_2 at RT.

The absorption spectrum of **(89)** displays a maxima at 354 nm and an onset of absorption at 396 nm (3.13 eV). The emission spectrum of **(89)** displays a maxima at 466 nm. Shoulder peaks are present in both the absorption and emission spectra of **(89)**, although these are particularly broad therefore vibrational energy spacings can not be determined accurately.

Table 5.2 summarises photophysical data of complexes **(3)**, **(12)**, **(86)** and **(89)**. When comparing the spectra of **(86)** to the non-fluorinated analogue **(12)** it can be seen that there is a shift to higher optical gap energy for **(86)**. This is believed to be due to the steric interactions of the tetrafluoride groups with the *ortho* protons on the adjacent arene rings. This interaction is believed to enforce a large dihedral angle between the arene rings on the spacer ligand, thus reducing the effective π- conjugation through the complex.

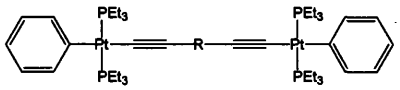

R=	Onset of absorption (nm)	(eV)	λ_{max} (nm)	ε ($dm^3mol^{-1}cm^{-1}$)
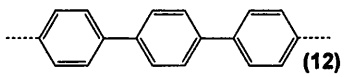 (12)	409	3.04	350	72,300
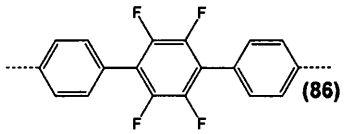 (86)	392	3.16	340	69,400
 (3)	388	3.20	349	51,400
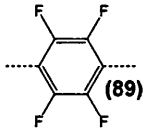 (89)	396	3.13	354	87,000

Table 5.2 Summary of photophysical data of complexes (3), (12), (86) and (89).

Comparison of the spectra of **(89)** with **(3)** has shown a shift to lower optical gap energy for **(89)**. This is due to the electron withdrawing effects of fluorine altering the energy of the molecular frontier orbitals. In the "three- ring" system **(86)**, the fluorides are also acting to reduce the optical energy gap, but this is counteracted with the steric influences of the fluorides enforcing a large dihedral angle between the arene rings on the spacer ligand, thus reducing the effective π- conjugation through the complex.

5.5 Synthesis of 4,4''-*di*-(*trans*-(phenyl,*bis*-triethylphosphine) platinum) ethynyl-2',3',5',6'-tetramethyl-terphenyl (95)

The second system in which sterically demanding groups were used to attempt to enforce a twist due to steric interactions was the tetramethyl complex **(95)**. The synthesis of complex **(95)** was achieved *via* a 5 step reaction scheme shown in Figure 5.7.

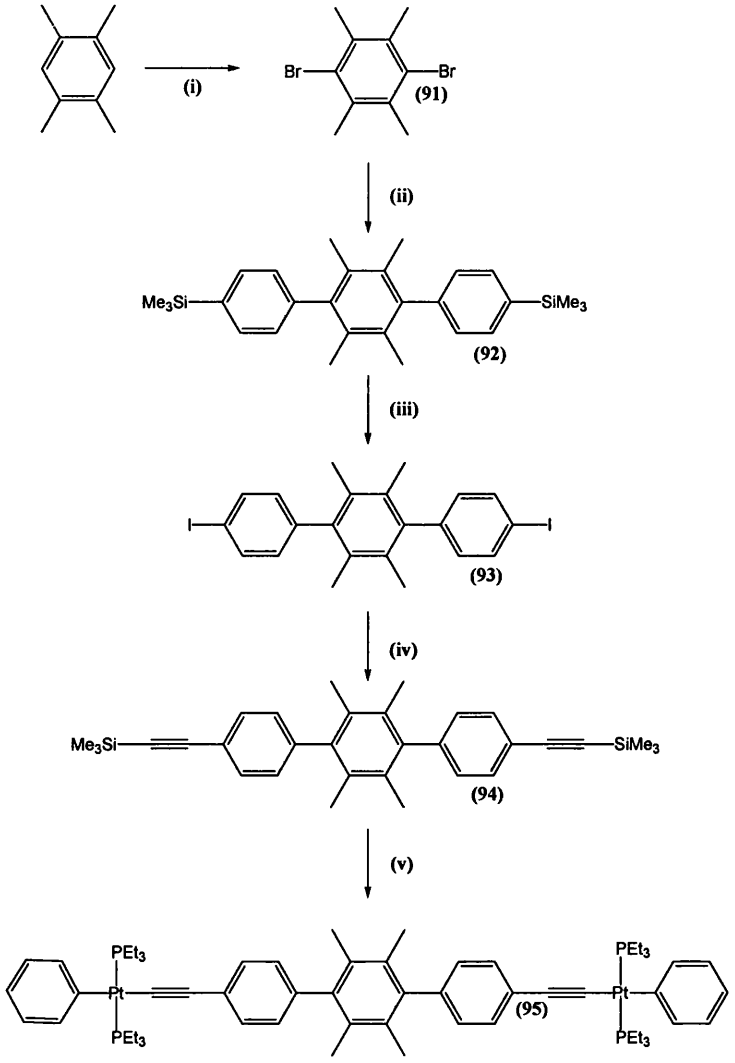

Figure 5.7 Synthesis of complex (95) (i) Br_2, CH_2Cl_2,[9] (ii) *p*-$Me_3Si(C_6H_4)B(OH)_2$, $Pd(PPh_3)_4$, $NaHCO_{3(aq)}$, toluene, Δ (iii) ICl, $CHCl_3$, (iv) Me_3SiCCH, $Pd(PPh_3)_2Cl_2$, CuI, $^iPr_2NH$, CH_2Cl_2 (v) NaOMe, $PhPt(PEt_3)_2Cl$, CuI, $^iPr_2NH$, CH_2Cl_2.

1,2,4,5-Tetramethyl-benzene was brominated in the 3 and 6- positions using literature procedures to afford 1,4-dibromo-2,3,5,6-tetramethyl-benzene.[9] Compound **(91)** was then subsequently reacted with *p*-trimethylsilyl-phenyl boronic acid in a Suzuki coupling reaction under standard conditions.[5] The

analytically pure product **(92)** was achieved after purification by chromatography in an 84% yield. The product was characterised by ^{1}H and ^{13}C NMR spectroscopy, with the proton NMR spectrum showing the characteristic singlet resonance at 0.32 ppm corresponding to the 18 protons of the trimethylsilyl groups.

Compound **(92)** was subsequently reacted with iodine monochloride in a chloroform solution yielding the di-iodide compound **(93)** in a yield of 96%. The cleavage of the trimethylsilyl groups was confirmed by the absence of the singlet at 0.32 ppm. Further analysis by EI mass spectrometry confirmed the molecular formula of **(93)** to be $C_{22}H_{20}I_2$.

Compound **(93)** was then used in the Sonogashira coupling reaction with trimethylsilyl acetylene to give the protected di-yne ligand **(94)**. The reaction was carried out in the presence of *bis*(triphenylphosphine)palladium(II)chloride and copper iodide catalyst, in diisopropyl amine and dichloromethane solution. After 18 hours the volatiles were removed and the crude product was purified by chromatography to afford **(94)** in an 80%. The product was characterised by ^{1}H and ^{13}C spectroscopy. The 18 proton resonance at 0.27 ppm in the ^{1}H NMR spectrum, along with quaternary carbon resonances at 94.10 and 105.17 ppm in the ^{13}C NMR spectrum were the most indicative features in the NMR spectra obtained.

Complex **(95)** was synthesised by the direct reaction of the trimethylsilyl protected di-yne ligand **(94)**. This was achieved by the *in situ* deprotection of the alkyne ligand in the dehydrohalogenation reaction with *trans-bis*(triethylphosphine)(phenyl)platinum(II) chloride. Sodium methoxide was added to the reaction mixture in order to deprotect the ligand, with standard conditions used as previously detailed in the synthesis of **(86)** in Section 5.2. The pure product was obtained after purification by chromatography and recrystallisation in a 48% yield. The complex was characterised by ^{1}H, ^{13}C, and ^{31}P NMR spectroscopies. The ^{1}H and ^{13}C NMR spectra both exhibited the expected resonances consistent with the expected molecular structure. The ^{31}P

NMR spectrum showed a singlet at 10.02 ppm with coupling observed to ^{195}Pt nuclei in the form of satellites corresponding to a coupling constant of $^{1}J_{PtP}$ = 2638 Hz. The elemental analysis results were consistent with the molecular formula $C_{62}H_{90}P_4Pt_2$.

5.6 UV-visible studies of complex (95)

To investigate the effects of the tetramethyl groups in complex **(95)** on the photophysical properties of the system, UV-visible absorption spectra as 0.01 mM dichloromethane solutions, at room temperature, were determined. Figure 5.8 shows the UV-visible absorption and emission spectra of the di-platinum complex **(95)** and the terphenyl analogue **(12)** for comparison.

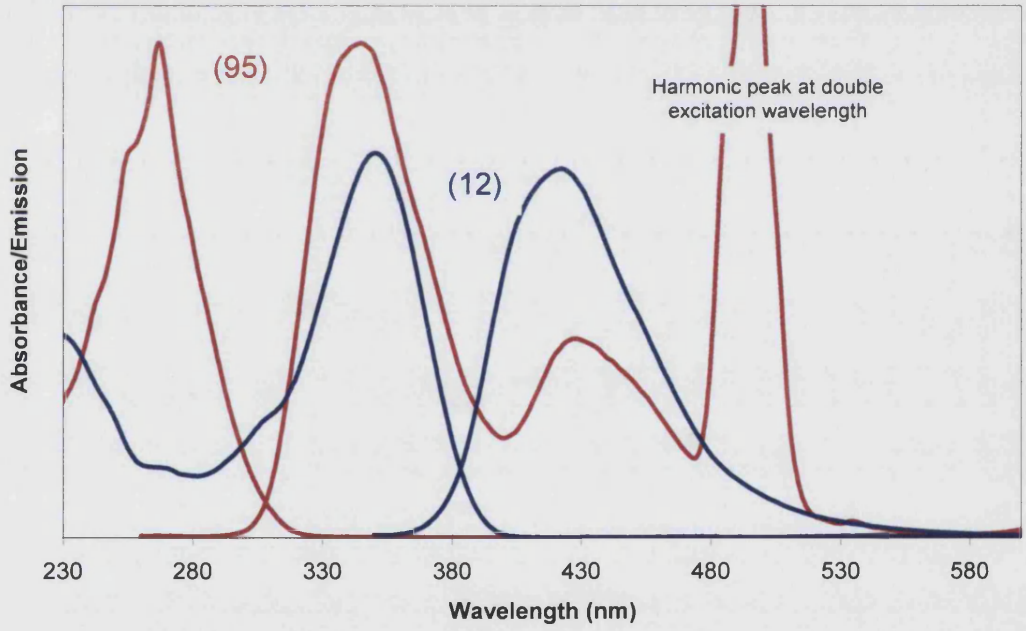

Figure 5.8 Absorption and emission spectra of (12) and (95) in CH_2Cl_2 solution at RT.

The absorption spectrum of **(95)** displays a sharp maximum peak at 267 nm and an onset of absorption at 335 nm (3.70 eV). The emission spectrum of **(95)** displays a maximum at 345 nm with a second peak at 428 nm. The energy difference between these two peaks equates to 0.7 eV. The existence of a second emission peak was observed and previously in the spectrum of **(55)**.

This was tentatively assigned to the emission from an excimer in solution and is also thought to be the case in this example.[10]

When comparing the spectra of **(95)** to the terphenyl analogue **(12)** it can be seen that there is a large shift to a higher optical energy gap for **(95)**. This is believed to be due to the steric interactions of the methyl groups with the *ortho* protons on the adjacent arene rings. This interaction is believed to enforce a large dihedral angle between the arene rings on the spacer ligand, thus reducing the effective π- conjugation through the complex.

5.7 Synthesis and UV-visible studies of complex (90)

In the extreme case, where the steric demands of the central di-yne ligand force the dihedral angle between adjacent rings to be close to 90°, within previously seen conjugated systems in this Thesis (Figure 5.9), the effective π- conjugation can be blocked at the point where the two rings are linked. This reduces the size of the choromophore and increases the optical energy gap of the system.

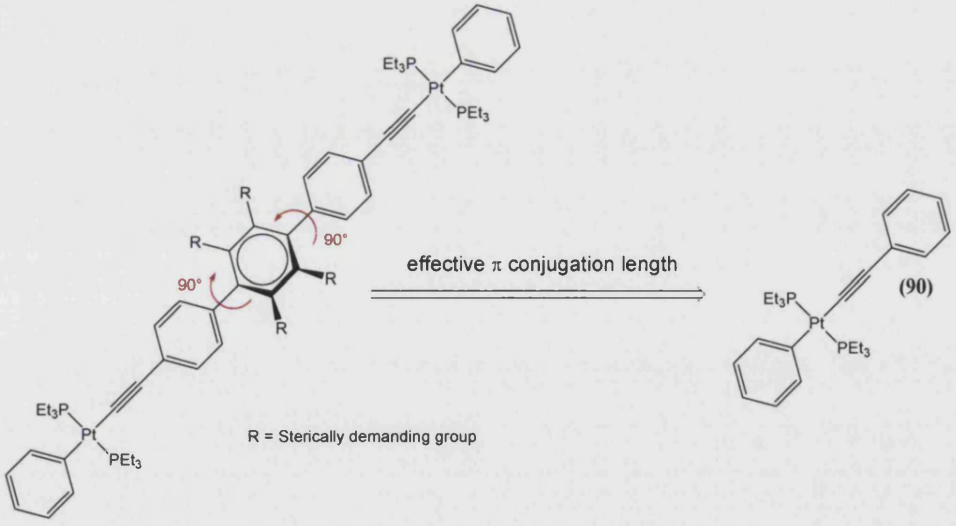

Figure 5.9 Complex (90) shown as a model complex for when π-conjugation is lost at the di-yne spacer group.

To model this situation complex **(90)** was synthesised and the photophysical properties studied by UV-visible spectroscopy. The results for this study can then be compared back to previously discussed complexes.

The synthesis of **(90)** was achieved by a one step reaction as shown in Figure 5.10. *Trans- bis*(triethylphosphine)(phenyl)platinum(II) chloride was reacted with ethynyl benzene, in a tetrahydrofuran and diisopropylamine solution. Copper(I) iodide was added as catalyst and the reaction was worked up as for previously seen dehydrohalogenation reaction involving di-yne ligands in this Thesis.

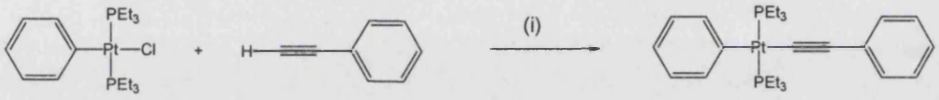

Figure 5.10 Synthesis of (90). (i) CuI, THF, $^{i}Pr_2NH$.

Complex **(90)** was achieved in a 91% yield and was characterised by ^{1}H, ^{13}C and ^{31}P NMR spectroscopies. The ^{31}P NMR spectrum exhibited a single resonance with ^{195}Pt satellites, at 10.10 ppm and $^{1}J_{PtP}$ coupling constant of 2642 Hz. The complex was structurally characterised by single crystal X-ray diffraction.

The molecular structure of **(90)** was determined by X-ray crystallography from a single crystal obtained from an ethanolic solution and is shown in Figure 5.11. Selected bond lengths and angles are provided in Table 5.3, with crystallographic data provided in Appendix 1.

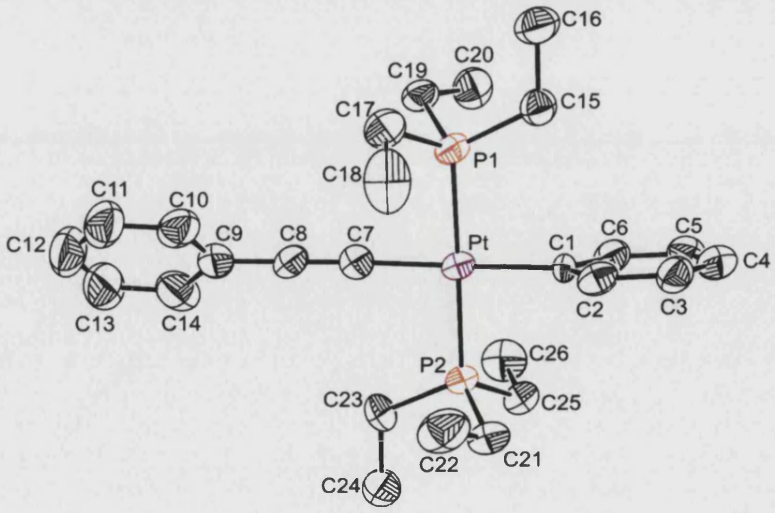

Figure 5.11 Molecular structure of (90) depicted with a 50% ellipsoid probability. Hydrogen atoms have been omitted for clarity.

The bond lengths and bond angles around the metal centre are comparable to similar platinum alkyne complexes characterised previously within the group and this Thesis.

Bond Lengths (Å)		**Bond Angles (°)**	
Pt-C_1	2.039(7)	Pt-C_7-C_8	173.3(9)
Pt-C_7	1.959(11)	P_1-Pt-P_2	177.92(10)
Pt-P_1	2.293(2)	C_1-Pt-C_7	173.9(4)
Pt-P_2	2.284(2)	**Dihedral Angles (°)**	
C_7-C_8	1.253(16)	C_{9-14}/C_1,C_7,P_1,P_2,Pt	45.19(17)
		C_{1-6}/C_1,C_7,P_1,P_2,Pt	84.34(17)

Table 5.3 Selected bond length and bond angle data for (90).

The geometry around the Pt centre is confirmed as pseudo square planar with the C_1-Pt-C_7 and P_1-Pt-P_2 bond angles being close to 180°. The square plane of the metal centre is related to the terminal arene ring (C_1-C_6) by a dihedral angle of 84.34(17)° and is related to the arene ring on the alkyne (C_9-C_{14}) by a dihedral angle of 45.19(17)°.

Once the identity and purity of **(90)** was confirmed, the photophysical properties of the complex were studied by solution UV-visible spectroscopy, in a 0.01 mM dichloromethane solution. The UV-visible absorption and emission spectra of **(90)** are shown in Figure 5.12. The emission spectrum was obtained after exciting the sample at 267 nm.

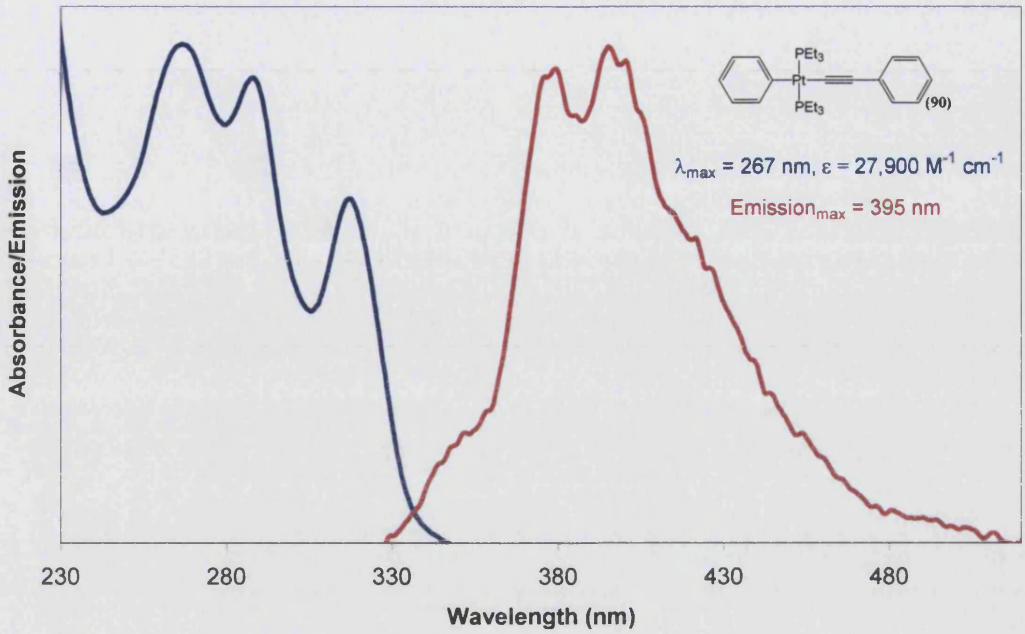

Figure 5.12 Absorption and emission spectra of (90) in CH_2Cl_2 at RT.

The absorption spectrum of **(90)** exhibits three main bands centred at 316, 287 and 267 nm. The onset of absorption is observed at 356 nm (3.48 eV). This is the second highest optical energy gap observed for all the Pt(II) complexes reported in this Thesis. The high optical energy gap for **(90)** is to be expected as this complex should contain the shortest length of the π- conjugated chromophore compared to the other Pt(II) complexes reported here. The duryl-containing Pt(II) complex **(95)** has an optical energy gap of 3.70 eV, the highest optical energy gap observed in this Thesis. The fact that complex **(95)** absorbs at an even higher energy implies that the four electron donating methyl groups on the central arene ring of the spacer group in **(95)** are causing the HOMO-LUMO gap to increase. The opposite effect is observed for the tetrafluoride complex **(85)** which has a relatively low optical gap of 3.19 eV due to the electron withdrawing effect of the fluoride groups.

5.8 Synthesis of Aza-cyclic ligands (99) and (101)

As part of the objectives outlined for this Chapter, it was intended to design new ligands where measures were taken to minimise the steric interactions between adjacent arene rings. Inspiration was taken from Chapter 3, where the protons were "removed" from the central heterocyclic ring, by synthesising diazole analogues. This section outlines the synthesis of two aza-cycle- containing ligands, where protons are "removed" and "replaced" with nitrogen atoms. The synthesis of a pyrimidine- **(99)** and tetrazine- **(101)** containing ligands is outlined below.

The synthetic strategy towards **(99)** required 5-bromo-2-iodo-pyrimidine as a starting material in the Suzuki coupling reaction with *p*-trimethylsilyl-phenyl boronic acid. The synthesis of the dihalide was achieved using literature preparations as outlined in Figure 5.13.

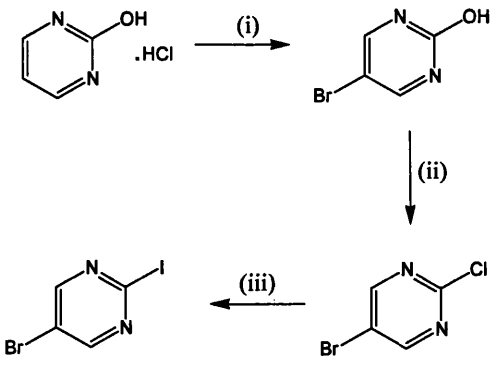

Figure 5.13 Synthesis of 5-bromo-2-iodo-pyrimidine. (i) Br_2, H_2O,[11] (ii) $POCl_3$, $PhNMe_2$, Δ,[12] (iii) conc. HI, CH_2Cl_2, 0 °C.[13]

5-Bromo-2-iodo-pyrimidine was subsequently reacted with *p*-trimethylsilyl-phenyl boronic acid in a Suzuki coupling reaction under standard conditions (Figure 5.14).[5] The analytically pure product **(98)** was achieved after purification by chromatography in an 82% yield. The product was characterised by ^1H and ^{13}C NMR spectroscopy, with the proton NMR spectrum showing the characteristic singlet resonance at 0.32 ppm corresponding to the 18 protons of the trimethylsilyl groups. The molecular formula of **(98)** was confirmed as $C_{22}H_{28}N_2Si_2$ by EI mass spectrometry and elemental analysis.

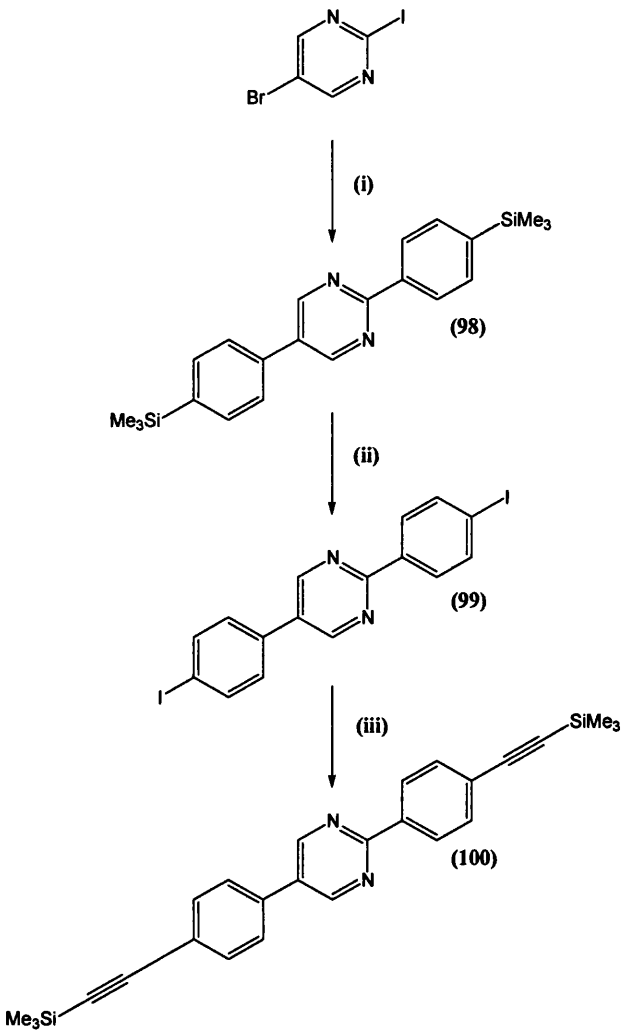

Figure 5.14 Synthesis of compound (100) (i) *p*-$Me_3Si(C_6H_4)B(OH)_2$, $Pd(PPh_3)_4$, $NaHCO_{3(aq)}$, toluene, Δ (ii) ICl, $CHCl_3$, (iii) Me_3SiCCH, $Pd(PPh_3)_2Cl_2$, CuI, $^iPr_2NH$, CH_2Cl_2.

Compound **(98)** was then reacted with iodine monochloride in a chloroform solution yielding the di-iodide compound **(99)** in a 70% yield. The cleavage of the trimethylsilyl groups was confirmed by the absence of the singlet at 0.32 ppm. Further analysis by EI mass spectrometry and elemental analysis confirmed the molecular formula of **(99)** to be $C_{16}H_{10}I_2N_2$.

Compound **(99)** was used in the Sonogashira coupling reaction with trimethylsilyl acetylene to give the protected di-yne ligand **(100)**. The conditions and work up of the reaction were similar to those outlined for previously discussed di-yne ligands in this Chapter. **(100)** was characterised by ^1H and ^{13}C NMR spectroscopy, with the ^1H NMR spectrum exhibiting two

resonances for trimethylsilyl groups at 0.02 and 0.07 ppm, each with a 9 proton integral.

The synthesis of the tetrazine- containing ligand **(102)** is detailed in Figure 5.15.

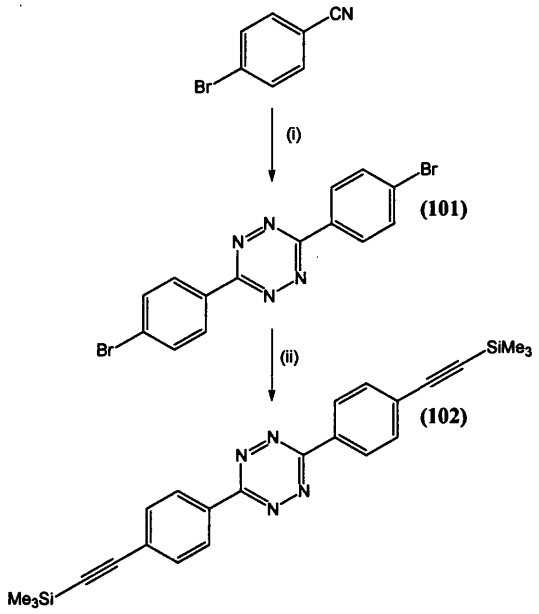

Figure 5.15 Synthesis of (102). (i) $Cu(NO_3)_2.3H_2O$, EtOH, $H_2NNH_2.H_2O$,[14] (ii) Me_3SiCCH, $Pd(PPh_3)_2Cl_2$, CuI, $^iPr_2NH$, DMF.

Compound **(101)** was synthesised by a literature preparation,[14] although the reported yield of 45% could not be obtained. **(101)** was achieved in 5% yield and was characterised by elemental analysis and EI mass spectrometry. NMR spectroscopic analysis was not obtained for **(101)** as the product was insoluble in all common organic solvents.

(101) was subsequently employed in the Sonogashira coupling reaction with trimethylsilylacetylene. Standard reaction conditions were used as previously described in this Thesis, with the exception of the solvent used, dimethylformamide was needed to solubalise the starting materials and the reaction was heated to 70 °C. After purification the pure product was obtained in 50% yield, and was characterised by ^1H and ^{13}C NMR spectroscopy. The presence of the alkynyl groups were confirmed by the observation of the characteristic ^{13}C NMR spectroscopic resonances at 98.42 and 104.33 ppm.

5.9 UV-visible studies of Aza-cyclic ligands (99) and (101)

Having successfully synthesised ligands **(100)** and **(102)**, the photophysical properties of these systems were investigated by UV-visible spectroscopy as 0.01 mM dichloromethane solutions. Figure 5.16 displays the UV-visible absorption and emission spectra of **(100)** and **(102)** along with **(10)** for comparison.

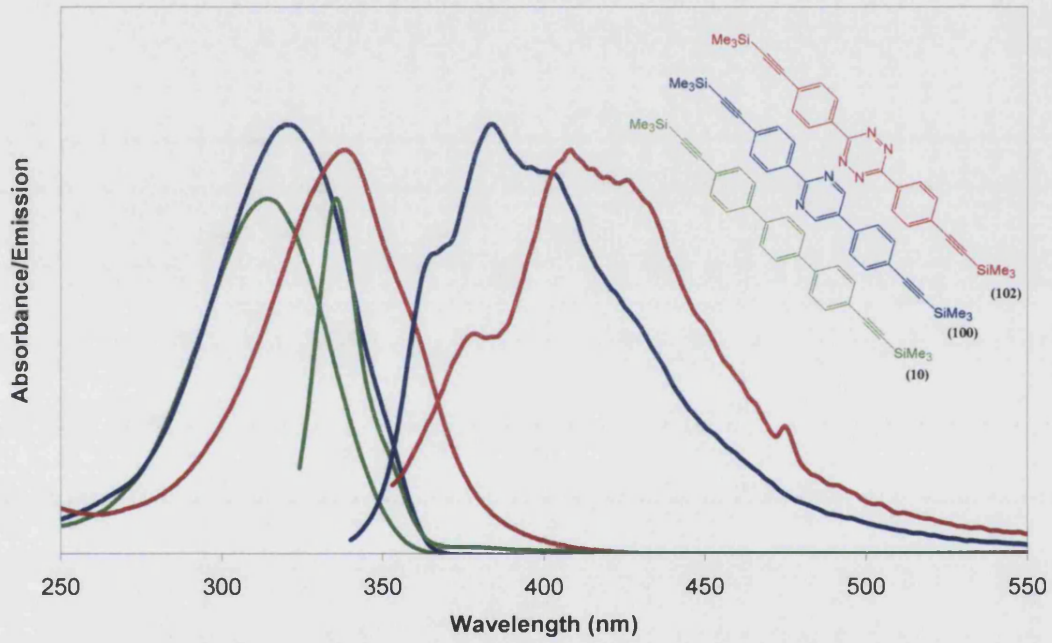

Figure 5.16 Absorption and emission spectra of compounds (10), (100) and (102), in CH_2Cl_2 solution at RT.

The absorption spectrum of **(100)** displays a maximum peak at 321 nm and an onset of absorption at 377 nm (3.29 eV). The emission spectrum of **(100)** displays a broad band with a maximum observed at 381 nm. Compound **(102)** displays a maximum peak at 338 nm in the absorption spectrum and an onset of absorption at 422 nm (2.94 eV). The emission spectrum of **(102)** displays a broad band with a maximum peak at 409 nm.

Me_3Si—≡—R—≡—$SiMe_3$					
R =	Onset of absorption (nm)	(eV)	λ_{max} (nm)	ε ($dm^3mol^{-1}cm^{-1}$)	Stokes Shift (nm)
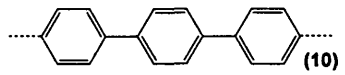 (10)	370	3.35	314	45,600	28
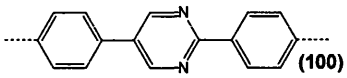 (100)	377	3.29	321	55,000	63
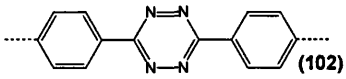 (102)	422	2.94	338	51,800	71

Table 5.4 Summary of photophysical data of complexes (10), (100) and (102).

Table 5.4 summarises the photophysical data obtained from solution UV-visible spectroscopy of **(10)**, **(100)** and **(102)**. A trend is observed in the optical energy gaps of the systems, with the magnitude of the optical energy decreasing in the order of **(10)>(100)>(102)**. This trend can be related to the number relative planar nature of the systems. The pyrimidine- containing ligand **(100)** has the possibility of one planar adjacent arene ring at the 2- position of the pyrimidine, and the tetrazine has the possibility of two planar adjacent arene rings at the 2- and 5- positions of the tetrazine ring. For this reason it can be concluded that the "minimising of steric effects" of the nitrogens are the cause of the trend observed for the optical energy gap. It can also be concluded the trend is not due to the electronic influence of increasing the number of nitrogen atoms, as it was observed in Chapter 3, with the diazole- containing systems, that the nitrogen atoms have an adverse effect on the optical energy gap.

5.10 Synthesis and characterisation of complex (106)

This section of work describes the synthesis of a new tri- platinum complex **(106)** with a tri-yne ligand. The motivation for this work was to investigate the effect of incorporation of a third metal centre as well as studying the effect of branching out the π- conjugation in two positions of the central arene ring of the spacer group.

The synthesis of the tri-yne ligand was achieved using literature procedures and is outlined in Figure 5.17.[15,16]

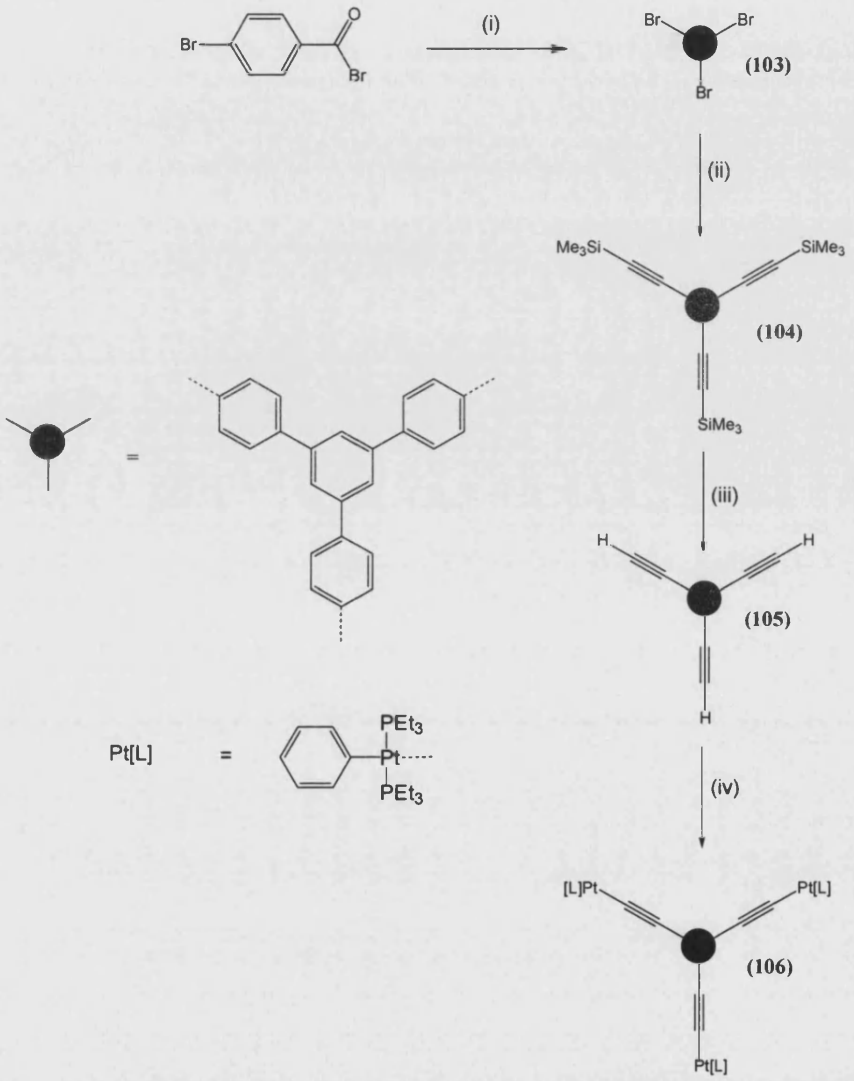

Figure 5.17 Synthesis of (106). (i) $SiCl_4$, EtOH, [15] (ii) $Pd(PPh_3)_2Cl_2$, CuI, Et_2NH, CH_2Cl_2,[16] (iii) KOH(aq) MeOH,[16] (iv) $Pt(Ph)(PEt_3)_2Cl$, CuI, Et_2NH, CH_2Cl_2.

The synthesis of complex **(106)** was achieved by the dehydrohalogenation reaction of **(105)** and three molar equivalents of *trans-bis*(triethylphosphine)(phenyl)platinum(II) chloride. The reaction was carried out in the presence of copper iodide catalyst in a dichloromethane and diethylamine solvent mixture. The reaction was worked up as previously seen for di-nuclear platinum complexes in this Thesis and was purified by recrystallisation from ethanol. **(106)** was achieved in a 69% yield, and was

characterised by multinuclear NMR spectroscopy, with the ^{31}P NMR displaying a single resonance at 11.09 ppm and ^{195}Pt satellites ($^{1}J_{PtP}$ = 2367 Hz). Characterisation was supported by elemental analysis, as well as structural characterisation achieved by single crystal X-ray diffraction.

The molecular structure of **(106)** was determined by X-ray crystallography from a single crystal obtained from an ethanolic solution and is shown in Figure 5.18. Selected bond lengths and angles are provided in Table 5.5, with crystallographic data provided in Appendix 1.

All three Pt centres are surrounded by four ligands in a square planar geometry. The central arene ring (C_1-C_6) on the spacer ligand is related to the adjacent arene rings by three dihedral angles; 25.96(16)° (C_7-C_{12}), 23.06(15)° (C_{13}-C_{18}) and 42.79(16)° (C_{19}-C_{24}). The dihedral angle between adjacent spacer group rings of the related complex **(12)** in Chapter 2 (terphenyl spacer) was found to be 34.4(3)°. It could be predicted that the dihedral angles observed in **(106)** would be greater than the analogous complex **(12)**, because the arene rings are arranged in a *para* arrangement in **(12)** and a *meta* arrangement in **(106)**, giving rise to greater steric interactions in the latter.

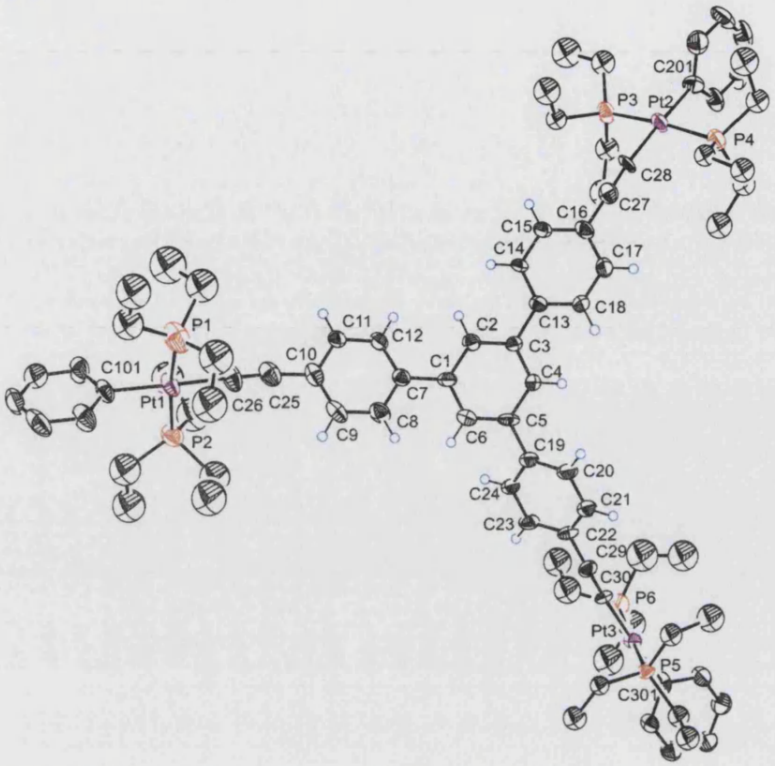

Figure 5.18 Molecular structure of (106) depicted with a 50% ellipsoid probability. Hydrogens have been omitted for clarity, except for those on the tri-yne ligand which are shown in blue.

Bond Lengths (Å)		Bond Angles (°)	
Pt_1-C_{26}	1.994(18)	Pt_1-C_{26}-C_{25}	177.21(18)
Pt_2-C_{28}	2.002(12)	Pt_2-C_{28}-C_{27}	169.90(21)
Pt_3-C_{30}	2.002(16)	Pt_3-C_{30}-C_{29}	175.92(15)
Pt_1-P_1	2.288(13)	P_1-Pt_1-P_2	171.57(16)
Pt_1-P_2	2.264(12)	P_3-Pt_2-P_4	173.55(20)
Pt_2-P_3	2.287(13)	P_5-Pt_3-P_6	173.34(16)
Pt_2-P_4	2.289(14)	C_{26}-Pt_1-C_{101}	178.36(19)
Pt_3-P_5	2.290(12)	C_{28}-Pt_2-C_{201}	175.51(17)
Pt_3-P_6	2.280(13)	C_{30}-Pt_3-C_{301}	177.94(17)
Pt_1-C_{101}	2.084(13)	**Dihedral Angles (°)**	
Pt_2-C_{201}	2.057(11)	$C_{1\text{-}6}$/$C_{7\text{-}12}$	25.96(16)
Pt_3-C_{301}	2.044(12)	$C_{1\text{-}6}$/$C_{13\text{-}18}$	23.06(15)
C_{25}-C_{26}	1.245(12)	$C_{1\text{-}6}$/$C_{19\text{-}24}$	42.79(16)
C_{27}-C_{28}	1.211(9)		
C_{29}-C_{30}	1.216(10)		

Table 5.5 Selected bond angles and bond lengths of (106).

5.11 UV-visible studies of complex (106)

Once the identity and purity of **(106)** was confirmed, the photophysical properties of the complex were studied by solution UV-visible spectroscopy, as 0.01 mM dichloromethane solution. The UV-visible absorption and emission spectra of **(106)** are shown in Figure 5.19. The emission spectrum was obtained after exciting the sample at 392 nm. The electronic spectra of **(12)** are also shown in Figure 5.19 for comparison.

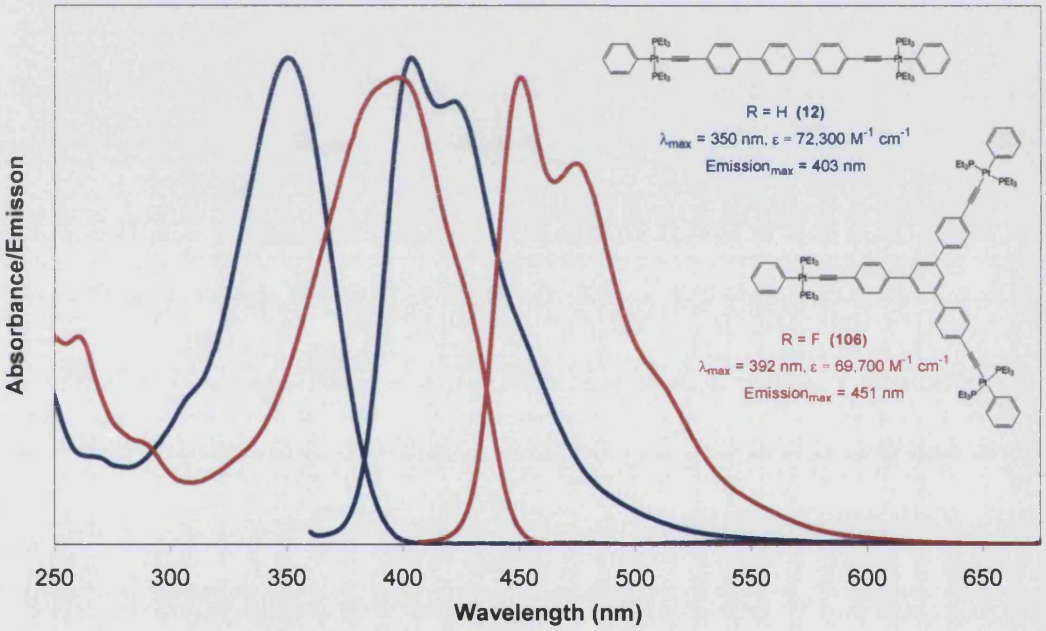

Figure 5.19 UV-visible absorption and emission spectra of (106) and (12) in CH_2Cl_2 at RT.

The absorption spectrum of **(106)** exhibits one major broad band centred at 392 nm. The onset of absorption is observed at 470 nm (2.64 eV), this is 0.4 eV lower than **(12)**. The drop in the optical energy gap of **(106)** compared to **(12)** is consistent with the increase in the size of the chromophore and suggests that delocalisation is spread over the whole of the system between all three Pt(II) centres. The emission spectrum of **(106)** shows two main peaks at 450 and 477 nm, and is similar in peak shape to the emission spectrum of **(12)** with a shift to higher wavelength.

5.12 Conclusions

The aim of the work in this Chapter was to design a series of new di-yne ligands in order to study the effects of steric interactions within the spacer group on the photophysical properties of the di-yne ligands and corresponding complexes.

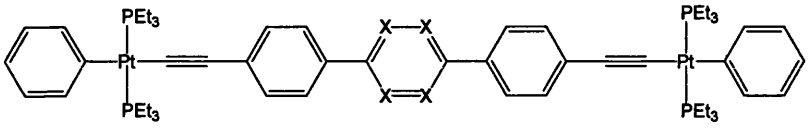

Fluorine and methyl groups were used on the central arene ring of the spacer groups in complexes **(86)** (X= CF) and **(95)** (X= CCH_3), respectively, to impose greater steric interactions between adjacent rings than in **(12)** (X= CH). The effect of the substitution of these sterically demanding groups produced a bathochromic shift in the solution UV-visible spectra. The observation of the bathochromic shift is consistent with the reduction in the delocalisation of the system as the twist angle increases. However, the electron donating or withdrawing properties of the methyl and fluorine groups, respectively have a secondary influence on the position of the absorption band which may reinforce or negate the steric effect. The presence of the fluorine groups was proven to decrease the optical gap, as complex **(89)** displayed an optical gap 0.07 eV lower than the non-fluorinated analogue **(3)**.

Planarisation of the spacer group was attempted in the hope to increase the orbital overlap of the system to increase delocalisation, by the synthesis of the new di-yne ligand **(102)**. This new tetrazine- containing ligand displayed an optical energy gap of 2.94 eV, which was 0.41 eV lower than the terphenyl-containing ligand **(10)**. Partial planarisation was achieved by the synthesis of the new pyrimidine- containing ligand **(100)**, which displayed an optical gap of 3.29 eV, 0.06 eV lower than **(10)**. This shows the ability to influence the electronic properties by introducing a more planar central chromophore.

Increase in the size of the chromophore of **(12)** was investigated by synthesising a tri-nuclear Pt(II) complex **(106)**. The solution state UV-visible spectra of these two complexes were compared, with **(106)** displaying a lower optical energy gap of 0.4 eV. The solid state structure of **(106)** showed greater dihedral angles between adjacent arene rings of the spacer group when compared to **(12)**, this will have had a energy increasing effect on the HOMO-LUMO energy gap of the system.

To summarise all the optical energy gaps of all the compounds examined in this Thesis Table 5.6 lists the compound reference number along with the associated optical energy gap.

Compound	Optical Gap (eV)	Compound	Optical Gap (eV)
(2)	4.14	**(55)**	3.11
(3)	3.20	**(57)**	2.80
(5)	3.76	**(61)**	2.77
(6)	3.13	**(65)**	2.77
(11)	3.22	**(69)**	2.77
(12)	3.04	**(73)**	3.01
(22)	2.83	**(77)**	3.00
(26)	2.69	**(86)**	3.16
(32)	2.66	**(89)**	3.13
(36)	3.01	**(90)**	3.48
(40)	2.65	**(95)**	3.70
(43)	2.58	**(100)**	3.29
(48)	2.88	**(102)**	2.94
(52)	2.71	**(106)**	2.64

Table 5.6 Summary of optical energy gaps for compounds studied in this Thesis.

Increase in the size of the chromophore of **(12)** was investigated by synthesising a tri-nuclear Pt(II) complex **(106)**. The solution state UV-visible spectra of these two complexes were compared, with **(106)** displaying a lower optical energy gap of 0.4 eV. The solid state structure of **(106)** showed greater dihedral angles between adjacent arene rings of the spacer group when compared to **(12)**, this will have had a energy increasing effect on the HOMO-LUMO energy gap of the system.

5.13 References

[1] A. P. Monkman, L. Pålsson, R. W. T. Higgins, C. Wang, M. R. Bryce, A. S. Batsanov, J. A. K. Howard, *J. Am. Chem. Soc.*, 2002, **124**, 6049

[2] J. L. Segura, N. Martin, *J. Mater. Chem.*, 2000, **10**, 2403

[3] A. Onipko, Y. Klymenko, L. Malysheva, *J. Chem. Phys.*, 1997, **107**, 7331

[4] J. J. S. Lamba, J. M. Tour, *J. Am. Chem. Soc.*, 1994, **116**, 11723

[5] N. Miyaura, T. Yanagi, A. Suzuki., *Synth. Commun.*, 1981, **11**, 513

[6] M. S. Khan, M. R. A. Al-Mandhary, M. K. Al-Suti, T. C. Corcoran, Y. Al-Mahrooqi, J. P. Attfield, N. Feeder, W. I. F. David, K. Shankland, R. H. Friend, A. Köhler, E. A. Marseglia, E. Tedesco, C. C. Tang, P. R. Raithby, J. C. Collings, K. P. Roscoe, A. S. Batsanov, L. M. Stimson, T. B. Marder, *New. J. Chem.*, 2003, **27**, 140

[7] F. Waugh, D. R. M. Walton, *J. Organomet. Chem.*, 1972, **39**, 275

[8] H. B. Fyfe, M. Mlekuz, D. Zargarian, N. J. Taylor, T. B. Marder, *J. Chem. Soc., Chem. Commun.*, 1991, 188

[9] M. J. Ahrens, L. E. Sinks, B. Rybtchinski, W. Liu, B. A. Jones, J. M. Giaimo, A.V. Gusev, A. J. Goshe, D. M. Tiede, M. R. Wasielewski, *J. Am. Chem. Soc.*, 2004, **126**, 8284

[10] C. E.Wayne, R. P. Wayne, *Photochemistry*, Oxford, University Press. 2001

[11] J. W. Goodby, M. Hird, R. A. Lewis, K. J. Toyne, *Chem. Commun.*, 1996, **24**, 2719

[12] T. Shibata, S. Yonekubo, K. Soai, *Angew. Chem. Int. Ed.*,1999, **38**, 659

[13] G. Vlad, I. T. Horvath, *J. Org. Chem.*, 2002, **67**, 6550

[14] C. L. Lim, S. H. Pyo, T. Y. Kim, E. S. Yim, B. H Han, *Bull. Korean Chem. Soc.*, 1995, **16**, 374

[15] S. Kotha, M. Kashinath, S. Dhurke, P. Lahiri, K. Kakali, W. Sunoj, B. Raghavan, *Eur. J. Org. Chem.*, 2004, **19**, 4003

[16] E. Weber, M. Hecker, E. Koepp, W. Orlia, M. Czugler, I. Csoeregh, *J. Chem. Soc. Perkin Trans. 2*, 1988, 1251

Chapter 6

Experimental

6. Experimental Details

6.1 General methods and instrumentation

All air sensitive reactions were carried out under dinitrogen or argon atmospheres using either standard Schlenk line or dry box techniques.[1] Dichloromethane and tetrahydrofuran were dried and degassed under an argon atmosphere over activated alumina columns using an Innovative Technology Solvent Purification System (SPS) and degassed using argon prior to use in air sensitive reactions. All secondary and tertiary amines were purified by distillation using calcium hydride as a drying agent and stored under argon in Young's ampoules over 4 Å molecular sieves.

NMR spectra were recorded on Bruker AV300 or AVANCE 400 spectrometers at 298 K unless otherwise stated. ^{1}H NMR spectra were referenced internally to residual protio-solvent ($CHCl_3$ at 7.26 ppm) and ^{13}C NMR spectra referenced to deuterio-solvent resonance ($CDCl_3$ at 77.0 ppm). ^{19}F NMR spectra were referenced to $C_6H_5CF_3$ (-63.72 ppm), ^{31}P NMR spectra to 85% H_3PO_4 (0.00 ppm) and ^{77}Se NMR spectra to selenophene (605.0 ppm). Assignments were supported by ^{13}C PENDANT NMR and homo- and hetero-nuclear, one- and two-dimensional experiments as appropriate.

IR spectra were recorded as KBr discs on a Nicolet – Nexus FTIR spectrometer in the range of 4000 – 400 cm^{-1} and averaged over 16 scans, and data quoted in wavenumbers (cm^{-1}).

Mass spectra were recorded at the EPSRC National Mass Spectrometry Service at the University of Wales, Swansea, using either Electron Impact (EI) or Chemical Ionisation (CI) as the method of ionisation.

Electronic absorption spectra were recorded using a Perkin Elmer Lambda 650 UV-vis Spectrometer. Samples were prepared in "Grade A" volumetric glassware and analysed in 1.0 cm path length quartz cells at 200 nm/min band pass rate, and spectra recorded as an average of three scans. Emission spectra were recorded using a Perkin Elmer LS55 Luminescence Spectrometer. Samples were analysed in 1.0 cm path

length quartz cells using a 10.0 nm excitation slit width and 240 nm/min band pass rate.

Elemental analyses were carried out in house using an Exeter Analytical CE 440 elemental analyser.

Single crystals for X-ray analysis were mounted onto the goniometer head by means of a glass fibre and perfluoro polyether oil. Data was collected using a Brüker Nonius Kappa CCD diffractometer fitted with a CCD area detector and cryostream to cool the sample to low temperature.

Unless stated otherwise chemicals were obtained commercially and used as received. Precursor compounds were prepared by literature methods. Where it was necessary to alter the work-up or purification procedure to obtain satisfactory results, or where characterisation of the materials was incomplete in literature, full synthetic procedures and characterisation data is reported here. The following compounds were synthesised by literature methods; 1,4-diethynyl-benzene,[2] 4,4'-diethynyl-biphenyl,[3] 2-bromo-1-(4-bromo-phenyl)-ethanone, [4] 2,5-diethynyl-thiophene, [5] 1,4-dibromo-durene, [6] 5-bromo-2-chloropyrimidine, [7] 5-bromo-2-iodopyrimidine, [8] 1,3,5-*tris*-[(4-bromo)phenyl]benzene,[9] 1,3,5-tris-[(4-trimethylsilylethynyl)phenyl]benzene,[10] *trans-bis*(triethylphosphine)(phenyl)platinum(II) chloride, [11] *trans- bis* (diethylphenyl-phosphine)(phenyl)platinum(II) chloride,[11] triphenylphosphine-gold(I) chloride.[12]

6.2 Experimental details for Chapter Two

6.2.1 Synthesis of 1,4-*di*-(*trans*-(phenyl,*bis*-triethylphosphine)platinum) ethynyl-benzene (3)[13]

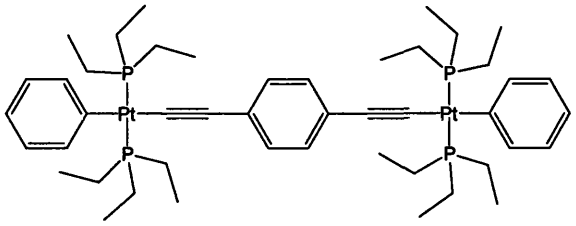

Trans-bis(triethylphosphine)(phenyl)platinum(II)chloride (250 mg, 0.458 mmol), 1,4-diethynylbenzene (28.8 mg, 0.229 mmol) and copper(I) iodide (~5 mg) were placed in a Schlenk tube. Dichloromethane (15 mL) and diisopropylamine (15 mL) were added and the reaction left to stir for 16 hr after which time completion of the reaction was confirmed by TLC (silica, dichloromethane). The volatiles were removed under reduced pressure to afford a solid. The crude product was then passed through a plug of alumina with ethyl acetate as the eluent, the volatiles again removed under reduced pressure, and the resulting solid recrystallised from ethanol to afford **(3)** as yellow crystals (196 mg, 75%).

^{1}H NMR ($CDCl_3$, 400.13 MHz)

1.05-1.12 (m, C*H*$_3$, 36H), 1.72-1.79 (m, C*H*$_2$, 24H), 6.80 (t, ^3J = 14.7 Hz, C*H*, 2H), 6.96 (t, ^3J = 14.7 Hz, C*H*, 4H), 7.14 (s, C*H*, 4H), 7.33 (m, C*H*, 4H)

^{13}C{^{1}H} NMR – PENDANT ($CDCl_3$, 100.61 MHz)

8.36	CH_3	($P(CH_2CH_3)_3$)	126.02	CH	(*para*, Pt-*Ph*)
15.45	CH_2	(($P(CH_2CH_3)_3$), t_{ps}, $^1J_{PC}+^3J_{PC}$ = 34 Hz)	127.58	CH	(*meta*, Pt-*Ph*)
			130.72	CH	(C_6H_4)
111.13	C_q	(C≡C-Pt)	139.60	C_{ipso}	(C_6H_5Pt)
113.28	C_q	(C≡C-Pt)	Inner phenyl C_{ipso} absent		
121.48	CH	(*ortho*, Pt-*Ph*)			

^{31}P{^{1}H} NMR ($CDCl_3$, 161.97 MHz)

9.89 ($^1J_{PtP}$ = 2642 Hz)

IR (KBr disc, ν cm^{-1}): 3046, 2968, 2936, 2855 (C-H), 2093 (C≡C)

UV/vis: λ_{max} = 349 nm, ε = 51,300 $dm^3mol^{-1}cm^{-1}$

Emission: λ_{max} = 366 nm

6.2.2 Synthesis of 4,4'-*di*-(*trans*-(phenyl,*bis*-triethylphosphine)platinum) ethynyl-biphenyl (6)

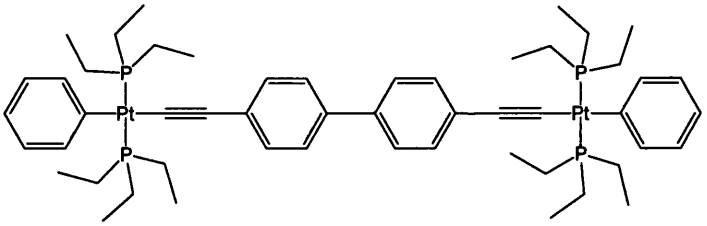

Trans-bis(triethylphosphine)(phenyl)platinum(II)chloride (272 mg, 0.50 mmol), 4,4′-diethynylbiphenyl (50.5 mg, 0.25 mmol) and copper(I) iodide (~5 mg) were placed in a Schlenk tube. Dichloromethane (10 mL) and diisopropylamine (10 mL) were added and the reaction left to stir for 12 hr after which time completion of the reaction was confirmed by TLC (silica, dichloromethane/hexane, 1:1 v/v). The volatiles were removed under reduced pressure. The crude product was then passed through a plug of alumina with ethyl acetate as the eluent, the volatiles were removed under reduced pressure, and the resulting solid recrystallised from ethanol to afford **(6)** as cream crystals (218 mg, 72%).

^{1}H NMR ($CDCl_3$, 400.13 MHz)

1.10 (m, C*H*$_3$, 36H), 1.77 (m, C*H*$_2$, 24H), 6.80 (m, C*H*, 2H), 6.96 (m, C*H*, 4H), 7.34 (d, ^3J = 8.0 Hz, 4H), 7.43 (d, ^3J = 8.0 Hz, 4H)

^{13}C{^{1}H} NMR – PENDANT ($CDCl_3$, 100.61 MHz)

8.03	CH_3	($P(CH_2CH_3)_3$)	127.28	*C*H	(*meta*, Pt-*Ph*)
15.12	CH_2	($P(CH_2CH_3)_3$, t_{ps}, $^1J_{PC}+^3J_{PC}$ = 34 Hz)	128.09	C_{ipso}	(C≡C-C_{ipso})
			137.23	C_{ipso}	(biphenyl)
110.13	C_q	(*C*≡C-Pt)	131.14	*C*H	(*meta* to alkyne)
114.28	C_q	(C≡*C*-Pt)	139.21	*C*H	(*ortho*, Pt-*Ph*)
121.20	*C*H	(*para*, Pt-*Ph*)	156.45	C_{ipso}	(Pt-*Ph*)
126.20	*C*H	(*ortho* to alkyne)			

^{31}P{^{1}H} NMR ($CDCl_3$, 161.97 MHz)

10.03 ($^1J_{PtP}$ = 2640 Hz)

Elemental Analysis: Result % (calculated %): C = 50.7 (51.3), H = 6.34 (6.46)

IR (KBr disc, ν cm^{-1}): 3046, 2968, 2936(C-H), 2090 (C≡C)

UV/vis: λ_{max} = 349 nm, ε = 58,800 dm^{3}mol^{-1}cm^{-1}

Emission: λ_{max} = 387 nm

6.2.3 Synthesis of 4,4''-*di*-(*trans*-(phenyl,*bis*-(diethyl) (phenyl) phosphine) platinum) ethynyl-biphenyl (7)

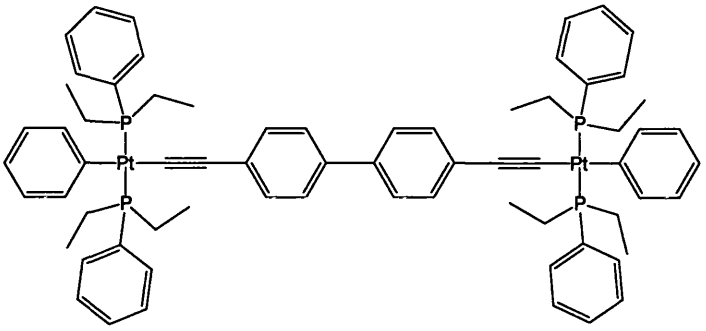

Trans-bis(diethylphenylphosphine)(phenyl)platinum(II)chloride (320 mg, 0.50 mmol), 4,4'-diethynylbiphenyl (50.5 mg, 0.25 mmol) and copper(I) iodide (~5 mg) were placed in a Schlenk tube. Dichloromethane (10 mL) and diisopropylamine (10 mL) were added and the reaction left to stir for 18 hr after which time completion of the reaction was confirmed by TLC (silica, dichloromethane/hexane, 2:1 v/v). The volatiles were removed under reduced pressure. The crude product was then passed through a small plug of alumina in ethyl acetate, and the eluted solvent was evaporated to dryness. The resulting solid was recrystallised from ethanol to afford **(7)** as yellow crystals (230 mg, 65%).

^{1}H NMR ($CDCl_3$, 400.13 MHz)

0.97-1.05 (m, C*H*$_3$, 18H), 1.97-2.08 (m, C*H*$_A$, 8H), 2.10-2.21 (m, C*H*$_B$, 8H), 6.69-6.77 (m, C*H*, 6H), 6.92 (d, ^3J = 6.3 Hz, C*H*, 4H), 7.24 (d, ^3J = 8.6 Hz, C*H*, 4H), 7.35-7.36 (m, C*H*, 12H), 7.41 (d, ^3J = 8.6 Hz, C*H*, 4H), 7.53-7.60 (m, C*H*, 8H)

^{13}C{^{1}H} NMR – PENDANT ($CDCl_3$, 100.61 MHz)

7.72	CH_3	($P(CH_2CH_3)_3$)	129.31	*C*H	(*ortho* to alkyne)
15.60	CH_2	(($P(CH_2CH_3)_3$), t_{ps}, $^1J_{PC}+^3J_{PC}$ = 34 Hz)	131.24	*C*H	(*meta*, Pt-*Ph*)
			131.62	C_{ipso}	(C≡C-C_{ipso})
111.12	C_q	(*C*≡C-Pt)	131.86	C_{ipso}	(biphenyl)
113.88	C_q	(C≡*C*-Pt)	132.08	*C*H	(*meta* to alkyne)
121.19	*C*H	(*para*, Pt-*Ph*)	137.27	C_{ipso}	(P(*Ph*))
126.13	*C*H	(P(*Ph*))	139.11	*C*H	(*ortho*, Pt-*Ph*)
126.96	*C*H	(P(*Ph*))	154.57	C_{ipso}	(Pt-*Ph*)
128.88	*C*H	(P(*Ph*))			

$^{31}P\{^{1}H\}$ NMR ($CDCl_3$, 161.97 MHz)

10.27 ($^{1}J_{PtP}$ = 2721 Hz)

Elemental Analysis: Result % (calculated %): C = 57.2 (58.0), H = 5.63 (5.58)

IR (KBr disc, ν cm^{-1}): 3046, 2968, 2936, 2875 (C-H), 2096 (C≡C)

UV/vis: λ_{max} = 351 nm, ε = 58,800 $dm^3mol^{-1}cm^{-1}$

Emission: λ_{max} = 388 nm

6.2.4 Synthesis of 4,4''-*bis*-(trimethylsilyl)-terphenyl (8)[14]

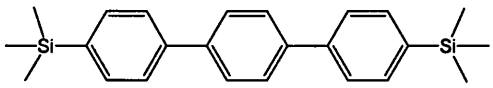

4-trimethylsilyl

4-trimethylsilyl phenylboronic acid (600 mg, 3.09 mmol), 1,4-diiodobenzene (339 mg, 1.03 mmol), tetrakis(triphenylphosphine)palladium(0) (173 mg, 1.50 mmol) were placed into a round bottomed flask. Toluene (30 mL) and sodium carbonate (2.0 M aqueous solution, 20 mL) were added and the solution refluxed under an inert atmosphere. The reaction was monitored by TLC (silica, dichloromethane) and after 48 hr was complete. The volatiles were removed under reduced pressure and the crude product was redissolved in chloroform, this was washed with saturated sodium hydrogen carbonate (2 x 50 mL) then water (2 x 50 mL). The organic phase was dried ($MgSO_4$) and the volatiles removed under reduced pressure to yield an off white solid. This solid was then recrystallised from methanol affording **(8)** as a white powder (262 mg, 68%).

^{1}H NMR ($CDCl_3$, 300.22 MHz)

0.32 (s, CH_3, 18H), 7.53-7.59 (m, CH, 8H), 7.60-7.65 (m, CH, 4H)

$^{13}C\{^{1}H\}$ NMR – PENDANT ($CDCl_3$, 75.49 MHz, δ ppm)

-2.10	CH_3	($SiCH_3$)	138.30	C_{ipso}	(central C_6H_4)
125.40	CH	(central C_6H_4)	139.10	C_{ipso}	(*para* to $SiMe_3$)
126.50	CH	(*meta* to $SiMe_3$)	140.04	C_{ipso}	($CSiMe_3$)
132.90	CH	(*ortho* to $SiMe_3$)			

6.2.5 Synthesis of 4,4''-diiodo-*p*-terphenyl (9)[15,16]

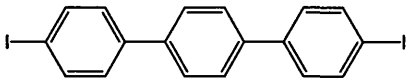

Iodine monochloride (1.18 mL, 1.00 M solution in dichloromethane) was added dropwise to a stirring solution of 4,4''-*bis*(trimethylsilyl)-*p*-terphenyl **(4)** (200 mg, 0.53 mmol) in chloroform (20 mL). On addition of the iodine monochloride the solution turned a bright orange colour and a white precipitate was formed. TLC (silica, dichloromethane/hexane, 1:1 v/v) of the mixture after 1 hr revealed the completion of reaction. Saturated sodium thiosulphate (10 mL) was added to quench excess iodine. The organic layer was separated, washed with water (2 x 20 mL) and then dried ($MgSO_4$). The solvent was removed under reduced pressure yielding an off white solid which was recrystallised from chloroform affording **(9)** as a white solid (180 mg, 62%).

^{1}H NMR ($CDCl_3$, 400.13 MHz)

7.37 (d, ^3J=8.0 Hz, C*H*, 4H), 7.63 (s, C*H*, 4H), 7.79 (d, ^3J=8.0 Hz, C*H*, 4H)

^{13}C{^{1}H} NMR ($CDCl_3$, 75.49 MHz)

127.31	CH	(central C_6H_4)	137.89	CH	(*ortho* to iodide)
128.78	CH	(*meta* to iodide)	140.00	C_{ipso}	(central C_6H_4)

Two *ipso* carbons are absent from the spectrum due to the poor solubility of the product in all common organic solvents.

6.2.6 Synthesis of 4,4''-*bis*trimethylsilylethynyl-*p*-terphenyl (10)[17]

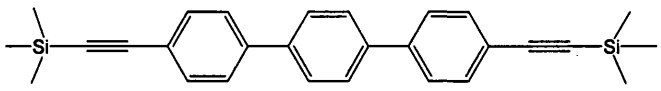

4,4''-diiodo-*p*-terphenyl **(5)** (150 mg, 0.27 mmol), copper iodide (5 mg, 0.03 mmol) and *bis*(triphenylphosphine)palladium(II)chloride (38 mg, 0.05 mmol) were placed in a Schlenk tube. Tetrahydrofuran (50 mL), diisopropylamine (10 mL) and trimethylsilylacetylene (0.12 mL, 0.82 mmol) were added respectively and the reaction was left to stir, under protection from light, for 16 hr. TLC (silica, dichloromethane/hexane, 4:1 v/v) revealed completion of reaction and the volatiles

were removed under reduced pressure. The resulting solid was dissolved in hexane/ethyl acetate (1:1 v/v) and passed through an alumina plug, after which the solvent was removed yielding a brown solid. Recrystallisation of the crude product from ethanol afforded **(10)** as an off white solid (110 mg, 96%).

^{1}H NMR ($CDCl_3$, 400.13 MHz)

0.21 (s, C*H*$_3$, 18H), 7.20 (s, C*H*, 4H), 7.48 (d, ^3J=8.4 Hz, C*H*, 4H), 7.52 (d, ^3J=8.4 Hz, C*H*, 4H)

^{13}C{^{1}H} NMR – PENDANT ($CDCl_3$, 100.61 MHz)

-1.01	CH_3	($SiCH_3$)	126.42	*C*H	(central C_6H_4)
94.08	C_q	(C≡*C*-Si)	131.46	*C*H	(*ortho* to alkyne)
103.94	C_q	(C≡*C*-C)	138.56	C_{ipso}	(central C_6H_4)
121.23	C_{ipso}	(C≡C-*C*)	139.45	C_{ipso}	(*para* to alkyne)
125.71	*C*H	(*meta* to alkyne)			

IR (KBr disc, ν cm^{-1}): 3122, 2959, 2889 (C-H), 2156 (C≡C), 1250 (Si-C)

6.2.7 Synthesis of 4,4''-*di*-ethynyl-terphenyl (11)

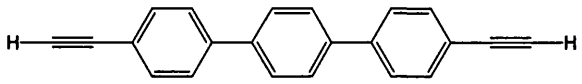

Potassium hydroxide (0.24 mL, 2.00 M aqueous solution) was added to a stirring solution of 4,4''-*bis*-trimethylsilylethynyl-terphenyl **(10)** (90 mg, 0.21 mmol) in dichloromethane/methanol (40 mL, 1:1 mixture). The solution was left to stir, in the absence light, for 18 hr and the reaction progress was monitored by TLC (silica, dichloromethane/hexane, 4:1 v/v). The volatiles were removed under reduced pressure; the solid was redissolved in dichloromethane and washed with water (2 x 50 mL). The organic phase was dried ($MgSO_4$) and the volatiles were removed to afford **(11)** as a pale yellow solid (42 mg, 72%).

^{1}H NMR ($CDCl_3$, 300.22 MHz)

3.14 (s, C≡C*H*, 2H), 7.60 (m, C*H*, 8H), 7.68 (m, C*H*, 4H)

$^{13}C\{^1H\}$ NMR – PENDANT ($CDCl_3$, 100.61 MHz)

83.84	*C*H	(C≡*C*H)	127.86	*C*H	(central C_6H_4)
96.93	C_q	(C≡*C*Ph)	132.99	*C*H	(*meta* to alkyne)
121.53	C_q	(C≡C*Ph*)	139.92	C_{ipso}	(central C_6H_4)
127.23	*C*H	(*ortho* to alkyne)	141.19	C_{ipso}	(*para* to alkyne)

IR (KBr disc, ν cm^{-1}): 3023, 2989 (C-H), 2100 (C≡C), 1921 (C≡C-H)

6.2.8 Synthesis of 4,4''-*bis*-(*trans*-(phenyl,*bis*-triethylphosphine)platinum) ethynyl-terphenyl (12)

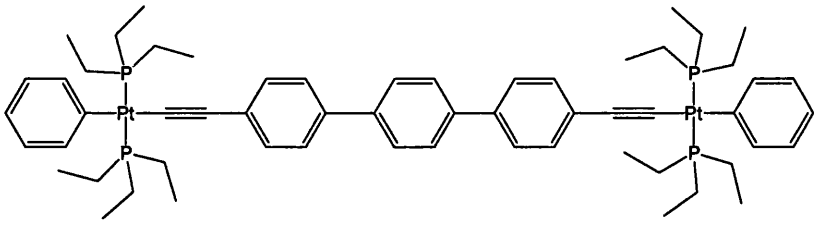

Trans-bis(triethylphosphine)(phenyl)platinum(II)chloride (124 mg, 0.23 mmol), 4,4''-*di*-ethynylterphenyl **(11)** (30 mg, 0.11 mmol), and copper(I) iodide (5 mg) were placed in a Schlenk tube. Dichloromethane (20 mL) and diisopropylamine (10 mL) were added and the reaction was left to stir for 6 hr, after which time TLC (silica, dichloromethane/hexane, 2:1 v/v) confirmed completion of the reaction. The volatiles were removed under reduced pressure and the solid was dissolved in ethyl acetate. The solution was passed through a plug of alumina and the solvent was evaporated to dryness. The resulting solid was recrystallised from ethanol/chloroform (9:1 v/v) yielding **(12)** as yellow crystals (93 mg, 67%).

^1H NMR ($CDCl_3$, 400.13 MHz)

1.07-1.15 (m, CH_3, 36H), 1.74-1.82 (m, CH_2, 24H), 6.79-6.83 (m, C*H*, 2H), 6.95-6.99 (m, C*H*, 4H), 7.33-7.39 (m, C*H*, 8H), 7.50 (d, ^3J = 8.6 Hz, 4H), 7.64 (d, ^3J = 8.6 Hz, C*H*, 4H)

$^{13}C\{^1H\}$ NMR – PENDANT ($CDCl_3$, 75.5 MHz)

8.38	CH_3	($P(CH_2CH_3)_3$)	126.66	*C*H	(central C_6H_4)
15.47	CH_2	(($P(CH_2CH_3)_3$), t_{ps}, $^1J_{PC}+^3J_{PC}$ = 34 Hz)	127.86	*C*H	(*meta* to alkyne)
			132.99	*C*H	(central C_6H_4)
110.37	C_q	(*C*≡C-Pt)	138.98	C_{ipso}	(central C_6H_4)
112.28	C_q	(C≡*C*-Pt)	141.19	C_{ipso}	(*para* to alkyne)
121.54	*C*H	(*para*, Pt-*Ph*)	139.55	*C*H	(*ortho*, Pt-*Ph*)
122.13	*C*H	(*ortho* to alkyne)			

$^{31}P\{^1H\}$ NMR ($CDCl_3$, 161.97 MHz)

10.04 ($^1J_{PtP}$ = 2640 Hz)

Elemental Analysis: Result % (calculated %): C = 53.5 (53.9), H = 6.44 (6.39)

IR (KBr disc, ν cm^{-1}): 2954, 2927(C-H), 2090 (C≡C)

UV/vis: λ_{max} = 350 nm, ε = 72,300 $dm^3mol^{-1}cm^{-1}$

Emission: λ_{max} = 422 nm

6.2.9 Synthesis of 4,4'''-*bis*-(trimethylsilyl)-quaterphenyl (13) [18]

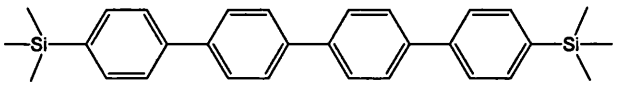

4-trimethylsilyl phenylboronic acid (800 mg, 4.12 mmol), 4,4'-diiodo-biphenyl (556 mg, 1.37 mmol), tetrakis(triphenylphosphine)palladium(0) (238 mg, 4.12 mmol) were placed in a round bottomed flask. Toluene (60 mL) and sodium carbonate (2.0 M aqueous solution, 40 mL) were added and the solution was refluxed under an inert atmosphere. The reaction was monitored by TLC (alumina, 40:60 petroleum ether) and was complete after 52 hr. The reaction mixture was concentrated to low volume (~10 mL) and the resulting solid was filtered and dried under reduced pressure. The crude product was then recrystallised from chloroform affording **(13)** as a white powder (364 mg, 59%).

^1H NMR ($CDCl_3$, 400.13 MHz)

0.32 (s, CH_3, 18H), 7.64 (m, *CH*, 8H), 7.72 (m, *CH*, 8H)

$^{13}C\{^1H\}$ NMR – PENDANT ($CDCl_3$, 75.49 MHz)

-0.73	CH_3	($SiCH_3$)	139.77	C_{ipso}	(C_6H_4)
126.71	CH	(C_6H_4)	140.02	C_{ipso}	(C_6H_4)
127.74	CH	(C_6H_4)	140.50	C_{ipso}	(C_6H_4)
127.90	CH	(C_6H_4)	141.40	C_{ipso}	(C_6H_4)
134.24	CH	(C_6H_4)			

Elemental Analysis: Result % (calculated %): C = 78.9 (79.9), H = 7.48 (7.60)

6.2.10 Synthesis 4,4'''-diiodo-*p*-quaterphenyl (14)

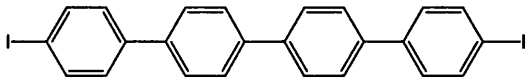

Iodine monochloride (1.47 mL, 1.00 M solution in dichloromethane) was added, dropwise to a stirring solution of 4,4'''-*bis*-(trimethylsilyl)-quaterphenyl (300 mg, 0.67 mmol) in chloroform (60 mL). After several minutes a white precipitate was formed. TLCs of the reaction mixture proved to be inconclusive as the product was insoluble in all common organic solvents. The reaction was left to stir for 18 hr after which time excess iodine was quenched with saturated sodium thiosulphate solution (10 mL). The volatiles were removed under reduced pressure and the crude product was washed with chloroform (50 mL) affording **(14)** as a white powder (180 mg, 48%). The product was very insoluble in all common organic solvents; therefore NMR spectroscopic characterisation was not possible.

EI-mass spectrum: ($C_{24}H_{16}I_2$) *m/z* 558.2; calc. 558.2

Elemental Analysis: Result % (calculated %): C = 51.0 (51.6), H = 2.66 (2.89)

6.2.11 Synthesis of 4,4'''-*bis*-(trimethylsilylethynyl)-quaterphenyl (15)

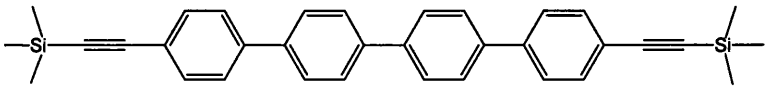

4,4'''-diiodo-*p*-quaterphenyl **(14)** (150 mg, 0.27 mmol), copper iodide (5 mg, 0.03 mmol) and *bis*(triphenylphosphine)palladium(II)chloride (38 mg, 0.05 mmol) were placed in a Schlenk tube. Dimethylformamide (150 mL), diisopropylamine (50 mL) and trimethylsilylacetylene (0.22 mL, 1.50 mmol) were added, respectively, and the

reaction was left to stir, under protection from light, for 28 hr. TLC (silica, dichloromethane/hexane, 4:1 v/v) revealed completion of reaction and the volatiles were removed under reduced pressure. The crude product was dissolved in hexane/ethyl acetate (1:3 v/v) and passed through a short alumina plug after which the solvent was removed yielding a brown solid. Recrystallisation of the crude product from ethanol afforded **(15)** as an off white solid (55 mg, 40%).

^{1}H NMR ($CDCl_3$, 400.13 MHz)

0.27 (s, C*H*$_3$, 18H), 7.58 (m, C*H*, 8H), 7.71 (m, C*H*, 8H)

^{13}C{^{1}H} NMR – PENDANT ($CDCl_3$, 75.5 MHz, δ ppm)

0.00	CH_3	Si*Me*$_3$	132.46	*C*H	(*C*$_6$H$_4$)
95.04	C_q	*C*CSiMe$_3$	133.20	*C*H	(*C*$_6$H$_4$)
104.95	C_q	*C*CSiMe$_3$	139.36	C_{ipso}	(*C*$_6$H$_4$)
122.16	C_{ipso}	(C≡C-*C*)	139.81	C_{ipso}	(*C*$_6$H$_4$)
126.71	*C*H	(*C*$_6$H$_4$)	140.55	C_{ipso}	(*C*$_6$H$_4$)
127.44	*C*H	(*C*$_6$H$_4$)			

IR (KBr disc, ν cm^{-1}): 3046, 2968, 2936, 2875 (C-H), 2086 (C≡C)

6.2.12 Attempted synthesis of 4,4'''-*di*-(ethynyl)-quaterphenyl (16)

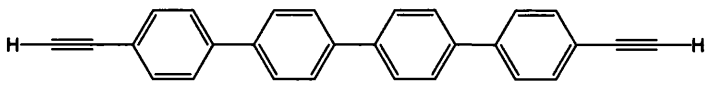

4,4'''-*bis*-trimethylsilylethynyl-quaterphenyl **(15)** (20 mg, 0.56 mmol) was dissolved in dichloromethane/methanol (50 mL, 2:1 mixture) and potassium hydroxide (0.20 mL, 2.00 M aqueous solution) was added. The solution was left to stir in the absence of light for 18 hr and the reaction progress was monitored by TLC (silica, dichloromethane/hexane, 5:1 v/v). The solvent was removed under reduced pressure, and the solid was suspended in dichloromethane (100 mL) and washed with water (2 x 50 mL). The organic phase was dried ($MgSO_4$) and the volatiles were removed affording **(16)** as a pale brown solid (10 mg, 42%). The product was found to be insoluble in all common organic solvents.

6.2.13 Synthesis of 4,4'''-*di*-(*trans*-(phenyl,*bis*-triethylphosphine) platinum)ethynyl-tetraphenyl (17)

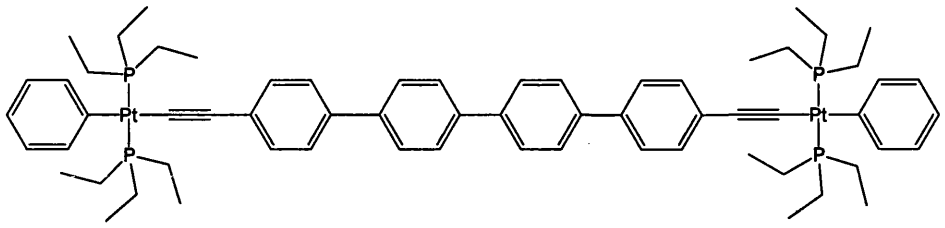

4,4'''-*bis*-trimethylsilylethynyl-quaterphenyl **(15)** (30 mg, 0.09 mmol) and sodium methoxide (30 mg) were placed in a Young's ampoule and dissolved in dichloromethane/methanol (2:1 v/v, 50 mL). The reaction was left to stir in the absence of light for 30 minutes. *Trans-bis*(triethylphosphine)(phenyl)platinum(II) chloride (90 mg, 0.18 mmol) and diisopropylamine (10 mL) was added to the stirring solution. The reaction was left to stir for a further 26 hr after which time TLC (silica, dichloromethane) revealed consumption of ligand and platinum starting materials. The volatiles were removed under reduced pressure and the solid was dissolved in ethyl acetate. The solution was passed through a plug of alumina and the solvent was evaporated to dryness. The resulting solid was recrystallised from ethanol/chloroform (6:1 v/v) affording **(17)** as a yellow solid (48 mg, 43%).

^{1}H NMR ($CDCl_3$, 400.13 MHz)

1.04-1.15 (m, C*H*$_3$, 36H), 1.74-1.82 (m, C*H*$_2$, 24H), 6.79-6.83 (m, C*H*, 2H), 6.95-6.99 (m, C*H*, 8H), 7.33-7.39 (m, C*H*, 12H), 7.46-7.59 (m, C*H*, 8H)

^{31}P{^{1}H} NMR ($CDCl_3$, 161.97 MHz)

10.00 ($^1J_{PtP}$ = 2644 Hz)

6.3 Experimental details for Chapter Three

6.3.1 Synthesis of 1,4-*di*-(4-bromo-phenyl)-butane-1,4-dione (18)

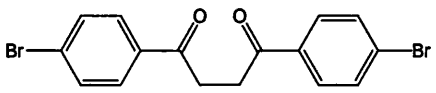

Freshly dehydrated zinc chloride (2.72 g, 20.0 mmol) was placed in a Young's ampoule, benzene (10 mL), diethylamine (1.57 mL, 15.0 mmol) and *tert*-butanol (1.4 mL, 15 mmol) were successively added. The mixture was stirred for 3 hr then 4'-bromo-2-bromoacetophenone (1.99 g, 10.0 mmol) and 4-bromoacetophenone (4.17 g, 15.0 mmol) were successively added. The mixture was stirred for 7 days and monitored by TLC (silica, hexane/dichloromethane). The reaction was quenched with 5% sulphuric acid (20 mL). The organic layer was separated and washed with 5% sodium chloride and dried ($MgSO_4$). The volatiles were removed under reduced pressure and the product was crystallised from methanol affording **(18)** as a white solid (3.29 g, 85%).

^{1}H NMR ($CDCl_3$, 300.22 Hz)

3.33 (s, C*H*$_2$, 2H), 7.56 (d, ^3J = 8.6 Hz, C*H*, 2H), 7.83 (d, ^3J = 8.6 Hz, C*H*, 2H)

^{13}C{^{1}H} NMR – PENDANT ($CDCl_3$, 75.5 MHz)

32.8	*C*H$_2$		135.8	C$_{ipso}$	(*para* to bromine)
130.1	*C*H	(*ortho* to bromine)	197.9	C$_{ipso}$	*C*=O
132.4	*C*H	(*meta* to bromine)			

Elemental Analysis: Result % (calculated %): C = 48.3 (48.5), H = 3.04 (3.05)

6.3.2 Synthesis of 2,5-*di*-(4-bromo-phenyl)-furan (19)[19]

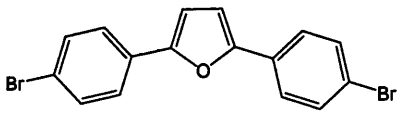

1,4-*bis*-(4-bromo-phenyl)-butane-1,4-dione (800 mg, 2.02 mmol) and phosphorous pentoxide (4.00 g, 10.1 mmol) were dissolved in xylene (30 mL) and the solution was refluxed for 2 hr. TLC of the reaction mixture (silica, hexane/dichloromethane, 2:1 v/v) revealed completion of the reaction. After cooling, cold water was added

dropwise (30 mL) and the reaction mixture was heated to 80 °C for 30 minutes. The volatiles were then removed under reduced pressure, dichloromethane (40 mL) was added, and the organic phase was separated and washed with water (2 x 50 mL). The dichloromethane was dried ($MgSO_4$) and evaporated to low volume and methanol was added to precipitate **(19)** as a white solid (610 mg, 80%).

^{1}H NMR ($CDCl_3$, 400.13 MHz)

6.74 (s, C*H*, 2H), 7.52 (d, ^3J = 8.6 Hz, C*H*, 4H), 7.59 (d, ^3J = 8.6 Hz, C*H*, 4H)

^{13}C{^{1}H} NMR – PENDANT ($CDCl_3$, 100.62 MHz)

108.25	*C*H	(*furan*)	129.79	C_{ipso}	(*furan*)
121.65	C_{ipso}	(*C*Br)	132.26	*C*H	(*meta* to furan)
125.58	*C*H	(*ortho* to furan)	153.02	C_{ipso}	(*para* to bromine)

Elemental Analysis: Result % (calculated %): C = 49.9 (50.8), H = 2.70 (2.67)

EI/Mass Spectrum: ($C_{16}H_{10}Br_2O$) *m/z* 378.0, calc. 378.0

6.3.3 Synthesis of 2,5-*bis*-(4-trimethylsilylethynyl-phenyl)-furan (20)

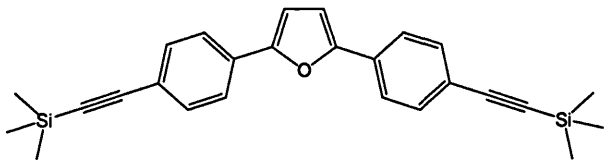

2,5-*di*-(4-bromo-phenyl)-furan (500 mg, 1.32 mmol), copper (I) iodide (7.5 mg, 0.04 mmol), *bis*(triphenylphosphine)palladium(II)chloride (55.6 mg, 0.08 mmol) were placed in a Schlenk tube. Dichloromethane (20 mL), diisopropylamine (10 mL) and trimethylsilylacetylene (0.58 mL, 3.96 mmol) were added successively and the reaction was left to stir, under the protection of light, for 26 hr. The volatiles were removed under reduced pressure and the resultant solid was passed through a short alumina plug using ethyl acetate/hexane (1:1 v/v) as the eluent. The solvent was then removed and the solid was further purified by chromatography (silica, hexane/dichloromethane, 4:1 v/v) affording **(20)** as an off white solid (340 mg, 63%).

^{1}H NMR ($CDCl_3$, 400.13 MHz)

0.27 (s, CH_3, 18H), 6.77 (s, C*H*, 2H), 7.49 (d, ^3J = 8.4 Hz, C*H*, 4H), 7.67 (d, ^3J = 8.4 Hz, C*H*, 4H)

$^{13}C\{^1H\}$ NMR – PENDANT ($CDCl_3$, 100.62 MHz)

0.34	CH_3	($SiCH_3$)	123.77	CH	(*meta* to TMS)
95.66	C_q	($SiC{\equiv}C$)	130.67	C_{ipso}	(*para* to TMS)
105.40	C_q	($C{\equiv}CPh$)	132.75	CH	(*ortho* to TMS)
108.83	CH	(*furan*)	153.50	C_{ipso}	(*furan*)
122.30	C_{ipso}	($CSiCH_3$)			

Elemental Analysis: Result % (calculated %): C = 74.6 (75.7), H = 6.63 (6.83)

IR (KBr disc, ν cm^{-1}): 2959, 2899 (C-H), 2158 (C≡C), 1251 (Si-C)

6.3.4 Synthesis of 2,5-*di*-(4-ethynyl-phenyl)-furan (21)

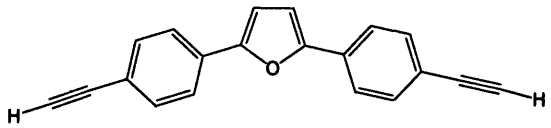

Potassium hydroxide (2.00 M aqueous solution, 0.24 mL) was added to a stirring solution of 2,5-*bis*-(4-trimethylsilylethynyl-phenyl)-furan (100 mg, 0.24 mmol) in dichloromethane/methanol (1:1 v/v, 20 mL). The reaction was left to stir for 4 hr after which time TLC revealed the completion of the reaction (alumina, hexane/dichloromethane, 4:1 v/v). The volatiles were removed under reduced pressure and the solid was redissolved in dichloromethane and washed with water (2 x 50 mL). The organic phase was separated and dried ($MgSO_4$). The volatiles were removed under reduced pressure affording **(21)** as an off white solid (55 mg, 86%).

^1H NMR ($CDCl_3$, 300.22 MHz)

3.15 (s, C*H*, 2H), 6.79 (s, C*H*, 2H), 7.53 (d, ^3J = 8.4 Hz, C*H*, 4H), 7.70 (d, ^3J = 8.4 Hz, C*H*, 4H)

$^{13}C\{^1H\}$ NMR – PENDANT ($CDCl_3$, 100.62 MHz, δ ppm)

78.46	CH	($HC{\equiv}C$)	123.88	CH	(*ortho* to furan)
83.97	C_{ipso}	($C{\equiv}CPh$)	131.00	C_{ipso}	(*para* to alkyne)
108.93	CH	(*furan*)	132.92	CH	(*meta* to furan)
121.30	C_{ipso}	(*para* to furan)	153.44	C_{ipso}	(*furan*)

IR (KBr disc, ν cm^{-1}): 2949, 2823 (C-H), 2158 (C≡C)

6.3.5 Synthesis of 2,5-*di*-(4-(*trans*-(phenyl,*bis*-triethylphosphine)platinum ethynyl))phenyl)-furan (22)

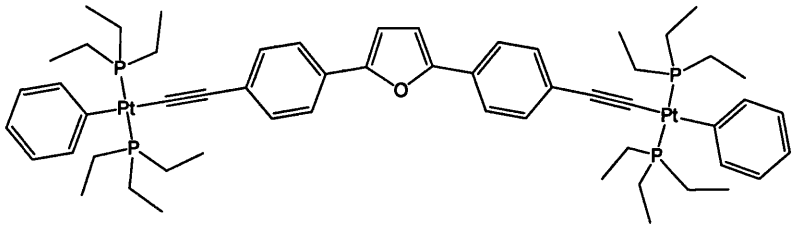

Trans-bis(triethylphosphine)(phenyl)platinum(II)chloride (250 mg, 0.35 mmol) and 2,5-*di*-(4-ethynyl-phenyl)-furan (47 mg, 0.18 mmol) were placed in a Schlenk tube. Dichloromethane (15 mL) and diisopropylamine (15 mL) were added and the reaction was left to stir for 18 hr after which time completion of the reaction was confirmed by TLC (silica, dichloromethane). The volatiles were removed under reduced pressure. The crude product was then passed through a small plug of alumina in ethyl acetate, and the eluted solvent was evaporated to dryness. The resulting solid was recrystallised from ethanol to afford **(22)** as yellow crystals (140 mg, 61%).

^{1}H NMR ($CDCl_3$, 400.13 MHz)

1.08-1.14 (m, C*H*$_3$, 36H), 1.71-1.81 (m, C*H*$_2$, 24H), 6.77 (s, C*H*, 2H), 6.80 (t, ^{3}J = 14.5 Hz, C*H*, 2H), 6.97 (t, ^{3}J = 14.5 Hz, C*H*, 4H), 7.34 (m, C*H*, 2H), 7.53 (d, ^{3}J = 8.4 Hz, C*H*, 4H), 7.70 (d, ^{3}J = 8.4 Hz, C*H*, 4H)

^{13}C{^{1}H} NMR – PENDANT ($CDCl_3$, 100.62 MHz)

8.04	*C*H$_3$	(P(CH$_2$C*H*$_3$)$_3$)	127.29	*C*H	(*ortho* to furan)
15.11	*C*H$_2$	((P(C*H*$_2$CH$_3$)$_3$), t_{ps}, $^{1}J_{PC}$+$^{3}J_{PC}$ = 33 Hz)	128.69	C_{ipso}	(C≡C-C_{ipso})
			131.35	C_{ipso}	(*para* to alkyne)
107.48	*C*H	(*furan*)	133.19	*C*H	(C_6H_5Pt)
110.22	C_{ipso}	(PtC≡C)	139.18	*C*H	(C_6H_5Pt)
114.48	C_{ipso}	(C≡C*Ph*)	153.21	C_{ipso}	(*furan*)
121.22	*C*H	(C_6H_5Pt)	156.34	C_{ipso}	(C_6H_5Pt)

^{31}P{^{1}H} NMR ($CDCl_3$, 161.97 MHz)

10.03 ($^{1}J_{PtP}$ = 2641 Hz)

IR (KBr disc, ν cm^{-1}): 2973, 2968, 2855 (ethyl), 2092 (C≡C)

Elemental Analysis: Result % (Calculated %): C = 52.3 (52.4), H = 6.61 (6.28)

UV/vis: λ_{max} = 375 nm, ε = 75,300 dm^{3}mol^{-1}cm^{-1}

Emission: λ_{max} = 398 nm

6.3.6 Synthesis of 2,5-*di*-(4-bromo-phenyl)-thiophene (23)

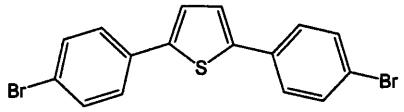

1,4-*bis*-(4-bromo-phenyl)-butane-1,4-dione (500 mg, 1.26 mmol) and Lawesson's reagent (764 mg, 1.89 mmol) was dissolved in xylene (30 mL) and refluxed under an inert atmosphere for 18 hr. TLC of the mixture revealed completion of the reaction (silica, hexane: dichloromethane, 2:1 v/v). After cooling, cold water was added dropwise (30 mL) and the reaction mixture was heated to 80 °C for 30 min. The volatiles were removed under reduced pressure, dichloromethane (40 mL) was added, and the organic phase was separated and washed with water (2 x 50 mL). The dichloromethane solution was dried ($MgSO_4$) and evaporated to low volume, followed by the addition of methanol to precipitate **(23)** as a white solid (409 mg, 83%).

^{1}H NMR ($CDCl_3$, 400.13 MHz)

7.27 (s, C*H*, 2H), 7.47 (d, ^3J = 9.0 Hz, C*H*, 4H), 7.52 (d, ^3J = 9.0 Hz, C*H*, 4H)

^{13}C{1H} NMR – PENDANT ($CDCl_3$, 100.62 MHz)

121.86	C_{ipso}	(*para* to bromine)	132.41	*C*H	(*ortho* to thiophene)
124.85	*C*H	(*thiophene*)	133.42	C_{ipso}	(*C*Br)
127.44	*C*H	(*meta* to thiophene)	143.08	C_{ipso}	(*thiophene*)

EI/Mass Spectrum: ($C_{16}H_{10}Br_2S$) *m/z* 394.0, calc. 394.0

6.3.7 Synthesis of 2,5-*bis*-(4-trimethylsilylethynyl-phenyl)-thiophene (24)

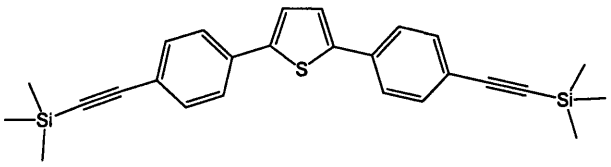

2,5-*di*-(4-bromo-phenyl)-thiophene (300 mg, 0.76 mmol), copper (I) iodide (7.5 mg, 0.04 mmol), *bis*(triphenylphosphine)palladium(II)chloride (55.6 mg, 0.08 mmol) were placed in a Schlenk tube. Dichloromethane (20 mL), diisopropylamine (10 mL) and trimethylsilylacetylene (0.33 mL, 2.28 mmol) were added successively and the

reaction was left to stir, in the absence of light, for 18 hr. The volatiles were removed under reduced pressure and the resultant solid was passed through an alumina plug using ethyl acetate/hexane (1:1 v/v). The volatiles were removed and the crude product was further purified by chromatography (silica, hexane/dichloromethane 1:1 v/v) affording **(24)** as an off white solid (270 mg, 83%).

^{1}H NMR ($CDCl_3$, 400.13 MHz)

0.26 (s, C*H*$_3$, 18H), 7.31 (s, C*H*, 2H), 7.47 (d, ^3J = 8.4 Hz, C*H*, 4H), 7.55 (d, ^3J = 8.4 Hz, C*H*, 4H)

^{13}C{^{1}H} NMR – PENDANT ($CDCl_3$, 100.62 MHz)

0.32	*C*H$_3$	(Si*C*H$_3$)	125.45	*C*H	(*ortho* to thiophene)
95.70	C_q	(Si*C*≡C)	132.88	*C*H	(*meta* to thiophene)
105.09	C_q	(C≡*C*Ph)	134.40	C_{ipso}	(*para* to thiophene)
122.45	C_{ipso}	(*para* to alkyne)	143.73	C_{ipso}	(*thiophene*)
124.93	*C*H	(*thiophene*)			

Elemental Analysis: Result % (Calculated %): C = 71.4 (70.4), H = 6.61 (7.19)

IR (KBr disc, ν cm^{-1}): 3075, 3028, 2956, 2898 (C-H), 2155 (C≡C), 1250 (Si-C)

6.3.8 Synthesis of 2,5-*d*-(4-ethynyl-phenyl)-thiophene (25)

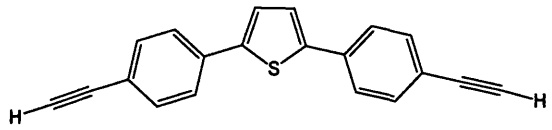

Potassium hydroxide (2.00 M aqueous solution, 0.47 mL) was added to a stirring solution of 2,5-*bis*-(4-trimethylsilylethynyl-phenyl)-thiophene (200 mg, 0.47 mmol) in dichloromethane/methanol (2:1 v/v, 20 mL). The reaction was left to stir for 16 hr after which time TLC revealed the completion of the reaction (silica, hexane/dichloromethane, 4:1 v/v). The volatiles were removed under reduced pressure and the solid was redissolved in dichloromethane and washed with water (2 x 50 mL). The organic phase was separated and dried ($MgSO_4$). The solvent was removed affording **(25)** as a yellow solid (130 mg, 98%).

^{1}H NMR ($CDCl_3$, 300.22 MHz)

3.09 (s, C*H*, 2H), 7.20 (s, C*H*, 2H), 7.44 (d, ^3J = 8.7 Hz, C*H*, 4H), 7.52 (d, ^3J = 8.7 Hz, C*H*, 4H)

^{13}C{^{1}H} NMR – PENDANT ($CDCl_3$, 75.49 MHz)

78.60	*C*H	(H*C*≡C)	125.74	*C*H	(*ortho* to thiophene)
85.82	C_q	(C≡*C*Ph)	133.10	*C*H	(*meta* to thiophene)
121.59	C_{ipso}	(*para* to alkyne)	134.81	C_{ipso}	(*para* to thiophene)
125.20	*C*H	(*thiophene*)	134.75	C_{ipso}	(*thiophene*)

IR (KBr disc, ν cm^{-1}): 2949, (C-H), 2158 (C≡C), 1939 (C≡C-H)

6.3.9 Synthesis of 2,5-*di*-(4-(*trans*-(phenyl,*bis*-triethylphosphine)platinum ethynyl))phenyl)-thiophene (26)

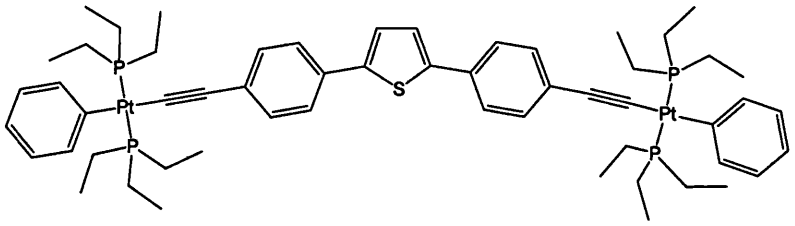

Trans-bis(triethylphosphine)(phenyl)platinum(II) chloride (272 mg, 0.50 mmol), 2,5-*di*-(4-ethynyl-phenyl)-thiophene (59 mg, 0.25 mmol) and copper(I) iodide (~5 mg) were transferred to a Schlenk tube. Dichloromethane (15 mL) and diisopropylamine (15 mL) were added and the reaction was left to stir for 18 hr after which time completion of the reaction was confirmed by TLC (silica, dichloromethane). The volatiles were removed under reduced pressure and the crude product was then passed through a plug of alumina in hexane/ethyl acetate (1:1 v/v), and the eluted solvent was evaporated to dryness. The crude product was recrystallised from ethanol/chloroform (6:1 v/v) to afford **(26)** as yellow crystals (210 mg, 66%).

^{1}H NMR ($CDCl_3$, 400.13 MHz)

1.07-1.14 (m, CH_3, 36H), 1.73-1.81 (m, CH_2, 24H), 6.81 (t, ^3J = 14.5 Hz, C*H*, 2H), 6.97 (t, ^3J = 14.5 Hz, C*H*, 4H), 7.21 (s, C*H*, 2H), 7.29 (d, ^3J = 8.4 Hz, C*H*, 4H), 7.34 (m, C*H*, 2H), 7.47 (d, ^3J = 8.4 Hz, C*H*, 4H)

$^{13}C\{^1H\}$ NMR – PENDANT ($CDCl_3$, 75.5 MHz)

8.07	CH_3	($P(CH_2CH_3)_3$)	128.69	C_{ipso}	($C{\equiv}C\text{-}C_{ipso}$)
15.22	CH_2	(($P(CH_2CH_3)_3$), t_{ps},	131.35	C_{ipso}	(*para* to alkyne)
		$^1J_{PC}+^3J_{PC}$ = 34 Hz)	132.21	C_{ipso}	(*thiophene*)
124.48	CH	(*thiophene*)	133.29	CH	(C_6H_5Pt)
110.22	C_q	($PtC{\equiv}C$)	139.18	CH	(*ortho* C_6H_5Pt)
114.48	C_q	($C{\equiv}CPh$)	156.34	C_{ipso}	(Pt-*Ph*)
121.22	CH	(*para* C_6H_5Pt)			
127.29	CH	(*ortho* to thiophene)			

$^{31}P\{^1H\}$ NMR ($CDCl_3$, 161.97 MHz)

10.00 ($^1J_{PtP}$ = 2638 Hz)

Elemental Analysis: Result % (calculated %): C = 51.8 (51.7), H = 6.21 (6.30)

UV/vis: λ_{max} = 388 nm, ε = 77,300 $dm^3mol^{-1}cm^{-1}$

Emission: λ_{max} = 438 nm

6.3.10 Synthesis of 2,5-dibromoselenophene (27)

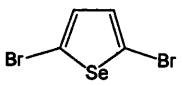

Selenophene (2.00 g, 15.26 mmol) was dissolved in hydrobromic acid (20 mL) and diethyl ether (20 mL) at -10 °C. A solution of bromine (4.88 g, 30.52 mmol) in hydrobromic acid (30 mL) was added dropwise over a period of 1 hr whilst maintaining the temperature at -10 °C. The solution was left to stir for a further 1hr at room temperature. TLC (silica, hexane) revealed the completion of the reaction and a saturated solution of sodium thiosulphate (15 mL) was added to quench the excess bromine. The organic layer was separated, washed with water (2 x 30 mL) and dried ($MgSO_4$). The solvent was removed under reduced pressure and the crude product was passed through a silica plug in hexane. The crude dark yellow oil was further purified by vacuum distillation (42 °C, 0.02 mmHg) to afford **(27)** as a pale yellow oil (2.83 g, 64%).

^1H NMR ($CDCl_3$, 300.22 MHz)

7.00 (s, CH, 2H)

$^{13}C\{^1H\}$ NMR ($CDCl_3$, 75.5 MHz)

115.57 *C*H 132.98 C_{ipso}

^{77}Se NMR ($CDCl_3$, 76.31 MHz)

730.5

6.3.11 Synthesis of 2,5-*bis*-(4-trimethylsilyl-phenyl)-selenophene (28)

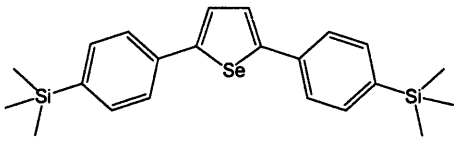

4-trimethylsilyl phenylboronic acid (1.75 g, 9.00 mmol), 2,5-dibromoselenophene (864 mg, 3.00 mmol), tetrakis(triphenylphosphine)palladium(0) (693 mg, 6.00 mmol) were placed in a round bottomed flask. Toluene (50 mL) and an aqueous solution of sodium carbonate (30 mL, 2.00 M) were added and the solution refluxed under an inert atmosphere. The reaction was monitored by TLC (silica, hexane/dichloromethane, 4:1 v/v) and after 76 hr was complete. The organic phase was decanted and the volatiles were removed under reduced pressure yielding a pale brown solid. The crude product was purified by chromatography (silica, hexane/dichloromethane, 5:1 v/v) yielding a yellow solid. Recrystallisation from ethanol/chloroform (9:1 v/v) afforded **(28)** as a bright yellow solid (831 mg, 65%).

^1H NMR ($CDCl_3$, 400.13 MHz)

0.29 (s, CH_3, 18H), 7.48 (s, C*H*, 2H), 7.52 (d, ^3J = 8.3 Hz, 4H), 7.56 (d, ^3J = 8.3 Hz, 4H)

$^{13}C\{^1H\}$ NMR ($CDCl_3$, 100.62 MHz)

-1.19	CH_3	($SiCH_3$)	136.62	C_{ipso}	(C_6H_4 *para* to $SiCH_3$)
125.25	*C*H	(C_6H_4 *ortho* to selenophene)	139.98	C_{ipso}	(C_6H_4 *para* to selenophene
126.26	*C*H	(*Selenophene*)	149.92	C_{ipso}	(*Selenophene*)
133.89	*C*H	(C_6H_4 *meta* to selenophene)			

^{77}Se NMR ($CDCl_3$, 76.31 MHz)

572.6 ($^3J_{SeH}$ = 8.5 Hz)

Elemental Analysis: Result % (calculated %): C = 61.6 (61.8), H = 6.62 (6.60)

6.3.12 Synthesis of 2,5-*di*-(4-iodo-phenyl)selenophene (29)

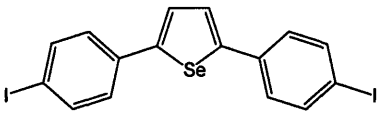

Iodine monochloride (1.00 M solution in dichloromethane, 2.34 mL) was added dropwise to the stirring solution of 2,5-*bis*-(4-trimethylsilyl-phenyl)-selenophene (500 mg, 1.17 mmol) in chloroform (20 mL), and after 5 min a yellow precipitate was formed. After 15 hr of stirring TLC (silica, hexane/dichloromethane, 9:1 v/v) revealed completion of reaction and a saturated solution of sodium thiosulphate (~5 mL) was added. The solid was filtered off and washed with ethanol (2 x 20 mL). The crude product was recrystallised from chloroform affording **(29)** as a bright yellow solid (520 mg, 83%).

^{1}H NMR ($CDCl_3$, 400.13 MHz)

7.29 (d, ^3J = 8.4 Hz, *C*H, 4H), 7.43 (s, *C*H, 2H), 7.70 (d, ^3J = 8.4 Hz, *C*H, 4H)

^{13}C{^{1}H} NMR ($CDCl_3$, 100.62 MHz)

92.20	C_{ipso}	(*C*I)	135.58	C_{ipso}	(*Selenophene*)
126.76	*C*H	(*Selenophene*)	138.01	*C*H	(C_6H_4 *meta* to selenophene
127.67	*C*H	(C_6H_4 *ortho* to selenophene)			

^{77}Se NMR ($CDCl_3$, 76.31 MHz)

574.41 ($^3J_{SeH}$ = 8.4 Hz)

Elemental Analysis: Result % (calculated %): C = 33.3 (35.9), H = 1.78 (1.88)

6.3.13 Synthesis of 2,5-*bis*-(4-trimethylsilylethynyl-phenyl)selenophene (30)

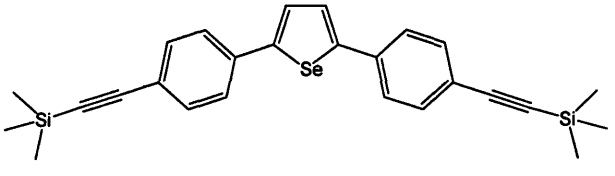

2,5-*di*-(4-iodo-phenyl)selenophene (450 mg, 0.84 mmol), copper (I) iodide (16 mg, 0.08 mmol), and *bis*(triphenylphosphine)palladium(II)chloride (118 mg, 0.17 mmol) were placed in a Schlenk tube. Dichloromethane (30 mL), diisopropylamine (15 mL) and trimethylsilylacetylene (0.30 mL, 2.08 mmol) were added successively and the reaction was left to stir, in the absence of light, for 4 hr. TLC (silica, hexane)

revealed the completion of the reaction and the volatiles were removed under reduced pressure. The resultant solid was passed through a silica plug in hexane, and the solvent removed to afford **(30)** as bright yellow material (270 mg, 68%).

^{1}H NMR ($CDCl_3$, 400.13 MHz)

0.26 (s, *C*H, 18H), 7.45 (d, ^3J = 8.6 Hz, *C*H, 4H), 7.47 (s, *C*H, 2H), 7.49 (d, ^3J = 8.6 Hz, *C*H, 4H)

^{13}C PENDANT NMR ($CDCl_3$, 100.62 MHz)

-0.04	CH_3	($SiCH_3$)	126.91	*C*H	(*Selenophene*)
95.65	C_q	($SiC{\equiv}C$)	132.54	*C*H	(C_6H_4 ortho to selenophen
104.84	C_q	($C{\equiv}CPh$)	136.08	C_{ipso}	(*Selenophene*)
122.32	C_{ipso}	(C_6H_4 para to selenophene)	149.56	C_{ipso}	(C_6H_4 para to $SiCH_3$)
125.65	*C*H	(C_6H_4 meta to selenophene)			

^{77}Se NMR ($CDCl_3$, 76.31 MHz)

572.98 ($^3J_{SeH}$ = 6.2 Hz)

Elemental Analysis: Result % (calculated %): C = 65.5 (65.7), H = 5.93 (5.95)

IR (KBr disc, v cm^{-1}): 2954, 2898 (C-H), 2154 (C≡C), 1249 (Si-C)

6.3.14 Synthesis of 2,5-*di*-(4-ethynyl-phenyl)selenophene (31)

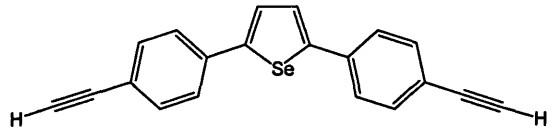

Potassium hydroxide (2.00 M aqueous solution, 0.24 mL) was added to the stirring solution of 2,5-*bis*-(4-trimethylsilylethynyl-phenyl)selenophene (150 mg, 0.32 mmol) in methanol: dichloromethane (1:1 v/v, 20 mL). The reaction was left to stir in the absence of light for 3 hr. TLC (silica, hexane: dichloromethane, 4:1 v/v) revealed the completion of the reaction and the volatiles were removed under reduced pressure, and the solid was redissolved in dichloromethane and washed with water (2 x 50 mL). The organic phase was separated and dried ($MgSO_4$). The volatiles were removed affording **(31)** as an off white solid (109 mg, 99%).

^{1}H NMR ($CDCl_3$, 400.13 MHz)

3.16 (s, *C*H, 2H), 7.48-7.53 (m, *C*H, 10H)

^{13}C PENDANT NMR ($CDCl_3$, 100.62 MHz)

78.48	C_q	(HC≡C)	127.04	CH	(*Selenophene*)
83.42	C_q	(C≡CPh)	132.72	CH	(C_6H_4 ortho to selenophen
121.29	C_{ipso}	(C_6H_4 para to selenophene)	136.42	C_{ipso}	(*Selenophene*)
125.79	CH	(C_6H_4 meta to selenophene)	149.53	C_{ipso}	(C_6H_4 para to alkyne)

^{77}Se NMR ($CDCl_3$, 76.31 MHz)

574.77 ($^3J_{SeH}$ = 5.9 Hz)

IR (KBr disc, ν cm^{-1}): 3045, 2949 (C-H), 2145 (C≡C), 1944 (C≡C-H)

6.3.15 Synthesis of 2,5-*di*-(4-(*trans*-(phenyl,*bis*-triethylphosphine)platinum ethynyl))phenyl)- selenophene (32)

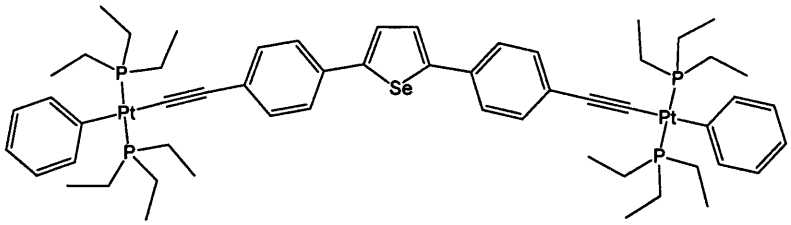

2,5-*di*-(4-ethynyl-phenyl)selenophene (65 mg, 0.20 mmol), *trans-bis* (triethylphosphine)(phenyl)platinum(II)chloride (215 mg, 0.40 mmol), and copper iodide (5 mg) were placed in a Schlenk tube, dichloromethane (15 mL) and di-isopropylamine (10 mL) were added and the solution was left to stir, under protection from light, for 3 hr. TLC (silica, hexane: dichloromethane, 1:1 v/v) revealed completion of the reaction and the volatiles were removed under reduced pressure. The crude product was dissolved in hexane: ethyl acetate (2:1 v/v) and passed through a plug of silica, the solution was then evaporated to dryness and recrystallised from ethanol affording **(32)** as yellow crystals (218 mg, 82%).

^{1}H NMR ($CDCl_3$, 400.13 MHz)

1.07 (m, C*H*$_3$, 36H), 1.73 (m, C*H*$_2$, 24H), 6.81 (t, ^3J = 7.6 Hz, C*H*, 2H), 6.97 (t, ^3J = 7.6 Hz, C*H*, 4H), 7.27 (d, ^3J = 8.6 Hz, C*H*, 4H), 7.34 (m, C*H*, 2H), 7.37 (s, C*H*, 2H), 7.41 (d, ^3J = 8.6 Hz)

^{13}C PENDANT NMR ($CDCl_3$, 100.62 MHz)

8.03	CH_3	($P(CH_2CH_3)_3$)	128.49	C_{ipso}	($C{\equiv}C\text{-}C_{ipso}$)
15.12	CH_2	(($P(CH_2CH_3)_3$), t_{ps}, $^1J_{PC}+^3J_{PC}$ = 34 Hz)	130.35	C_{ipso}	(*para* to alkyne)
			132.22	C_{ipso}	(*selenophene*)
110.34	C_q	($PtC{\equiv}C$)	133.66	CH	(C_6H_5Pt)
114.78	C_q	($C{\equiv}CPh$)	140.19	CH	(*ortho* C_6H_5Pt)
121.24	CH	(*para* C_6H_5Pt)	156.34	C_{ipso}	(C_6H_5Pt)
126.64	CH	(*selenophene*)			
127.55	CH	(*ortho* to selenophene)			

^{31}P{^{1}H} NMR ($CDCl_3$, 161.98 MHz)

10.01 ($^1J_{PtP}$ = 2639 Hz)

^{77}Se NMR ($CDCl_3$, 76.31 MHz)

563.22 ($^3J_{SeH}$ = 6.0 Hz)

Elemental Analysis: Result % (calculated %): C = 49.7 (50.0), H = 5.99 (5.92)

UV/vis: λ_{max} = 397 nm, ε = 69,700 $dm^3mol^{-1}cm^{-1}$

Emission: λ_{max} = 451 nm

6.3.16 Synthesis of 2,5-dibromofuran (33)

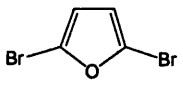

Bromine (4.70 g, 29.4 mmol) was added dropwise to the stirring solution of furan (1.00 g, 14.7 mmol) in chloroform (30 mL). The reaction was monitored by TLC (silica, hexane: dichloromethane, 4:1 v/v) and after 3 hr was complete. A saturated solution of sodium thiosulphate (20 mL) was added followed by water (30 mL) and dichloromethane (50 mL). The organic layer was separated and dried ($MgSO_4$), and the volatiles were removed under reduced pressure. The crude product was passed through a silica column in pentane affording **(33)** as a yellow oil (1.99 g, 60%).

^{1}H NMR ($CDCl_3$, 400.13 MHz)

6.30 (s, CH_2)

^{13}C{^{1}H} NMR ($CDCl_3$, 100.61 MHz)

114.21	CH	121.88	C_{ipso}

6.3.17 Synthesis of 2,5-*bis*(trimethylsilyethynyl)furan (34)

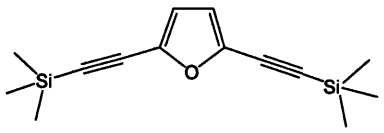

2,5-dibromofuran (903 mg, 4.00 mmol) was placed in a Young's ampoule and dissolved in dichloromethane (10 mL). In a separate Schlenk tube copper iodide (76.0 mg, 0.4 mmol), and *bis*(triphenylphosphine)palladium(II)chloride (560 mg, 0.80 mmol) were dissolved in dichloromethane (30 mL) and diisopropylamine (15 mL). The 2,5-dibromofuran solution was then added to the catalyst mixture followed by the addition of trimethylsilylacetylene (1.46 mL, 10.0 mmol). The reaction was left to stir for 3 hr after which time TLC (silica, hexane/dichloromethane, 4:1 v/v) revealed the reaction was complete. The volatiles were removed under reduced pressure and the resulting solid was passed through a plug of silica in hexane: ethyl acetate (4:1 v/v) as the eluent. The volatiles were removed under reduced pressure and the crude product was purified by sublimation (25 °C, 0.05 mmHg) affording **(34)** as an off white solid (692 mg, 67%).

^{1}H NMR ($CDCl_3$, 400.13 MHz)

0.24 (s, C*H*$_3$, 18H), 6.53 (s, C*H*, 2H)

^{13}C{^{1}H} NMR ($CDCl_3$, 100.61 MHz)

0.40	CH_3	($SiCH_3$)	116.28	*C*H	(*furan*)
93.68	C_q	(Si*C*≡C)	137.39	C_{ipso}	(*furan*)
100.45	C_q	(C≡*C*furan)			

6.3.18 Synthesis of 2,5-diethynyl furan (35)

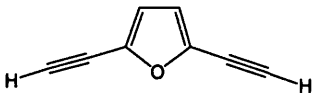

Potassium hydroxide (2.0 M aqueous solution, 0.87 mL) was added to the stirring solution of 2,5-*bis*(trimethylsilyethynyl)furan (150 mg, 0.60 mmol) in methanol/ dichloromethane (1:1 v/v, 20 mL). The reaction was left to stir, in the absence of light, for 1 hr. TLC (silica, hexane: dichloromethane, 9:1 v/v) revealed the completion of the reaction and the volatiles were removed under reduced pressure.

The crude product was extracted into diethyl ether (30 mL) from water (30 mL), the organic layer was separated and dried ($MgSO_4$). The solvent was removed under reduced pressure in a water bath at 15 °C affording **(35)** as a colourless oil (61 mg, 92%) which decomposed after several hours.

^{1}H NMR ($CDCl_3$, 400.13 MHz)

3.39 (s, C*H*, 2H), 6.61(s, C*H*, 2H)

^{13}C{^{1}H} NMR ($CDCl_3$, 100.61 MHz)

73.29	*C*H	(HC≡C)	116.80	*C*H	(*furan*)
82.30	C_q	(C≡*C*furan)	129.29	C_{ipso}	(*furan*)

6.3.19 Synthesis of 2,5-di(*trans-bis*(triethylphosphine)(phenyl)platinum)ethynyl furan (36)

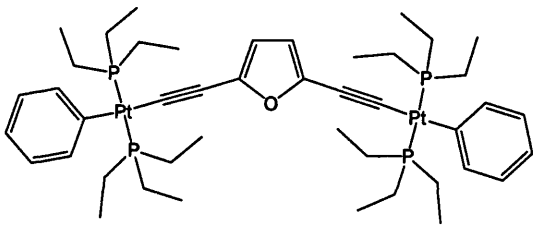

2,5-diethynyl furan (16 mg, 0.14 mmol) was placed in a Young's ampoule and dissolved in dichloromethane (10 mL). In a separate Schlenk tube copper iodide (5 mg), and *trans-bis*(triethylphosphine)(phenyl)platinum(II)chloride (150 mg, 0.28 mmol) were dissolved in tetrahydrofuran (30 mL) and diisopropylamine (15 mL). The 2,5-diethynyl furan solution was then added to the Schlenk tube and the reaction was left to stir for 6 hr. TLC (silica, hexane: dichloromethane, 1:1 v/v) revealed the completion of the reaction and the volatiles were then removed under reduced pressure. The crude product was passed through a silica plug in hexane: ethyl acetate (2:1 v/v) and the solvent was removed under reduced pressure. The brown solid was recrystallised from ethanol affording **(36)** as colourless crystals (145 mg, 93%).

^{1}H NMR ($CDCl_3$, 400.13 MHz)

1.04-1.12 (m, CH_3, 36H), 1.70-1.78 (m, CH_2, 24H), 6.04 (s, C*H*, 2H), 6.79 (t, ^3J= 7.3 Hz, CH, 2H), 6.95 (t, ^3J= 7.3 Hz, CH, 4H), 7.31 (d, ^3J= 7.3 Hz, C*H*, 2H)

$^{13}C\{^1H\}$ NMR ($CDCl_3$, 100.61 MHz)

7.96	CH_3	($P(CH_2CH_3)_3$)	121.21	*C*H	(*ortho* PtC_6H_5)
15.01	CH_2	(($P(CH_2CH_3)_3$), t_{ps}, $^1J_{PC}+^3J_{PC}$ = 34 Hz)	127.27	*C*H	(*para* PtC_6H_5)
			Absent	C_{ipso}	(*furan*)
100.47	C_q	(C≡*C*furan)	139.10	*C*H	(*meta* PtC_6H_5)
110.28	*C*H	(*furan*)	156.10	C_{ipso}	(PtC_6H_5)
117.92	C_q	(Pt*C*≡C)			

$^{31}P\{^1H\}$ NMR ($CDCl_3$, 121.5 MHz)

10.04 ($^1J_{PtP}$ = 2361 Hz)

Elemental Analysis: Result % (calculated %): C = 46.3 (46.7), H = 6.08 (6.42)

UV/vis: λ_{max} = 358 nm, ε = 32,100 $dm^3mol^{-1}cm^{-1}$

Emission: λ_{max} = 398 nm

6.3.20 Synthesis of 2,5-di(*trans-bis*(triethylphosphine)(phenyl)platinum)ethynyl thiophene (40)

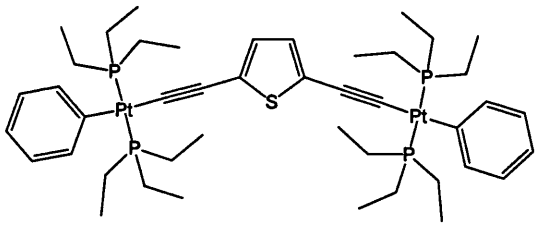

2,5-diethynyl thiophene (16 mg, 0.14 mmol) was placed in a Young's ampoule and dissolved in dichloromethane (10 mL). In a separate Schlenk tube copper iodide (5 mg), and *trans-bis*(triethylphosphine)(phenyl)platinum(II)chloride (150 mg, 0.28 mmol) were dissolved in tetrahydrofuran (30 mL) and diisopropylamine (15 mL). 2,5-diethynyl thiophene solution was then added to the Schlenk tube and the reaction was left to stir for 6 hr. TLC (silica, hexane: dichloromethane, 1:1 v/v) revealed the completion of the reaction and the volatiles were then removed under reduced pressure. The crude product was passed through a silica plug in hexane: ethyl acetate (2:1, v/v) and the solvent was removed under reduced pressure. The brown solid was recrystallised from ethanol affording **(40)** as colourless crystals (130 mg, 81%).

^{1}H NMR ($CDCl_3$, 400.13 MHz)

1.04 – 1.12 (m, C*H*$_3$, 36H), 1.69 – 1.77 (m, C*H*$_2$, 24H), 6.61 (s, C*H*, 2H), 6.79 (m, C*H*, 2H), 6.95 (t, ^3J = 7.4 Hz, C*H*, 4H), 7.31 (d, ^3J = 7.4 Hz, C*H*, 4H)

^{13}C{^{1}H} NMR - PENDANT ($CDCl_3$, 75.5 MHz)

7.97	*C*H$_3$	(P(CH$_2$*C*H$_3$)$_3$)	126.38	*C*H	(*thiophene*)
15.09	*C*H$_2$	((P(*C*H$_2$CH$_3$)$_3$), t_{ps},	127.20	*C*H	(*para* Pt*C*$_6$H$_5$)
		$^1J_{PC}+^3J_{PC}$ = 34 Hz)	126.80	C_{ipso}	(*thiophene*)
102.75	C_q	(C≡*C*thiophene)	139.12	*C*H	(*meta* Pt*C*$_6$H$_5$)
117.98	C_q	(Pt*C*≡C)	156.23	C_{ipso}	(Pt*C*$_6$H$_5$)
121.15	*C*H	(*ortho* Pt*C*$_6$H$_5$)			

^{31}P{^{1}H} NMR ($CDCl_3$, 161.98 MHz)

10.09 ($^1J_{PtP}$ = 2365 Hz)

IR (KBr disc, ν cm^{-1})

3043, 2963, 2930, 2875 (C-H), 2085 (C≡C)

UV/vis: λ_{max} = 377 nm, ε = 45,800 dm^{3}mol^{-1}cm^{-1}

Emission: λ_{max} = 399 nm

6.3.21 Synthesis of 2,5-*bis*(trimethylsilyethynyl)selenophene (41)

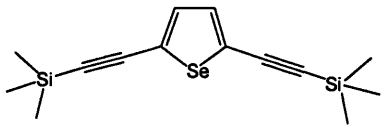

2,5-dibromoselenophene (1150 mg, 4 mmol), copper (I) iodide (76 mg, 0.40 mmol), and *bis*(triphenylphosphine)palladium(II)chloride (560 mg, 0.80 mmol) were placed in a Schlenk tube. Dichloromethane (20 mL), diisopropylamine (10 mL) and trimethylsilylacetylene (1.46 mL, 10 mmol) were added successively and the reaction was left to stir, in the absence of light, for 2 hr. TLC (silica, hexane) revealed the completion of the reaction and the volatiles were removed under reduced pressure. The resultant solid was passed through an alumina plug in hexane/ethyl acetate (2:1 v/v). The solvent was then removed and the crude product was purified by chromatography (silica, hexane) and recrystallisation from ethanol to afford **(41)** as pale gold material (970 mg, 76%).

^{1}H NMR ($CDCl_3$, 300.22 MHz)

0.24 (s, C*H*$_3$, 18H), 7.22 (s, C*H*, 2H)

^{13}C{^{1}H} NMR ($CDCl_3$, 75.5 MHz)

-0.23	CH_3	(Si*C*H$_3$)	129.29	C_{ipso}	(*selenophene*)
99.10	C_q	(Si*C*≡C)	134.73	*C*H	(*selenophene*)
101.75	C_q	(C≡*C*selenophene)			

^{77}Se NMR ($CDCl_3$, 76.31 MHz)

758.9 ($^3J_{SeH}$ = 7.00 Hz)

Elemental Analysis: Result % (calculated %): C = 52.0 (52.0), H = 6.15 (6.23)

6.3.22 Synthesis of 2,5-diethynyl selenophene (42)

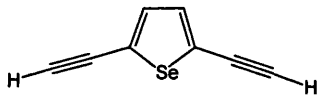

Potassium hydroxide (2.0 M aqueous solution, 1.10 mL) was added to a stirring solution of 2,5-*bis*(trimethylsilyethynyl)selenophene (323 mg, 1.00 mmol) in dichloromethane/methanol (2:1 v/v, 20 mL). The reaction was left to stir for 2 hr after which time TLC revealed the completion of the reaction (silica, hexane). The reaction mixture was reduced to a low volume under reduced pressure, in a water bath at 15°C, and the remaining viscous oil was redissolved in dichloromethane and washed with water (2 x 50 mL). The organic phase was separated and dried ($MgSO_4$). The volatiles were removed affording **(42)** as a dark yellow oil (110 mg, 62%).

^{1}H NMR ($CDCl_3$, 400.13 MHz)

3.53 (s, C*H*, 2H), 7.30 (s, C*H*, 2H)

^{13}C{^{1}H} NMR ($CDCl_3$, 100.62 MHz)

78.49	C_q	(C≡*C*selenophene)	128.55	C_{ipso}	(*selenophene*)
83.87	*CH*	(H*C*≡C)	135.10	*C*H	(*selenophene*)

^{77}Se NMR ($CDCl_3$, 76.36 MHz)

761.16 ($^3J_{SeH}$ = 8.25 Hz)

6.3.22 Synthesis of 2,5-di(*trans-bis*(triethylphosphine)(phenyl)platinum)ethynyl selenophene (43)

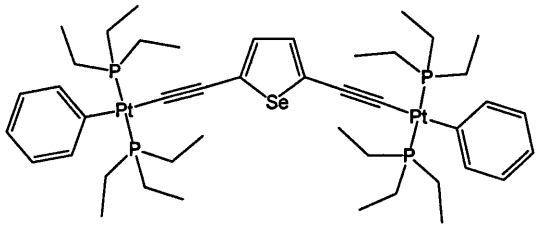

Trans-bis(triethylphosphine)(phenyl)platinum(II) chloride (250 mg, 0.46 mmol), 2,5-diethynyl selenophene (41 mg, 0.23 mmol) and copper(I) iodide (~5 mg) were placed in a Schlenk tube. Dichloromethane (30 mL) and diisopropylamine (20 mL) were added and the reaction was left to stir for 18 hr after which time completion of the reaction was confirmed by TLC (silica, hexane/dichloromethane, 1:1 v/v). The volatiles were removed under reduced pressure. The crude product was passed through a plug of silica in hexane/ethyl acetate (4:1 v/v), and the eluted solvent was removed under reduced pressure and the resulting solid was recrystallised from ethanol/chloroform (6:1 v/v) to afford **(43)** as yellow crystals (193 mg, 70%).

^{1}H NMR ($CDCl_3$, 400.13 MHz)

1.04 – 1.12 (m, C*H*$_3$, 36H), 1.69 – 1.77 (m, C*H*$_2$, 24H), 6.75 (s, C*H*, 2H), 6.79 (t, ^{3}J = 7.4 Hz, C*H*, 2H), 6.95 (t, ^{3}J = 7.4 Hz, C*H*, 4H), 7.31 (d, ^{3}J = 7.4 Hz, C*H*, 4H)

^{13}C{^{1}H} NMR - PENDANT ($CDCl_3$, 75.5 MHz)

8.03	CH_3	($P(CH_2CH_3)_3$)	127.27	CH	(*Selenophene*)
15.17	CH_2	(($P(CH_2CH_3)_3$), t_{ps}, $^{1}J_{PC}+^{3}J_{PC}$ = 33 Hz)	128.54	CH	(*para* PtC_6H_5)
			131.52	C_{ipso}	(*Selenophene*)
105.58	C_q	(C≡CSelenophene)	139.16	CH	(*meta* PtC_6H_5)
121.04	C_q	(PtC≡C)	156.28	C_{ipso}	(PtC_6H_5)
121.22	CH	(*ortho* PtC_6H_5)			

^{31}P{^{1}H} NMR ($CDCl_3$, 161.98 MHz)

10.13 ($^{1}J_{PtP}$ = 2365 Hz)

^{77}Se NMR ($CDCl_3$, 76.31 MHz)

709.0 ($^{3}J_{SeH}$ = 7.5 Hz)

IR (KBr disc, ν cm^{-1})

3042, 2962, 2929, 2875 (C-H), 2076 (C≡C)

Elemental Analysis: Result % (calculated %): C = 44.2 (44.3), H = 5.99 (6.08)

UV/vis: λ_{max} = 425 nm, ε = 40,500 $dm^3mol^{-1}cm^{-1}$

Emission: λ_{max} = 452 nm

6.3.23 Synthesis of 1,2-di(4-bromobenzoyl)hydrazine (44)

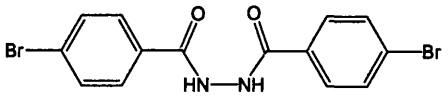

4-bromobenzoyl chloride (2.20g, 10.0 mmol) was heated under reflux in a stirred solution of hydrazine hydrate (0.24 mL, 5.00 mmol) for 1 hr. After cooling, cold water was added to precipitate by products. The filtrate was then evaporated to low volume to give a white crude product which was recrystallised from toluene to afford **(44)** as a white product (1.20 g, 60%).

^{1}H NMR ($CDCl_3$, 300.22 Hz)

1.25 (s, N*H*, 2H), 7.62 (d, ^3J = 8.5 Hz, C*H*, 2H), 7.96 (d, ^3J = 8.5 Hz, C*H*, 2H)

Elemental Analysis: Result % (calculated %): C = 42.5 (42.2), H = 2.51 (2.53), N = 7.18 (7.04)

6.3.24 Synthesis of 2,5-di(4-bromophenyl)-1,3,4-oxadiazole (45)

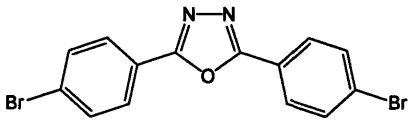

1,2-di(4-bromobenzoyl)hydrazine (1.00 g, 2.50 mmol) was dissolved in phosphorus oxychloride (50 mL) and refluxed for 18 hr. The volatiles were removed under reduced pressure. The crude product was washed with chloroform (100 mL) and water (100 mL) to quench any remaining phosphorus oxychloride. The resulting solid was filtered and recrystallised from ethanol/chloroform (1:1 v/v) to afford **(45)** as colourless crystals (0.90 g, 94%).

^{1}H NMR ($CDCl_3$, 300.22 Hz)

7.68 (d, ^3J = 8.5 Hz, C*H*, 4H), 8.01 (d, ^3J = 8.5 Hz, C*H*, 4H)

$^{13}C\{^1H\}$ NMR – PENDANT ($CDCl_3$, 75.5 MHz)

122.6	C_{ipso}	(*C*Br)	132.5	*C*H	(*meta* to oxadiazole)
126.6	C_{ipso}	(*para* to bromine)	164.0	C_{ipso}	(*oxadiazole*)
128.3	*C*H	(*ortho* to oxadiazole)			

Elemental Analysis: Result % (calculated %): C = 44.2 (44.3), H = 2.13 (2.12), N = 7.51 (7.37)

6.3.25 Synthesis of 2,5-*bis*(4-trimethylsilylethynylphenyl)-1,3,4-oxadiazole (46)

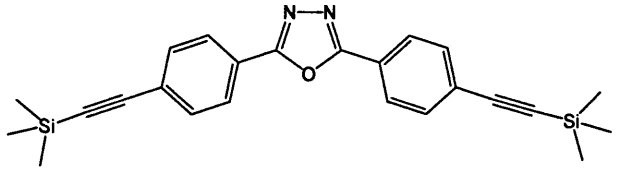

2,5-di(4-bromophenyl)-1,3,4-oxadiazole (0.76 g, 2.00 mmol), copper iodide (10 mg, 0.06 mol), and *bis*(triphenylphosphine)palladium(II)chloride (80 mg, 0.12 mmol) were placed in a Schlenk tube. Tetrahydrofuran (20 mL), diisopropylethylamine (0.60 mL), and trimethylsilylacetylene (0.42 mL) were added successively and the reaction left to stir, under protection from light, for 24 hr. TLC (silica, hexane/dichloromethane, 1:1 v/v) revealed that the reaction was complete and the volatiles were removed under reduced pressure. The resultant solid was dissolved in dichloromethane/ethyl acetate (1:1 v/v) and was passed through a plug of alumina. The volatiles were removed under reduced pressure and the crude product was recrystallised from ethanol/chloroform (1:1 v/v) affording **(46)** as white crystals (0.77 g, 93%).

^1H NMR ($CDCl_3$, 300.22 Hz)

0.28 (s, CH_3, 18H), 7.62 (d, ^3J = 8.4 Hz, C*H*, 4H), 8.07 (d, ^3J = 8.4 Hz, C*H*, 4H)

$^{13}C\{^1H\}$ NMR – PENDANT ($CDCl_3$, 75.5 MHz)

0.21	CH_3	(SiCH_3)	128.01	*C*H	(*ortho* to oxadiazole)
97.83	C_q	(C≡*C*Si)	130.09	C_{ipso}	(*para* to alkyne)
104.39	C_q	(Ph*C*≡C)	133.02	*C*H	(*meta* to oxadiazole)
126.41	C_{ipso}	(*para* to oxadiazole)	167.95	C_{ipso}	(*oxadiazole*)

IR (KBr disc, ν cm^{-1})

2960, 2900 (C-H), 2158 (C≡C), 1685, 1653 (C=N), 1250 (Si-C)

6.3.26 Synthesis of 2,5-di(4-ethynylphenyl)-1,3,4-oxadiazole (47)

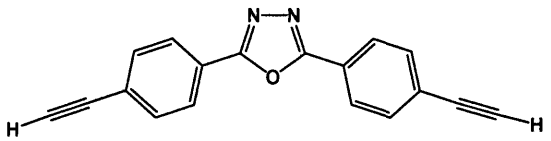

Potassium hydroxide (2.00 M aqueous solution, 0.75 mL) was added to a stirred solution of 2,5-di(4-trimethylsilylethynylphenyl)-1,3,4-oxadiazole (0.31 g, 0.75 mmol) in methanol/dichloromethane (20 mL, 1:1 v/v). The reaction was left to stir for 2 hr. TLC (silica, dichloromethane) revealed the completion of the reaction and the volatiles were removed under reduced pressure. The resulting solid was extracted into dichloromethane (70 mL) and washed with water (70 mL). The organic phase was then dried ($MgSO_4$) and evaporated to dryness affording **(47)** as a white solid (0.21 g, 98%).

^{1}H NMR ($CDCl_3$, 300.22 MHz)

3.26 (s, C*H*, 2H), 7.64 (d, ^3J = 8.4 Hz, C*H*, 4H), 8.09 (d, ^3J = 8.4 Hz, C*H*, 4H)

^{13}C{^{1}H} NMR – PENDANT ($CDCl_3$, 75.5 MHz)

80.19	*C*H	(H*C*≡C)	126.74	*C*H	(*ortho* to oxadiazole)
82.61	C_q	(C≡*C*Ph)	132.74	*C*H	(*meta* to oxadiazole)
123.65	C_{ipso}	(*para* to alkyne)	164.12	C_{ipso}	(*oxadiazole*)
125.67	C_{ipso}	(*para* to oxadiazole)			

IR (KBr disc, ν cm^{-1})

3058 (C-H), 2105 (C≡C), 1934 (C≡C-H)

Elemental Analysis: Result % (calculated %): C = 79.5 (80.0), H = 3.70 (3.73), N = 10.5 (10.4)

UV/vis: λ_{max} = 308 nm, ε = 68,000 $dm^3mol^{-1}cm^{-1}$

6.3.27 Synthesis of 2,5-*di*-(4-(*trans*-(phenyl,*bis*-triethylphosphine)platinum ethynyl))phenyl)-1,3,4-oxadiazole (48)

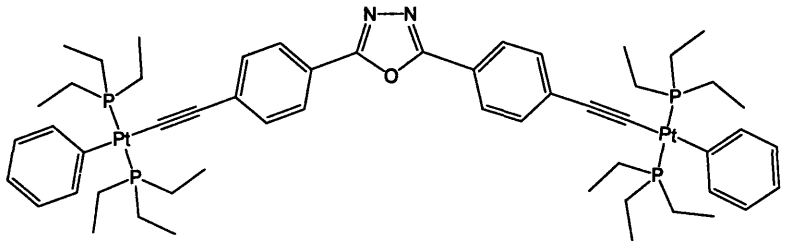

2,5-di(4-ethynylphenyl)-1,3,4-oxadiazole (68 mg, 0.25 mmol), *trans-bis*(triethylphosphine)(phenyl)platinum(II) chloride (273 mg, 0.5 mmol), and copper iodide (5 mg) were placed in a Schlenk tube and dissolved in dichloromethane (15 mL) and diisopropylamine (10 mL). The reaction was left to stir, under protection from the light, for 6 hr. TLC (silica, dichloromethane) revealed that the reaction was complete and the volatiles were removed under reduced pressure. The crude product was passed through a plug of alumina with ethyl acetate, and the eluted solvent was evaporated to dryness. The crude product was recrystallised from ethanol affording **(48)** as a yellow compound (198 mg, 75%).

^{1}H NMR ($CDCl_3$, 300.22 MHz)

1.06-1.16 (m, C*H*$_3$, 36H), 1.72-1.82 (m, C*H*$_2$, 24H), 6.82 (t, ^{3}J = 7.2 Hz, C*H*, 2H), 6.98 (t, ^{3}J = 7.2 Hz, C*H*, 4H), 7.33 (d, ^{3}J = 7.2 Hz, C*H*, 4H), 7.40 (d, ^{3}J = 8.4 Hz, C*H*, 4H), 7.96 (d, ^{3}J = 8.4 Hz, C*H*, 4H)

^{13}C{^{1}H} NMR – PENDANT ($CDCl_3$, 75.5 MHz)

8.03	*C*H$_3$	(P(CH$_2$*C*H$_3$)$_3$)	127.37	*C*H	(*ortho* to oxadiazole)
15.05	*C*H$_2$	((P(*C*H$_2$CH$_3$)$_3$), t_{ps},	131.30	*C*H	(*meta* to oxadiazole)
		$^{1}J_{PC}+^{3}J_{PC}$ = 34 Hz)	132.89	C_{ipso}	(*para* to oxadiazole)
114.57	C_q	(Pt*C*≡C)	139.02	*C*H	(*ortho* C$_6$H$_5$Pt)
119.65	C_q	(C≡*C*Ph)	164.56	C_{ipso}	(*oxadiazole*)
121.36	*C*H	(*para* C$_6$H$_5$Pt)			
126.47	C_{ipso}	(*para* to alkyne on C$_6$H$_4$)			

^{31}P{^{1}H} NMR ($CDCl_3$, 121.5 MHz)

10.20 ($^{1}J_{PtP}$ = 2629 Hz)

IR (KBr disc, ν cm^{-1})

2963, 2931, 2875 (C-H), 2092 (C≡C)

Elemental Analysis: Result % (calculated %): C = 50.1 (50.5), H = 5.94 (6.12), N = 1.99 (2.18)

UV/vis: λ_{max} = 366 nm, ε = 95,000 $dm^3mol^{-1}cm^{-1}$

Emission: λ_{max} = 407, 423 nm

6.3.28 Synthesis of 2,5-di(4-bromophenyl)-1,3,4-thiadiazole (49)

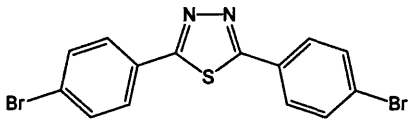

1,2-di(4-bromobenzoyl)hydrazine (1.00 g, 2.50 mmol) and phosphorous pentasulphide (0.67 g, 1.50 mmol) were dissolved in xylene (20 mL) and refluxed for 14 hr. TLC (silica, dichloromethane) revealed the completion of the reaction. After cooling, cold water (15 mL) was added dropwise, and the solution was heated to 80°C for 2 hr. The solution was cooled to 0 °C and sodium hydrogen carbonate was added until the pH of the solution was ~7-8. The neutralised solution was stirred for 12 hr. The volatiles were removed and the resulting brown solid was washed with water (2 x 50 mL) and dried in air. The crude product was washed in ethanol to leave a beige powder that was recrystallised from xylene to afford **(49)** as an off white crystalline material (0.61 g, 62%).

^{1}H NMR ($CDCl_3$, 300.22 MHz)

7.65 (d, ^3J = 8.4 Hz, C*H*, 4H) 7.88 (d, ^3J = 8.4 Hz, C*H*, 4H)

Elemental Analysis: Result % (calculated %): C = 42.0 (42.5), H = 2.01 (2.04), N = 7.05 (7.07)

6.3.29 Synthesis of 2,5-*bis*(4-trimethylsilylethynylphenyl)-1,3,4-thiadiazole (50)

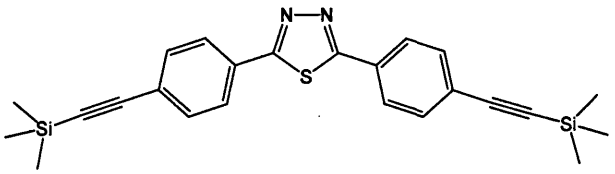

2,5-di(4-bromophenyl)-1,3,4-thiadiazole (550 mg, 1.39 mmol), copper iodide (8 mg, 0.04 mmol) and *bis*(triphenylphosphine)palladium(II)chloride (58.5 mg, 6 mol%) were placed in a Schlenk tube. Tetrahydrofuran (20 mL), di-isopropylethylamine (0.5 mL) and trimethylsilylacetylene (0.295 mL) were added successively and the reaction was left to stir, under protection from light, for 18 hr. TLC (silica, hexane/dichloromethane, 1:1 v/v) revealed that the reaction was complete and the volatiles were removed under reduced pressure. The resultant solid was dissolved in dichloromethane/ethyl acetate (1:1 v/v) and was passed through a plug of alumina. The volatiles were removed under reduced pressure and recrystallised from ethanol/chloroform (2:1 v/v) affording **(50)** as an off white solid (460 mg, 76 %).

^{1}H NMR ($CDCl_3$, 300.22 MHz)

0.27 (s, CH_3, 18H), 7.59 (d, ^3J = 8.5 Hz, CH, 4H), 7.94 (d, ^3J = 8.5 Hz, CH, 4H)

^{13}C NMR ($CDCl_3$, 75.5 MHz)

0.21	CH_3	($SiCH_3$)	128.01	CH	(*ortho* to thiadiazole)
97.80	C_q	(C≡CSi)	130.09	C_{ipso}	(*para* to alkyne)
104.39	C_q	(PhC≡C)	133.02	CH	(*meta* to thiadiazole)
126.41	C_{ipso}	(*para* to oxadiazole)	167.95	C_{ipso}	(*thiadiazole*)

IR (KBr disc, ν cm^{-1})

2959, 2898 (C-H), 2157 (C≡C), 1253 (Si-C)

Elemental Analysis: Result % (calculated %): C = 66.3 (66.9), H = 5.94 (6.08), N = 6.48 (6.50)

UV/vis: λ_{max} = 334 nm, ε = 62,000 $dm^3mol^{-1}cm^{-1}$

6.3.30 Synthesis of 2,5-di(4-ethynylphenyl)-1,3,4-thiadiazole (51)

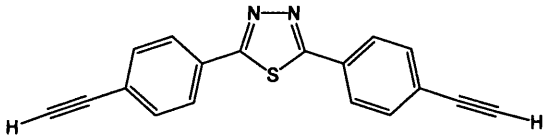

Potassium hydroxide (2.00 M aqueous solution, 0.75 mL) was added to a stirring solution of 2,5-*bis*(4-trimethylsilylethynylphenyl)-1,3,4-thiadiazole (0.32 g, 0.75 mmol) dichloromethane/methanol (1:1 v/v). The reaction was left to stir, under protection from light, for 2 hr. TLC (alumina, dichloromethane) revealed that the reaction was complete. The product was extracted using dichloromethane (50 mL) and water (50 mL). The organic phase was separated and dried ($MgSO_4$). The crude product was dissolved in dichloromethane and passed through a plug of silica, and the eluted solvent was evaporated to dryness affording **(51)** as an off white solid (0.21 g, 96%).

^{1}H NMR ($CDCl_3$, 300.22 MHz)

3.24 (s, C*H*, 2H), 7.63 (d, ^3J = 8.5 Hz, C*H*, 4H), 7.97 (d, ^3J = 8.5 Hz, C*H*, 4H)

^{13}C{^{1}H} NMR ($CDCl_3$, 75.5 MHz)

79.85	*C*H	(HC≡C)	130.09	C_{ipso}	(*para* to alkyne)
82.75	C_q	(C≡*C*Ph)	132.87	*C*H	(*meta* to thiadiazole)
125.05	C_{ipso}	(*para* to thiadiazole)	167.56	C_{ipso}	(*thiadiazole*)
127.77	C_{ipso}	(*ortho* to thiadiazole)			

IR (KBr disc, ν cm^{-1})

3046 (C-H), 2110 (C≡C), 1933 (C≡C-H)

Elemental Analysis: Result % (calculated %): C = 75.0 (75.5), H = 3.50 (3.52), N = 9.81 (9.78)

UV/vis: λ_{max} = 326 nm, ε = 68,000 $dm^3mol^{-1}cm^{-1}$

6.3.31 Synthesis of 2,5-*di*-(4-(*trans*-(phenyl,*bis*-triethylphosphine)platinum ethynyl))phenyl)-1,3,4-thiadiazole (52)

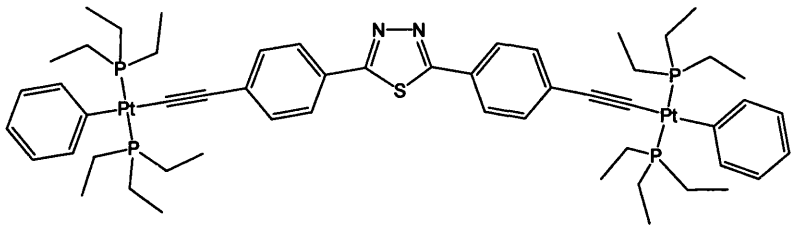

2,5-di(4-ethynylphenyl)-1,3,4-thiadiazole (72 mg, 0.25 mmol), *trans-bis*(triethylphosphine)(phenyl)platinum(II)chloride (272 mg, 0.50 mmol), and copper iodide (5 mg) were placed in a Schlenk tube. Dichloromethane (15 mL) and diisopropylamine (10 mL) were added and the solution was left to stir, under protection from light, for 3 hr. TLC (silica, dichloromethane) revealed the completion of the reaction, and the volatiles were removed under reduced pressure. The solid was dissolved in ethyl acetate and passed through a short plug of silica, and the volatiles were then evaporated. The crude product was recrystallised from ethanol to afford **(52)** as yellow crystals (190 mg, 73%).

^{1}H NMR ($CDCl_3$, 300.22 MHz)

1.06-1.16 (m, CH_3, 36H), 1.72-1.81 (m, CH_2, 24H), 6.82 (t, ^{3}J = 7.4 Hz, CH, 2H), 6.98 (t, ^{3}J = 7.4 Hz, CH, 4H), 7.33 (d, ^{3}J = 7.4 Hz, CH, 4H), 7.37 (d, ^{3}J = 8.5 Hz, CH, 4H), 7.85 (d, ^{3}J = 8.5 Hz, CH, 4H)

^{13}C{^{1}H} NMR - PENDANT ($CDCl_3$, 75.5 MHz)

8.03	CH_3	($P(CH_2CH_3)_3$)	127.47	CH	(*ortho* to thiadiazole)
15.05	CH_2	(($P(CH_2CH_3)_3$), t_{ps},	131.37	CH	(*meta* to thiadiazole)
		$^{1}J_{PC}+^{3}J_{PC}$ = 34 Hz)	132.33	C_{ipso}	(*para* to alkyne)
110.43	C_q	(C≡C)	139.04	CH	(*ortho* to C_6H_5Pt)
121.35	CH	(*para* C_6H_5Pt)	167.75	C_{ipso}	(*thiadiazole*)
126.18	C_{ipso}	(*para* to thiadiazole)			

^{31}P{^{1}H} NMR ($CDCl_3$, 121.5 MHz)

10.12 ($^{1}J_{PtP}$ = 2630 Hz)

IR (KBr disc, ν cm^{-1})

2962, 2931, 2874 (C-H), 2092 (C≡C)

UV/vis: λ_{max} = 384 nm, ε = 94,000 $dm^3mol^{-1}cm^{-1}$

Emission: λ_{max} = 458 nm

6.3.32 Synthesis of 1,4-*bis*-(4-(trimethylsilylethynyl)phenyl)-butane-1,4-dione (53)

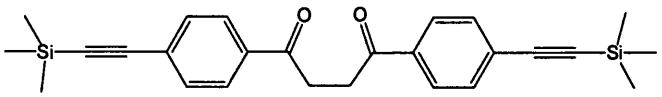

1,4-*di*-(4-bromo-phenyl)-butane-1,4-dione (600 mg, 1.52 mmol), copper (I) iodide (15 mg, 0.04 mmol), and *bis*(triphenylphosphine)palladium(II)chloride (111 mg, 0.08 mmol) were placed in a Schlenk tube. Tetrahydrofuran (20 mL), diisopropylamine (10 mL) and trimethylsilylacetylene (0.33 mL, 2.28 mmol) were added successively and the reaction was left to stir, in the absence of light, for 2 hr. The volatiles were removed under reduced pressure and the resultant solid was passed through a short alumina plug using ethyl acetate as the eluent. The volatiles were removed under reduced pressure and the resultant solid was dissolved in dichloromethane (20 mL). Hexane (150 mL) was added to precipitate the crude product. The solid was filtered and recrystallised from ethanol affording **(53)** as a silvery white solid (560 mg, 86%).

^{1}H NMR ($CDCl_3$, 300.22 MHz)

0.27 (s, C*H*$_3$, 18H), 3.43 (s, C*H*$_2$, 4H), 7.55 (d, ^3J = 8.5 Hz, C*H*, 4H), 7.96 (d, ^3J = 8.5 Hz, C*H*, 4H)

^{13}C{^{1}H} NMR – PENDANT ($CDCl_3$, 100.62 MHz)

0.17	*C*H$_3$	(Si*C*H$_3$)	128.41	*C*$_{ipso}$	(*para* to carbonyl)
32.93	*C*H$_2$		132.46	*C*H	(*meta* to carbonyl)
98.47	*C*$_q$	(Si*C*≡C)	136.34	*C*$_{ipso}$	(*para* to alkyne)
104.40	*C*$_q$	(C≡*C*Ph)	198.16	*C*$_q$	(*C*=O)
128.28	*C*H	(*meta* to carbonyl)			

Elemental Analysis: Result % (calculated %): C = 72.0 (72.5), H = 7.40 (7.02)

6.3.33 Synthesis of 1,4-*bis*-(4-(ethynyl)phenyl)-butane-1,4-dione (54)

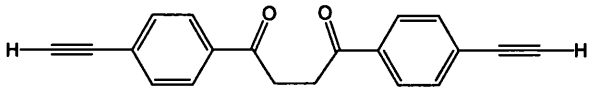

Potassium hydroxide (2.0 M aqueous solution, 0.77 mL) was added to a stirring solution of 1,4-*bis*-(4-trimethylsilylethynyl)-butane-1,4-dione (300 mg, 0.70 mmol) in dichloromethane/methanol (2:1 v/v, 20 mL). The reaction was left to stir for 2 hr after which time TLC revealed the completion of the reaction (silica, hexane/dichloromethane, 2:1 v/v). The volatiles were removed under reduced pressure and the solid was redissolved in dichloromethane and washed with water (2 x 50 mL). The organic phase was separated and dried ($MgSO_4$). The solvent was removed, and the solid was crystallised from ethanol affording **(54)** as a yellow solid (155 mg, 78%).

^{1}H NMR ($CDCl_3$, 300.22 MHz)

3.25 (s, C*H*, 2H), 3.44 (s, CH_2, 4H), 7.59 (d, ^3J = 8.5 Hz, C*H*, 4H) 7.99 (d, ^3J = 8.5 Hz, C*H*, 4H)

^{13}C{^{1}H} NMR – PENDANT ($CDCl_3$, 100.62 MHz)

33.60	CH_2		128.01	C_{ipso}	(*para* to carbonyl)
80.36	*C*H	(HC≡C)	132.34	*C*H	(*ortho* to carbonyl)
82.78	C_q	(C≡*C*Ph)	136.39	C_{ipso}	(*para* to alkyne)
127.02	*C*H	(*meta* to carbonyl)	197.72	C_q	(*C*=O)

6.3.34 Synthesis of 2,5-*di*-(4-(*trans*-(phenyl,*bis*-triethylphosphine)platinum ethynyl))phenyl)- butane-1,4-dione (55)

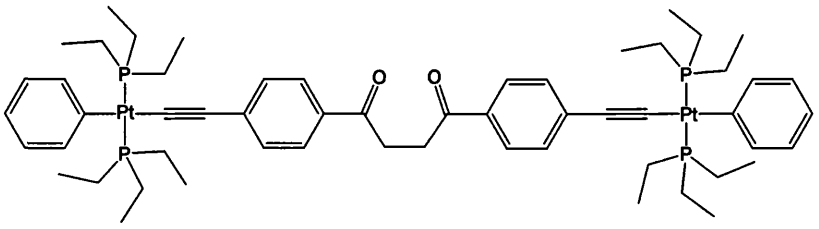

Trans-bis(triethylphosphine)(phenyl)platinum(II)chloride (250 mg, 0.46 mmol), 1,4-*di*-(4-ethynyl)-butane-1,4-dione (66 mg, 0.23 mmol) and copper(I) iodide (5 mg) were placed in a Schlenk tube. Dichloromethane (15 mL) and diisopropylamine (10 mL)

were added and the reaction was left to stir, under protection from light, for 18 hr. TLC (silica, dichloromethane) revealed the completion of the reaction and the volatiles were removed under reduced pressure. The crude product was then passed through a small plug of alumina in hexane/ethyl acetate (2:1 v/v), and the eluted solvent was evaporated to dryness. The resulting solid was recrystallised from ethanol/chloroform (5:1 v/v) to yield **(55)** as yellow crystals (220 mg, 74%).

^{1}H NMR ($CDCl_3$, 400.13 MHz)

1.06-1.14 (m, C*H*$_3$, 36H), 1.71-1.79 (m, C*H*$_2$, 24H), 3.40 (s, C*H*$_2$, 4H), 6.81 (t, ^{3}J = 14.5 Hz, C*H*, 2H), 6.97 (m, C*H*, 4H), 7.33 (t, ^{3}J = 8.5 Hz, C*H*, 8H), 7.90 (d, ^{3}J = 8.5 Hz, C*H*, 4H)

^{13}C{^{1}H} NMR – PENDANT ($CDCl_3$, 75.5 MHz)

8.01	*C*H$_3$	(P(CH$_2$*C*H$_3$)$_3$)	130.77	*C*H	(C$_6$H$_4$)
15.01	*C*H$_2$	((P(*C*H$_2$CH$_3$)$_3$), t$_{ps}$, $^{1}J_{PC}$+$^{3}J_{PC}$ = 34 Hz)	132.68	*C*$_{ipso}$	(*C*$_6$H$_5$)
			134.70	*C*$_{ipso}$	(C$_6$H$_4$)
32.54	*C*H$_2$	(CO*C*H$_2$)	139.04	*C*H	(*C*$_6$H$_5$)
110.71	*C*$_q$	(C≡*C*Ph)	155.88	*C*$_{ipso}$	(Pt(*C*$_6$H$_5$))
121.38	*C*H	(C$_6$H$_4$)	198.16	*C*$_q$	(*C*O)
127.38	*C*H	(*C*$_6$H$_5$)			
128.01	*C*H	(*C*$_6$H$_5$)			

^{31}P{^{1}H} NMR ($CDCl_3$, 161.97 MHz)

10.08 ($^{1}J_{PtP}$ = 2628 Hz)

Elemental Analysis: Result % (calculated %): C = 51.4 (51.7), H = 6.29 (6.35)

IR (KBr disc, ν cm^{-1}): 3046, 2963, 2930, 2910, 2874 (C-H), 2089 (C≡C), 1681 (C=O)

UV/vis: λ_{max} = 349 nm, ε = 63,100 dm^{3}mol^{-1}cm^{-1}

Emission: λ_{max} = 409 nm

6.3.35 Synthesis of 2,5-*bis*-(4-triphenylphosphine gold(I)ethynyl-phenyl)-1,3,4-oxadiazole (56)

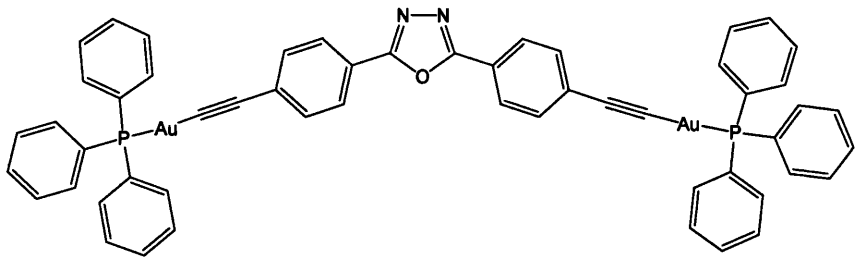

2,5-di(4-ethynylphenyl)-1,3,4-oxadiazole (41 mg, 0.15 mmol) was dissolved in methanol (30 mL), sodium methoxide (50 mg, 0.1 mmol) and triphenylphosphine-gold(I) chloride (200 mg, 0.41 mmol) was added to the solution and the reaction was left to stir for 18 hr. The precipitate was filtered and washed with methanol (10 mL), water (10 mL) then methanol (10 mL). The crude product was recrystallised from ethanol/chloroform (6:1 v/v) to afford **(56)** as a yellow crystals (135 mg, 67%).

^{1}H NMR ($CDCl_3$, 400.13 MHz)

7.44-7.59 (m, C*H*, 30H), 7.63 (d, ^{3}J = 8.4 Hz, C*H*, 4H), 8.02 (d, ^{3}J = 8.4 Hz, C*H*, 4H)

^{13}C PENDANT NMR ($CDCl_3$, 100.62 MHz)

103.40	C_q	(Au*C*≡C)	130.01	C_{ipso}	(C_6H_4 para to oxadiazole)
121.80	C_q	(C≡*C*Ph)	131.56	*C*H	(d, $^{5}J_{PC}$ = 2.09 Hz, *Ph*P)
126.55	*C*H	(C_6H_4 ortho to oxadiazole)	132.84	*C*H	(*oxadiazole*)
126.26	*C*H	(C_6H_4 meta to oxadiazole)	134.32	C_{ipso}	(d, $^{3}J_{PC}$ = 14.1 Hz, *Ph*P)
129.15	*C*H	(d, $^{4}J_{PC}$ = 11.1 Hz, *Ph*P)	134.62	C_{ipso}	(C_6H_4 para to alkyne)
129.46	C_{ipso}	(*Ph*P)	149.52	C_{ipso}	(*oxadiazole*)

^{31}P{^{1}H} NMR ($CDCl_3$, 161.98 MHz)

42.31

UV/vis: λ_{max} = 341 nm, ε = 81,000 $dm^3mol^{-1}cm^{-1}$

Emission: λ_{max} = 369 nm

6.3.36 Synthesis of 2,5-*bis*-(4-triphenylphosphine gold(I)ethynyl-phenyl)selenophene (57)

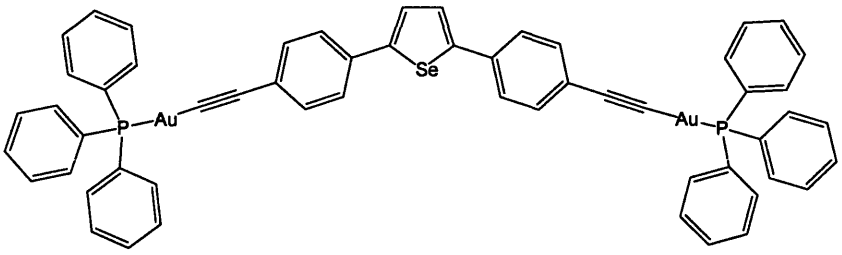

2,5-*bis*-(4-trimethylsilylethynyl-phenyl)selenophene (48 mg, 0.10 mmol) was dissolved in methanol (30 mL), and sodium methoxide (50 mg, 1.0 mmol) was added to the stirring solution. The reaction was left to stir for 1 hr. Triphenylphosphine-gold(I) chloride (100 mg, 0.20 mmol) was added to the solution and the reaction was left to stir for 18 hr. The precipitate was filtered and washed with methanol (10 mL), water (10 mL) then methanol (10 mL). The crude product was then recrystallised from ethanol to afford **(57)** as a yellow crystals (107 mg, 86%).

^{1}H NMR ($CDCl_3$, 400.13 MHz)

7.41 (s, C*H*, 2H), 7.43-7.59 (m, C*H*, 38H)

^{13}C PENDANT NMR ($CDCl_3$, 100.62 MHz)

104.13	C_q	(Au*C*≡C)	130.01	C_{ipso}	(C_6H_4 para to selenophene)
124.04	C_q	(C≡*C*Ph)	131.56	*C*H	(d, $^{5}J_{PC}$ = 2.09 Hz, *Ph*P)
125.50	*C*H	(C_6H_4 ortho to selenophene)	132.84	*C*H	(*selenophene*)
126.26	*C*H	(C_6H_4 meta to selenophene)	134.32	C_{ipso}	(d, $^{3}J_{PC}$ = 14.1 Hz, *Ph*P)
129.15	*C*H	(d, $^{4}J_{PC}$ = 11.1 Hz, *Ph*P)	134.62	C_{ipso}	(C_6H_4 para to alkyne)
129.46	C_{ipso}	(*Ph*P)	149.52	C_{ipso}	(*selenophene*)

^{31}P{^{1}H} NMR ($CDCl_3$, 161.98 MHz)

42.46

^{77}Se NMR ($CDCl_3$, 76.31 MHz)

568.03 ($^{3}J_{SeH}$ = 5.8 Hz)

Elemental Analysis: Result % (calculated %): C = 52.8 (53.9), H = 3.14 (3.23)

UV/vis: λ_{max} = 376 nm, ε = 71,700 $dm^3mol^{-1}cm^{-1}$

6.4 Experimental details for Chapter Four

6.4.1 Synthesis of 2,5-*di*-(4-bromo-phenyl)-pyrrole (58)

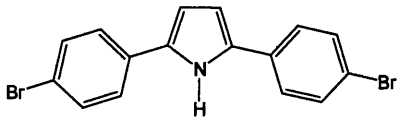

1,4-*di*-(4-bromo-phenyl)-butane-1,4-dione (500 mg, 1.27 mmol) and ammonium acetate (532 mg, 6.35 mmol) were dissolved in ethanol (20 mL) and sealed in a Young's Ampoule. The reaction was heated to 80 °C and left to stir for 3 hr after which time TLC (silica, dichloromethane) revealed completion of the reaction. The solvent was evaporated to low volume (~5 mL) precipitating out white needles. The product was filtered, washed with cold ethanol and dried under reduced pressure affording **(58)** as a white solid (450 mg, 94%).

^{1}H NMR ($CDCl_3$, 400.13 Hz, δ ppm)

6.57 (d, $^4J_{NH}$ = 2.5 Hz, C*H*, 2H), 7.38 (d, ^3J = 8.6 Hz, C*H*, 4H), 7.51 (d, ^3J = 8.6 Hz, C*H*, 4H), 8.48 (s, N*H*, 1H)

^{13}C{^{1}H} NMR – PENDANT ($CDCl_3$, 75.5 MHz, δ ppm)

108.98	*C*H	(*pyrrole*)	131.53	C_{ipso}	(*C*Br)
120.48	C_{ipso}	(*pyrrole*)	132.43	*C*H	(*meta* to pyrrole)
125.64	*C*H	(*ortho* to pyrrole)	132.8	C_{ipso}	(*para* to bromine)

Elemental Analysis: Result % (calculated %): C = 51.1 (51.0), H = 2.97 (2.94), N = 3.77 (3.71)

EI/Mass Spectrum: ($C_{16}H_{11}Br_2N$) *m/z* 377.0, calc. 377.0

6.4.2 Synthesis of 2,5-*bis*-(4-trimethylsilylethynyl-phenyl)-pyrrole (59)

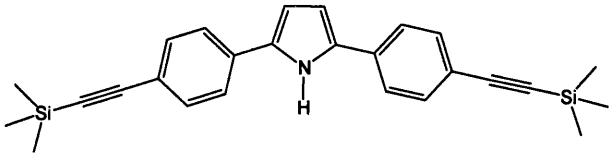

2,5-*di*-(4-bromo-phenyl)-pyrrole (500 mg, 1.33 mmol), copper (I) iodide (25 mg, 0.13 mmol), and *bis*(triphenylphosphine)palladium(II)chloride (186 mg, 0.27 mmol) were

placed in a Schlenk tube. Dichloromethane (20 mL), diisopropylamine (10 mL) and trimethylsilylacetylene (0.58 mL, 3.99 mmol) were added successively and the reaction was stirred, in the absence of light, for 22 hr. The volatiles were removed under reduced pressure and the resultant solid was passed through a short alumina plug using hexane/ethyl acetate (4:1 v/v) as the eluent. The solvent was then removed and the solid redissolved in hexane (20 mL) and passed through a silica column. The eluted solvent was removed under reduced pressure affording **(59)** as a yellow solid (460 mg, 86%).

^{1}H NMR ($CDCl_3$, 400.13 Hz, δ ppm)

0.26 (s, C*H*$_3$, 18H), 6.62 (d, $^4J_{NH}$ = 2.0 Hz, C*H*, 2H), 7.45 (d, ^3J = 8.4 Hz, C*H*, 4H), 7.49 (d, ^3J = 8.4 Hz, C*H*, 4H), 8.58 (s, N*H*, 1H)

^{13}C{^{1}H} NMR – PENDANT ($CDCl_3$, 75.5 MHz, δ ppm)

-0.02	*C*H$_3$	(Si*C*H$_3$)	123.29	*C*H	(*ortho* to pyrrole)
94.91	C_q	(Si*C*≡C)	132.00	C_{ipso}	(*para* to pyrrole)
105.03	C_q	(C≡*C*Ph)	132.62	*C*H	(*meta* to pyrrole)
109.12	*C*H	(*pyrrole*)	133.00	C_{ipso}	(*para* to alkyne)
120.89	C_{ipso}	(*pyrrole*)			

Elemental Analysis: Result % (calculated %): C = 73.8 (75.9), H = 7.13 (7.10), N = 3.05 (3.40)

6.3.3 Synthesis of 2,5-*di*-(4-ethynyl-phenyl)-1*H*-pyrrole (60)

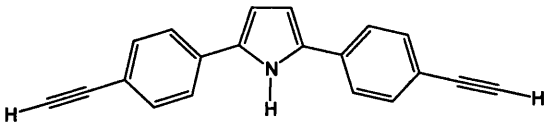

Potassium hydroxide (1.24 mL, 2.00 M aqueous solution) was added to a stirring solution of 2,5-*bis*-(4-trimethylsilylethynyl-phenyl)-pyrrole (300 mg, 0.73 mmol) in methanol/dichloromethane (1:1 v/v, 20 mL). The reaction was left to stir, in the absence of light, for 2 hr. TLC (silica, ethyl acetate) revealed completion of the reaction and the volatiles were removed under reduced pressure. The solid was redissolved in dichloromethane (20 mL) and washed with water (2 x 20 mL). The organic phase was separated, dried ($MgSO_4$) and evaporated to dryness affording **(60)** as a brown solid (160 mg, 98%).

^{1}H NMR ($CDCl_3$, 400.13 Hz, δ ppm)

3.13 (s, C*H*, 2H), 6.63 (d, $^4J_{NH}$ = 2.5 Hz, C*H*, 2H), 7.47 (d, ^3J = 8.2 Hz, C*H*, 4H), 7.52 (d, ^3J = 8.2 Hz, C*H*, 4H), 8.58 (s, N*H*, 1H)

^{13}C{^{1}H} NMR – PENDANT ($CDCl_3$, 75.5 MHz, δ ppm)

77.78	C_{ipso}	(HC≡C)	123.43	CH	(*ortho* to pyrrole)
83.58	C_{ipso}	(C≡CPh)	132.35	C_{ipso}	(*para* to pyrrole)
109.21	CH	(*pyrrole*)	132.77	CH	(*meta* to pyrrole)
119.89	C_{ipso}	(*pyrrole*)	132.93	C_{ipso}	(*para* to alkyne)

IR (KBr disc, ν cm^{-1})

3066 (C-H), 2112 (C≡C), 1941 (C≡C-H)

Elemental Analysis: Result % (calculated %): C = 88.0 (89.9), H = 4.82 (4.90), N = 5.10 (5.24)

6.4.4 Synthesis of 2,5-*bis*-(4-(*trans*-(phenyl,*bis*-triethylphosphine)platinum ethynyl))phenyl)-1*H*-pyrrole (61)

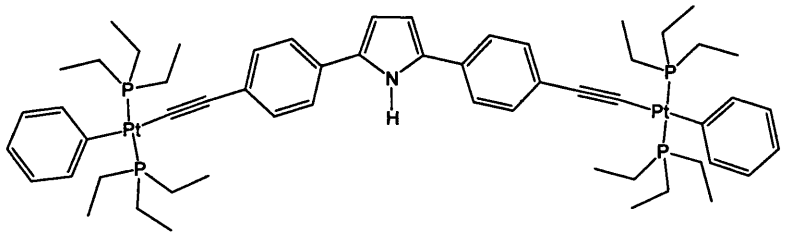

Trans- *bis*(triethylphosphine)(phenyl)platinum(II) chloride (356 mg, 0.50 mmol), 2,5-*di*-(4-ethynyl-phenyl)-pyrrole (67 mg, 0.25 mmol), and copper iodide (5 mg) were transferred to a Schlenk tube, tetrahydrofuran (15 mL) and diisopropylamine (15 mL) were added and the solution was left to stir, under protection from light. The progress of the reaction was monitored by TLC (silica, dichloromethane). After 2 hr the reaction was complete and the volatiles were removed under reduced pressure. The solid was dissolved in hexane/ethyl acetate (2:1 v/v) and passed through a short alumina plug. The solvent was then removed and the crude product was purified further by chromatography (silica, dichloromethane/hexane, 9:1 v/v) affording **(61)** as yellow crystals (248 mg, 77%).

^{1}H NMR ($CDCl_3$, 300.22 MHz, δ ppm)

1.07-1.15 (m, C*H*$_3$, 36H), 1.74-1.81 (m, C*H*$_2$, 24H), 6.52 (d, $^4J_{NH}$ = 2.5 Hz, C*H*, 2H), 6.81 (t, ^3J = 14.9 Hz, C*H*, 2H), 6.97 (t, ^3J = 14.9 Hz, C*H*, 4H), 7.31 (d, ^3J = 8.6 Hz, C*H*, 4H), 7.36 (d, ^3J = 8.6 Hz, C*H*, 4H), 8.46 (s, N*H*, 1H)

^{13}C{^{1}H} NMR – PENDANT ($CDCl_3$, 75.5 MHz, δ ppm)

8.04	*C*H$_3$	(PCH$_2$*C*H$_3$)	127.29	*C*H	(*C*$_6$H$_4$)
15.11	*C*H$_2$	((P(*C*H$_2$CH$_3$)$_3$), t$_{ps}$, $^1J_{PC}$+$^3J_{PC}$ = 34 Hz)	128.69	*C*H	(*C*$_6$H$_4$)
			131.35	*C*$_{ipso}$	(*para* to alkyne)
107.48	*C*H	(*pyrrole*)	133.19	*C*$_{ipso}$	(P(*Ph*))
110.22	*C*$_q$	(Pt*C*≡C)	139.18	*C*H	(*ortho*, Pt-*Ph*)
114.48	*C*$_q$	(C≡*C*Ph)	156.34	*C*$_{ipso}$	(Pt-*Ph*)
121.22	*C*H	(*para* C$_6$H$_5$Pt)			
123.21	*C*$_{ipso}$	(*pyrrole*)			

^{31}P{^{1}H} NMR ($CDCl_3$, 121.5 MHz, δ ppm)

9.99 ($^1J_{PtP}$ = 2641 Hz)

IR (KBr disc, ν cm^{-1}): 2962, 2931, 2873 (C-H), 2090 (C≡C)

Elemental Analysis: Result % (calculated %): C = 52.4 (52.5), H = 6.39 (6.37), N = 0.94 (1.10)

UV/Vis: λ_{max} = 381 nm, ε = 65,500 dm^{3}mol^{-1}cm^{-1}

Emission: λ_{max} = 421, 445 nm

6.4.5 Synthesis of 2,5-*di*-(4-bromo-phenyl)-1-methyl-pyrrole (62)

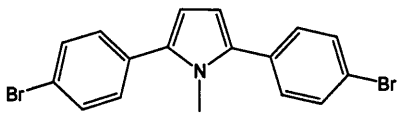

Methylamine (8.00 M solution in ethanol, 0.24 mL) was added to a stirring solution of 1,4-*di*-(4-bromo-phenyl)-butane-1,4-dione (250 mg, 0.63 mmol) in ethanol (50 mL). The mixture was refluxed for 14 hr after which time the solution had turned bright yellow and a white precipitate had formed. The solid was filtered off and washed with ethanol affording **(62)** as a white solid (220 mg, 86%).

^{1}H NMR ($CDCl_3$, 400.13 Hz, δ ppm)

3.57 (s, C*H*$_3$, 3H), 6.31 (s, C*H*, 2H), 7.32 (d, ^3J = 8.5 Hz, C*H*, 4H), 7.55 (d, ^3J = 8.5 Hz, C*H*, 4H)

^{13}C{^{1}H} NMR – PENDANT ($CDCl_3$, 75.5 MHz, δ ppm)

34.67	*C*H$_3$	(N*C*H$_3$)	132.06	*C*H	(*meta* to pyrrole)
109.62	*C*H	(*pyrrole*)	132.59	C_{ipso}	(*para* to pyrrole)
121.44	C_{ipso}	(*pyrrole*)	136.51	C_{ipso}	(*para* to bromine)
130.53	*C*H	(*ortho* to pyrrole)			

EI/Mass Spectrum: ($C_{17}H_{13}Br_2N$) *m/z* 391.0, calc. 391.1

6.4.6 Synthesis of 2,5-*bis*-(4-trimethylsilylethynyl-phenyl)-1-methyl-pyrrole (63)

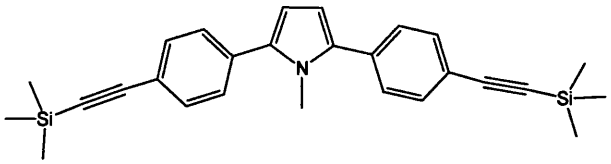

2,5-*di*-(4-bromo-phenyl)-1-methyl-pyrrole (150 mg, 0.39 mmol), copper (I) iodide (10 mg, 0.04 mmol), and *bis*(triphenylphosphine)palladium(II)chloride (42 mg, 0.08 mmol) were placed in a Schlenk tube. Dichloromethane (20 mL), diisopropylamine (10 mL) and trimethylsilylacetylene (0.17 mL, 1.15 mmol) were added successively and the reaction was left to stir for 18 hr. The volatiles were removed under reduced pressure and the resultant solid was passed through a short alumina plug using ethyl acetate/hexane (1:1 v/v) as the eluent. The solvent was then removed and crude product was further purified by chromatography (silica, hexane/dichloromethane, 4:1 v/v) affording **(63)** as an off white solid (130 mg, 78%).

^{1}H NMR ($CDCl_3$, 300.22 Hz, δ ppm)

0.26 (s, C*H*$_3$, 18H), 3.59 (s, C*H*$_3$, 3H), 6.34 (s, C*H*, 2H), 7.39 (d, ^3J = 8.5 Hz, C*H*, 4H), 7.51 (d, ^3J = 8.5 Hz, C*H*, 4H)

^{13}C{^{1}H} NMR – PENDANT ($CDCl_3$, 75.5 MHz, δ ppm)

0.33	*C*H$_3$	(Si*C*H$_3$)	121.41	C_{ipso}	(*pyrrole*)
35.07	*C*H$_3$	(N*C*H$_3$)	128.15	*C*H	(*ortho* to pyrrole)
95.36	C_q	(Si*C*≡C)	132.11	*C*H	(*meta* to pyrrole)
105.32	C_q	(C≡*C*Ph)	133.27	C_{ipso}	(*para* to pyrrole)
109.61	*C*H	(*pyrrole*)	137.08	C_{ipso}	(*para* to alkyne)

6.4.14 Synthesis of 2,5-*di*-(4-ethynyl-phenyl)-1-phenyl-pyrrole (72)

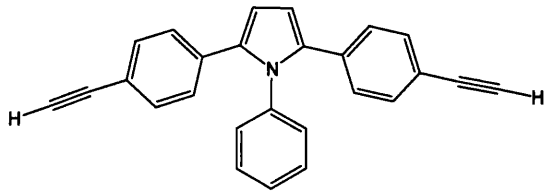

Potassium hydroxide (2.00 M solution, 0.45 mL) was added to the stirring solution of 2,5-*bis*-(4-trimethylsilylethynyl-phenyl)-1-phenyl-pyrrole (200 mg, 0.41 mmol) in dichloromethane/methanol (1:1 v/v, 10 mL), and the reaction was left to stir, under protection from light, for 4 hr. The solvent was removed under reduced pressure and the product extracted into dichloromethane and washed with water (2 x 50 mL). The organic phase was separated and dried ($MgSO_4$), and evaporated to dryness under reduced pressure affording **(72)** as an off white solid (98 mg, 70%).

^{1}H NMR ($CDCl_3$, 400.13 Hz, δ ppm)

3.10 (s, C*H*, 2H), 6.50 (s, C*H*, 2H), 6.93-7.01 (m, C*H*, 6H), 7.24–7.27 (m, C*H*, 7H)

^{13}C{^{1}H} NMR – PENDANT ($CDCl_3$, 75.5 MHz, δ ppm)

84.62	*C*H	(C≡*C*H)	128.76	*C*H	(C_6H_5)
104.00	C_{ipso}	(Ph*C*≡C)	129.00	*C*H	(C_6H_4)
110.34	*C*H	(*pyrrole*)	131.55	*C*H	(C_6H_4)
120.71	C_{ipso}	(*pyrrole*)	133.10	C_{ipso}	(C_6H_4)
127.57	*C*H	(C_6H_5)	135.58	C_{ipso}	(C_6H_5)
128.18	*C*H	(C_6H_5)			

IR (KBr disc, ν cm^{-1}): 3055 (C-H), 2112 (C≡C), 1943 (C≡C-H)

6.4.15 Synthesis of 2,5-*di*-(4-(*trans*-(phenyl,*bis*-triethylphosphine)platinum ethynyl))phenyl)-1-phenyl-1H-pyrrole (73)

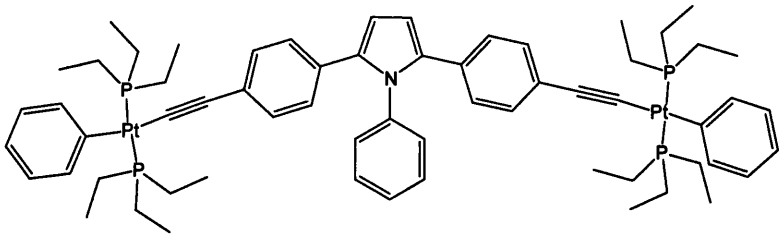

6.4.7 Synthesis of 2,5-*di*-(4-ethynyl-phenyl)-1-methyl-pyrrole (64)

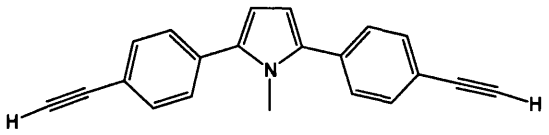

Potassium hydroxide (2.0 M aqueous solution, 0.26 mL) was added to a stirring solution of 2,5-*bis*-(4-trimethylsilylethynyl-phenyl)-1-methyl-pyrrole (90 mg, 0.21 mmol) in dichloromethane/methanol (1:1 mixture, 30 mL) and the reaction stirred for 5 hr. TLC (silica, hexane/dichloromethane, 4:1 v/v) confirmed the completion of the reaction and the volatiles were removed under reduced pressure. The resultant solid was dissolved in dichloromethane (30 mL) and washed with water (2 x 30 mL). The organic phase was separated and dried ($MgSO_4$). The volatiles were removed under reduced pressure affording **(64)** as an off white solid (52 mg, 91%).

^{1}H NMR ($CDCl_3$, 300.22 Hz, δ ppm)

3.13 (s, C*H*, 2H), 3.62 (s, CH_3, 3H), 6.36 (s, C*H*, 2H), 7.43 (d, ^3J = 8.5 Hz, CH, 4H), 7.55 (d, ^3J = 8.5 Hz, CH, 4H)

^{13}C{^{1}H} NMR – PENDANT ($CDCl_3$, 75.5 MHz, δ ppm)

34.63	CH_3	(NCH_3)	128.41	*C*H	(*ortho* to pyrrole)
78.20	C_{ipso}	(HC≡*C*)	132.27	*C*H	(*meta* to pyrrole)
83.52	C_{ipso}	(*C*≡CPh)	133.60	C_{ipso}	(*para* to pyrrole)
109.67	*C*H	(*pyrrole*)	136.93	C_{ipso}	(*para* to alkyne)
120.41	C_{ipso}	(*pyrrole*)			

IR (KBr disc, ν cm^{-1}): 3061 (C-H), 2106 (C≡C), 1943 (C≡C-H)

6.4.7 Synthesis of 2,5-*di*-(4-(*trans*-(phenyl,*bis*-triethylphosphine)platinum ethynyl))phenyl)-1-methyl-pyrrole (65)

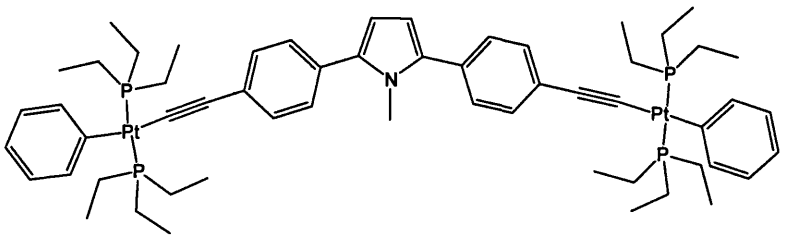

Trans- *bis*(triethylphosphine)(phenyl)platinum(II) chloride (234 mg, 0.43 mmol), 2,5-*di*-(4-ethynyl-phenyl)-1-methyl-pyrrole (60 mg, 0.22 mmol), and copper iodide (5 mg) were placed in a Schlenk tube, dichloromethane (15 mL) and di-isopropylamine (10 mL) were added and the solution stirred in the absence of light. The progress of the reaction was monitored by TLC (silica, hexane/dichloromethane, 1:1 v/v). After 18 hr the reaction was complete and the volatiles were removed under reduced pressure. The residue was passed through a silica plug (hexane: ethyl acetate, 2:1 v/v), the solvent was removed and the crude product was recrystallised from ethanol affording **(65)** as yellow crystals (230 mg, 83%).

^{1}H NMR ($CDCl_3$, 300.22 Hz, δ ppm)

1.07-1.15 (m, CH_3, 36H), 1.74 (m, CH_2, 24H), 3.60 (s, CH_3, 3H), 6.28 (s, C*H*, 2H), 6.81 (t, ^3J = 7.4 Hz, C*H*, 2H), 6.97 (t, ^3J = 7.4 Hz, C*H*, 4H), 7.30-7.35 (m, CH, 12H)

^{13}C{^{1}H} NMR – PENDANT ($CDCl_3$, 75.5 MHz, δ ppm)

8.02	CH_3	(PCH_2CH_3)	127.83	C_{ipso}	(*pyrrole*)
15.11	CH_2	(PCH_2CH_3)	128.16	*C*H	(C_6H_4)
31.87	CH_3	(NCH_3)	129.67	C_{ipso}	(C_6H_4)
110.00	C_q	(Pt*C*≡C)	130.81	*C*H	(C_6H_5)
114.40	C_q	(C≡*C*Ph)	137.13	C_{ipso}	(C_6H_4)
121.20	*C*H	(C_6H_5)	139.81	*C*H	(C_6H_5)
127.28	*C*H	(C_6H_4)	156.32	C_{ipso}	(C_6H_5)

^{31}P{^{1}H} NMR ($CDCl_3$, 121.5 MHz, δ ppm)

10.08 ($^1J_{PtP}$ = 2639 Hz)

IR (KBr disc, ν cm^{-1}): 2975, 2951, 2872 (C-H), 2089 (C≡C)

Elemental Analysis: Result % (calculated %): C = 53.4 (52.8), H = 6.39 (6.45), N = 0.91 (1.08)

UV/Vis: λ_{max} = 381 nm, ε = 65,500 $dm^3mol^{-1}cm^{-1}$

Emission: λ_{max} = 420 nm

6.4.8 Synthesis of 2,5-*di*-(4-bromo-phenyl)-1-n-butyl-pyrrole (66)

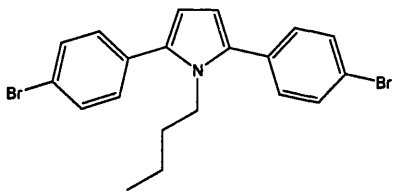

n-Butylamine (5 mL) was added to the stirring solution of 1,4-*di*-(4-bromo-phenyl)-butane-1,4-dione (250 mg, 0.63 mmol) in ethanol (50 mL). The reaction was refluxed for 14 hr after which time the solution had turned bright yellow. TLC (silica, dichloromethane) revealed completion of the reaction, and the solvent was evaporated to low volume precipitating the crude product. The solid was filtered and washed with ethanol affording **(66)** as a white solid (235 mg, 86%).

^{1}H NMR ($CDCl_3$, 400.13 Hz, δ ppm)

0.58 (t, ^3J = 14.7 Hz, C*H*$_3$, 3H), 0.80 – 0.89 (m, C*H*$_2$, 2H), 1.12 – 1.20 (m, C*H*$_2$, 2H), 4.01 (t, ^3J = 14.7 Hz, C*H*$_2$, 2H), 6.24 (s, C*H*, 2H), 7.31 (d, ^3J = 8.4 Hz, C*H*, 4H), 7.55 (d, ^3J = 8.4 Hz, C*H*, 4H)

^{13}C{^{1}H} NMR – PENDANT ($CDCl_3$, 75.5 MHz, δ ppm)

13.36	*C*H$_3$	(*C*H$_3$ pyrrole)	121.08	*C*$_{ipso}$	(*pyrrole*)
19.31	*C*H$_2$	(α-*C*H$_2$ pyrrole)	130.36	*C*H	(*ortho* to pyrrole)
32.73	*C*H$_2$	(β-*C*H$_2$ pyrrole)	131.66	*C*H	(*meta* to pyrrole)
45.10	*C*H$_2$	(γ-*C*H$_2$ pyrrole)	132.91	*C*$_{ipso}$	(*para* to bromine)
109.98	*C*H	(*pyrrole*)	135.72	*C*$_{ipso}$	(*C*Br)

EI/Mass Spectrum: ($C_{20}H_{19}Br_2N$) *m/z* 433.2, calc. 433.2

6.4.9 Synthesis of 2,5-*bis*-(4-trimethylsilylethynyl-phenyl)-1-n-butyl-pyrrole (67)

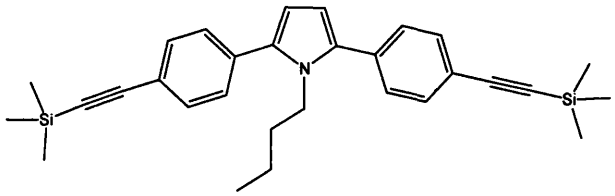

2,5-*di*-(4-bromo-phenyl)-1-n-butyl-pyrrole (200 mg, 0.46 mmol), copper (I) iodide (15 mg, 0.05 mmol), and *bis*(triphenylphosphine)palladium(II)chloride (45 mg, 0.10 mmol) were placed in to a Schlenk tube. Dichloromethane (20 mL), diisopropylamine (10 mL) and trimethylsilylacetylene (0.20 mL, 1.38 mmol) were added successively and the reaction was left to stir, under the protection from light, for 18 hr. The volatiles were removed under reduced pressure and the resultant solid was passed through a short alumina plug using ethyl acetate/hexane (1:1 v/v) as the eluent. The solvent was then removed and solid was further purified by chromatography (silica, hexane/dichloromethane, 3:1 v/v) affording **(67)** as an off white solid (168 mg, 78%).

^{1}H NMR ($CDCl_3$, 400.13 Hz, δ ppm)

0.27 (s, C*H*$_3$, 18H), 0.54 (t, ^3J = 14.7 Hz, C*H*$_3$, 3H), 0.75 – 0.85 (m, C*H*$_2$, 2H), 1.08 – 1.16 (m, C*H*$_2$, 2H), 4.05 (t, ^3J = 14.5 Hz, C*H*$_2$, 2H), 6.27 (s, C*H*, 2H), 7.38 (d, ^3J = 8.2 Hz, C*H*, 4H), 7.51 (d, ^3J = 8.2 Hz, C*H*, 4H)

^{13}C{^{1}H} NMR – PENDANT ($CDCl_3$, 75.5 MHz, δ ppm)

0.33	*C*H$_3$	(Si*C*H$_3$)	110.68	*C*H	(*pyrrole*)
13.70	*C*H$_3$	(*C*H$_3$ pyrrole)	121.78	*C*$_{ipso}$	(pyrrole)
19.63	*C*H$_2$	(α-*C*H$_2$ pyrrole)	128.73	*C*H	(*ortho* to pyrrole)
32.98	*C*H$_2$	(β-*C*H$_2$ pyrrole)	132.48	*C*H	(*meta* to pyrrole)
45.69	*C*H$_2$	(γ-*C*H$_2$ pyrrole)	134.42	*C*$_{ipso}$	(*para* to pyrrole)
95.21	*C*$_q$	(Si*C*≡C)	137.05	*C*$_{ipso}$	(*para* to alkyne)
105.36	*C*$_q$	(C≡*C*Ph)			

6.4.10 Synthesis of 2,5-*bis*-(4-trimethylsilylethynyl-phenyl)-1-n-butyl-pyrrole (68)

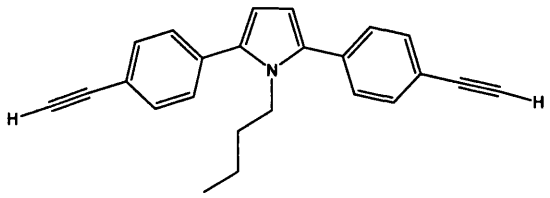

Potassium hydroxide (2.0 M solution, 0.11 mL) was added to a stirring solution of 2,5-*bis*-(4-trimethylsilylethynyl-phenyl)-1-n-butyl-pyrrole (100 mg, 0.21 mmol) in dichloromethane/methanol (1:1 v/v, 10 mL), and the reaction stirred, with protection from light, for 4 hr. The volatiles were removed under reduced pressure and the solid extracted from water into dichloromethane (2 x 50 mL). The organic phase was dried with ($MgSO_4$) and evaporated to dryness under reduced pressure affording **(68)** as an off white solid (61 mg, 90%).

^{1}H NMR ($CDCl_3$, 400.13 Hz, δ ppm)

0.54 (t, ^3J = 14.7 Hz, CH_3, 3H), 0.74 – 0.84 (m, CH_2, 2H), 1.08 – 1.16 (m, CH_2, 2H), 3.14 (s, C*H*, 2H), 4.05 (t, ^3J = 14.5 Hz, CH_2, 2H), 6.37 (s, C*H*, 2H), 7.37 (d, ^3J = 8.2 Hz, C*H*, 4H), 7.51 (d, ^3J = 8.2 Hz, C*H*, 4H)

^{13}C{^{1}H} NMR – PENDANT ($CDCl_3$, 75.5 MHz, δ ppm)

13.16	*C*H$_3$	(*C*H$_3$ pyrrole)	122.28	C_{ipso}	(pyrrole)
19.33	*C*H$_2$	(α-*C*H$_2$ pyrrole)	123.44	*C*H	(*ortho* to pyrrole)
32.63	*C*H$_2$	(β-*C*H$_2$ pyrrole)	131.33	*C*H	(*meta* to pyrrole)
45.16	*C*H$_2$	(γ-*C*H$_2$ pyrrole)	134.63	C_{ipso}	(*para* to pyrrole)
85.44	C_q	(H*C*≡C)	135.65	C_{ipso}	(*para* to alkyne)
109.21	C_q	(C≡*C*Ph)			
111.68	*C*H	(*pyrrole*)			

IR (KBr disc, ν cm^{-1}): 3058 (C-H), 2110 (C≡C), 1944 (C≡C-H)

6.4.11 Synthesis of 2,5-*bis*-(4-(*trans*-(phenyl,*bis*-triethylphosphine)platinum ethynyl))phenyl)-1-butyl-1H-pyrrole (69)

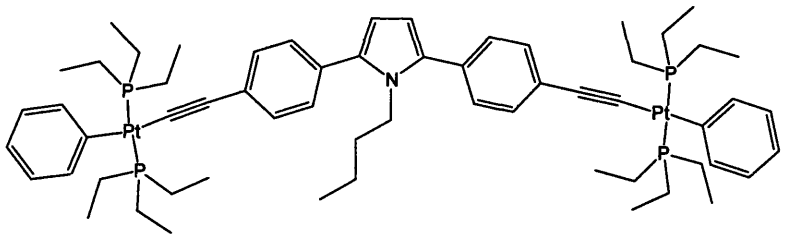

Trans- *bis*(triethylphosphine)(phenyl)platinum(II) chloride (200 mg, 0.40 mmol), 2,5-*di*-(4-ethynyl-phenyl)-1-butyl-pyrrole (65 mg, 0.20 mmol), and copper iodide (5 mg) were placed in a Schlenk tube, dichloromethane (25 mL) and diisopropylamine (10 mL) were added and the solution was left to stir under protection from light. The progress of the reaction was monitored by TLC (silica, hexane: dichloromethane, 2:1 v/v). After 16 hr the reaction was complete and the volatiles were removed under reduced pressure. The residue was passed through a silica plug (hexane: ethyl acetate, 2:1 v/v), the solvent was removed and the crude product was recrystallised from ethanol affording **(69)** as yellow crystals (230 mg, 83%).

^{1}H NMR ($CDCl_3$, 300.22 Hz, δ ppm)

0.54 (t, ^3J = 14.7 Hz, CH_3, 3H), 0.75 – 0.85 (m, CH_2, 2H), 1.07 – 1.16 (m, CH_2 & CH_3, 38H), 1.74 – 1.81 (m, CH_2, 24H), 6.28 (s, C*H*, 2H), 6.80 (t, ^3J = 7.1 Hz, C*H*, 2H), 6.96 (t, ^3J = 7.4 Hz, C*H*, 4H), 7.30-7.35 (m, CH, 12H)

^{13}C{^{1}H} NMR – PENDANT ($CDCl_3$, 75.5 MHz, δ ppm)

8.05	CH_3	(PCH_2CH_3)	127.28	*C*H	(C_6H_4)
13.22	CH_3	(CH_3 pyrrole)	128.23	C_{ipso}	(*pyrrole*)
15.11	CH_2	(($P(CH_2CH_3)_3$), t_{ps},	128.77	*C*H	(C_6H_4)
		$^1J_{PC}+^3J_{PC}$ = 33 Hz)	129.22	C_{ipso}	(C_6H_4)
20.53	CH_2	(α-CH_2 pyrrole)	129.71	*C*H	(C_6H_5)
32.61	CH_2	(β-CH_2 pyrrole)	138.13	C_{ipso}	(C_6H_4)
43.36	CH_2	(γ-CH_2 pyrrole)	139.81	*C*H	(C_6H_5)
111.67	C_q	(PtC≡C)	156.32	C_{ipso}	(C_6H_5)
115.50	C_q	(C≡CPh)			
121.21	*C*H	(C_6H_5)			

$^{31}P\{^{1}H\}$ NMR ($CDCl_3$, 121.5 MHz, δ ppm)

10.09 ($^{1}J_{PtP}$ = 2639 Hz)

IR (KBr disc, ν cm^{-1}): 2966, 2957, 2877 (C-H), 2091 (C≡C)

Elemental Analysis: Result % (calculated %): C = 52.4 (53.8), H = 6.49 (6.70), N = 0.93 (1.05)

UV/Vis: λ_{max} = 382 nm, ε = 68,900 $dm^3mol^{-1}cm^{-1}$

Emission: λ_{max} = 421 nm

6.4.12 Synthesis of 2,5-*di*-(4-bromo-phenyl)-1-phenyl-pyrrole (70)

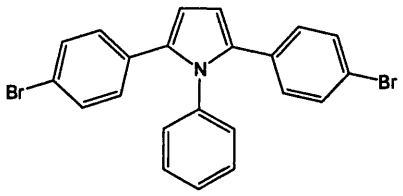

1,4-*di*-(4-bromo-phenyl)-butane-1,4-dione (792 mg, 2.00 mmol) and aniline (930 mg, 10 mmol) were placed into a Young's Ampoule, acetic acid (30 mL) was added and the solution was left to stir at 110 °C for 3 hr after which time a white precipitate was formed. The solid was filtered and washed with acetic acid (2 x 20 mL), then ethanol (2 x 20 mL) and dried under reduced pressure to afford **(70)** as a white solid (720 mg, 80%).

^{1}H NMR ($CDCl_3$, 400.13 Hz, δ ppm)

6.47 (s, C*H*, 2H), 6.90 (d, ^{3}J = 8.4 Hz, C*H*, 4H), 7.00 – 7.02 (m, C*H*, 2H), 7.28 – 7.30 (m, C*H*, 7H)

$^{13}C\{^{1}H\}$ NMR – PENDANT ($CDCl_3$, 75.5 MHz, δ ppm)

110.70	*C*H	(*pyrrole*)	130.42	*C*H	(*ortho* to pyrrole)
120.86	C_{ipso}	(*pyrrole*)	131.46	*C*H	(*meta* to pyrrole)
128.08	*C*H	(*C*H, C_6H_5 1-pyr)	132.30	C_{ipso}	(*C*Br)
129.13	*C*H	(*C*H, C_6H_5 1-pyr)	135.31	C_{ipso}	(*para* to bromine)
129.47	*C*H	(*C*H, C_6H_5 1-pyr)	138.77	C_{ipso}	(C_6H_5 1-pyr)

EI/Mass Spectrum: ($C_{22}H_{15}Br_2N$) *m/z* 453.0, calc. 453.0

Elemental Analysis: Result % (calculated %): C = 57.5 (58.3), H = 3.37 (3.34), N = 3.11 (3.09)

6.4.13 Synthesis of 2,5-bis-(4-trimethylsilylethynyl-phenyl)-1-phenyl-pyrrole (71)

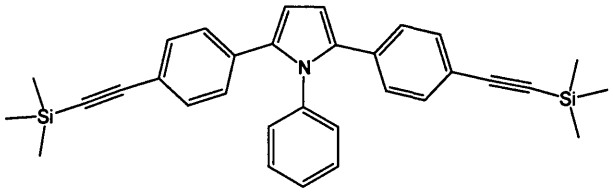

2,5-di-(4-bromo-phenyl)-1-phenyl-pyrrole (600 mg, 1.32 mmol), copper (I) iodide (38.0 mg, 0.20 mmol), and *bis*(triphenylphosphine)palladium(II)chloride (279 mg, 0.40 mmol) were placed in a Schlenk tube. Dichloromethane (30 mL), diethylamine (10 mL) and trimethylsilylacetylene (0.58 mL, 3.97 mmol) were added successively and the reaction was stirred, in the absence of light, for 46 hr after which TLC revealed completion of reaction (silica, hexane/dichloromethane, 9:1 v/v). The volatiles were removed under reduced pressure and the crude product was passed through an alumina plug in hexane/ethyl acetate (1:1 v/v). The solvent was then removed and solid was further purified by washing with cold hexane (2 x 20 mL) and recrystallisation from ethanol to afford **(71)** as an off white solid (505 mg, 78%).

^{1}H NMR ($CDCl_3$, 400.13 Hz, δ ppm)

0.22 (s, C*H*$_3$, 18H), 6.50 (s, C*H*, 2H), 6.93-7.01 (m, C*H*, 6H), 7.24–7.27 (m, C*H*, 7H)

^{13}C{^{1}H} NMR – PENDANT ($CDCl_3$, 75.5 MHz, δ ppm)

-0.05	CH_3	($SiCH_3$)	128.18	CH	(C_6H_5)
94.62	C_{ipso}	(C≡*C*Si)	128.76	CH	(C_6H_5)
105.05	C_{ipso}	(Ph*C*≡C)	129.00	CH	(C_6H_4)
110.65	CH	(*pyrrole*)	131.55	CH	(C_6H_4)
120.71	C_{ipso}	(*pyrrole*)	133.10	C_{ipso}	(C_6H_4)
127.57	CH	(C_6H_5)	135.58	C_{ipso}	(C_6H_5)

IR (KBr disc, ν cm^{-1})

3049, 2958, 2889 (C-H), 2153 (C≡C), 1251 (Si-C)

Trans- bis(triethylphosphine)(phenyl)platinum(II) chloride (117 mg, 0.22 mmol), 2,5-*di*-(4-ethynyl-phenyl)-1-phenyl-pyrrole (37.8 mg, 0.11 mmol) and copper iodide (5 mg) were placed in a Schlenk tube, dichloromethane (25 mL) and triethylamine (25 mL) were added and the solution was left to stir under protection from light. The progress of the reaction was monitored by TLC (silica, hexane/dichloromethane, 1:1 v/v). After 12 hr the reaction was complete and the volatiles were removed under reduced pressure. The residue was passed through a silica plug (hexane: ethyl acetate, 1:1 v/v), the volatiles were removed under reduced pressure and the crude product was recrystallised from ethanol affording **(73)** as yellow crystals (94 mg, 63%).

^{1}H NMR ($CDCl_3$, 400.13 Hz, δ ppm)

1.07-1.14 (m, C*H*$_3$, 36H), 1.74-1.81 (m, C*H*$_2$, 24H), 6.48 (s, C*H*, 2H), 6.80 (t, ^{3}J = 7.4 Hz, C*H*, 2H), 6.98 (t, ^{3}J = 7.4 Hz, C*H*, 4H), 7.30-7.35 (m, CH, 12H)

^{13}C{^{1}H} NMR – PENDANT ($CDCl_3$, 75.5 MHz, δ ppm)

8.09	CH_3	(PCH_2CH_3)	127.57	CH	(C_6H_5)
15.15	CH_2	(($P(CH_2CH_3)_3$), t_{ps},	128.18	CH	(C_6H_5)
		$^{1}J_{PC}+^{3}J_{PC}$ = 34 Hz)	128.69	CH	(C_6H_4)
108.88	CH	(*pyrrole*)	128.76	CH	(C_6H_5)
110.25	C_q	($PtC{\equiv}C$)	131.35	C_{ipso}	(C_6H_4)
115.58	C_q	($C{\equiv}CPh$)	133.19	C_{ipso}	(C_6H_4)
121.62	CH	(*para* C_6H_5Pt)	139.18	CH	(C_6H_5)
122.28	C_{ipso}	(*pyrrole*)	156.34	C_{ipso}	(C_6H_5)
127.29	CH	(C_6H_4)			

^{31}P{^{1}H} NMR ($CDCl_3$, 121.5 MHz, δ ppm)

10.04 ($^{1}J_{PtP}$ = 2633 Hz)

IR (KBr disc, ν cm^{-1}): 2967, 2955, 2869 (C-H), 2096 (C≡C)

Elemental Analysis: Result % (calculated %): C = 55.5 (54.8), H = 6.37 (6.31), N = 0.94 (1.03)

UV/Vis: λ_{max} = 342 nm, ε = 41,200 $dm^3mol^{-1}cm^{-1}$

Emission: λ_{max} = 411 nm

6.4.16 Synthesis of 2,5-*di*-(4-bromo-phenyl)-1-methoxyphenyl-pyrrole (74)

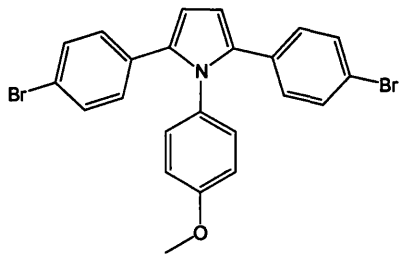

1,4-*bis*-(4-bromo-phenyl)-butane-1,4-dione (792 mg, 2.00 mmol) and *para*-anistidine (246 mg, 4.00 mmol) was placed into a Young's Ampoule, acetic acid (100 mL) was added and the solution was left to stir at 110 °C for 18 hr after which time a white precipitate was formed. The solid was filtered off and washed with acetic acid (2 x 20 mL), ethanol (2 x 20 mL) and dried under reduced pressure affording **(74)** as an off white solid (669 mg, 69%).

^{1}H NMR ($CDCl_3$, 400.13 Hz, δ ppm)

3.81 (s, C*H*$_3$, 3H), 6.45 (s, C*H*, 2H), 6.79 (d, ^3J = 8.6 Hz, 4H), 6.92 (m, C*H*, 8H), 7.30 (d, ^3J = 8.6 Hz, C*H*, 4H)

^{13}C{^{1}H} NMR – PENDANT ($CDCl_3$, 75.5 MHz, δ ppm)

75.86	*C*H$_3$	O*Me*	79.78	*C*H	(*pyrrole*)
78.74	*C*H	*C*$_6$H$_4$OMe	79.79	*C*H	(*C*$_6$H$_4$Br)
78.96	*C*H	*C*$_6$H$_4$OMe	79.85	*C*H	(*C*$_6$H$_4$Br)

EI/Mass Spectrum: ($C_{23}H_{17}Br_2NO$) *m/z* 483.0, calc. 483.0

Elemental Analysis: Result % (calculated %): C = 56.8 (57.2), H = 3.58 (3.55), N = 2.78 (2.90)

6.4.17 Synthesis of 2,5-*bis*-(4-trimethylsilylethynyl-phenyl)-1-methoxyphenyl-pyrrole (75)

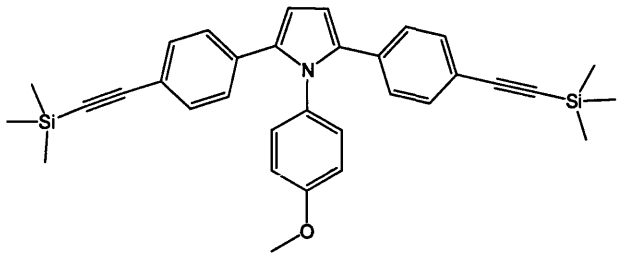

2,5-*di*-(4-bromo-phenyl)-1-methoxyphenyl-pyrrole (210 mg, 0.44 mmol), copper (I) iodide (23.0 mg, 0.15 mmol), and *bis*(triphenylphosphine)palladium(II) chloride (150 mg, 0.30 mmol) were placed in a Schlenk tube. Dichloromethane (30 mL), diethylamine (10 mL) and trimethylsilylacetylene (0.30 mL, 2.00 mmol) were successively added and the reaction was left to stir for 18 hr. The volatiles were removed under reduced pressure and the crude product was passed through an alumina plug in hexane/ethyl acetate (1:1 v/v). The solvent was then removed and the solid was further purified by column chromatography (silica, hexane/dichloromethane, 3:1 v/v) and recrystallisation from ethanol to afford **(75)** as an off white solid (172 mg, 79 %).

^{1}H NMR ($CDCl_3$, 400.13 Hz, δ ppm)

0.22 (s, C*H*$_3$, 18H), 3.80 (s, C*H*$_3$, 3H), 6.49 (s, C*H*, 2H), 6.76 (d, ^3J = 8.9 Hz, C*H*, 2H), 6.91 (d, ^3J = 8.9 Hz, C*H*, 2H), 6.98 (d, ^3J = 8.3 Hz, C*H*, 4H), 7.27 (d, ^3J = 8.3 Hz, C*H*, 4H)

^{13}C{^{1}H} NMR – PENDANT ($CDCl_3$, 75.5 MHz, δ ppm)

-0.04	*C*H$_3$	(Si*C*H$_3$)	129.68	*C*H	(*C*$_6$H$_4$)
55.35	*C*H$_3$	(O*C*H$_3$)	131.44	*C*$_{ipso}$	(*C*$_6$H$_4$)
94.59	*C*$_q$	(C≡*C*Si)	131.57	*C*H	(*C*$_6$H$_4$)
105.11	*C*$_q$	(PhC≡*C*)	133.20	*C*$_{ipso}$	(*C*$_6$H$_4$)
110.36	*C*H	(*pyrrole*)	135.70	*C*$_{ipso}$	*C*$_6$H$_4$OMe
114.15	*C*H	*C*$_6$H$_4$OMe	158.75	*C*$_{ipso}$	(*C*OCH$_3$)
120.60	*C*$_{ipso}$	(*pyrrole*)			
128.15	*C*H	*C*$_6$H$_4$OMe			

IR (KBr disc, ν cm^{-1}): 3049, 2945, 2889 (C-H), 2155 (C≡C), 1251 (Si-C)

6.4.18 Synthesis of 2,5-*di*-(4-(*trans*-(phenyl,*bis*-triethylphosphine)platinum ethynyl))phenyl-1-(4-methoxy-phenyl)-1H-pyrrole (77)

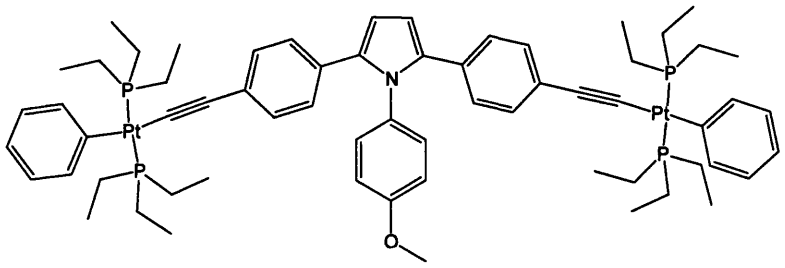

2,5-*bis*-(4-trimethylsilylethynyl-phenyl)-1-methoxyphenyl-pyrrole (93 mg, 0.18 mmol) and sodium methoxide (30 mg) were placed into a Young's Ampoule and dissolved in dichloromethane/methanol (1:1 v/v, 90 mL). The solution was stirred, in the absence of light, for 30 min. *Trans-bis*(triethylphosphine)(phenyl)platinum(II) chloride (180 mg, 0.36 mmol), copper iodide (5 mg) and diisopropylamine (10 mL) were added to the stirring solution. The reaction was left to stir for 18 hr after which time TLC revealed consumption of ligand and platinum starting materials. The solvent was removed under reduced pressure and the solid was dissolved in ethyl acetate. The solution was passed through a plug of alumina and the solvent was evaporated to dryness. The resulting solid was recrystallised from ethanol/chloroform (5:1 v/v) yielding **(77)** as a yellow solid (132 mg, 53%).

^{1}H NMR ($CDCl_3$, 400.13 Hz, δ ppm)

1.04-1.12 (m, C*H*$_3$, 36H), 1.71-1.78 (m, C*H*$_2$, 24H), 3.82 (s, C*H*$_3$, 3H), 6.41 (s, C*H*, 2H), 6.78 (d, ^3J = 9.0 Hz, C*H*, 4H), 6.93-7.00 (m, C*H*, 8H), 7.11 (d, ^3J = 8.4 Hz, C*H*, 4H), 7.31 (d, ^3J = 7.4 Hz, C*H*, 4H)

^{13}C{^{1}H} NMR – PENDANT ($CDCl_3$, 75.5 MHz, δ ppm)

8.11	*C*H$_3$	(PCH$_2$*C*H$_3$)	126.29	*C*H	(*C*$_6$H$_4$)
15.13	*C*H$_2$	((P(*C*H$_2$CH$_3$)$_3$), t_{ps},	128.57	*C*H	(*C*$_6$H$_5$)
		$^1J_{PC}+^3J_{PC}$ = 34 Hz)	129.18	*C*H	(*C*$_6$H$_5$)
54.55	*C*H$_3$	(O*C*H$_3$)	130.66	*C*H	(*C*$_6$H$_4$)
107.58	*C*H	(*pyrrole*)	130.96	*C*H	(*C*$_6$H$_5$)
110.15	C_q	(PtC≡C)	131.35	C_{ipso}	(*C*$_6$H$_4$)
115.58	C_q	(C≡*C*Ph)	132.29	C_{ipso}	(*C*$_6$H$_4$)
122.12	*C*H	(*para* C$_6$H$_5$Pt)	139.48	*C*H	(*C*$_6$H$_5$)
123.38	C_{ipso}	(*pyrrole*)	156.36	C_{ipso}	(*C*$_6$H$_5$)

$^{31}P\{^{1}H\}$ NMR ($CDCl_3$, 121.5 MHz, δ ppm)

10.10 ($^{1}J_{PtP}$ = 2644 Hz)

IR (KBr disc, ν cm^{-1}): 2975, 2951, 2872 (C-H), 2093 (C≡C)

Elemental Analysis: Result % (calculated %): C = 55.7 (54.5), H = 6.27 (6.32), N = 0.92 (1.01)

UV/Vis: λ_{max} = 345 nm, ε = 46,100 $dm^3mol^{-1}cm^{-1}$

Emission: λ_{max} = 411 nm

6.4.19 Synthesis of 2,5-*di*-(4-bromo-phenyl)-1-phenol-pyrrole (78)

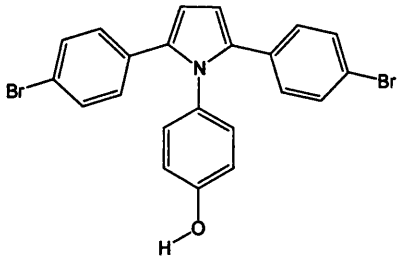

1,4-*di*-(4-bromo-phenyl)-butane-1,4-dione (792 mg, 2.00 mmol) and 4-aminophenol (436 mg, 4.00 mmol) were placed into a Young's ampoule, acetic acid (100 mL) was added and the solution was left to stir at 110 °C for 36 hr after which time a white precipitate was formed. The solid was filtered off and washed with acetic acid (2 x 20 mL), ethanol (2 x 20 mL) and dried under reduced pressure affording **(78)** as an off white solid (600 mg, 64%).

^{1}H NMR ($CDCl_3$, 400.13 Hz, δ ppm)

4.81 (s, O*H*, 1H), 6.35 (s, C*H*, 2H), 6.92 (d, ^{3}J = 7.6 Hz, C*H*, 4H), 7.30 (d, ^{3}J = 7.6 Hz, C*H*, 4H), 7.42-7.57 (m, C*H*, 4H)

EI/Mass Spectrum: ($C_{22}H_{15}Br_2NO$) *m/z* 469.0, calc. 469.0

6.4.20 Synthesis of 2,5-*di*-(4-bromo-phenyl)-1-pyren-1-yl-1H-pyrrole (79)

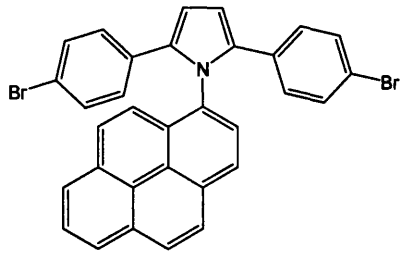

1,4-*di*-(4-bromo-phenyl)-butane-1,4-dione (396 mg, 1.00 mmol) and 1-aminopyrene (434 mg, 2.00 mmol) were placed into a Young's ampoule, acetic acid (100 mL) was added and the solution was left to stir at 110 °C for 46 hr after which time a precipitate was formed. The solid was filtered off and washed with acetic acid (2 x 20 mL), ethanol (2 x 20 mL) and dried in air affording **(79)** as a dark solid (306 mg, 53%).

^{1}H NMR ($CDCl_3$, 400.13 Hz, δ ppm)

6.45 (s, C*H*, 2H), 6.39 (d, ^3J = 7.8 Hz, C*H*, 4H), 7.29 (d, ^3J = 7.8 Hz, C*H*, 4H), 7.46-7.88 (m, C*H*, 9H)

6.4.21 Synthesis of 4-[2,5-*di*-(4-bromo-phenyl)-pyrrol-1-yl]-benzonitrile (80)

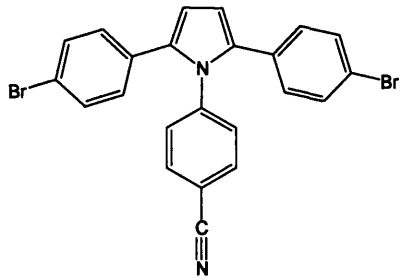

1,4-*di*-(4-bromo-phenyl)-butane-1,4-dione (396 mg, 1.00 mmol) and 4-aminobenzonitrile (354 mg, 3.00 mmol) were placed into a Young's ampoule, acetic acid (100 mL) was added and the solution was refluxed for 74 hr. The solvent was reduced to low volume (~10 mL) to precipitate the crude product. The solid was filtered off and washed with ethanol (2 x 20 mL) and dried under reduced pressure affording **(80)** as a white solid (239 mg, 50%).

^{1}H NMR ($CDCl_3$, 400.13 Hz, δ ppm)

6.55 (s, C*H*, 2H), 7.01 (d, ^3J = 7.6 Hz, C*H*, 4H), 7.30 (d, ^3J = 7.6 Hz, C*H*, 4H), 7.45-7.67 (m, C*H*, 4H)

EI/Mass Spectrum: ($C_{23}H_{14}Br_2N_2$) *m/z* 478.1, calc. 478.1

6.4.22 Synthesis of 4-[2,5-*di*-(4-bromo-phenyl)-pyrrol-1-yl]-phenylamine (81)

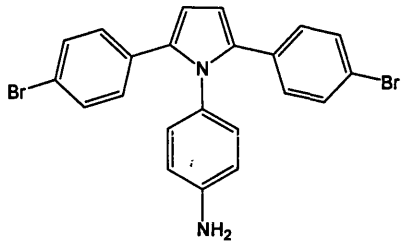

1,4-*bis*-(4-bromo-phenyl)-butane-1,4-dione (396 mg, 1.00 mmol) and benzene-1,4-diamine (108 mg, 1.00 mmol) were placed into a Young's ampoule, acetic acid (150 mL) was added and the solution was refluxed for 74 hr. The solvent was reduced to low volume (~10 mL) to precipitate the crude product. The solid was filtered off and washed with ethanol (2 x 20 mL) and dried under reduced pressure affording **(81)** (271 mg, 58%).

^{1}H NMR ($CDCl_3$, 400.13 Hz, δ ppm)

4.05 (s, N*H*$_2$, 1H), 6.39 (s, C*H*, 2H), 6.85 (d, ^3J = 7.6 Hz, C*H*, 4H), 7.30 (d, ^3J = 7.6 Hz, C*H*, 4H), 7.44-7.55 (m, C*H*, 4H)

6.5 Experimental details for Chapter Five

6.5.1 Synthesis of 1,2,4,5-tetrafluoro-3,6-(*bis*-*p*-trimethylsilylphenyl)benzene (82)

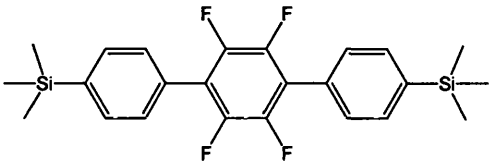

4-trimethylsilyl phenylboronic acid (1.00 g, 5.15 mmol), 1,4-diiodotetrafluorobenzene (690 mg, 1.72 mmol), and tetrakis(triphenylphosphine)palladium(0) (397 mg, 3.44 mmol) were placed into a round bottomed flask. Toluene (30 mL) and sodium carbonate (20 mL, 2.0 M aqueous solution) were added and the solution was refluxed under an inert atmosphere. The reaction was monitored by TLC (silica, hexane/dichloromethane, 9:1 v/v) and after 96 hr was complete. The organic phase was decanted, dried ($MgSO_4$) and the solvent removed under reduced pressure yielding a brown solid. The crude product was purified by chromatography (silica, hexane/dichloromethane, 9:1 v/v) yielding a white solid which was further purified by recrystallisation from ethanol to afford **(82)** as shiny white flakes (630 mg, 82%).

^{1}H NMR ($CDCl_3$, 400.13 MHz)

0.32 (s, C*H*$_3$, 18H), 7.50 (d, ^3J = 8.3 Hz, 4H), 7.67 (d, ^3J = 8.3 Hz, 4H)

^{13}C{^{1}H} NMR – PENDANT ($CDCl_3$, 100.61 MHz)

-1.19	CH_3	($SiCH_3$)	133.54	*C*H	(*ortho* to TMS)
127.85	C_{ipso}	(*para* to TMS)	141.98	C_{ipso}	($CSiCH_3$)
119.60	C_{ipso}	(*C*F, m, $^2J_{FC} + {}^3J_{FC}$)	144.17	C_{ipso}	(*C*F, dm, $^1J_{FC}$ = 246 Hz)
129.31	*C*H	(*meta* to TMS)			

^{19}F NMR ($CDCl_3$, 376.5 MHz)

-144.25 (C*F*)

Elemental Analysis: Result % (calculated %): C = 64.9 (64.5), H = 5.77 (5.87)

6.5.2 Synthesis of 1,2,4,5-tetrafluoro-3,6-(*di-p*-iodophenyl)benzene (83)

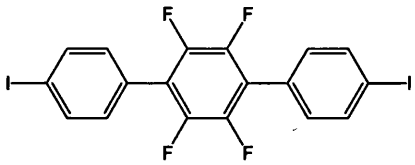

Iodine monochloride (1.0 M solution in dichloromethane, 2.20 mL) was added to a stirring solution of 1,2,4,5-tetrafluoro-3,6-(*bis-p*-trimethylsilylphenyl)benzene (446 mg, 1.00 mmol) in chloroform (20 mL). After 5 mins a white precipitate was formed. After 30 mins of stirring TLC (silica, hexane/dichloromethane, 9:1 v/v) revealed completion of the reaction and a saturated solution of sodium thiosulphate (~5 mL) was added. The solid was filtered off and washed with cold chloroform (2 x 10 mL) affording **(83)** as a white solid (440 mg, 80 %).

^{1}H NMR ($CDCl_3$, 400.13 MHz)

7.24 (d, ^3J = 8.2 Hz, 4H), 7.85 (d, ^3J = 8.2 Hz, 4H)

$^{13}C\{^1H\}$ NMR – PENDANT ($CDCl_3$, 100.61 MHz)

95.60	C_{ipso}	(*C*I)	137.92	*C*H	(*ortho* to iodide)
126.80	C_{ipso}	(*para* to iodine)	143.95	C_{ipso}	(*C*F, dm, $^1J_{FC}$ = 247 Hz)
131.77	*C*H	(*meta* to iodine)	Ipso carbon on central ring absent		

^{19}F NMR ($CDCl_3$, 376.5 MHz)

-143.70 (C*F*)

EI-mass spectrum: ($C_{18}H_8F_4I_2$) *m/z* 553.9; calc. 553.9

Elemental Analysis: Result % (calculated %): C = 38.3 (39.0), H = 1.49 (1.46)

6.5.3 Synthesis of 1,2,4,5-tetrafluoro-3,6-(*bis-p*-trimethylsilylethynylphenyl)-benzene (84)

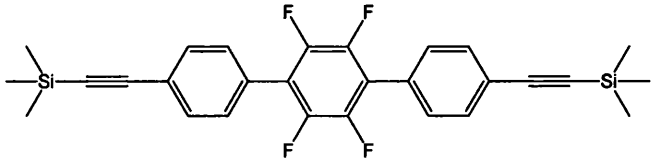

1,2,4,5-tetrafluoro-3,6-(*di-p*-iodophenyl)benzene (300 mg, 0.54 mmol), copper (I) iodide (10.0 mg, 0.05 mmol), and *bis*(triphenylphosphine) palladium(II)chloride (70.0 mg, 0.10 mmol) were placed to a Schlenk tube. Dichloromethane (30 mL),

diisopropylamine (15 mL) and trimethylsilylacetylene (0.16 mL, 1.62 mmol) were added successively and the reaction was left to stir, in the absence of light, for 4 hr. TLC (silica, hexane) revealed the completion of the reaction and the volatiles were removed under reduced pressure. The resulting solid was passed through a silica plug in hexane/dichloromethane (1:1 v/v) as the eluant. The volatiles were then removed to afford **(84)** as yellow solid (270 mg, 68%).

^{1}H NMR ($CDCl_3$, 400.13 MHz)

0.28 (s, CH_3, 18H), 7.26 (d, ^3J = 8.4 Hz, 4H), 7.59 (d, ^3J = 8.4 Hz, 4H)

$^{13}C\{^1H\}$ NMR – PENDANT ($CDCl_3$, 100.61 MHz)

-0.10	CH_3	($SiCH_3$)	130.02	CH	(C_6H_4 *meta* to alkyne)
96.05	C_q	($SiC{\equiv}C$)	132.10	CH	(C_6H_4 *ortho* to alkyne)
104.30	C_q	($C{\equiv}CPh$)	142.82	C_{ipso}	(CF, dm, $^1J_{FC}$ = 246 Hz)
124.17	C_{ipso}	(C_6H_4 *para* to alkyne)	145.25	C_{ipso}	(C_6F_4)
127.37	C_{ipso}	(C_6H_4)			

^{19}F NMR ($CDCl_3$, 376.5 MHz)

-145.12 (CF)

Elemental Analysis: Result % (calculated %): C = 67.2 (68.0), H = 5.33 (5.30)

6.5.4 Synthesis 1,2,4,5-tetrafluoro-3,6-(*di-p*-ethynylphenyl)benzene (85)

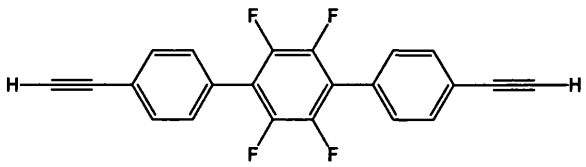

Potassium hydroxide (2.0 M aqueous solution, 1.20 mL) was added to a stirring solution of 1,2,4,5-tetrafluoro-3,6-(*bis-p*-trimethylsilylethynylphenyl)benzene (200 mg, 0.40 mmol) in dichloromethane/methanol (1:1 v/v, 50 mL). After 1 hr TLC (silica, hexane: dichloromethane, 4:1 v/v) revealed the completion of the reaction. The volatiles were removed under reduced pressure and the solid was redissolved in dichloromethane (50 mL) and washed with water (2 x 50 mL). The organic layer was separated and dried ($MgSO_4$). The volatiles were then removed to afford **(85)** as a white solid (120 mg, 85%).

^{1}H NMR ($CDCl_3$, 400.13 MHz)

3.17 (s, C*H*, 18H), 7.49 (d, ^3J = 8.2 Hz, C*H*, 4H), 7.63 (d, ^3J = 8.2 Hz, C*H*, 4H)

^{13}C{^{1}H} NMR – PENDANT ($CDCl_3$, 100.61 MHz)

78.66	CH	(*H*C≡C)	130.14	*C*H	(C_6H_4 *meta* to alkyne)
82.96	C_q	(C≡*C*Ph)	132.33	*C*H	(C_6H_4 *ortho* to alkyne)
123.20	C_{ipso}	(C_6H_4 *para* to alkyne)	142.76	C_{ipso}	(*C*F, dm, $^1J_{FC}$ = 247 Hz)
127.77	C_{ipso}	(*C*$_6$H$_4$)	145.25	C_{ipso}	(*C*$_6$F$_4$)

^{19}F NMR ($CDCl_3$, 376.5 MHz)

-145.02 (C*F*)

6.5.5 Synthesis of 4,4''-*bis*-(*trans*-(phenyl,*bis*-triethylphosphine)platinum) ethynyl-2',3',5',6'-tetrafluoro-terphenyl (86)

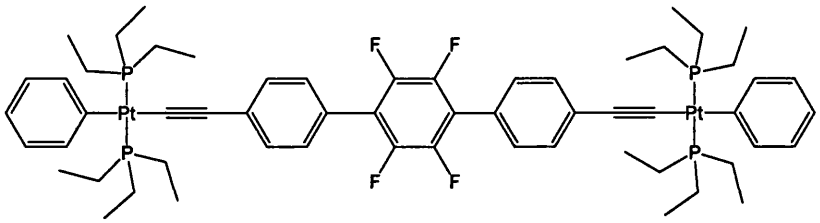

Trans- bis(triethylphosphine)(phenyl)platinum(II) chloride (200 mg, 0.64 mmol), 1,2,4,5-tetrafluoro-3,6-(*di-p*-ethynylphenyl)benzene (64 mg, 0.184 mmol), and copper iodide (5 mg) were dissolved in dichloromethane (30 mL) and diisopropylamine (20 mL). The reaction was left to stir under an argon atmosphere and was monitored by TLC (silica, hexane/dichloromethane 2:1 v/v). After 14 hr the solvent was removed under reduced pressure. The crude product was then passed through a silica plug (hexane/dichloromethane 1:1 v/v) and the volatiles were removed to give an off white solid. The solid was recrystallised from ethanol/chloroform (9:1 v/v) to afford **(86)** as colourless crystals (245 mg, 90%).

^{1}H NMR ($CDCl_3$, 400.13 MHz)

1.07-1.15 (m, CH_3, 36H), 1.74-81 (m, CH_2, 24H), 6.81 (t, ^3J = 7.2 Hz, C*H*, 2H), 6.97 (t, ^3J = 7.4 Hz, C*H*, 4H), 7.33-67 (m, C*H*, 12H)

$^{13}C\{^1H\}$ NMR – PENDANT ($CDCl_3$, 75.5 MHz, δ ppm)

8.03	CH_3	($P(CH_2CH_3)_3$)	129.75	CH	(C_6H_4)
15.13	CH_2	($P(CH_2CH_3)_3$), t_{ps}, $^1J_{PC}+^3J_{PC}$ = 34 Hz)	130.37	C_{ipso}	(C_6H_4)
			130.89	CH	(C_6H_4)
109.95	C_q	(PtC≡C)	139.14	CH	(C_6H_5)
116.62	C_q	(C≡CPh)	142.86	C_{ipso}	(CF, dm, $^1J_{FC}$ = 247 Hz)
121.29	CH	(*para* C_6H_5Pt)	145.16	C_{ipso}	(C_6F_4)
123.36	C_{ipso}	(C_6H_4)	156.18	C_{ipso}	(C_6H_5)
127.33	CH	(*ortho* to C_6F_4)			

^{19}F NMR ($CDCl_3$, 376.5 MHz)

-145.09 (C*F*)

$^{31}P\{^1H\}$ NMR ($CDCl_3$, 121.5 MHz, δ ppm)

10.03 ($^1J_{PtP}$ = 2636 Hz)

IR (KBr disc, ν cm^{-1})

3044, 2964, 2908, 2876 (C-H), 2093 (C≡C)

Elemental Analysis: Result % (calculated %): C = 50.5 (51.0), H = 5.67 (5.76)

UV/vis: λ_{max} = 340 nm, ε = 69,400 $dm^3mol^{-1}cm^{-1}$

Emission: λ_{max} = 422 nm

6.5.6 Synthesis of 1,2,4,5-tetrafluoro-3,6-*bis*-trimethylsilylethynyl-benzene (87)

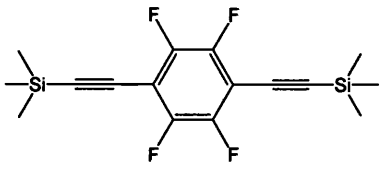

1,2,4,5-Tetrafluoro-3,6-diiodo-benzene (740 mg, 1.85 mmol), copper (I) iodide (17.6 mg, 0.09 mmol), and *bis*(triphenylphosphine)palladium(II)chloride (126 mg, 0.18 mmol) was placed in a Schlenk tube. Dichloromethane (30 mL), diisopropylamine (20 mL) and trimethylsilylacetylene (0.81 mL, 5.55 mmol) were added successively and the reaction was left to stir, in the absence of light, for 12 hr. TLC (silica, hexane) revealed the completion of the reaction and the volatiles were removed under reduced pressure, in a cold water bath. The resultant solid was passed through an alumina plug in hexane/ethyl acetate (4:1 v/v). The volatiles were then removed and the crude

product was purified by sublimation (25 °C, 0.01 mmHg) affording **(87)** as colourless crystals (432 mg, 68%).

^{1}H NMR ($CDCl_3$, 400.13 MHz)

0.19 (s, C*H*$_3$)

^{13}C{^{1}H} NMR – PENDANT ($CDCl_3$, 75.5 MHz, δ ppm)

-0.04	CH_3	(Si*C*H$_3$)	130.22	C_{ipso}	(C_6F_4)
95.05	C_q	(Si*C*≡C)	143.33	C_{ipso}	(*C*F)
100.30	C_q	(C≡*C*(C$_6$F$_4$))			

^{19}F NMR ($CDCl_3$, 376.5 MHz)

-136.67 (C*F*)

Elemental Analysis: Result % (calculated %): C = 55.5 (56.1), H = 5.67 (5.30)

6.5.7 Synthesis of 1,2,4,5-tetrafluoro-3,6-*di*-ethynyl-benzene (88)

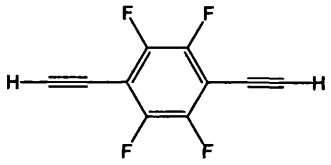

Potassium hydroxide (2.0 M aqueous solution, 1.46 mL) was added to a stirring solution of 1,2,4,5-tetrafluoro-3,6-*bis*-trimethylsilylethynyl-benzene (250 mg, 0.73 mmol) in dichloromethane/methanol (1:1 v/v, 50 mL). After 1 hr TLC (silica, hexane: dichloromethane, 6:1 v/v) revealed the completion of the reaction. The volatiles were removed under reduced pressure and the solid was redissolved in diethyl ether (30 mL) and washed with water (2 x 30 mL). The organic layer was separated and dried ($MgSO_4$). The solvent was then removed and the crude product was sublimed (25°C, 0.01 mmHg) to afford **(88)** as a white solid (101 mg, 70%).

^{1}H NMR ($CDCl_3$, 400.13 MHz)

3.04 (s, C*H*$_3$)

^{13}C{^{1}H} NMR – PENDANT ($CDCl_3$, 75.5 MHz, δ ppm)

81.65	*C*H	(H*C*≡C)	123.67	C_{ipso}	(C_6F_4)
96.30	C_q	(C≡*C*(C$_6$F$_4$))	145.35	C_{ipso}	(*C*F)

^{19}F NMR ($CDCl_3$, 376.5 MHz)

-137.57 (C*F*)

6.5.8 Synthesis of 1,4-*bis*-((*trans*-(phenyl,*bis*-triethylphosphine)platinum) ethynyl) 2,3,5,6-tetrafluoro-benzene (89)

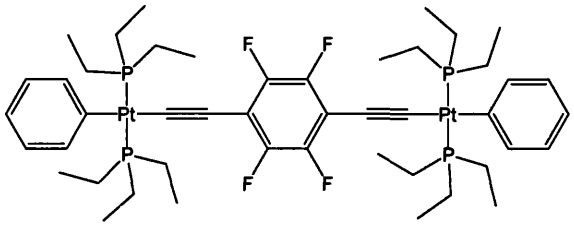

1,2,4,5-Tetrafluoro-3,6-*di*-ethynyl-benzene (27.7 mg, 0.14 mmol) was placed in a Young's ampoule and dissolved in dichloromethane (10 mL). In a separate Schlenk tube *trans-bis*(triethylphosphine)(phenyl)platinum(II)chloride (150 mg, 0.28 mmol) and copper iodide (5 mg) were dissolved in dichloromethane (30 mL) and diisopropylamine (15 mL). The diyne solution was then added to the Schlenk tube and the reaction was left to stir for 6 hr. TLC (silica, hexane: dichloromethane, 1:1 v/v) revealed the completion of the reaction and the volatiles were then removed under reduced pressure. The crude product was passed through a silica plug in hexane: ethyl acetate (3:1 v/v) and the solvent was removed under reduced pressure. The crude product was recrystallised from ethanol affording **(89)** as colourless crystals (135 mg, 79%).

^{1}H NMR ($CDCl_3$, 400.13 MHz)

1.04-1.12 (m, C*H*$_3$, 36H), 1.73-1.81 (m, C*H*$_2$, 24H), 6.81 (t, ^{3}J = 7.2 Hz, C*H*, 2H), 6.97 (t, ^{3}J = 7.4 Hz, C*H*, 4H), 7.30 (d, ^{3}J = 7.4 Hz, C*H*, 4H)

^{13}C{^{1}H} NMR – PENDANT ($CDCl_3$, 75.5 MHz, δ ppm)

7.99	CH_3	($P(CH_2CH_3)_3$)	127.36	CH	(*ortho* C_6H_5Pt)
14.90	CH_2	($P(CH_2CH_3)_3$), t_{ps}, $^{1}J_{PC}+^{3}J_{PC}$ = 34 Hz)	130.84	C_{ipso}	(C_6F_4)
			138.95	CH	(*meta* C_6H_5Pt)
94.36	C_{ipso}	(PtC≡C)	146.20	C_{ipso}	(CF)
105.20	C_{ipso}	(C≡C(C_6F_4))	155.76	C_{ipso}	(C_6H_5Pt)
121.35	CH	(*para* C_6H_5Pt)			

^{19}F NMR ($CDCl_3$, 376.5 MHz)

-144.00 (C*F*)

^{31}P{^{1}H} NMR ($CDCl_3$, 121.5 MHz, δ ppm)

10.28 ($^{1}J_{PtP}$ = 2613 Hz)

Elemental Analysis: Result % (calculated %): C = 45.5 (45.4), H = 5.79 (5.82)

UV/vis: λ_{max} = 354 nm, ε = 87,000 $dm^3mol^{-1}cm^{-1}$

Emission: λ_{max} = 371 nm

6.5.9 Synthesis of *trans- bis*(triethylphosphine)(phenyl)platinum(II) ethynyl benzene (90)

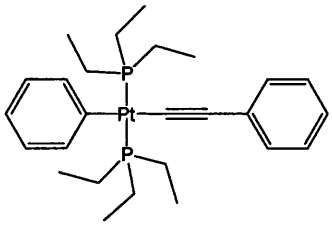

Trans- bis(triethylphosphine)(phenyl)platinum(II) chloride (150 mg, 0.28 mmol) and copper iodide (5 mg) were dissolved in tetrahydrofuran (20 mL) and diisopropylamine (10 mL). Ethynyl benzene (0.36 mL, 0.33 mmol) was added to the stirring solution and the reaction was left to stir for 1 hr in the absence of light. TLC (silica, hexane/dichloromethane, 2:1 v/v) confirmed the completion of the reaction and the volatiles were removed under reduced pressure. The solid was passed through a silica plug (hexane/ethyl acetate, 4:1 v/v). The solvent was removed under reduced pressure and the crude product was recrystallised from ethanol to afford **(90)** as yellow crystals (155 mg, 91%).

^{1}H NMR ($CDCl_3$, 400.13 MHz)

1.06-1.13 (m, C*H*$_3$, 18H), 1.73-1.80 (m, C*H*$_2$, 12H), 6.80 (t, ^3J = 7.2 Hz, C*H*, 1H) 6.96 (t, ^3J = 7.4 Hz, C*H*, 2H), 7.09 (t, ^3J = 7.2 Hz, C*H*, 1H), 7.20 (t, ^3J = 7.2 Hz, C*H*, 2H), 7.29-7.34 (m, C*H*, 4H)

^{13}C{^{1}H} NMR – PENDANT ($CDCl_3$, 100.61 MHz)

8.02	CH_3	($P(CH_2CH_3)_3$)	127.28	C*H*	($Pt(C_6H_5)$
15.11	CH_2	($P(CH_2CH_3)_3$), t_{ps}, $^1J_{PC}+^3J_{PC}$ = 35 Hz)	127.85	*CH*	($C{\equiv}C(C_6H_5)$
			129.40	C_{ipso}	($C{\equiv}C(C_6H_5)$
110.10	C_q	($C{\equiv}C(C_6H_5)$	130.88	C*H*	($C{\equiv}C(C_6H_5)$
113.07	C_q	($C{\equiv}C(C_6H_5)$	139.20	C*H*	($Pt(C_6H_5)$
121.23	*C*H	($C{\equiv}C(C_6H_5)$	156.40	C_{ipso}	($Pt(C_6H_5)$
124.53	*C*H	($Pt(C_6H_5)$			

$^{31}P\{^1H\}$ NMR ($CDCl_3$, 121.5 MHz, δ ppm)

10.10 ($^1J_{PtP}$ = 2642 Hz)

Elemental Analysis: Result % (calculated %): C = 51.9 (51.2), H = 5.99 (6.61)

UV/vis: λ_{max} = 267 nm, ε = 27,900 $dm^3mol^{-1}cm^{-1}$

Emission: λ_{max} = 395 nm

6.5.10 Synthesis of 1,2,4,5-tetramethyl-3,6-(*bis-p*-trimethylsilylphenyl)benzene (92)

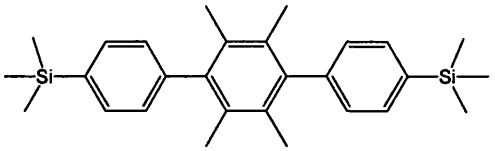

4-trimethylsilyl phenylboronic acid (1.00 g, 5.15 mmol), 1,4-dibromodurene (501 mg, 1.72 mmol), and tetrakis(triphenylphosphine)palladium(0) (397 mg, 3.44 mmol) were placed into a round bottomed flask. Toluene (30 mL) and sodium carbonate (20 mL, 2.00 M aqueous solution) were added and the solution was refluxed under an inert atmosphere. The reaction was monitored by TLC (silica, hexane/dichloromethane, 9:1 v/v) and after 72 hr was complete. The reaction mixture was evaporated to low volume and then made up in dichloromethane, this was washed with a saturated aqueous solution of sodium hydrogen carbonate (2 x 50 mL) then with water (2 x 50 mL). The organic phase was dried ($MgSO_4$) and evaporated to low volume and with addition of methanol (20 mL) a grey solid precipitated out of solution. The solid was then further purified by chromatography (silica, hexane/dichloromethane, 4:1 v/v) affording **(92)** as a pale yellow solid (620 mg, 84%).

^1H NMR ($CDCl_3$, 400.13 MHz)

0.32 (s, C*H*$_3$, 18H), 1.96 (s, C*H*$_3$, 12H), 7.18 (d, ^3J = 8.1 Hz, 4H), 7.58 (d, ^3J = 8.1 Hz, 4H)

$^{13}C\{^1H\}$ NMR – PENDANT ($CDCl_3$, 100.61 MHz)

-0.97	CH_3	($SiCH_3$)	133.24	CH	(*ortho* to TMS)
18.16	CH_3	(C_6-CH_3)	137.98	C_{ipso}	(central ring)
128.82	CH	(*meta* to TMS)	141.18	C_{ipso}	(*para* to TMS)
131.83	C_{ipso}	(CCH_3)	143.15	C_{ipso}	($CSiCH_3$)

6.5.11 Synthesis of 1,2,4,5-tetramethyl-3,6-(*di-p*-iodophenyl)benzene (93)

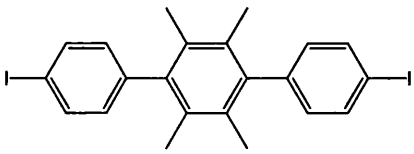

1,2,4,5-tetramethyl-3,6-(*bis-p*-trimethylsilylphenyl)benzene (500 mg, 1.16 mmol) was dissolved in dry methanol (60 mL) and silver trifluoromethanesulfonate (1250 mg, 4.88 mmol) was added to the stirring solution, at 0 °C, under an inert atmosphere. After 20 minutes of stirring iodine (1.18 g, 4.64 mmol) was added, and the reaction was left to stir for a further 30 minutes at 0 °C, followed by 10 hr at room temperature. The reaction was monitored by TLC (silica, hexane/dichloromethane, 4:1 v/v). The volatiles were then removed under reduced pressure, the solid was dissolved in ethyl acetate (60 mL) and then washed with 2.0 M aqueous sodium thiosulphate (2 x 60 mL). The organic phase was separated and dried ($MgSO_4$). The solvent was then removed under reduced pressure affording **(93)** as an off white solid (600 mg, 96%).

^{1}H NMR ($CDCl_3$, 400.13 MHz)

1.93 (s, C*H*$_3$, 12H), 6.92 (d, ^3J = 8.3 Hz, C*H*, 4H), 7.77 (d, ^3J = 8.3 Hz, C*H*, 4H)

^{13}C{^{1}H} NMR – PENDANT ($CDCl_3$, 100.61 MHz)

18.08	CH_3		137.52	CH	*ortho* to iodide
92.00	C_{ipso}	CI	140.28	C_{ipso}	$C_6(CH_3)_4$
131.51	CH	*meta* to iodide	142.13	C_{ipso}	C_6H_4
131.79	C_{ipso}	CCH_3			

EI-mass spectrum: ($C_{22}H_{20}I_2$) *m/z* 538.0; calc. 538.0

6.5.12 Synthesis of 1,2,4,5-tetramethyl-3,6-(*bis-p*-trimethylsilylethynyl)benzene (94)

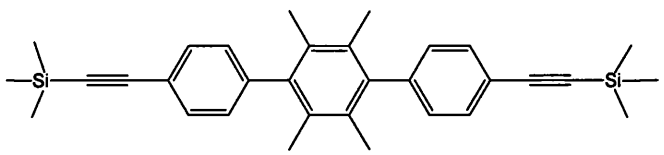

1,2,4,5-tetramethyl-3,6-(*di-p*-iodophenyl)benzene (500 mg, 0.94 mmol), copper (I) iodide (17.8 mg, 0.09 mmol), and *bis*(triphenylphosphine)palladium(II) chloride (132

mg, 0.18 mmol) were placed in a Schlenk tube. Dichloromethane (30 mL), diisopropylamine (15 mL) and trimethylsilylacetylene (0.41 mL, 2.82 mmol) were added successively and the reaction was left to stir, in the absence of light, for 18 hr. TLC (silica, hexane) revealed the completion of the reaction and the volatiles were removed under reduced pressure. The resultant solid was passed through an alumina plug in hexane to remove impurities, and then the desired product was eluted in hexane/dichloromethane (4:1 v/v). The volatiles were then removed to afford **(94)** as a pale yellow solid (360 mg, 80%).

^{1}H NMR ($CDCl_3$, 400.13 MHz)

0.27 (s, C*H*$_3$, 18H), 1.91 (s, C*H*$_3$, 12H), 7.11 (d, ^3J = 8.4 Hz, C*H*, 4H), 7.55 (d, ^3J = 8.4 Hz, C*H*, 4H)

^{13}C{^{1}H} NMR – PENDANT ($CDCl_3$, 100.61 MHz)

0.00	CH_3	($SiCH_3$)	129.43	*C*H	(C_6H_4 *meta* to alkyne)
17.95	CH_3	$C_6(CH_3)_4$	131.68	C_{ipso}	
94.10	C_q	(Si*C*≡C)	132.03	*C*H	(C_6H_4 *ortho* to alkyne)
105.17	C_q	(C≡*C*Ph)	140.73	C_{ipso}	
121.17	C_{ipso}	(C_6H_4 *para* to alkyne)	143.17	C_{ipso}	

6.5.13 Synthesis of 4,4''-*bis*-(trans-(phenyl,*bis*-triethylphosphine)platinum) ethynyl-2',3',5',6'-tetramethyl-terphenyl (95)

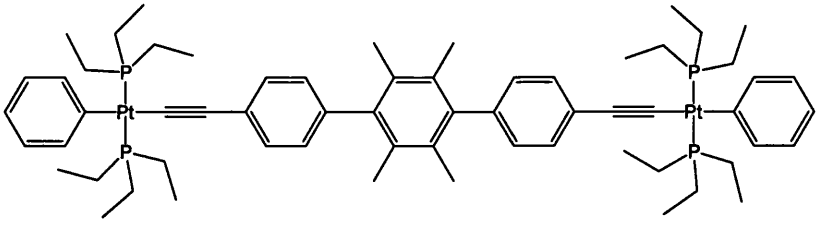

1,2,4,5-tetramethyl-3,6-(*bis-p*-trimethylsilylethynyl)benzene (86 mg, 0.18 mmol) and sodium methoxide (30 mg) were placed into a Young's Ampoule and dissolved in dichloromethane/methanol (1:1 v/v, 90 mL). The solution was left to stir in the absence light for 1 hr. *Trans-bis*(triethylphosphine)(phenyl)platinum(II) chloride (180 mg, 0.36 mmol), copper iodide (5 mg) and diisopropylamine (10 mL) were added to the stirring solution. The reaction was left to stir for 18 hr after which time TLC (silica, dichloromethane) revealed consumption of ligand and platinum starting materials. The volatiles were removed under reduced pressure and the solid was

dissolved in ethyl acetate. The solution was passed through a plug of alumina and the solvent was evaporated to dryness. The resulting solid was recrystallised from ethanol/chloroform (5:1 v/v) affording **(95)** as a white solid (116 mg, 48%).

^{1}H NMR ($CDCl_3$, 400.13 MHz)

1.07-1.15 (m, C*H*$_3$, 36H), 1.76-1.83 (m, C*H*$_2$, 24H), 1.94 (s, C*H*$_3$, 12H), 6.79-6.83 (m, C*H*, 2H), 6.95-6.99 (m, C*H*, 4H), 7.33-7.39 (m, C*H*, 8H), 7.43 (d, ^3J = 8.5 Hz, 4H), 7.59 (d, ^3J = 8.5 Hz, C*H*, 4H)

^{13}C{^{1}H} NMR – PENDANT ($CDCl_3$, 75.5 MHz)

8.39	CH_3	($P(CH_2CH_3)_3$)	123.43	*C*H	(*ortho* to alkyne)
15.47	CH_2	(($P(CH_2CH_3)_3$), t_{ps},	126.66	*C*H	(central C_6H_4)
		$^1J_{PC}+^3J_{PC}$ = 34 Hz)	127.86	*C*H	(*meta* to alkyne)
18.34	CH_3	$C_6(CH_3)_4$	132.99	*C*H	(central C_6H_4)
110.37	C_q	(*C*≡C-Pt)	138.98	C_{ipso}	(central C_6H_4)
112.28	C_q	(C≡*C*-Pt)	139.55	*C*H	(*ortho*, Pt-*Ph*)
121.44	*C*H	(*para*, Pt-*Ph*)	141.19	C_{ipso}	(*para* to alkyne)

^{31}P{^{1}H} NMR ($CDCl_3$, 161.97 MHz)

10.02 ($^1J_{PtP}$ = 2638 Hz)

Elemental Analysis: Result % (calculated %): C = 53.2 (55.1), H = 6.90 (6.72)

IR (KBr disc, ν cm^{-1}): 3045, 2954, 2927(C-H), 2090 (C≡C)

UV/vis: λ_{max} = 267 nm, ε = 93,000 dm^{3}mol^{-1}cm^{-1}

Emission: λ_{max} = 345 nm

6.5.14 Synthesis of 2,5-*bis*-(4-trimethylsilyl-phenyl)-pyrimidine (98)

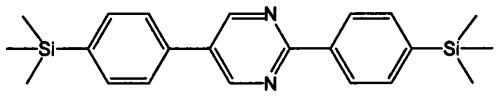

4-trimethylsilyl phenylboronic acid (1.07 g, 5.51 mmol), 5-bromo-2-iodopyrimidine (500 mg, 1.84 mmol), and tetrakis(triphenylphosphine)palladium(0) (318 mg, 2.76 mmol) were charged into a round bottomed flask. Toluene (50 mL) and sodium carbonate (40 mL, 2.00 M aqueous solution) were added and the solution was refluxed under an inert atmosphere. The reaction was monitored by TLC (silica,

hexane: dichloromethane, 2:1) and after 2 hr was complete. The reaction mixture was evaporated to dryness, dissolved in dichloromethane (50 mL) and washed with water (2 x 50 mL). The organic phase was separated and dried ($MgSO_4$). The volatiles were removed under reduced pressure and the crude solid was purified using chromatography (silica, hexane: dichloromethane, 2:1 v/v) affording **(98)** as a white solid (484 mg, 82%).

^{1}H NMR ($CDCl_3$, 300.22 MHz, δ ppm)

0.32 (s, C*H*$_3$, 18H), 7.60-7.71 (m, C*H*, 6H), 8.45 (d, ^3J = 8.1 Hz, C*H*, 2H), 9.03 (s, *C*H, 2H)

Elemental Analysis: Result % (calculated %): C = 69.7 (70.1), H = 7.25 (7.49), N = 7.22 (7.44)

EI/Mass Spectrum: ($C_{22}H_{28}N_2Si_2$) *m/z* 476.2, calc. 476.6

6.5.15 Synthesis of 2,5-*di*-(4-iodo-phenyl)-pyrimidine (99)

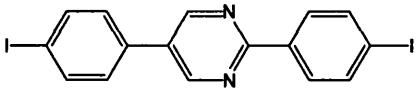

Iodine monochloride (2.20 mL, 1.00 M solution in dichloromethane) was added dropwise to a stirring solution of 3,6-*bis*-(4-trimethylsilyl-phenyl)-pyrimidine (320 mg, 1.00 mmol) in chloroform (20 mL). On addition of the iodine monochloride the solution turned a bright orange colour with a white precipitate forming after 5 min. TLC (silica, dichloromethane/hexane, 3:1 v/v) of the mixture after 1 hr revealed the completion of reaction. Saturated sodium thiosulphate solution (10 mL) was added to quench any excess iodine. The organic layer was separated, washed with water (2 x 20mL) and then dried ($MgSO_4$). The solvent was removed under reduced pressure yielding an off white solid which was recrystallised from chloroform (200 mL) affording **(99)** as a white solid (340 mg, 70%).

^{1}H NMR ($CDCl_3$, 300.22 MHz, δ ppm)

7.36 (d, ^3J = 8.5 Hz, C*H*, 2H), 7.84-7.89 (m, C*H*, 4H), 8.22 (d, ^3J = 8.5 Hz, C*H*, 2H), 8.97 (s, *C*H, 2H)

Elemental Analysis: Result % (calculated %): C = 39.5 (39.7), H = 2.10 (2.08), N = 5.71 (5.79)

EI/Mass Spectrum: *m/z* 484.0, calc. 484.0

6.5.16 Synthesis of 2,5-*bis*-(4-trimethylsilylethynyl-phenyl)-pyrimidine (100)

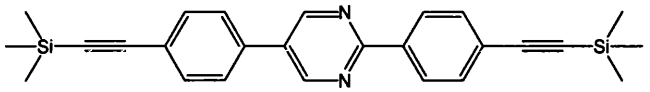

2,5-*di*-(4-iodo-phenyl)-pyrimidine (200 mg, 0.41 mmol), copper iodide (7 mg, 0.05 mmol) and *bis*(triphenylphosphine)palladium(II)chloride (72 mg, 0.10 mmol) were placed in a Schlenk tube. Tetrahydrofuran (50 mL), diisopropylamine (10 mL) and trimethylsilylacetylene (0.12 mL, 0.82 mmol) were added respectively and the reaction was left to stir, in the absence of light, for 16 hr. TLC (silica, dichloromethane/hexane, 4:1 v/v) revealed completion of reaction and the volatiles were removed under reduced pressure. The resulting solid was dissolved in hexane/ethyl acetate (1:1 v/v) and passed through a short alumina plug, after which the solvent was removed yielding a brown solid. Recrystallisation of the crude product from ethanol afforded **(99)** as an off white solid (142 mg, 72%).

^{1}H NMR ($CDCl_3$, 300.22 MHz, δ ppm)

0.02 (s, C*H*$_3$, 9H), 0.07 (s, C*H*$_3$, 9H), 7.30 (d, ^3J = 8.6 Hz, C*H*, 2H), 7.85-7.96 (m, C*H*, 4H), 8.22 (d, ^3J = 8.6 Hz, C*H*, 2H), 8.95 (s, *C*H, 2H)

^{13}C{^{1}H} NMR – PENDANT ($CDCl_3$, 75.5 MHz, δ ppm)

-0.07	CH_3	(Si*C*H$_3$, 5-*pym*)	127.92	*C*H	(*ortho* to alkyne, 2-*pym*)
1.01	CH_3	(Si*C*H$_3$, 2-*pym*)	131.01	C_{ipso}	(*para* to alkyne, 5-*pym*)
96.33	C_q	(C≡*C*-Si, 5-*pym*)	132.27	CH	(*meta* to alkyne, 5-*pym*)
96.50	C_q	(C≡*C*-Si, 2-*pym*)	132.95	*C*H	(*meta* to alkyne, 2-*pym*)
104.21	C_q	(C≡*C*-C, 5-*pym*)	134.27	C_{ipso}	(5-*pym*)
104.88	C_q	(C≡*C*-C, 2-*pym*)	137.00	C_{ipso}	(*para* to alkyne, 2-*pym*)
123.87	C_{ipso}	(C≡C-*C*, 5-*pym*)	155.07	*C*H	(4/6-*pym*)
125.55	C_{ipso}	(C≡C-*C*, 2-*pym*)	162.96	C_{ipso}	(2-*pym*)
126.45	CH	(*ortho* to alkyne, 5-*pym*)			

UV/vis: λ_{max} = 321 nm, ε = 55,000 $dm^3mol^{-1}cm^{-1}$

Emission: λ_{max} = 384 nm

6.5.17 Synthesis of 3,6-*di*-(4-bromo-phenyl)-[1,2,4,5]-tetrazine[20,21] (101)

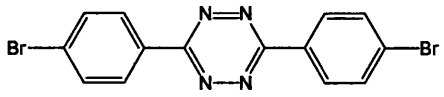

Copper nitrate trihydrate (2.46 g, 0.01 mol), zinc (1.30 g, 0.02 mol) and ethanol (10 mL) were placed in a two necked round bottomed flask. The mixture was stirred for 30 minutes under an inert atmosphere after which time the blue colour had almost all faded. 4-Bromo-benzonitrile (1.82 g, 0.01 mol) and hydrazine monohydrate (2.30 mL, 0.05 mol) were added to the stirring slurry. The reaction was refluxed for 12 hr, allowed to cool and filtered to remove the catalyst. The solid was washed with chloroform (2 x 50 mL) and the volatiles were removed under reduced pressure. The crude product was recrystallised from ethanol affording **(101)** as a pink solid (162 mg, 5%). The product was insoluble in all common organic solvents, therefore no NMR data was obtained.

Elemental Analysis: Result (calculated): C = 42.7% (42.9%), H = 2.26% (2.06%), N = 14.6% (14.3%)

EI-mass spectrum: ($C_{14}H_8Br_2N_4$) *m/z* 391.9; calc. 391.9

6.5.18 Synthesis of 3,6-*bis*-(4-trimethylsilylethynyl-phenyl)-[1,2,4,5]-tetrazine (102)

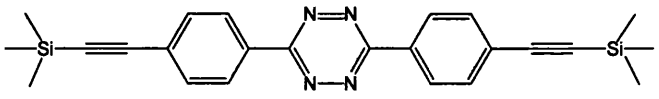

3,6-*bis*-(4-bromo-phenyl)-[1,2,4,5]-tetrazine (100 mg, 0.26 mmol), copper (I) iodide (5 mg, 0.04 mmol), and *bis*(triphenylphosphine)palladium(II)chloride (38 mg, 0.05 mmol) were placed in a Schlenk tube. Dimethylformamide (20 mL), diisopropylamine (10 mL) and trimethylsilylacetylene (0.06 mL, 0.55 mmol) were added successively and the reaction vessel was sealed and heated to 70 °C with stirring, under the protection of light, for 18 hr. TLC (silica, dichloromethane) revealed completion of reaction. The volatiles were removed under reduced pressure and the resultant solid was passed through a short alumina plug using ethyl

acetate/hexane (1:1 v/v) as the eluent. The volatiles were then removed and the crude product was further purified by chromatography (silica, hexane/dichloromethane, 1:1 v/v) affording **(102)** as a bright pink crystalline solid (55 mg, 50%).

^{1}H NMR ($CDCl_3$, 300.22 MHz, δ ppm)

0.29 (s, C*H*$_3$, 18H), 7.69 (d, ^3J = 8.7 Hz, C*H*, 4H), 8.60 (d, ^3J = 8.7 Hz, C*H*, 4H)

^{13}C{^{1}H} NMR – PENDANT ($CDCl_3$, 75.5 MHz, δ ppm)

0.00	CH_3	(SiCH_3)	131.48	C_{ipso}	(*para* to alkyne)
98.42	C_q	(SiC≡C)	132.96	*C*H	(*meta* to tetrazine)
104.33	C_q	(*C*≡*C*Ph)	164.56	C_{ipso}	(*tetrazine*)
127.86	*C*H	(*ortho* to tetrazine)			

UV/vis: λ_{max} = 338 nm, ε = 51,800 $dm^3mol^{-1}cm^{-1}$

Emission: λ_{max} = 409 nm

6.5.19 Synthesis of 1,3,5-*tris*-[(4-trimethylsilylethynyl)phenyl]benzene (106)

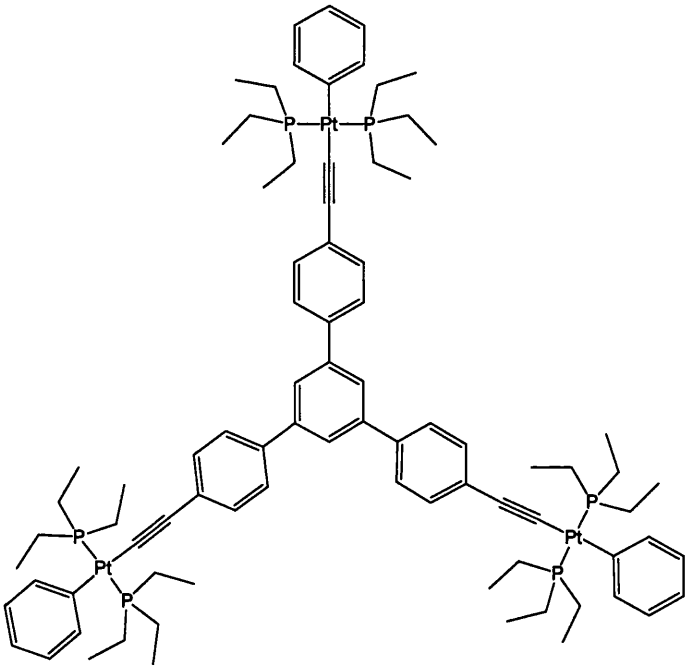

Trans-bis(triethylphosphine)(phenyl)platinum(II)chloride (250 mg, 0.46 mmol), 1,3,5-*tri*-[(4-ethynyl)phenyl]benzene (58 mg, 0.15 mmol), and copper(I) iodide (5 mg) were placed in a Schlenk tube. Dichloromethane (40 mL) and diisopropylamine (20 mL) were added and the reaction was left to stir for 18 hr, after which time TLC (silica, dichloromethane/hexane, 1:1 v/v) confirmed completion of the reaction. The volatiles were removed under reduced pressure and the solid was dissolved in ethyl

acetate. The solution was passed through a plug of alumina and the solvent was evaporated to dryness. The resulting solid was recrystallised from ethanol/chloroform (9:1 v/v) yielding **(106)** as yellow crystals (197 mg, 69%).

^{1}H NMR ($CDCl_3$, 300.22 MHz)

1.06-1.15 (m, C*H*$_3$, 54H), 1.76-1.85 (m, C*H*$_2$, 36H), 6.81 (t, ^3J = 7.2 Hz, C*H*, 3H), 6.97 (t, ^3J = 7.4 Hz, C*H*, 6H), 7.43 (d, ^3J = 8.5 Hz, 6H), 7.59 (d, ^3J = 8.5 Hz, C*H*, 6H), 7.66 (s, C*H*, 3H)

^{13}C{^{1}H} NMR – PENDANT ($CDCl_3$, 75.5 MHz, δ ppm)

8.38	*C*H$_3$	(P(CH$_2$C*H*$_3$)$_3$)	126.66	*C*H	(central C$_6$H$_4$)
15.47	*C*H$_2$	((P(C*H*$_2$CH$_3$)$_3$), t$_{ps}$, $^1J_{PC}$+$^3J_{PC}$ = 34 Hz)	127.86	*C*H	(*meta* to alkyne)
			132.99	*C*H	(central C$_6$H$_4$)
110.37	C_q	(*C*≡C-Pt)	138.98	C_{ipso}	(central C$_6$H$_4$)
112.28	C_q	(C≡*C*-Pt)	141.19	C_{ipso}	(*para* to alkyne)
121.54	*C*H	(*para*, Pt-*Ph*)	139.55	*C*H	(*ortho*, Pt-*Ph*)
122.13	*C*H	(*ortho* to alkyne)			

^{31}P{^{1}H} NMR ($CDCl_3$, 121.5 MHz, δ ppm)

11.09 ($^1J_{PtP}$ = 2367 Hz)

Elemental Analysis: Result (calculated): C = 53.7% (53.1%), H = 6.28% (6.36%),

UV/vis: λ_{max} = 355 nm, ε = 79,800 dm^{3}mol^{-1}cm^{-1}

Emission: λ_{max} = 451 nm

6.6 References

[1] R. J. Errington, *Advanced Practical Inorganic and Metalorganic Chemistry*, Blackie Academic and Professional, London, 1st Ed., 1997

[2] J. Plater, *Tetrahedron*, 2004, **60**, 6385

[3] G. Low, *J. Med. Chem*, 1999, **42**, 3167

[4] J. Stille, *Heterocycles*, 1997, **45**, 1363

[5] G. Whitesides, *J. Org. Chem*, 1988, **53**, 2489

[6] Y. Kim, S. Ahn, S. Kwon, *Bull. Korean Chem. Soc.*, 2001, **22**, 451

[7] G. Vlad, I. T. Horvath, *J. Org. Chem.*, 2002, **67**, 6550

[8] K.T. Wong, F.C. Fang, Y.M. Cheng, P.T. Chou, G.H. Lee, Y. Wang, *J. Org. Chem.*, 2004, **69**, 8038

[9] S. Kotha, M. Kashinath, S. Dhurke, P. Lahiri, K. Kakali, W. Sunoj, B. Raghavan, *Eur. J. Org. Chem.*, 2004, **19**, 4003

[10] E. Weber, M. Hecker, E. Koepp, W. Orlia, M. Czugler, I. Csoeregh, *J. Chem. Soc. Perkin Trans. 2*, 1988, 1251

[11] K. Siegmann, *Organometallics*, 1989, **8**, 2659

[12] M. Bruce, *Inorg. Synth.*, 1989, **26**, 324

[13] M. S. Khan, M. R. A. Al-Mandhary, M. K. Al-Suti, F. R. Al-Battashi, S. Al-Saadi, B.Ahrens, J. K. Bjernemose, M. F. Mahon, P. R. Raithby, M. Younus, N. Chawdhury, A. Köhler, E. A. Marseglia, E. Tedesco, N. Feeder, S. J. Teat, *Dalton Trans.*, 2004, 2377

[14] A. L. Allred, L. W. Bush, *J. Am. Chem. Soc.*, 1968, **90**, 3352

[15] M. R. Unroe, B. A. Reinhardt, *Synthesis*, 1987, **11**, 981

[16] K.A. Kovyrzina, T.A. Tsvetkova, *J.Org.Chem.USSR* (Engl.Transl.), 1974, **10**, 1078

[17] L. L. Schafer, J. R. Nitschke, S. S. H. Mao, F-Q. Liu, G. Harder, M. Haufe, T. D. Tilley, *Chem. Eur. J.*, 2002, **8**, 74

[18] A. L. Allred, L. W. Bush *J. Am. Chem. Soc.*, 1968, **90**, 3352

[19] F. Barba, V. M. Desamparados, A. Guirado, *Synthesis*, 1984, **7**, 593

[20] M. Santus, *Acta Pol. Pharm.*, 1993, **50**, 183

[21] C. L. Lim, S. H. Pyo, T. Y. Kim, E. S. Yim, B. H Han, *Bull. Korean Chem. Soc.*, 1995, **16**, 374

6.6 References

[1] R. J. Errington, *Advanced Practical Inorganic and Metalorganic Chemistry*, Blackie Academic and Professional, London, 1st Ed., 1997

[2] J. Plater, *Tetrahedron*, 2004, **60**, 6385

[3] G. Low, *J. Med. Chem*, 1999, **42**, 3167

[4] J. Stille, *Heterocycles*, 1997, **45**, 1363

[5] G. Whitesides, *J. Org. Chem*, 1988, **53**, 2489

[6] Y. Kim, S. Ahn, S. Kwon, *Bull. Korean Chem. Soc.*, 2001, **22**, 451

[7] G. Vlad, I. T. Horvath, *J. Org. Chem.*, 2002, **67**, 6550

[8] K.T. Wong, F.C. Fang, Y.M. Cheng, P.T. Chou, G.H. Lee, Y. Wang, *J. Org. Chem.*, 2004, **69**, 8038

[9] S. Kotha, M. Kashinath, S. Dhurke, P. Lahiri, K. Kakali, W. Sunoj, B. Raghavan, *Eur. J. Org. Chem.*, 2004, **19**, 4003

[10] E. Weber, M. Hecker, E. Koepp, W. Orlia, M. Czugler, I. Csoeregh, *J. Chem. Soc. Perkin Trans. 2*, 1988, 1251

[11] K. Siegmann, *Organometallics*, 1989, **8**, 2659

[12] M. Bruce, *Inorg. Synth.*, 1989, **26**, 324

[13] M. S. Khan, M. R. A. Al-Mandhary, M. K. Al-Suti, F. R. Al-Battashi, S. Al-Saadi, B.Ahrens, J. K. Bjernemose, M. F. Mahon, P. R. Raithby, M. Younus, N. Chawdhury, A. Köhler, E. A. Marseglia, E. Tedesco, N. Feeder, S. J. Teat, *Dalton Trans.*, 2004, 2377

[14] Allred A. L.; Bush L. W.; *J. Am. Chem. Soc.*, 1968, **90**, 3352

[15] Unroe, Marilyn R.; Reinhardt, Bruce A., *Synthesis*, 1987, **11**, 981

[16] Kovyrzina,K.A.; Tsvetkova,T.A.; *J.Org.Chem.USSR* (Engl.Transl.), 1974, **10**, 1078

[17] Schafer, Laurel L.; Nitschke, Jonathan R.; Mao, Shane S. H.; Liu, Feng-Q.; Harder, Gabriele; Haufe, Markus; Tilley, T. Don; *Chem. Europ. J.*, 2002, **8**, 74

[18] A. L. Allred, L. W. Bush *J. Am. Chem. Soc.*, 1968, **90**, 3352

[19] F. Barba, V. M. Desamparados, A. Guirado, *Synthesis*, 1984, **7**, 593

[20] M. Santus, *Acta Pol. Pharm.*, 1993, **50**, 183

[21] C. L. Lim, S. H. Pyo, T. Y. Kim, E. S. Yim, B. H Han, *Bull. Korean Chem. Soc.*, 1995, **16**, 374

Appendix

Found on attached Compact Disc